Engineered emulsions stabilised by thermoresponsive branched copolymers for pharmaceutical applications

Abhishek Rajbanshi

University of Hertfordshire

Life and Medical Sciences

August 2023

PhD thesis

submitted to the University of Hertfordshire in partial fulfilment of the requirements for the degree of Doctor of Philosophy

Dedicated to
My Grandparents and My Mother

Late Shiva Prasad Kayastha
(1931 – 2018 A.D.)

Late Nanichori Kayastha
(1935 – 2013 A.D.)

Late Anju Rajbanshi
(1963 – 2007 A.D)

Table of Contents

Author's declaration

I certify that the thesis titled '**Engineered emulsions stabilised by thermoresponsive branched copolymers for pharmaceutical applications**', submitted for the degree of Doctor of Philosophy, has not been previously submitted for another degree in this or any other educational institution. Moreover, I confirm that the experimental laboratory works, data analysis and interpretation are entirely my own work, except where otherwise acknowledged.

Abhishek Rajbanshi

31 August 2023

Acknowledgement

Behind every successful man, there is a woman – at the threshold of this PhD journey, I am profoundly grateful for my wife, Sony Chandi Shrestha's support upon which my accomplishments stand.

I dedicate this to my late grandparents and my late mother for their unconditional love, encouragement, and wonderful upbringing. I owe immense gratitude to my dad (Girendra Man Rajbanshi), sister (Queen Rajbanshi) and aunty (Anu Kayastha) whose support has woven the fabric of my journey. I am grateful for the love, support, and encouragement that I have received from the members of my maternal family (Biju Pradhan, Raju, Sagar, and Suresh Prasad Kayastha). I am profoundly grateful to my in-laws (Mohan and Nirmala Chandi Shrestha, and the entire family including Jatin Tandukar and his family) for their boundless love and heartfelt warmth; I consider myself truly blessed. I wholeheartedly thank my cousins and all my family members for their support.

I must acknowledge the remarkable individuals, Sundus and Ihab Twefik, whose words of encouragement, love, and unwavering support have been instrumental in my pursuit of this PhD degree.

Special thanks to Sudhir Sharan KC, Bachan Lal Shrestha, Saroj Shrestha, Suresh Katuwal Chhetri and the Maharaj group for the friendship they have shared.

List of abbreviations

ACNs	alkane carbon numbers
AIBN	alpha-azoisobutyronitrile
Al_2O_3	aluminium oxide
BCS	Branched copolymer surfactant
CCS	Core cross-linked star
CNC	cellulose nanocrystals
CO_2	carbon dioxide
CTA	Chain transfer agent
DDT	dodecanethiol
DEGMA	di (ethylene glycol) methyl ether methacrylate
DLS	Dynamic light scattering
DMA	2-(dimethylamino) ethyl methacrylate
DMCHA	N,N-dimethylcyclohexylamine
DMF	dimethylformamide
D_2O	deuterium oxide
DOX	doxorubicin
DSD	Droplet size distribution
EG	ethylene glycol
EGDMA	ethylene glycol dimethacrylate
El	Ellipsoid
G′	storage or elastic modulus
G″	loss or plastic modulus
GO	graphene oxide
GPC	Gel permeation chromatography
HDT	hexadecanethiol
HIPE	High internal phase emulsion
HPLC	High performance liquid chromatography
HS	Hardsphere
LCST	Lower critical solution temperature

LM	Light microscopy
MA	methacrylic acid
MAA	methyl methacrylic acid
MC	methylcellulose
ME	mercaptoethanol
MEA	2-methoxyethyl acrylate
Mn	number average molecular weight
Mw	weight average molecular weight
MWCO	molecular weight cut off
NMR	Nuclear magnetic resonance
NR	Neutron reflectivity
OEGMA	oligo (ethylene glycol) methyl ether methacrylate
O/W	oil-in-water
PDEA	poly(N,N-diethyl acrylamide)
PDM	poly (2-(dimethyl amino)ethyl methacrylate)
PDMAEMA	poly (N,N-dimethylaminoethyl methacrylate)
PEGA	poly (ethylene glycol) acrylate
PEGMA	poly (ethylene glycol) methyl ether methacrylate
PEO	poly (ethylene oxide)
PhD	Doctor of philosophy
PIPP	poly(2-isopropoxy-2-oxo1,3,2-dioxaphospholane)
PL	power law
PMMA	poly (methyl methacrylate)
PNIPAM	poly (N- isopropylacrylamide)
POEGMA	poly (oligoethylene glycol methyl ether methacrylates)
PS-BEIM	poly(styrene-2-(2- bromoisobutyryloxy)ethyl methacrylate)
PVA	polyvinyl alcohol
PVCL	poly(N-vinylcaprolactam)
PZW	polymer zwitterion
SANS	Small angle neutron scattering
SiC	silicon carbide
SHEMA	2-(sulfobenzoic acid) ethyl methacrylate

SHS	Sticky hardsphere
SL	shellac
SLD	Scattering light density
TA	tertiary amines
Tc	cloud point
TDT	tetradecanethiol
TEM	Transmission electron microscopy
Tgel	Thermoreversible gels
UCST	Upper critical solution temperature
UK	United Kingdom
UPy	2-ureido-4[1H] pyrimidin
W/O	water-in-oil
W/O/W	water-in-oil-in-water
XG	xanthan gum

List of publications

Rajbanshi, A. *et al.* Polymer architecture dictates thermoreversible gelation in engineered emulsions stabilised with branched copolymer surfactants. *Polym. Chem.* **13**, 5730–5744 (2022).

Rajbanshi, A. *et al.* Combining branched copolymers with additives generates stable thermoresponsive emulsions with in situ gelation upon exposure to body temperature. *Int. J. Pharm.* **637**, 122892 (2023).

Rajbanshi, A. *et al.* Branched copolymer surfactants as versatile templates for responsive emulsifiers with bespoke temperature-triggered emulsion-breaking or gelation. *Adv. Mater. Interfaces* **2300755**, 1–13 (2023).

Rajbanshi, A. *et al.* Development of engineered emulsions for nasal drug delivery. **(Research article in late draft)**

Rajbanshi, A. *et al.* Stimuli-responsive polymers for smart emulsions. **(Review article in late draft)**

List of presentations

Rajbanshi, A., Da Silva, M.A., Murnane, D., Dreiss, C.A. and Cook, M.T. (24 – 28 Jul 2023). Engineered emulsions stabilised by branched copolymer surfactants for pharmaceutical applications. Poster presentation at the Controlled Release Society 2023 Annual Meeting and Symposium.

Rajbanshi, A., Da Silva, M.A., Murnane, D., Dreiss, C.A. and Cook, M.T. (27 Apr 2023). Thermoresponsive engineered emulsion enabled by branched copolymer surfactants. Oral and Poster presentation at the London Polymer Group Symposium.

Rajbanshi, A., Da Silva, M.A., Murnane, D., Dreiss, C.A. and Cook, M.T. (04 – 09 Sep 2022). Thermoresponsive engineered emulsion enabled by branched copolymer surfactants. Poster presentation at the 36th Conference of the European Colloid and Interface Society.

Rajbanshi, A., Da Silva, M.A., Murnane, D., Dreiss, C.A. and Cook, M.T. (28 Apr 2022). Temperature-responsive engineered emulsion enabled by branched copolymer surfactants. Oral presentation at the Gel Permeation Celebration, Warwick Analytical Science Centre.

Rajbanshi, A., Da Silva, M.A., Murnane, D., Dreiss, C.A. and Cook, M.T. (12 - 14 Jan 2022). Thermoresponsive engineered emulsion enabled by branched copolymer surfactants. Oral presentation at the Mid-Winter Meeting, British Society of Rheology.

Rajbanshi, A., Da Silva, M.A., Murnane, D., Dreiss, C.A. and Cook, M.T. (12 - 15 Jul 2021). Polymeric surfactants enable thermoresponsive emulsions. Poster presentation at the 15th International Conference on Material Chemistry.

Abstract

This research work explored thermoresponsive emulsions and investigated their potential in delivering drugs through *in situ* gelling pharmaceutical formulations. Employing thermoresponsive branched copolymer surfactants (BCSs), this study established their efficacy in creating stable emulsions with reversible gelation triggered by changes in temperature. While previous research had shown BCSs' capacity to transition emulsions to gels via pH alteration, this study innovatively proposed the concept of thermoresponsive emulsions that respond at physiological temperatures.

The focus was on generating materials capable of shifting from a liquid to a gel state upon warming, promising enhanced healthcare technologies like in situ gel-forming materials for diverse drug delivery routes. The thermoresponsive BCSs used to stabilise the emulsions that showed sol-gel transition upon heating were synthesised with a lower critical solution temperature (LCST) monomer, a hydrophilic macromonomer, a cross-linker and a hydrophobic chain transfer agent. All these components were proven to contribute to the gelation behaviour.

The research investigated the interplay between temperature and BCS structure at both macro and nanoscales, dissecting how these engineered emulsions react to temperature shifts. Moreover, the emulsions held the potential for solubilisation of various drug chemistries and explored their drug delivery activities via *in situ* gelation. This thesis evaluated the rheology of the engineered emulsions based on polymer architecture, branching, molecular weight, and hydrophobic end groups, influencing gel formation on heating. Furthermore, poly(ethylene glycol) methyl ether methacrylate's role in controlling emulsion responsiveness was highlighted, with longer poly(ethylene glycol) chains inducing thermogelation and shorter chains causing emulsion breakdown upon mild heating. The ratio of LCST monomer to hydrophilic macromonomer tightly governed gelation temperature.

Expanding these findings, the research explored various pharmaceutically relevant oils in the emulsion system, along with additives to enhance stability. The addition of methylcellulose significantly improved stability, and small-angle neutron scattering (SANS) helped to understand the gelation mechanism and the nanoscale processes within

BCS-stabilised emulsions. Furthermore, these emulsion systems were investigated as pharmaceutical formulations, analysing drug release mechanisms and compatibility with nasal spray devices. These advanced emulsions showed promise in controlled drug release and nasal spray device compatibility.

In summary, this thesis showed a new frontier in drug delivery through temperature-responsive emulsions, offering smart dosage forms with transformative potential. The work not only advances understanding in thermoresponsive engineered emulsions but also lays the groundwork for personalised medicine and targeted drug delivery, promising improved patient outcomes and reduced dosing frequency.

Chapter 1: Introduction

1.1 Overview

Stimuli-responsive materials have had a significant impact on scientific research by enabling "smart" control over material properties upon activation with stimuli, such as pH[1–4], temperature[5–8], magnetic field[9–11], CO_2[12,13], light[14–17] and redox-reaction[18,19]. This control has revolutionised healthcare, leading to significant progress in the treatment of various diseases, as well as breakthroughs in tissue engineering, nanorobotics, and diagnostics. These advancements have opened up new possibilities and improved the quality of life for many individuals.[20] One reported class of smart materials are "engineered emulsions".[21] First reported by Weaver and co-workers, these systems use pH-sensitive branched copolymers to stabilise emulsion droplets, which respond to changes in pH by solidifying into gels.[21,22] This hierarchical process occurs due to intra-molecular hydrogen bonding between copolymers on adjacent emulsion droplets, leading to self-assembly of the droplets into a supracolloidal network structure. These materials offer exciting functionality, displaying stimulus-responsiveness, combined with the availability of organic and aqueous domains, which could be used as a reservoir or solubilisation locus for a large payload, released on demand. However, the current literature focuses on the fundamental behaviour of these materials and their use for drug delivery has not been assessed.

Emulsifiers are substances used to stabilise emulsions and prevent the dispersed phase from separating or coalescing. Typically, emulsifiers are small/macro molecules known as surfactants. However, using macromolecular surfactants provides a higher degree of flexibility compared to small molecules. By carefully selecting the macromolecular components, it is possible to create stimuli-responsive polymers with amphiphilic properties.[23] Thermo-thickening activity has been found in emulsions, which enables an increase in viscosity of a material during application and is beneficial for many medical applications. A low-viscosity fluid is easier to apply using syringes, pumps, or spray devices, while a gel-like solid improves retention, localisation, and stability over time. Previous studies have shown that branched copolymer surfactants (BCSs) can give

emulsions a pH-responsive behaviour, allowing solidification triggered by an acidic pH trigger.[23,24] Therefore, they serve as a foundation for developing emulsions that respond to temperature.

The aim of the research is to investigate the use of temperature-responsive polymers in topical or nasal drug delivery to generate novel "smart" medicines. Preliminary studies have reported thermo-rheological properties of BCSs stabilising oil-in-water emulsions.[25] This has led to the generation of materials exhibiting temperature-dependent gelation. For prior studies poly(N- isopropylacrylamide) (PNIPAM) was used as a temperature responsive unit to synthesise amphiphilic BCS. However, there are conflicting evidences regarding its biocompatibility, and the viscoelastic strength of gels was low.[25] The focus of this thesis is on the generation of novel BCSs to stabilise emulsions which are liquid-like at room temperature but switch to a gel state in response to temperature. These BCSs are synthesised with thermoresponsive units that belongs to the versatile and biocompatible oligo(ethylene glycol) methyl ether methacrylate family. Ultimately, this new blueprint for BCS aimed to give thermoreversible gel-forming emulsions with better performance than those reported to date.

This thesis is divided into 7 chapters, 4 of which focus on generation of optimal temperature responsive surfactants through polymer design, optimisation of emulsion formulations and fundamental understanding of these materials for drug delivery. Chapter 2 provides an overview of the available literature on responsive surfactants to generate engineered emulsions. Chapter 3 describes work conducted on synthesis of thermoresponsive BCSs generating a library of novel amphiphiles with varied branching, molecular weight and carbon length of hydrophobic domains. The relationship between polymer architecture and rheology of these emulsion systems is demonstrated and the mechanisms of gelation were probed by small angle neutron scattering (SANS). The design principles are discussed for this novel class of thermoresponsive materials that are 10 times stronger (storage modulus up to ca. 300 Pa) than the research activity led by Da Silva et al. (storage modulus ca. 30 Pa) and push the research further towards new advanced platforms for topical drug delivery.[25] This chapter has been published in Polymer Chemistry journal and are reproduced with amendments to the text.[26]

Chapter 4 focuses on optimisation and identification of optimal thermoresponsive systems. This chapter reports an optimised BCS with carefully controlled architecture and concentration that can create emulsions that undergo transition from a liquid to a gel state when heated above 32 °C, where materials produced in Chapter 3 required higher temperatures which were not physiologically relevant. This characteristic makes the system highly suitable for in-situ gelation upon contact with the body.

Chapter 5 is focused on the effect of co-surfactants and additives on the stability and performance of thermo-thickening emulsions and evaluates the optimal architecture in the presence of non-ionic and ionic surfactants. This chapter describes the evaluation of a range of pharmaceutically relevant oils in the BCS system as well as the evaluation of co-surfactants combined with BCS to overcome emulsion instabilities (i.e., creaming) and thermo-thickening performance. Overall, a novel thermoresponsive emulsion formulation was reported that can be used for in-situ gel forming dosage forms. The contents of this chapter have been published in International Journal of Pharmaceutics journal and are reproduced with amendments to the text.[27]

Chapter 6 explores the incorporation of drug molecules in the emulsion system and the effect of temperature stimulus on drug release profile. Furthermore, these thermoresponsive materials are incorporated into drug delivery devices and the effects of processing on the performance of the emulsion are explored.

Chapter 7 provides concluding remarks and future perspectives on the research. There is currently no study into the use of "engineered emulsions" stabilised by thermoresponsive polymers in drug delivery. The development of temperature-responsive emulsions will allow for "smart" dosage forms which can be triggered to increase viscosity after administration, enhancing retention of drug, thereby improving absorption and duration of effect. This in turn will allow for reduced number of doses and increased efficacy, overall improving treatment modalities and patient outcomes. There is also a paucity of information in this area in general and the progress made in this PhD has significantly increased understanding of thermoresponsive engineered emulsions.

1.2 References

1. Wang, Y., Zhu, L., Zhang, H., Huang, H. & Jiang, L. Formulation of pH and temperature dual-responsive Pickering emulsion stabilized by chitosan-based microgel for recyclable biocatalysis. *Carbohydr. Polym.* **241**, 116373 (2020).

2. Binks, B. P. & Rodrigues, J. A. Inversion of emulsions stabilized solely by ionizable nanoparticles. *Angew. Chemie - Int. Ed.* **44**, 441–444 (2005).

3. Sun, G., Li, Z. & Ngai, T. Inversion of particle-stabilized emulsions to form high-internalphase emulsions. *Angew. Chemie - Int. Ed.* **49**, 2163–2166 (2010).

4. Besnard, L. *et al.* Multiple emulsions controlled by stimuli-responsive polymers. *Adv. Mater.* **25**, 2844–2848 (2013).

5. Chen, F. *et al.* Nitrogen-aeration tuned ultrasonic synthesis of SiO2@PNIPAm nanoparticles and preparation of temperature responsive Pickering emulsion. *Ultrason. Sonochem.* **58**, 1–6 (2019).

6. Jiang, Y. *et al.* A Novel Temperature-Dependent Hydrogel Emulsion with Sol/Gel Reversible Phase Transition Behavior Based on Polystyrene-co-poly(N-isopropylacrylamide)/Poly(N-isopropylacrylamide) Core–Shell Nanoparticle. *Macromol. Rapid Commun.* **42**, 1–7 (2021).

7. Gao, Y., Xiang, Z., Zhao, X., Wang, G. & Qi, C. Pickering Emulsions Stabilized by Diblock Copolymer Worms Prepared via Reversible Addition-Fragmentation Chain Transfer Aqueous Dispersion Polymerization: How Does the Stimulus Sensitivity Affect the Rate of Demulsification? *Langmuir* **37**, 11695–11706 (2021).

8. Ranka, M., Katepalli, H., Blankschtein, D. & Hatton, T. A. Schizophrenic Diblock-Copolymer-Functionalized Nanoparticles as Temperature-Responsive Pickering Emulsifiers. *Langmuir* **33**, 13326–13331 (2017).

9. Peng, J., Liu, Q., Xu, Z. & Masliyah, J. Novel magnetic demulsifier for water removal from diluted bitumen emulsion. *Energy and Fuels* **26**, 2705–2710 (2012).

10. Flores, J. A., Jahnke, A. A., Pavia-Sanders, A., Cheng, Z. & Wooley, K. L. Magnetically-active Pickering emulsions stabilized by hybrid inorganic/organic networks. *Soft Matter* **12**, 9342–9354 (2016).

11. Lin, K. Y. A., Yang, H., Petit, C. & Lee, W. der. Magnetically controllable Pickering emulsion prepared by a reduced graphene oxide-iron oxide composite. *J. Colloid*

Interface Sci. **438**, 296–305 (2015).

12. Sun, Z., Zhao, Q., Haag, R. & Wu, C. Responsive Emulsions for Sequential Multienzyme Cascades. *Angew. Chemie - Int. Ed.* **60**, 8410–8414 (2021).

13. Jiang, J., Ma, Y., Cui, Z. & Binks, B. P. Pickering Emulsions Responsive to CO2/N2 and Light Dual Stimuli at Ambient Temperature. *Langmuir* **32**, 8668–8675 (2016).

14. Zhao, X. *et al.* Light-tuning amphiphility of host-guest Alginate-based supramolecular assemblies for photo-responsive Pickering emulsions. *Carbohydr. Polym.* **251**, 117072 (2021).

15. Li, Z. *et al.* Light-Responsive, Reversible Emulsification and Demulsification of Oil-in-Water Pickering Emulsions for Catalysis. *Angew. Chemie - Int. Ed.* **60**, 3928–3933 (2021).

16. Chen, Z. *et al.* Light controlled reversible inversion of nanophosphor-stabilized pickering emulsions for biphasic enantioselective biocatalysis. *J. Am. Chem. Soc.* **136**, 7498–7504 (2014).

17. Bai, R. X. *et al.* Light-Triggered Release from Pickering Emulsions Stabilized by TiO2 Nanoparticles with Tailored Wettability. *Langmuir* **32**, 9254–9264 (2016).

18. Zhang, H., Wu, J., Jiang, J., Cui, Z. & Xia, W. Redox-Responsive Oil-In-Dispersion Emulsions Stabilized by Similarly Charged Ferrocene Surfactants and Alumina Nanoparticles. *Langmuir* **36**, 14589–14596 (2020).

19. Yu, S. *et al.* Pickering emulsions of alumina nanoparticles and bola-type selenium surfactant yield a fully recyclable aqueous phase. *Green Chem.* **22**, 5470–5475 (2020).

20. Cook, M. T., Haddow, P., Kirton, S. B. & McAuley, W. J. Polymers Exhibiting Lower Critical Solution Temperatures as a Route to Thermoreversible Gelators for Healthcare. *Adv. Funct. Mater.* **31**, (2021).

21. Weaver, J. V. M., Rannard, S. P. & Cooper, A. I. Polymer-mediated hierarchical and reversible emulsion droplet assembly. *Angew. Chemie - Int. Ed.* **48**, 2131–2134 (2009).

22. Weaver, J. V. M. *et al.* PH-Responsive branched polymer nanoparticles. *Soft Matter* **4**, 985–992 (2008).

23. Woodward, R. T. *et al.* Controlling responsive emulsion properties via polymer design. *Chem. Commun.* 3554–3556 (2009) doi:10.1039/b904320a.

24. Koh, A. Y. C. & Saunders, B. R. Thermally induced gelation of an oil-in-water emulsion stabilised by a graft copolymer. *Chem. Commun.* **6**, 2461–2462 (2000).

25. da Silva, M. A. *et al.* Engineering Thermoresponsive Emulsions with Branched Copolymer Surfactants. *Macromol. Mater. Eng.* **307**, 1–14 (2022).

26. Rajbanshi, A. *et al.* Polymer architecture dictates thermoreversible gelation in engineered emulsions stabilised with branched copolymer surfactants. *Polym. Chem.* **13**, 5730–5744 (2022).

27. Rajbanshi, A. *et al.* Combining branched copolymers with additives generates stable thermoresponsive emulsions with in situ gelation upon exposure to body temperature. *Int. J. Pharm.* **637**, 122892 (2023).

Chapter 2: Literature review – stimuli responsive emulsions as advanced materials for pharmaceutical applications

2.1 Emulsions as a dosage form

Emulsions are a type of colloids that are metastable in nature. They are composed of at least two phases that are immiscible with each other, wherein one phase is dispersed and forms spherical droplets in the other phase.[1,2] They are used in a variety of industries, including food, cosmetics, and pharmaceuticals. Emulsions are thermodynamically unstable as compared to homogeneous and stable solutions. The difference in densities between the oil and aqueous phases and the undesirable interaction between oil and water molecules account for the instability.[3] Coalescence, flocculation, sedimentation or creaming, Ostwald ripening, and breaking are all instability mechanisms that are encountered with emulsions.[4] Coalescence, or the merging of separate droplets causing a reduction of the interfacial area, is one of the most common emulsion instabilities, which ultimately leads to phase separation.[3–5] The loose aggregation of droplets to form porous clusters is called flocculation, which occurs when the attraction between droplets is present, but a short-distance repulsion stops coalescence, described classically by Dearjaguin, Landau, Verwey and Overbeek (DLVO) theory. Sedimentation and creaming are comparable phenomena in which the droplets move to the bottom (sedimentation) or the surface (creaming) of the continuous phase depending on the density of the dispersed phase compared to the continuous phase.[3,4] Ostwald ripening also leads to deterioration of the emulsions, in which an increase in temperature leads smaller droplets to dissolve into the continuous phase and then separate from solution on the surface of the larger droplets upon cooling. The emulsion may then coalesce or phase invert as a result of this phenomenon.[3,4,6] When the emulsion is exposed to temperature variations, the interfacial layers between the dispersed and continuous phases can be destroyed, resulting in phase separation or breaking.[3,4]

Despite their instabilities, emulsions are significant materials in many products and formulations, and they can also be utilised as a platform for the synthesis of advanced materials.[7] Cosmetics, pharmaceuticals, food, oil recovery, and chemical processing

industries widely use emulsions.[2] Emulsions are employed in drug delivery, particularly as external applications or topical forms. They have demonstrated that they can increase the solubility of poorly aqueous soluble drugs as well as the partitioning of the drug from the oil to the water phase, which is faster than the disintegration and absorption procedures required for oral dosage forms such as tablets and capsules.[4,5]

Emulsions may exist in several forms. Simple emulsions include oil-in-water emulsions (o/w) and water-in-oil emulsions (w/o), whereas more complex systems such as multiple emulsions, e.g., oil-in-water-in-oil emulsions (o/w/o) and water-in-oil-in-water emulsions (w/o/w), or bicontinuous emulsions may also be prepared.[3-5] Other forms of emulsion are a dilute emulsion where the dispersed phase (the liquid forming droplets) is present in relatively small amounts compared to the continuous phase (the surrounding liquid).[3-5] A viscoelastic emulsion, is another class of emulsions that has properties of both a liquid and a solid, exhibiting characteristics of a gel-like material.[6] These emulsions can flow like liquids under shear stress but recover their shape and form when the stress is removed. They are used in various products, such as creams, lotions, and ointments, where a balance between spreadability and stability is desired. The different forms of emulsions offer unique properties and benefits for various applications. Complex emulsions allow for the encapsulation and controlled release of active ingredients, while viscoelastic emulsions provide desirable textures and enhanced stability. The choice of emulsion form depends on the intended use, the properties of the ingredients, and the desired characteristics of the final product. Several factors such as emulsion type, droplet size, continuous or dispersed phase volume ratio, and emulsion stability must be considered during the emulsification process.[6] Furthermore, emulsifiers such as small/macro molecule surfactants or polymeric stabilisers may be required.

Polymers are attractive emulsifying species because of their structural adaptability. Polymers can be utilised as traditional emulsifiers or as responsive systems to impart additional functionality.[6] On-demand demulsification and emulsion engineering have been achieved using stimuli-responsive polymers. Emulsions that respond to external stimuli such as light, temperature, pH, CO_2, redox reactions, magnetic fields, ions, or a combination of these stimuli have been developed for a variety of drug delivery platforms including injectables, topical, vaginal, and ocular applications.[6] While the major goal in the

formulation of emulsion systems is usually to achieve high stability against coalescence, several applications of emulsions require not only high stability against coalescence but also the break-up or phase inversion of the emulsion in a controlled manner. Phase inversion emulsions can be used to control the release of active pharmaceutical ingredients.[8] By changing the emulsion type, the rate of drug release can be adjusted. This is particularly important for topical medications where the desired drug release profile varies. In the petroleum industry, phase inversion emulsions can be employed for enhanced oil recovery methods.[8] With the advances in polymer science, it is feasible to create an emulsion that has great stability as well as on-demand breakdown or phase inversion.[8] As is typical of emulsions, these systems are complex and polymers imparting stimuli-responsive behaviour are required to stabilise emulsions with oils of widely varied polarity, droplet size and oil/water ratio as well as varied emulsification technique.[9]

2.2 Stimuli-responsive polymers

Synthetic techniques have enabled the creation of polymers with sophisticated structures. Polymers have proven particularly valuable in developing stimuli-responsive systems due to the presence of sensitive chemical moieties whose responsiveness enables modulation of properties, coupled with the intrinsic ability to control polymer properties through modification of architecture and inclusion of co-monomers.[10] There is well-established evidence that not only the sensitive units are responsible for the environmental sensitivity of the polymers, but their location, specific distribution, and molecular topology (morphology, molecular bond arrangement/cleavage and molecular motion)[11] also contribute to the responsiveness of smart materials.[12] Stimuli-responsive behaviour typically results from changes in physico-chemical structure enabled by functional groups that are amenable to a change in character (e.g., charge, polarity, and solvency) along a polymer backbone, leading to drastic transitions in macroscopic material properties as these chemical changes are invoked.[10] The response of the polymer in solution usually changes its chain dimensions/size, colour, secondary structure, solubility or degree of intermolecular interaction.[10,13,14] Another form of 'response' is caused by drastic changes in the polymeric structure, such as polymer degradation caused by bond breakage in the polymer backbone or at pendant cross-linking groups in response to a particular stimulus.

"Stimuli-responsive" polymeric materials undergo changes in their physical and chemical properties in response to changes in their environment. Stimulus-sensitive surfactants are currently undergoing extensive research due to their ability to respond and exhibit physico-chemical changes when exposed to external factors like mechanical stress, pH, light, temperature, and biological stimuli.[15–18] Surfactants come in a variety of structures, including conventional small molecules, nanoparticles, polymers, and microgels, all of which may impart stimuli-responsive behaviour.[17,19,20] They may also be referred to as 'smart', 'intelligent', or 'environmentally sensitive' polymers, without substantial differentiation between terminology.[21] These materials are being widely employed in healthcare research, enabling novel and improved therapies and diagnostics, amongst a plethora of applications. In response to stimuli (external and internal), a "smart" response prompted by polymers can lead to better localisation of pharmaceuticals, sustained release of payload, and triggered delivery at the pathological target site.[10] These stimuli-responsive materials are often influenced by similar processes in natural living cells and organisms.[21,22] For instance, certain plants such as wheat awns and pinecones respond to the external stimulus, humidity, by expanding or contracting to disperse their seeds.[22] Another common stimuli-response is the interaction of signal molecules and receptors producing physiological responses in animals. Single-celled organisms such as bacteria can sense and respond to environmental factors such as pH, light, temperature, and nutrients. The cis-trans isomerisation of retinal in response to light, which enables vision, is another instance of a stimuli-responsive behaviour.[22] Natural biopolymers, such as proteins and nucleic acids are all stimuli-responsive components of living organic systems and may be isolated or chemically adapted to utilise in healthcare applications. These 'natural' stimuli-responsive polymers have formed the basis for the development of numerous synthetic polymers that mimic their adaptive responses.[10]

The behaviour of stimuli-responsive polymers in solution broadly falls into three types based on their physical forms[23]: (i) linear free chains in solution that undergo physical changes such as reversible collapse in response to an environmental stimulus, (ii) covalently crosslinked gels that shrink or swell in response to a stimulus, and (iii) chain-adsorbed or surface-grafted forms that undergo reversible collapse on the surface.[12,23] Since stimuli-responsive behaviour occurs in aqueous solutions, these polymers are

gaining popularity in biotechnology and medicine for applications such as biosensors[24], "switch on-off" drug release[25], drug delivery systems[25,26], affinity precipitation[27], enzyme and cell immobilisation[28], tissue engineering, and artificial muscles[29].

Environmental stimuli that can be applied externally can trigger changes in properties such as physical state, colour, and shape.[21,30,31] The dynamic nature of these materials and sensitivity of the processes to the intended application are the most exciting characteristics of the smart materials.[21,31] Smart polymers may also exhibit reversibility of these modifications such that they return to their initial state as soon as the stimulus responsible for the modification is removed.[32] Based on the nature of stimuli, responsive behaviour can further be categorised into three major types as demonstrated in Figure 2.1: physical stimuli (mechanical stress, electrical/magnetic field, ultrasound, light, temperature, UV); chemical stimuli (electrochemical, pH, ionic strength, redox potential, H_2O_2); and biological stimuli (enzymes/receptors, biomolecules, antigens, ligands and other biochemical agents).[33,34] On a molecular level, physical stimuli trigger reversible changes in polymer chain dynamics and interactions. Reversible changes in polymer chain interactions with the environment are caused by chemical stimuli (nearby chains, solvents). Biological stimuli cause reversible changes in molecular enzymatic reactions, receptor recognition, antigen recognition, and ligand recognition. All of these can lead to changes in macroscopic properties such as changes in solubility, shape/ structure, chain dimension/ size, hydrophilic to hydrophobic balance and permeability.[35] In most cases, these responses are caused by the presence or disruption of secondary forces (hydrogen bonding, hydrophobic effects, electrostatic interactions, and so on), simple reactions (e.g., acid-base reactions) of moieties linked to the polymer backbone, and/or osmotic pressure variations.[10,13,14] Furthermore, some polymers can be designed to have dual or multiple stimuli-responsiveness.[10,35]
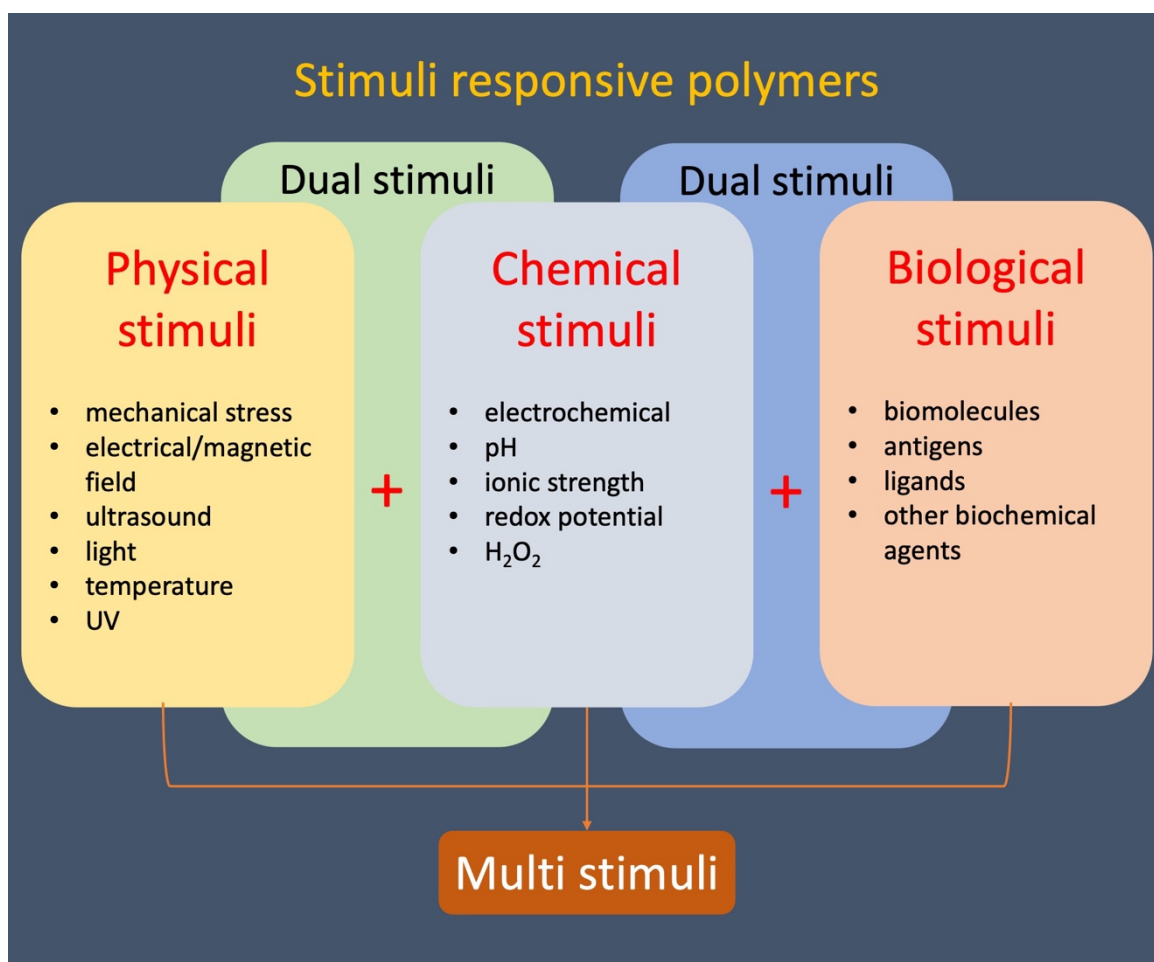
Figure 2.1: Classification of stimuli responsive polymers.[33,34]

Thermoresponsive polymers are stimuli-responsive macromolecules that modify their physical properties in response to temperature. Typically, the solubility of some of the constituent units varies with temperature, enabling promotion of polymer-polymer interactions only at specific temperatures. This phenomenon is typically considered to be related to the ratio of hydrophilic to lipophilic moieties on the polymer chain, and is governed by the thermodynamics of mixing.[31] The thermo-dependent miscibility or solubility gap of thermoresponsive polymers in aqueous systems is shown in phase diagrams of temperature versus polymer concentration as exemplified in Figure 2.2. Thermoresponsive polymers can be further classified into two groups based on their temperature responses: polymers that are insoluble beyond a critical temperature, known as the lower critical solution temperature (LCST), and polymers that precipitate or become

insoluble below a critical temperature, known as the upper critical solution temperature (UCST) as illustrated in Figure 2.2.[36]
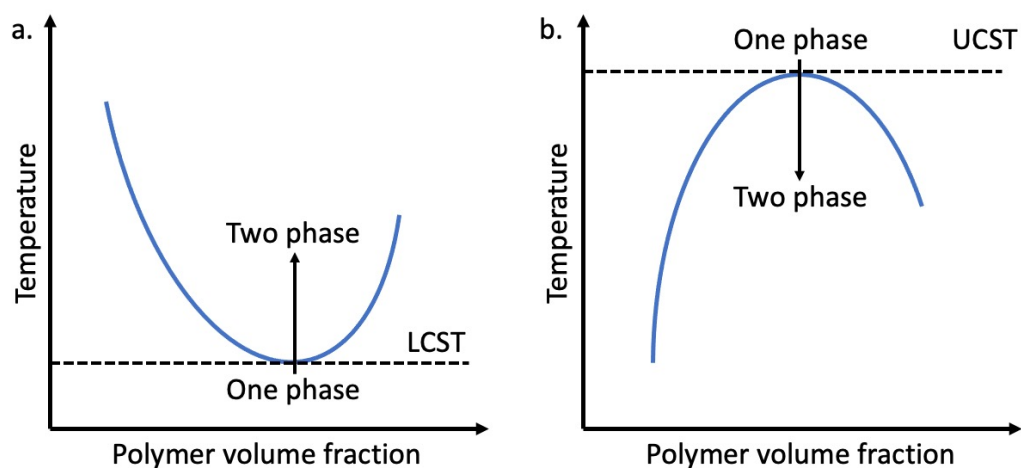
Figure 2.2: Curves illustrating the phase transition phenomenon: (a) Phase transition behaviour of thermo-responsive polymers in solution with a lower critical solution temperature (LCST), and (b) Phase transition behaviour with an upper critical solution temperature (UCST). Reproduced with permission.[36] Copyright 2020, MDPI.

In Figure 2.2(a), LCST is the point where the entropy of the water in the system increases owing to a less ordered arrangement of water molecules and is beyond the enthalpy of water hydrogen-bonded to the polymer. Consequently, the entropy of the system determines the LCST whereas the UCST (Figure 2.2(b)) is governed by the enthalpy of the system.[36] Since temperature alterations shift the entropy of solvation of the polymer chains in an aqueous solution, LCST-type polymers exhibit rapid, sharp, and reversible phase transitions.[37] They are fully soluble in water below this temperature and the polymer chains are usually in a random coil conformation due to hydrogen-bonding interactions between hydrophilic polymer moieties and surrounding water molecules. When the temperature increases above the LCST, hydrogen bonds are broken, and hydrophobic interactions become dominant. These hydrophobic interactions between polymer chains leads to phase separation, which enables polymers to self-assemble and aggregate in aqueous solutions.[38] Macroscopically, a polymer solution at LCST undergoes a phase transition from clear to cloudy (on the condition that the aggregates formed are sufficiently large to scatter light), this is also referred to as the clouding temperature or

cloud point (Tc).[38] From a practical standpoint, the LCST (or UCST) can also be referred to as the temperature at which the solution exhibits constant transmittance, either close to zero percent (i.e., turbid for the LCST polymer) or close to 100% (i.e., transparent for UCST polymers).[39]

When deciding which of these "smart" polymers to use in drug delivery, several factors should be considered. Polymers with LCST are widely employed for drug delivery since those polymers with UCST need high temperatures, which are not appropriate for thermo-labile drugs, biomolecules, or cells, in addition to being higher than body temperature.[31] Moreover, the LCST of many LCST polymers falls within the physiological temperature range (around 37°C for the human body). This property makes LCST polymers suitable for drug delivery applications, as they can respond to the natural temperature changes in the body. In contrast, UCST polymers typically have a phase transition temperature above the physiological range, making them less compatible with the body's conditions. The choice of the LCST or UCST type polymer also depends on the desired drug release profile. For example, if controlled or sustained release is required, a polymer with an LCST below physiological temperature can be selected. Below the LCST, the LCST polymer is hydrated and swells, creating a mesh-like structure that hinders drug diffusion. As the temperature increases above the LCST, the polymer undergoes a phase transition, becoming hydrophobic and collapsing. This collapse opens the polymer structure, allowing drug release. This mechanism enables precise control over drug release rates, as it is governed by the temperature. On the other hand, if triggered release is desired, a polymer with an LCST above body temperature can be chosen to ensure rapid drug release upon reaching the target site. External factors such as heat, infrared radiation, or localised hyperthermia techniques can be employed to precisely and locally trigger drug release from LCST polymers. This feature allows for spatiotemporal control over drug delivery, which is highly advantageous for targeted therapy.

Another important factor to be considered is the excretion path, toxicity, and degradation characteristics. An ideal polymer would be non-toxic, biodegradable, and, if non-biodegradable, have a size and structure that would allow for renal excretion.[40,41] Hence, the aqueous compatibility of the LCST type polymers is also considered to be advantageous in drug delivery. LCST polymers are typically water-soluble below their

14

LCST, facilitating their formulation into hydrogels or aqueous solutions. This property makes them easily compatible with aqueous physiological environments, simplifying their administration and ensuring good biocompatibility. Hence, LCST polymers are generally more widely utilised in drug delivery due to their physiological relevance, controlled release capabilities, versatility, compatibility with aqueous environments, and ease of temperature-based triggering mechanisms. However, UCST polymers have their own unique applications and advantages, such as using organic solvents for triggering phase transitions. UCST polymers often have better solubility in organic solvents compared to water. This characteristic enables the use of organic solvents to trigger the phase transition of the polymer, providing an alternative triggering mechanism for drug release. Organic solvents can be used as an external stimulus to induce the phase transition, allowing for controlled drug release in response to specific environmental cues.

Another exciting application is the compatibility with hydrophobic drugs. UCST polymers, being hydrophobic in their insoluble state, can effectively encapsulate and deliver hydrophobic drugs that are poorly soluble in aqueous environments.[42] This property makes UCST polymers attractive for the delivery of lipophilic or hydrophobic drugs. While UCST polymers possess advantages in certain drug delivery scenarios, their limited use in drug delivery can be attributed to factors such as their lack of physiological relevance, limited biocompatibility, challenges in formulation and stability, and the availability of fewer options for design and customisation.[42] The UCST of many UCST polymers is typically above the physiological temperature range. This makes it challenging to utilise these polymers for drug delivery applications in the body, as they do not respond to natural temperature changes. Achieving the desired temperature above the UCST for triggering drug release may require external heating methods, which adds complexity to the drug delivery system.[42] Some UCST polymers may exhibit poor biocompatibility, potentially causing adverse reactions or toxicity. This limited biocompatibility restricts their use in drug delivery applications, where safety is a paramount concern. Another major challenge is formulating UCST polymers into stable drug delivery systems. Maintaining the stability of the drug-polymer formulation and preventing premature drug release can be more difficult with UCST polymers compared to LCST polymers. The insoluble state of UCST polymers can lead to aggregation or precipitation of the polymer-

drug formulation, affecting its stability and drug release properties. Compared to LCST polymers, there are fewer UCST polymers available with well-defined and controllable UCST values. This limits the design flexibility and choices for UCST-based drug delivery systems and wider utilisation of LCST polymers in drug delivery applications.[42]

Polymer solutions that are capable of transforming a gel state with elevation of temperature on a critical point (Tgel) are termed as "Thermoreversible gels" or "Thermogelling materials".[42] A sol-gel transition occurs after heating a thermoreversible gel beyond a critical temperature, affected by an overall increase in hydrophobic unit above the LCST triggering self-assembly processes and physical interaction which increases the viscosity of the system.[43] Prior literature has divided these materials into two types.[43] The first class depends on a hydrophilic/hydrophobic balance and the second class that depends on temperature-responsive polymer component. Critical concentration and temperature are essential in making Tgel to exhibit a sol-gel transition which requires several mechanisms for the gelation process. Factors such as polymer architecture, molecular weight, additives, and polymer concentration are considered crucial in tuning the gelation properties of LCST-exhibiting thermoreversible gels.

2.3 Synthesis of branched polymers

Synthetic techniques have enabled the synthesis of polymers with sophisticated structures. These polymers have made it possible to fine-tune emulsion qualities to satisfy the demands of varied applications. Due to steric hindrance and multipoint irreversible anchoring at the oil-water interface, branched polymers can offer stronger emulsion stability than their linear counterparts.[44] For example, Weaver et al. produced a range of branched copolymer surfactants (BCSs) that gave substantially higher emulsion stability than their linear analogues.[44–46]

Polymeric surfactants are synthesised using polymerisation reactions, which can be a time-consuming and effort-intensive multistep process. To overcome these drawbacks, Weaver and colleagues employed the Strathclyde approach, a one-pot synthesis established by Sherrington and co-workers.[47] With this method, precise manipulation of hydrodynamic particle size and polymer chain ends is possible. It involves the use of a

radical initiator and a chain transfer agent to regulate the polymerisation reaction and control the growth of polymer chains. The reactive centre is a free radical, formed in the initiation step which is then followed by propagation and termination. In the initiation step, the radical initiator generates a reactive radical species, which initiates the polymerisation reaction by reacting with monomers. The initiator (I) undergoes homolytic cleavage in the rate determining step through thermal or photochemical decomposition. This decomposition occurs at a rate of kd and produces a free radical, R* which then adds to the vinyl group of a monomer, M at a rate constant of ki as illustrated below:

Initiator decomposition

$$I \xrightarrow{kd} 2R^*$$
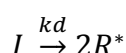
Monomer Initiation

$$R^* + M \xrightarrow{ki} RM^*$$
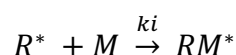
The polymerisation continues by the propagation of the growing chain radical, which reacts with additional monomer units. This involves the initiated monomer, RM*, typically undergoing a head-to-tail addition reaction with a radical. The resulting product is the growing polymer chain. Propagation is a bimolecular reaction that proceeds at a rate constant of *kp* as illustrated below:

$$RM_i^* \xrightarrow{kp} RM_{i+1}^*$$
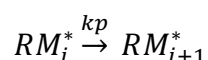
During the propagation stage, it is possible to introduce a chain transfer agent that can effectively control the growth of the polymer chain. The chain transfer agent can halt chain growth by transferring the radical from the growing chain to the transfer agent. This process can regulate the polymer chain length, leading to a polymer with a well-defined molecular weight.

$$(RM_{i+1}) + CTA \rightarrow (RM_{i+1}) + CTA_m$$
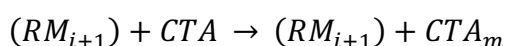
The creation of "dead" polymer chains and the removal of radicals from the system are achieved through a process called termination. This process can take two forms: combination and disproportionation. The occurrence of each type of termination process is influenced significantly by steric and electronic effects. In the combination process, two growing polymer chains (P_m/P_n) undergo a head-to-head addition reaction with each

other, resulting in the formation of a single polymer chain where the growth is terminated. It is also possible for a propagating chain to combine with an initiator radical or impurities within the polymerisation mixture. Disproportionation is another type of termination process that results in the formation of both saturated and vinyl-ended polymers. This process involves the removal of a hydrogen atom from one growing polymer chain. The occurrence of these two types of termination processes can lead to significant variations in the final polymer chain length, which can have an impact on the material properties of the resulting polymer as illustrated below:

$$P_m^* + P_n^* \xrightarrow{\text{combination}} P_{m+n}$$

$$P_m^* + P_n^* \xrightarrow{\text{disproportionation}} P_m + P_n$$
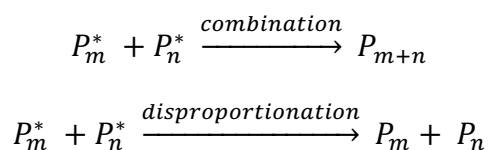
2.4 Polymer-stabilised emulsions with pH responsive behaviour

Weaver and colleagues described the synthesis and behaviour of pH-responsive branched amphiphilic copolymers.[47] The synthesis used a pH-responsive monomer 2-(diethylamino) ethyl methacrylate (DEA) and a hydrophilic macromonomer poly(ethyleneglycol) methacrylate (PEGMA) whilst introducing branches with ethylene glycol dimethacrylate and hydrophobic chain ends with an alkanethiol. This gave the researchers an efficient one-pot, single-step method to prepare materials which they theorise have similar structure to cross-linked micelles. They demonstrated that these copolymers exhibit pH-triggered uptake and release of a model hydrophobe, which depends on the chain-end of the polymer. The apparent pKa of the polyamine residues systematically varies with the degree of branching, increasing the versatility of these copolymers for triggered-release applications. This novel approach to synthesising copolymers represents a new and generic method for preparing core-shell materials. In basic pH aqueous solutions, the copolymers form well-defined micellar structures with hydrodynamic diameters ranging from 16 to 46 nm. When the pH is reduced, the branched copolymers undergo hydration and swelling, similar to pH-responsive self-assembled materials based on tertiary amine methacrylates. This behaviour is illustrated schematically in Figure 2.3,[47] comparing it to the swelling and deswelling behaviour of pH-responsive shell cross-linked micelles and microgels. Fluorescence experiments showed that the copolymers can uptake and release

pyrene depending on the solution's pH, and the extent of release can be fine-tuned by adjusting the degree of branching, hydrophobicity, and concentration of the chain transfer agent. Overall, this research presents a commercially viable method for synthesising pH-responsive core-shell polymeric nanostructures with various applications.
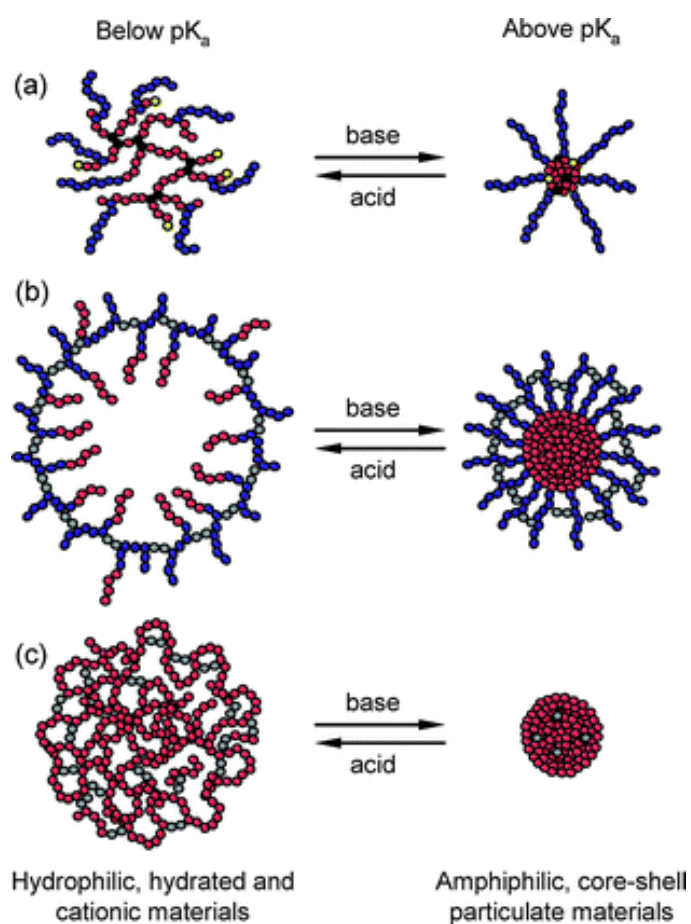
Figure 2.3: Comparison showing the behaviour of tertiary amine-based pH-responsive materials in aqueous solutions: (a) branched copolymer nanoparticles, (b) shell cross-linked micelles, and (c) microgels, both above and below their respective pKa values. Reproduced with permission.[47] Copyright 2008, The Royal Society of Chemistry.

Later in 2009, Weaver and researchers used their template to create a new class of responsive polymeric surfactants capable of producing stable and functional micrometer-sized emulsion droplets.[48] The surface functionality of these droplets has been carefully designed to allow for reversible hydrogen-bonding interactions, enabling the controlled trapping of droplets in specific geometries as illustrated in Figure 2.4 a–e.[48]
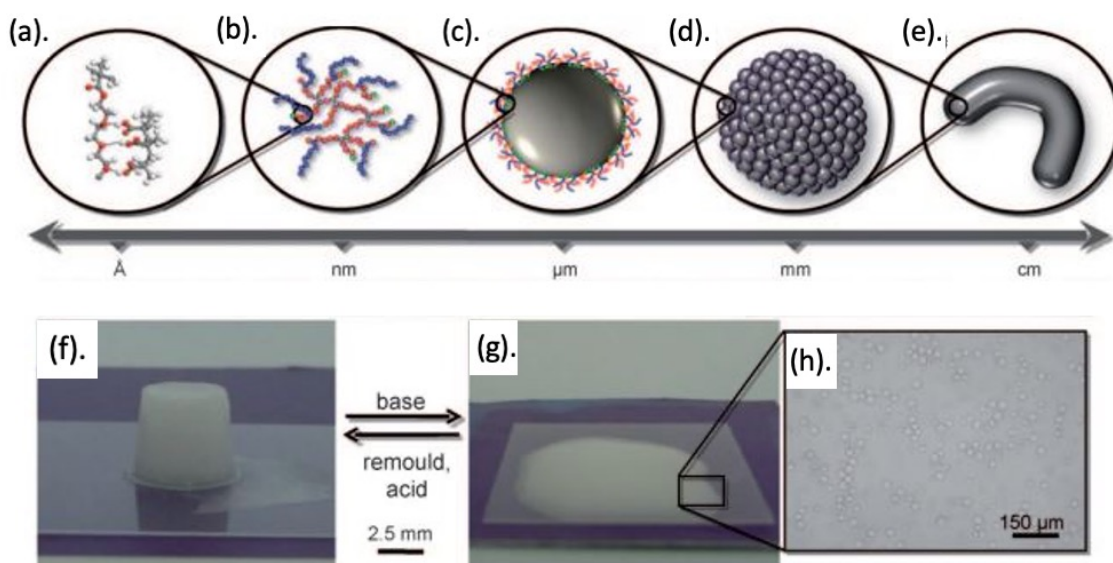
Figure 2.4: (a–e) Reversible assembly of emulsion droplets in a hierarchical manner; (f) assembly in a templated monolithic structure; (g) disassembly of the monolith shown in (f) observed 1 minute after adding base; (h) light micrograph capturing the image of (g). Reproduced with permission.[48] Copyright 2009, Wiley-VCH.

Referred to as "emulsion engineering," this concept utilises the polymeric surfactants to precisely mediate interactions between droplets, drawing inspiration from colloidal engineering and food science. Using these responsive surfactants, the researchers demonstrate the fabrication of various complex liquid-based structures with precise control and uniformity. Importantly, inter-droplet interactions are reversible, allowing the engineered emulsions to be easily disassembled back into stable individual droplets by adjusting the pH. The surfactants used in the study are amphiphilic branched copolymers synthesised from methacrylic acid (MA) and poly(ethyleneglycol) methacrylate (PEGMA) with hydrophobic dodecane chain ends. These macromonomers provide simultaneous steric and electrostatic stabilisation in basic conditions and can form multiple hydrogen bonds under acidic conditions. The branched architecture of the surfactants ensures multiple points of attachment to the droplet surface, while the dodecane chain ends mimic the oil phase. Disassembly of the engineered emulsions is achieved by raising the pH of the continuous phase, leading to the rapid decomplexation of hydrogen bonds and electrostatic repulsion of anionic MA residues on the droplet surfaces. To assess the

disassembly of the engineered emulsions, the pH of the continuous phase was raised. In all cases, the trapped structures underwent disassembly and reverted back to conventional, dispersed, and non-interacting emulsion droplets. The disassembly occurred rapidly, taking less than one minute for the monolith dissociation shown in Figure 2.4(f-g).[48] The integrity of the individual emulsion droplets was confirmed through light microscopy showing that they retained their structural integrity without any demulsification observed after the disassembly process. In summary, this study presents a novel strategy for the reversible assembly of stable and functional emulsion droplets into robust liquid structures. The assembly and disassembly processes are solely driven by interactions on the droplet surface, which can be controlled by subtle variations in the composition of the branched copolymer surfactants as shown in Figure 2.5.[49] These engineered emulsions hold significant potential for applications requiring encapsulation and controlled delivery of large payloads.
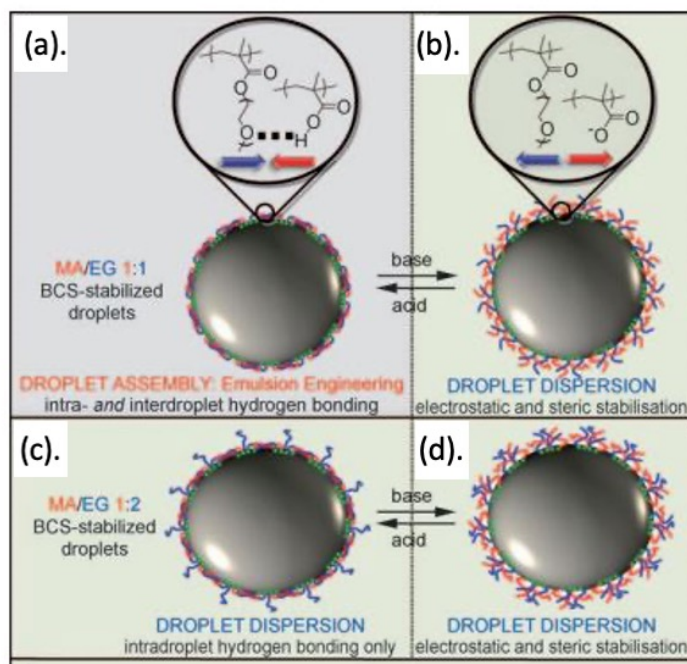
Figure 2.5: Influence of BCS composition on interdroplet interaction potentials: a) at low pH, intra- and interdroplet hydrogen bonding takes place in MA/EG 1:1 droplets, leading to interdroplet attraction and assembly; c) abundant steric stabilisation from MA/EG 1:2 droplets hinders interdroplet hydrogen bonding, resulting in interdroplet repulsion prevailing at low pH; b, d) steric and electrostatic stabilisation manifest at basic pH, causing interdroplet repulsion to dominate in both cases. Reproduced with permission.[49] Copyright 2010, The Royal Society of Chemistry.

In 2010 it was demonstrated that engineered emulsions with increased morphological and compositional complexity can be prepared using glucono-δ-lactone (GδL) while maintaining reversibility.[49] The assembled droplets can be easily disassembled into free-flowing emulsion dispersions without compromising their integrity. The hydrolysis of GδL in an aqueous solution uniformly lowers the pH. This pH-trigger is used to create significant quantities of functional and responsive emulsion droplet assemblies. The system maintains reversibility, and the surface-functional emulsion droplets retain their structural integrity during the assembly and disassembly processes. Unlike conventional acidification methods, this approach enabled the monitoring of engineered emulsion kinetics using rheometry, providing valuable insights. These advancements have the

potential to facilitate the widespread utilisation of this versatile encapsulation and reversible assembly process.

Again in 2011 it was reported by Weaver and co-workers that stable polymer-functionalised oil-in-water emulsion droplets can be prepared with precise surface compositions defined by a branched copolymer surfactant.[45] The study investigated the influence of composition, specifically the ratios of methacrylic acid (MA) to ethylene glycol (EG), on acid-triggered inter-polymer/inter-droplet hydrogen-bonding interactions. A one-pot branched vinyl polymerisation process is used to synthesise a series of copolymer surfactants with controlled compositions based on methacrylic acid and poly(ethylene glycol). These copolymers prove to be highly efficient emulsifiers for stable oil-in-water emulsions at basic pH. It was demonstrated that by varying the EG:MA ratio, the kinetics of inter-droplet interactions can be controlled, effectively switching to aggregated gel or dispersed liquid mediated by pH switch as demonstrated in Figure 2.6.[45] The equimolar ratios promote the fastest aggregation whereas the excess MA component retains droplet aggregation but at slower rates, while excess EG residues prevent inter-droplet hydrogen bonding and eliminate droplet aggregation at acidic pH. Additionally, rheometry studies showed that higher MA contents on droplet surfaces resulted in stiffer aggregated emulsion gels, with maximum structural integrity observed at stoichiometric EG:MA ratios. Hence, the study highlighted that the emulsion droplets stabilised with structurally similar branched copolymers, even with subtle functionality variations, can effectively control triggered inter-droplet interactions.
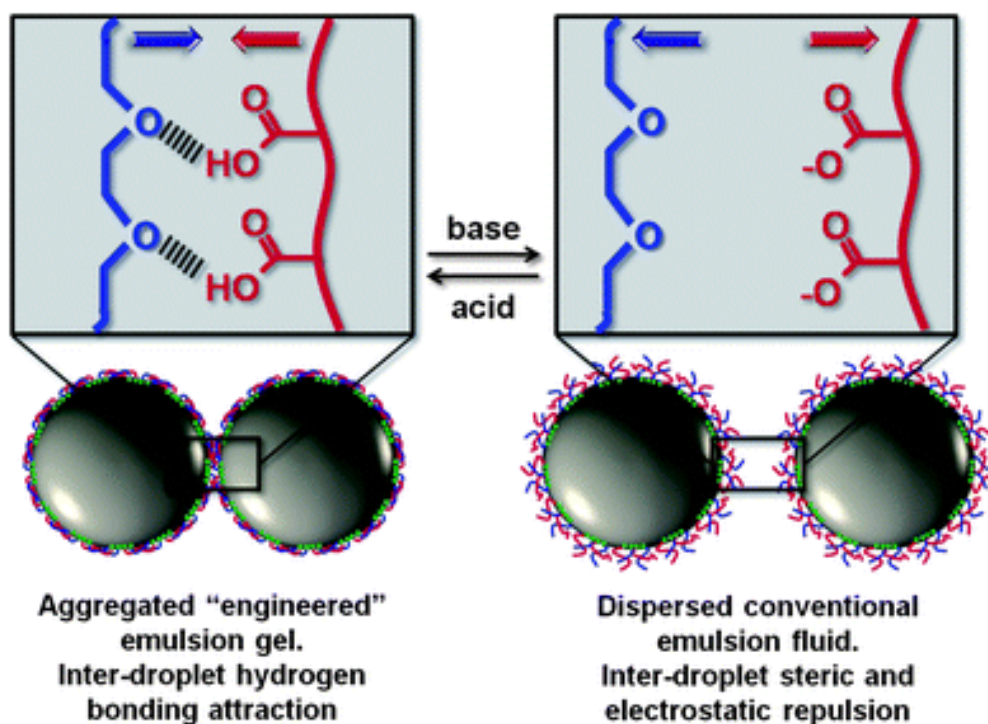
Figure 2.6: Schematic of the reversible shift from a fluid emulsion dispersion to a gelled engineered emulsion. The interactions between EG (blue) and MA (red) polymers situated on the surfaces of emulsion droplets are modulated through a pH-responsive mechanism. Reproduced with permission.[45] Copyright 2011, The Royal Society of Chemistry.

Woodward and colleagues described the utilisation of branched copolymers as emulsifiers to stabilise emulsion droplets which serve as templates for creating surface functionalised colloidal particles.[50] These copolymers have pH-responsive surface functionality that can control their solution behaviour, ranging from dispersion to aggregation. These assembled colloids can be rehydrated and remain stable in acidic water, but they disassemble into dispersed colloids when the solution as in Figure 2.7.[50] These colloids can encapsulate hydrophobic molecules and form macroscopic monolithic aggregates with controllable internal porosities. The aggregated colloids can be used to fabricate 3D monolithic structures, and the drying method employed can regulate the macroporosity within these structures. With further optimisation, these hierarchically structured biological scaffolds may serve as convenient monolithic structures capable of disassembling, making them potentially suitable for regenerative medical applications.
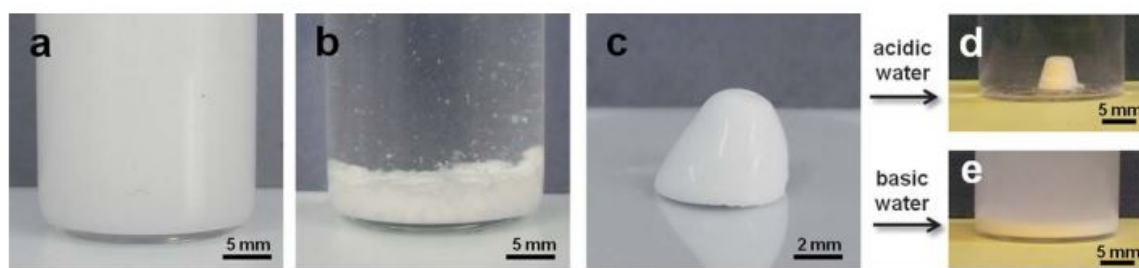
Figure 2.7: Images illustrating the reversible process of pH-induced colloid aggregation and monolith formation. (a) Dispersed surface-functionalised colloids at pH 10 in the presence of free EG:MA 1:1 branched copolymer as an aggregation aide. (b) The same system after undergoing aggregation and settling for 24 hours under acidic conditions (pH 2). (c) The resultant pellet formed upon centrifugation of (b). (d) Colloid pellet (c) remaining stable in acidic water. (e) Pellet (c) being dispersed in alkaline water. Reproduced with permission.[50] Copyright 2011, The Royal Society of Chemistry.

A similar study on pH-responsive emulsions stabilised by xanthan gum and shellac was conducted by Patel et al.,[51] and demonstrated a reversible mechanism of transition between a flocculated and a stable state at acidic pH and under neutral conditions, respectively as shown in Figure 2.8 (a). The solubility of shellac is pH-dependent, which has been used widely in the pharmaceutical sector to develop enteric release systems. Shellac can be dissolved at alkaline pH due to the presence of a significant number of hydroxyl groups, but it is practically insoluble at acidic pH. Because of shellac's acid resistance, colloidal particles generated at neutral to alkaline pH display instant aggregation in acidic medium. Considering the pH-dependent solubility profile of shellac, the oil-in-water emulsion was stabilised by colloidal interaction of Xanthan gum (XG) and shellac (SL) at the oil-water interface. The stable emulsion prepared at neutral pH showed instant flocculation on changing the pH to acidic ($\sim$1.2), neutralising the pH back to 7.2 resulted in switching the emulsion back to the stabilised state assisted by mild shaking as shown in Figure 2.8. Acidification causes the XG : SL network that stabilises the oil droplets in the emulsion to undergo phase separation, resulting in the flocculation of the emulsion. However, upon restoring the pH back to neutral, the XG : SL becomes re-dispersed in the bulk phase, thereby stabilising the emulsion and leading to the formation of distinct oil droplets. The ability of these emulsions to undergo pH-dependent flocculation was

exploited to control the assembly of oil droplets into desired shapes by extruding the emulsion using a syringe and needle in an acidic medium. Figure 2.8(b)[51] displays a photograph of an extruded emulsion, while Figure 2.8(c)[51] provides a microscopy image that reveals the confined flocculation of the emulsion droplets. Thus, this study demonstrated a straightforward way to utilise the pH-triggered flocculation of these emulsions to produce soft structures with controlled shapes.[51]
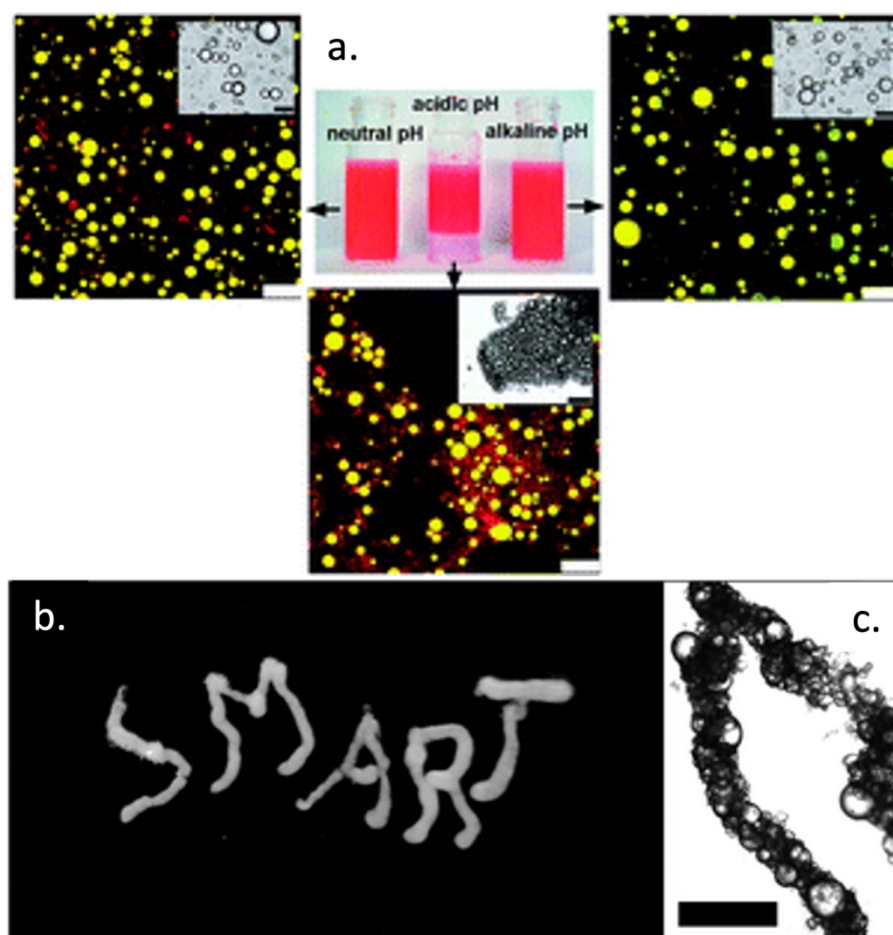
Figure 2.8: (a) Images obtained through confocal microscopy, depicting emulsions formulated with 10 wt% oil and stabilised by a 1:1 w/w blend of XG:SL. From left to right: a stable emulsion created under neutral pH conditions; an emulsion that has undergone flocculation after acidification; and a stable emulsion that has been neutralised back to a neutral pH (scale bars = 50 μm). (b) Photo capturing a concentrated emulsion (prepared using 60 wt% oil and stabilised by a 1:1 w/w mixture of XG:SL) being extruded using a syringe and needle within an acidic environment. (c) Microscopic image of the extruded strand composed of emulsion droplets (scale bars = 400 μm).Reproduced with permission.[51] Copyright 2013, The Royal Society of Chemistry.

High Internal Phase Emulsions (HIPE) are concentrated emulsion systems with a large volume fraction (> 0.74) of dispersed phase.[52] In 1907, S. U. Pickering described a new type of emulsions referred to as "Pickering Emulsion",[53] in which solid surface-active colloid particles adsorb at the interface between the two phases acting as a physical barrier to the coalescence of droplets and stabilising the emulsion kinetically.[54,55] Pickering emulsions are employed to generate colloid particles that can change from surface-active to surface-inactive in response to a stimulus.[55] Pickering described the production of oil-in-water HIPE with up to 99% oil content using soap.[53] The HIPE presents yield stress from the jammed emulsion droplets, which allows it to retain shape. HIPEs are both kinetically and thermodynamically unstable compared to conventional dilute emulsions. However, it is feasible to prepare metastable emulsion systems with no variation in appearance and properties over a lengthy period.[52] In 2010, Ngai and colleagues used a different strategy observing emulsion-type inversion from standard oil-in-water (O/W) emulsion to water-in-oil (W/O) HIPE at a fixed oil: water ratio of 23:73, utilising pH-responsive colloidal particles (5 wt%) made of polystyrene and poly(methacrylic acid) copolymer.[56] At a constant oil:water ratio, the inversion from oil-in-water to water-in-oil can be easily caused by lowering the pH or the addition of salt quantity in a single system.

Core cross-linked star (CCS)[57,58] polymers of poly(N,N-dimethylaminoethyl methacrylate) (PDMAEMA) have been employed as novel emulsifiers for the fabrication of gelled oil-in-water HIPEs.[2] The CCS is a new form of efficient emulsifier made up of polymers with hydrophilic arm polymers that are attached to a small central core that is smaller in size than the arms' dimensions.[58,59] These CCS polymer decreased the interfacial tension between water and oil in a pH-dependent manner. Gelled HIPEs were manufactured at high oil volume fractions ranging from 80-89 vol% and pH between 2-12. The emulsion properties such as oil droplet size, long-term stability and rheology were influenced by pH. The addition of base allows for pH-triggered complete demulsification of HIPEs because of the responsiveness of the PDMAEMA CCS polymer. The CCS polymers occur as distinct entities and exhibit positive zeta potentials at low pH solutions where PDMAEMA is heavily protonated. As the pH value increases from pH 3 to pH 8, protonation degree decreases, and the CCS polymers are present as loose aggregates with larger sizes and

greater zeta potentials. These findings are consistent with PDMAEMA-stabilised particles exhibiting flocculation at intermediate degree of protonation. As the pH continues to increase, the zeta potential decreases significantly due to deprotonation, approaching and exceeding the isoelectric point (pH 9.5) of PDMAEMA. At high pH values (pH > 8), the zeta potential is slightly negative, possibly due to partial hydrolysis of the ester groups, which leads to the formation of carboxylate anions. The conductivity of the CCS polymer was also influenced by pH, and a decline in conductivity at the isoelectric point (pH 9.5) was detected, which is in good accordance with the zeta potential measurements. Stable emulsions can be reformed by changing the pH to acidic conditions (initial value of pH 2.0) and re-applying a shearing force. CCS-stabilised HIPEs facilitates the preparation of hydrophilic polyHIPEs, and the polymer characteristics impact interfacial tension, droplet size and configurational changes. This has an effect on the wettability, viscoelasticity of the CCS polymer at the interface and the inter-droplet interactions.[2] Research conducted by An et al. synthesised pH-responsive CCS polymers with poly(N,N-dimethyl aminoethyl methacrylate) (PDMAEMA) arms that were deprotonated and gave w/o emulsions at basic pH due to the arms' higher solubility in the toluene phase. The arms were protonated in acidic pH, and the hydrophilicity increased, resulting in intermediate o/w/o and w/o/w multiple emulsions, as well as o/w HIPEs. It was postulated that CCS polymers serve as a link between linear polymers and colloidal particles.[59]

In a study conducted by Garcia-Tunon and co-workers, branched copolymer surfactants (BCS), based on methyl methacrylic acid (MAA) and polyethylene glycol methacrylate (PEGMA), were employed to in situ surface functionalisation of the oil droplets and to create smart inorganic particles of Aluminium Oxide (Al_2O_3) and Silicon Carbide (SiC) that can disperse or aggregate when triggered by pH as illustrated in Figure 2.9.[60] The process of attachment and functionalisation is accomplished through three mechanisms: 1) interactions between the hydrophobic chain ends (DDT) and the surfaces, 2) electrostatic interactions between the carboxylic anions in the MAA residues (COO−) and the positively charged particle surfaces, and 3) formation of chemical covalent bonds between the carboxylic residues and the metal oxides present on the particle surfaces. The functionalisation of with BCS enhances the wettability of ceramic particle surfaces resulting in increased contact angle with water. This amphiphilic polymer can segregate

at the oil-water interfaces, causing flocculation at acidic pH and stabilisation in basic conditions. The versatility of the method is not reliant on the pH triggered interactions between the BCS molecules that are used to functionalise the oil droplets but also the approach using Al_2O_3 and SiC ceramic particles. This system could be used in a wide range of applications, such as injection moulding and tissue engineering due to their potential to fabricate highly porous materials and increase the strength of lightweight materials.[60]
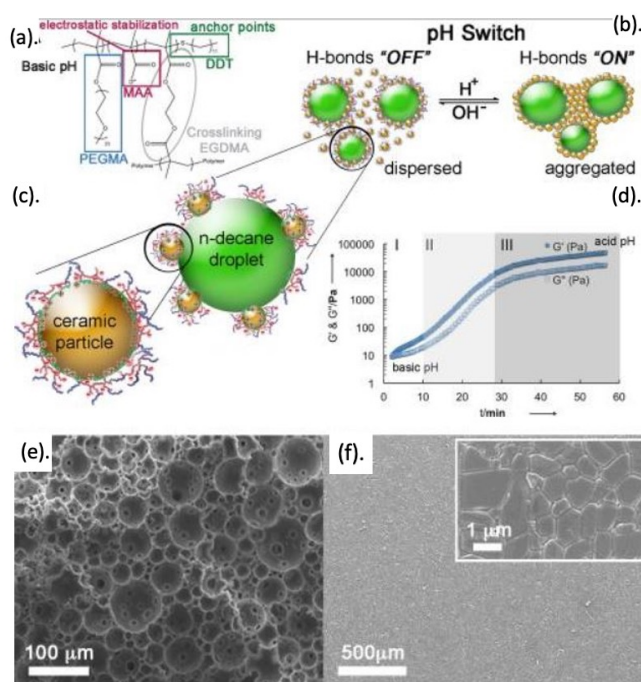
Figure 2.9: a) Structure of BCS highlighting the branching functionalities. b) pH-triggered assembly of ceramic particles functionalised with BCS in an oil-in-water emulsified suspension. c) Interactions between BCS-particles-droplets and BCS-particle entities. d) Changes in viscoelastic properties (G', G'') of an emulsified suspension during pH variation, illustrating the assembly process. Initially, particles and droplets are steric and electrostatically stabilised at high pH, where MAA branches are anionic and hydrogen bonds are inactive. Upon pH decrease below 5 (over longer durations), the MA branches become fully protonated (activating hydrogen bonds), causing functionalised particles and droplets (b) to bond, forming a network; G' (filled symbols) and G'' (open symbols) exceed 20 kPa. e, f) Exemplars of ceramic structures formed via responsive self-assembly: e) Porous SiC generated from an emulsion, and f) Sintered highly dense (>99% theoretical value) alumina acquired from a suspension (four-point bending strength: 200 + 50 MPa). Reproduced with permission.[60] Copyright 2013, Wiley-VCH.

Maçon et al. described the use of emulsion droplets as model-functionalised materials using electrostatic forces to induce the reversible synthesis of engineered emulsions. Two distinct BCSs with polymers of 2-(sulfobenzoic acid) ethyl methacrylate (SHEMA) or 2-(dimethylamino) ethyl methacrylate (DMA) were independently synthesised, then blended. DMA was positively charged in acidic condition, whereas SHEMA was always negatively charged. It was shown that by altering the chemical composition of these BCSs, inter-droplet assembly can be driven by electrostatic forces. The aggregation of dispersed emulsion droplets was found to be reversibly switchable when the pH was increased or decreased with respect to the pKa of poly(2-(dimethylamino) ethyl methacrylate). Due to their compact monomolecular structure and the presence of multiple hydrophobic anchoring sites, the BCSs demonstrated remarkable efficiency in maintaining the integrity of their associated emulsion droplets. There was no coalescence or separation of the droplets during the processes of aggregation and disaggregation. This innovative interaction mechanism observed in engineering emulsions holds significant promise as a model for investigating naturally occurring phenomena that involve dynamic electrostatic forces.[61]

In 2017, Yunhua and researchers presented a method for reversibly assembling emulsion micro-droplets stabilised by a graphene oxide/polyvinyl alcohol (GO/PVA) hybrid by simply regulating the hydrogen bonding interaction between the two materials, which is controlled by the ionisation of COOH groups on GO surface.[62] By injection moulding, the assembled emulsion droplets in an acidic state can be shaped into various macroscopic objects with a high degree of morphological control. Under basic pH condition, the assembled emulsion aggregates can be disassembled back into dispersed droplets due to reversible hydrogen bonding interactions. The macroporous composite hydrogel produced by utilising GO/PVA o/w stabiliser demonstrated biocompatibility and controlled release of Doxorubicin (DOX) over a period of 10 hours which was described by Ritger-Peppas release model. At pH 7.4, a slow release profile of DOX was observed as compared to the release profile at pH 4.0. The release properties exhibited potential as a carrier to deliver anti-neoplastic agents as most of the drugs are capable of retaining within the hydrogel at normal physiological pH conditions, while effectively releasing in acidic medium.[62]

Chalarca and co-worker exploited salt-responsive aggregation in polymer zwitterion stabilised oil-in-water droplets, which were amenable to processing into macroscopic, supracolloidal fibres by extrusion into aqueous media as shown in Figure 2.10.[63] The polymer zwitterions are monomers balanced by an equal number of positive and negative charges. These are hydrophilic, biocompatible and noninteracting possessing drug delivery applications. These droplet-based materials exhibited responsiveness, such as disaggregation when the salt concentration was increased, and rheology controlled by salt concentration and polymer composition. The ability to translate polymer zwitterions' solution properties to fluid–fluid interfaces, supracolloidal fibres, and bulk soft materials was demonstrated and it was anticipated that such soft assemblies could be employed as model systems to better understand how different stimuli affect self-interacting soft objects like tissues or cell aggregates.[63]
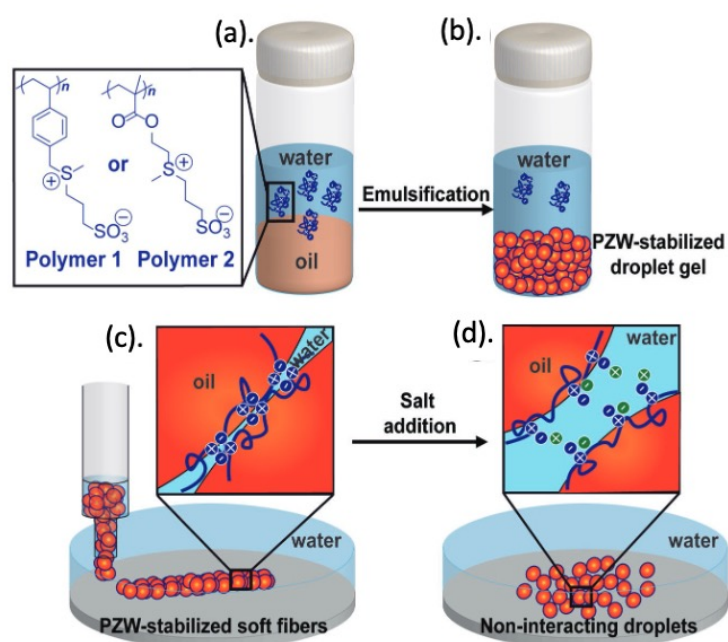
Figure 2.10: Schematic representations of droplet extrusion into soft fibres stabilised by PZW: a) Water-dispersed polymers 1 and 2 are blended with oil. b) Following emulsification and sedimentation, a droplet gel stabilised by PZW is formed. c) The supernatant is removed, and the droplet gel is loaded into a syringe, then extruded through a needle into a water reservoir, resulting in supracolloidal fibres. d) Fibre disaggregation is induced by introducing salt. Reproduced with permission.[63] Copyright 2018, Wiley-VCH.

2.5 Emulsions stabilised by thermoresponsive polymers

Verbrugghe et al. developed temperature-responsive poly(N-vinylcaprolactam) (PVCL) based graft copolymers and studied their emulsifying properties. Below the cloud point temperature, the graft copolymers acted as amphiphilic stabilisers however, temperatures above the LCST of PVCL caused the emulsions to break down as the graft polymers were no longer able to stabilise the emulsions due to the hydrophobic nature of the graft copolymers.[64] Moreover, the presence of branching points significantly impacted the phase separation behaviour of these smart materials. Unlike emulsions stabilised with PVCL-based graft copolymer by Verbrugghe et al., these PNIPAM-co-PEGMA graft polymer-stabilised emulsions did not break with temperature increment. Temperature sensitive gelation was observed, which was due to steric stabilisation.[65] It was proposed that the mechanism for emulsion gelation involved flocculation triggered by the collapse of the adsorbed PNIPAM-co-PEGMA layer at temperatures above the solution LCST. Higher temperatures lead to stronger flocculation due to a decrease in copolymer layer thickness. The collapse of the adsorbed layer created a rigid interface that prevented coalescence of the flocculated droplets. The reversibility of the gelation process is attributed to the interpenetration and entanglement of interfacial copolymer chains. Hence, the use of PNIPAM-co-PEGMA graft copolymers enabled temperature induced reversible gelation of oil-in-water emulsions switching from a liquid emulsion to a highly viscous gel. Following this study, Koh and colleagues studied temperature sensitive emulsions stabilised with poly(N-isopropylacrylamide)-co-poly(ethyleneglycol methacrylate) (PNIPAM-co-PEGMA) graft polymers, then performed a rheological analysis on the emulsions to study thermo-reversibility.[65,66] When heated, the viscosity of the emulsions decreased and then significantly increased at 48°C exhibiting gelation due to flocculation between neighbouring droplets, forming a network that entraps the aqueous phase. The strength of the network increased with temperature. The emulsion gelation was reversible and sensitive to shear. The mechanism proposed involves an increase in polymer-solvent interaction parameter with temperature, leading to transient network formation. The reversible gelation phenomenon was observed for various oil phases such as toluene, poly(dimethylsiloxane) and perfluorodecalin and has significant technological implications in transforming fluid emulsions into gels using temperature as the trigger.

This study provides a comprehensive rheological investigation of temperature-induced gelation in oil-in-water emulsions stabilised by PNIPAM-co-PEGMA, revealing its unique behaviour and potential applications in the field of emulsion technology.

Using poly(ethylene oxide) (PEO) star polymers as emulsifiers synthesised via atomic transfer radical polymerisation,a controlled polymerisation technique, Saigal et al. formed stable emulsions with temperature-sensitive microstructure and rheology. The majority of non-flocculated droplets were found in emulsions produced at room temperature. When heated above the cloud point of the polymers and cooled to room temperature, these emulsions contained mostly flocculated droplets and showed more gel-like rheological activity with rises in both the viscous and elastic moduli compared to the original emulsion. Emulsions made at the same high temperature and cooled to room temperature behaved differently, with non-flocculated droplets, more liquid-like rheology, and lower viscous and elastic moduli than emulsions made at room temperature.[67] Feng et al. synthesised di(ethylene glycol) methacrylate and poly(ethylene glycol) methacrylate thermoresponsive surfactants via Atom Transfer Radical Polymerisation and LCST could be tuned between 90 to 28°C by altering the molar ratio of the monomers. The copolymer displayed LCST of 34°C which was independent of chain length and around this temperature a viscous immiscible phase was formed at the oil-water interface because of collapsed surfactant. In the emulsion system stabilised by these thermoresponsive surfactants, the hydrophilic block collapsed and coalescence between the emulsion droplets occurred when the temperature exceeded the LCST but were stable for more than four months below the LCST.[8]

In the study conducted by Iwasaki et al., utilised poly[2-isopropoxy-2-oxo1,3,2-dioxaphospholane] (PIPP) was used to alter cellulose nanocrystals (CNCs). The resulting grafted copolymer (CNC-g-PIPP) was then used in creating emulsions.[68] The CNC-g-PIPP-based emulsions exhibited superior stability against coalescence compared to emulsions formed with unmodified CNCs. The emulsions with different concentrations of grafted particles had varying droplet sizes. The LCST was be triggered by using polyphosphoester, which has biodegradability and biocompatibility. The PIPP brushes make the CNCs hydrophobic, resulting in increased interfacial activity. The CNC-g-PIPP was utilised to stabilise a heptane-in-water Pickering emulsion, with demulsification induced by heating

the emulsion beyond the LCST of PPIP as illustrated in Figure 2.11.[68] Stable heptane-in-water emulsions were formed at 4 °C due to strong adsorption of CNC-g-PIPP at the oil-water interface. However, the emulsions disintegrated rapidly at 45 °C, as the hydrophobised CNC-g-PIPP desorbed from the interface. This thermally induced reversible emulsification/demulsification showed promising alternative for controlling emulsion stability in response to temperature, especially for biomedical applications.
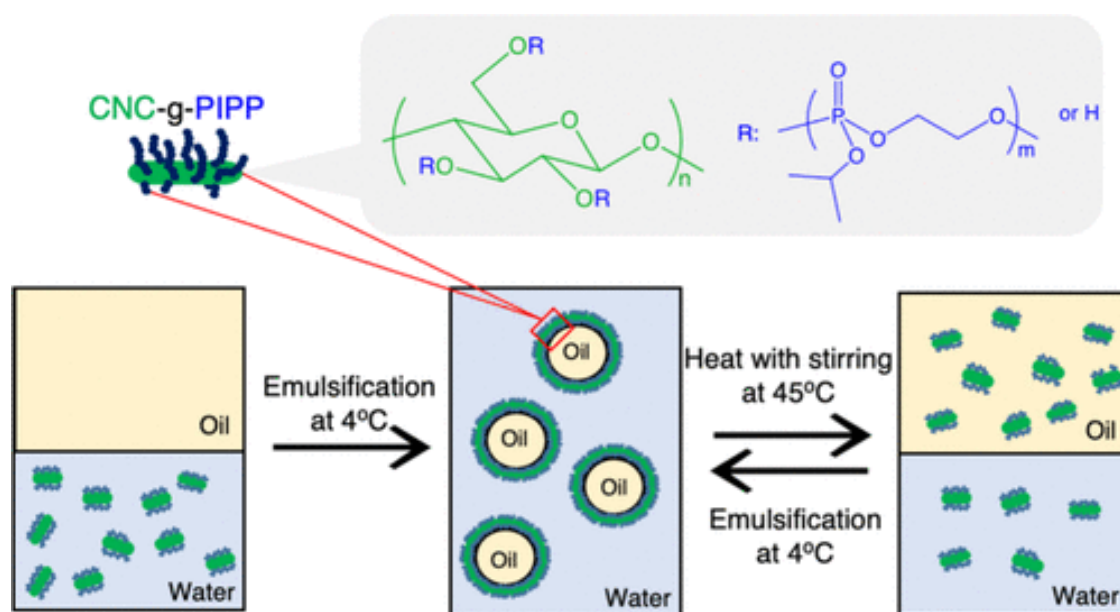
Figure 2.11: Proposed schematic illustrating potential mechanisms behind the reversible emulsification/demulsification of the CNC-g-PIPP-stabilised emulsion. Reproduced with permission.[68] Copyright 2019, American Chemical Society.

Combining the concept of "engineered emulsion" and HIPE gels, it was demonstrated by Chen's group that by altering the amount of nanogel particles used, the mechanical strength of the HIPE hydrogels can be adjusted. These HIPE hydrogels were synthesised from water-borne poly(N-isopropylacrylamide) nanogel dispersions and are non-covalently crosslinked by 2-ureido-4[1H] pyrimidinone (UPy) quadruple hydrogen bond groups which allows the HIPE gels to possess thermoresponsive activity.[69] By using injection moulding, it was shown that HIPE hydrogels may be formed into reconfigurable shaped objects. Furthermore, because of the PNIPAM's LCST behaviour, the structures can be shrunk significantly at high temperatures, permitting triggered delivery of guest molecules.[69]

2.6 Dual responsive emulsion

In 2008, Brugger and colleagues explored the stability and effective break-down of poly(N-isopropylacrylamide)-co-methacrylic acid (PNIPAM-co-MAA) microgel- stabilised emulsions alongside responsiveness with a view to identifying dually-responsive emulsions.[19] The polarity of the oil determined how the emulsion responded to changes in pH and temperature. The emulsions were destabilised and the oil separated from the water only when both the pH was reduced and the temperature increased well above the volume phase transition temperature of PNIPAM. The rheology results showed that the interface was extremely elastic at low temperature and high pH, and thus stabilised the emulsion. Around pH 5, the transition from a highly elastic to a less elastic interface strongly indicates that weakly acidic MAA groups play a significant role in the elastic properties. Successive increase in temperature and decrease in pH value led to the break-down of the emulsion, resulting in destabilisation. The water and oil ratio, and microgel concentration affect the emulsion's stability and type. The oil-in-water was the favoured stable form of PNIPAM-co-MAA microgel-stabilised heptane-water emulsions.[19]

Yamagami and researchers synthesised micrometer-sized, monodisperse, non-spherical poly(methyl methacrylate)/poly(styrene-2-(2- bromoisobutyryloxy)ethyl methacrylate)-graft-poly(2-(dimethyl amino)ethyl methacrylate) (PMMA/PS-BIEM-g-PDM) particles for use as emulsifiers.[70] Particles obtained in the 5-wt% PS-BIEM system had a closed mushroom-cap-like PDM layer that reversibly responded to temperature and pH as described in Figure 2.12.[70] With control over the hydrophilic/lipophilic balance, the dual stimuli non-spherical particles effectively acted as a particulate surfactant, resulting in a solid 1-octanol-in-water emulsion. At pH 5.5, the opened mushroom-cap was so hydrophilic that the particles could not adsorb at the interface and the emulsion was destabilised. However, the PDM phase had a strong affinity for 1-octanol at pH values of 5.8 and 6.0, resulting in the particles acting as particulate surfactants. Further increasing the pH to 6.5 the droplets collapsed, indicating the necessity of appropriate hydrophilicity. In addition to pH, the PDM phase became lipophilic with the rise in temperature above the LCST. This indicated that the temperature and pH could be adjusted to control the emulsion's stability.[70]
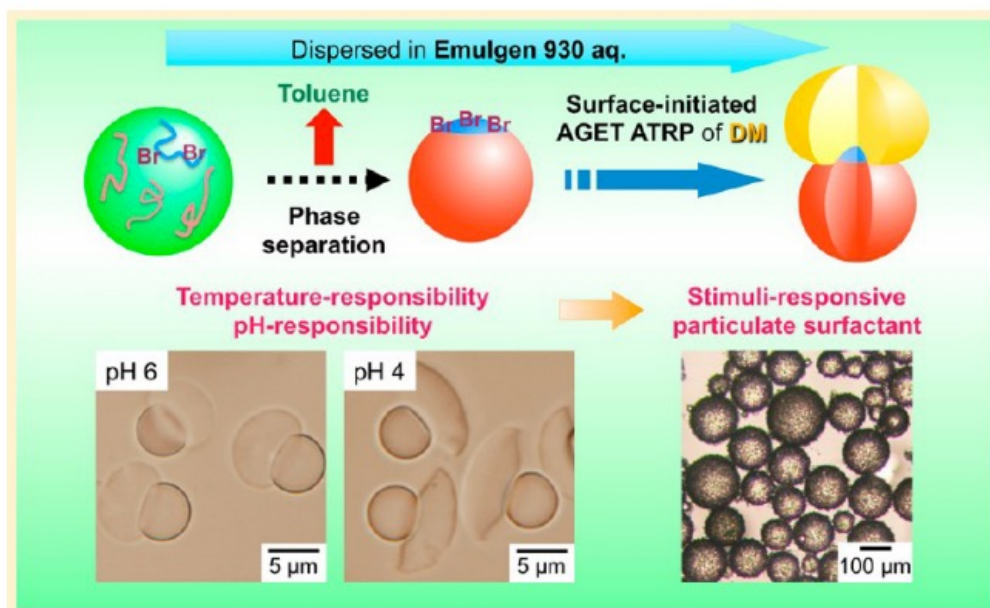
Figure 2.12: a) Diagram showing the process of crafting "mushroom-like" Janus particles, comprising PMMA/P(S-BIEM)-g-PDM, through site-selective surface-initiated activator generated by electron transfer for atom transfer radical polymerisation (AGET ATRP) of DM. This process takes place in an aqueous medium using biphasic-separated spherical PMMA/P(S-BIEM) Janus particles featuring bromine groups on one surface, which serve as macroinitiators. The macroinitiator Janus particles are produced through controlled release of toluene from a uniform PMMA/P(S-BIEM)/toluene droplet dispersed in the aqueous medium. Capitalising on their dual-responsive attributes, these asymmetrical particles effectively function as particulate surfactants in Pickering emulsions. This facilitates the creation of a stable emulsion of 1-octanol in water under optimal temperature and pH conditions. Additionally, the Pickering emulsion can be readily destabilised by manipulating these particles, enabling swift separation of the emulsion constituents. Reproduced with permission.[70] Copyright 2014, American Chemical Society.

Zhao et al. 2015[71] employed a general method to make dually sensitive Janus composite nanosheets that can serve as surfactants to stabilise emulsions. ATRP was used to selectively graft the pH sensitive 2-(dimethylamino)ethyl methacrylate and the thermally responsive N-Isopropylacrylamide onto the corresponding sides of the silica Janus nanosheets. By adjusting the pH or temperature, each side's wettability between

hydrophilic and hydrophobic could be adjusted separately. The composite nanosheets could act as a sensitive solid emulsifier, allowing emulsions to be stabilised by simply adjusting pH or (and) temperature. Janus nanosheets with dual responses could be useful in phase transfer catalysis.[71]

Ngai and co-workers demonstrated that by utilising a waterborne dispersion of poly(N-isopropylacrylamide)-co-(methacrylic acid) microgels, oil-in-water HIPE gel structures with internal phases of up to 90% can be generated.[72] It was suggested that hydrogen bond interactions cause the hydrogel-like continuous phase to form. Later in 2010, Ngai improved on this method for assembling HIPE-gels by employing core-shell particles with a polystyrene core and a microgel polymer outer shell and designed HIPEs using pH- and temperature-responsive microgels.[56,73]

In another research activity by Li et al., dual responsive Y-shaped amphiphilic PS-(PDMAEMA)$_2$ miktoarm star copolymers comprising of two hydrophilic PDMAEMA arms and a hydrophobic PS arm were synthesised. Depending on the volume ratio, the star copolymers could stabilise both o/w and w/o emulsions with toluene as the oil phase. Demulsification could be achieved by the pH increment, and phase inversion from an o/w to an o/w/o emulsion could be attained by increasing the temperature with mild stirring.[74]

An and colleagues[75] used the arms of dual responsive CCS polymers of p(MEA-co-PEGA) comprising of 2-methoxyethyl acrylate (MEA) and poly(ethylene glycol) acrylate (PEGA) of varying compositions. Heating the dodecane-in-water HIPEs over the LCST of the arms resulted in demulsification as shown in Figure 2.13.[75] The inclusion of kosmotropes and chaotropes, which are solutes that increase or decrease the structure of water molecules, could be used to adjust the emulsion's stability and demulsification efficiency. The kosmotropes decreased the cloud point and improved demulsification efficiency, whereas the chaotropes increased the cloud point and improved the emulsions' thermal stability.[75]
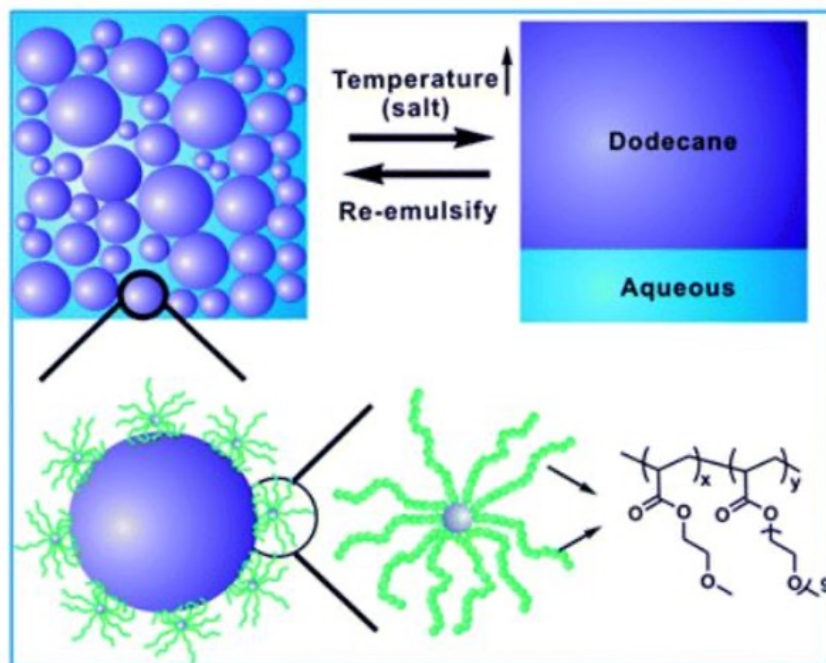
Figure 2.13: Diagram represensting the concept of responsive HIPEs stabilised by CCS polymers. Reproduced with permission.[75] Copyright 2014, The Royal Society of Chemistry.

2.7 Magnetic and CO_2 responsive emulsions

Jia et al. [76], created a poly(ethylene oxide)-block-poly(2-methacryloyloxyethyl pentynoate-graft-poly(acrylic acid))-block-polystyrene (PEO-b-P(MAPA-g-PAA)-b-PS) composite emulsifier having interfacial activity. Due to the amphiphilicity conferred by the PEO and PS linear polymers on two ends, the centre bottlebrush block was transformed into composite nanorods that stood vertically at the oil-water interface. With polymer/Ni composite Janus nanorods, magnetic responsive emulsions were formed.[76]

Li and colleagues used N,N-dimethylcyclohexylamine (DMCHA), a switchable hydrophobic tertiary amine, to prepare a CO_2 responsive emulsion as CO_2 causes formation of carbonic acid in water, reducing the pH. DMCHA was combined with paraffin oil to make CO_2 sensitive oil in water emulsions, which were emulsified using a standard surfactant, sodium dodecyl benzene sulfonate (SDBS). When exposed to CO_2, however, the majority of the paraffin oil and water separate from the emulsion, resulting in the creation of a middle phase microemulsion. More importantly, by removing CO_2, DMCHA could be isolated from the lower water phase and recycled.[77]

Dai et al. prepared a series of CO_2-responsive oil-in-water emulsion by introducing hydrophobic tertiary amines (TAs) with variable alkane carbon numbers (ACNs) into an emulsion stabilised by sodium dodecyl benzene sulfonate (SDBS). When exposed to CO_2, TAs undergo a transformation into bicarbonate salts. These salts can then interact with SDBS through electrostatic contact to form ion pairs, ultimately leading to the destabilisation of the emulsion. It was demonstrated that the elimination of CO_2 could activate the reversible switch as demonstrated in Figure 2.14.[78] Conductivity, interfacial tension, micrographs, and the water separation rate showed that the emulsion properties relied on the ACN prior to CO_2 bubbling. The ACN of the TA, TA/SDBS concentration, and CO_2 settling time were considered to examine the controllable mechanism of these CO_2-responsive emulsions. TAs with larger ACNs had enhanced miscibility with oil, facilitating adhesion to the oil phase and accelerating oil droplet rupture. The electrostatic interaction between the protonated TA and SDBS altered the interfacial tension and phase separation time. UV-vis spectrophotometer analysis of the water phase elucidated the content of separated ion pairs, aiding in understanding the significance of ACN and the corresponding controllable mechanism. However, due to the strong electrostatic force, not all ion pairs broke during N_2 bubbling, preventing complete re-emulsification of the system to its original state. This study primarily focused on the first round of CO_2-responsive properties.
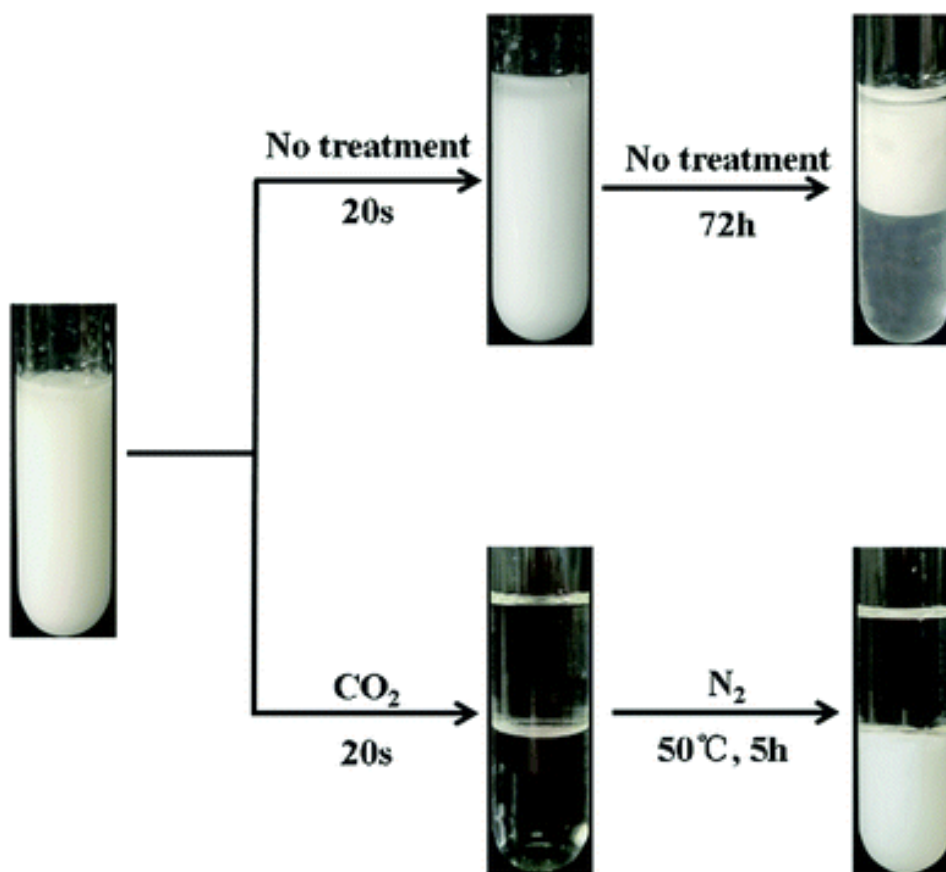
Figure 2.14: Sequential images capturing the process of demulsification and subsequent re-stabilisation of CO_2-responsive Oil-in-Water (O/W) emulsions. Reproduced with permission.[78] Copyright 2018, The Royal Society of Chemistry.

Liang and colleagues [79] showcased the creation of emulsions without the need for surfactants. They achieved this by designing particles with responsive and non-responsive surface groups, resulting in emulsions with adjustable properties. CO_2 switchable functional groups were grafted onto the surface of silica particles to form oil-in-water emulsions that responded to CO_2 triggers as shown in Figure 2.15.[79] It was shown that the surfactant free oil-in water emulsions can be stabilised by silica particles possessing both CO_2-responsive and hydrophobic chemical functional groups on their surface. When the wettability of the stabilising particle was adjusted by initiating CO_2 into the biphasic mixture, phase separation of emulsions occurred. With the removal of CO_2 from the emulsion and air sparging it, the emulsion's stability could be restored. This reversible change was verified by monitoring the zeta potential and contact angle of particles and model surfaces.[79]
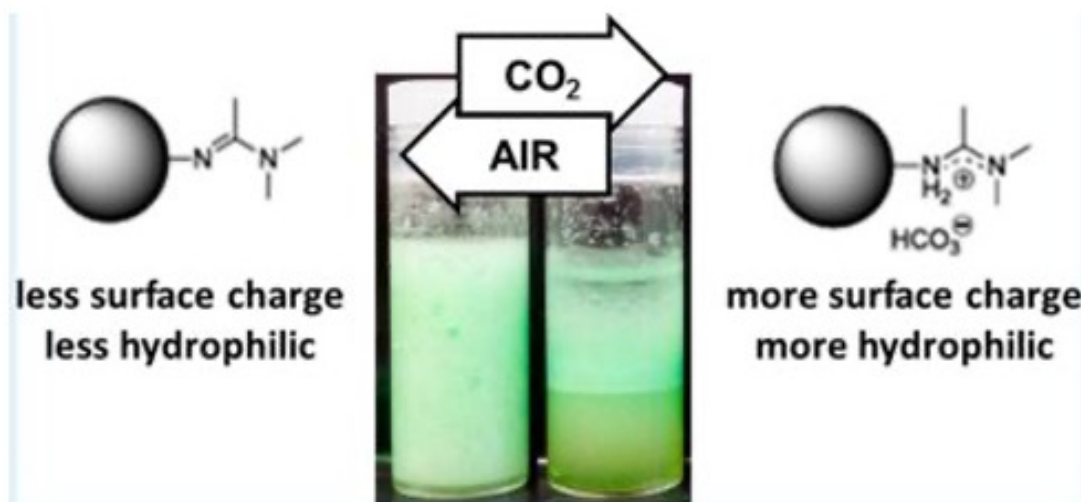
Figure 2.15: Illustration of switchable particles coated with CO_2-responsive surface groups, which undergo increased ionisation upon exposure to CO_2 leading to increased hydrophilicity and subsequently triggering the destabilisation of emulsions. Reproduced with permission.[79] Copyright 2014, American Chemical Society.

2.8 Engineering thermoresponsive emulsions

For the first time, Da Silva and co-workers reported the generation of thermoresponsive engineered emulsions stabilised with BCSs.[80] A one-pot free-radical polymerisation method to synthesise the BCSs. This involved combining a mixture of a "functional" monomer poly(N-isopropylacrylamide), (PNIPAM)-bearing temperature responsive characteristics, a hydrophilic monomer poly(ethylene glycol) methyl ether methacrylate (PEGMA), a cross-linker ethylene glycol dimethylacrylate (EGDMA), and a hydrophobic chain transfer agent 1-dodecanethiol (DDT). This resulted in a macromolecule that exhibited both thermoresponsiveness and amphiphilic properties. Preliminary investigations using these BCSs have shown their effectiveness as emulsifiers to stabilise dodecane-in-water emulsions and their ability to exhibit thermoresponsive behaviour.[80] Upon heating, the emulsions solidified and became non-flowing gels. This marked the first instance of successfully creating thermoresponsive engineered emulsions stabilised by BCSs. The thermo-rheological properties of the emulsions stabilised with these BCS were studied using shear oscillatory rheology. Additionally, small angle neutron scattering, and neutron reflectivity techniques were employed to investigate the nanoscale morphology

of the BCSs above and below the transition temperature. This provided insights on the nanoscale assembly processes that contribute to the thermoresponsive behaviour of these engineered emulsions. Furthermore, the influence of molecular weight on the characteristics of thermoresponsive engineered emulsions, a study was conducted using four distinct BCSs with increasing Mn (number average molecular weight) at varying concentrations. The mechanism for gelation in thermo-thickening engineered emulsions was hypothesised which involves the collapse of poly(N-isopropylacrylamide) (PNIPAM) above its lower critical solution temperature (LCST), resulting in polymer-polymer interactions that cause the aggregation of BCS clusters as shown in Figure 2.16.[80] In emulsion systems, these polymer-polymer interactions also occur between the nanoaggregates within the emulsion bulk and the polymer present at the interface, forming bridges that contribute to the elastic properties of the gel. These emulsions demonstrated successful thermoreversible gelation; however, the gel state was relatively weak, with storage modulus (G') of approximately 30 Pa, and it was limited to a narrow temperature range.
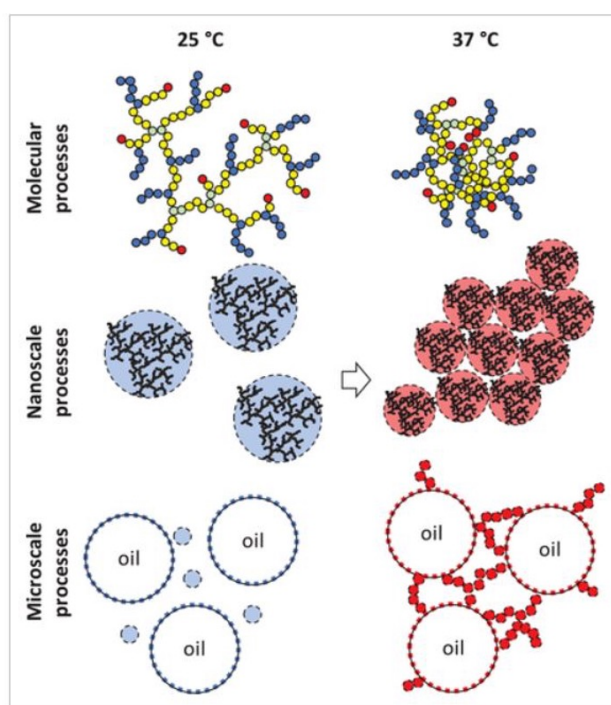
Figure 2.16: A hypothesis on the mechanism of gelation. Reproduced with permission.[80] Copyright 2022, Wiley-VCH.

The BCS were synthesised with poly(N-isopropyl acrylamide) (PNIPAM) as temperature sensitive unit as it is widely known for its sharp and environmentally-insensitive LCST at approximately 32 °C. Despite its attractiveness, there are conflicting reports on its biocompatibility.[81] An alternative polymer, poly(N,N-diethyl acrylamide) (PDEA), offers a controllable LCST ranging from about 25 to 36 °C, but its biocompatibility remains relatively unexplored.[82] Poly(N-vinyl caprolactam) is another biocompatible polymer commonly used in pharmaceutical excipients, exhibiting an LCST as low as 30 °C. However, the polymerisation of its monomer is challenging to control.[83] Poly(2-oxazolines) represent a novel class of thermoresponsive polymers that allow for LCST manipulation based on the pendant group attached. However, they have not yet found use in approved medications.[84]

Poly(oligoethylene glycol methyl ether methacrylates) (POEGMA) offer the advantage of precise control over the LCST by adjusting the pendant chain length and end group. They are considered biocompatible due to their resemblance to poly(ethylene glycol) (PEG) structures.[85] It is uncharged, water-soluble, non-toxic, and non-immunogenic, making it highly suitable for various biomedical applications. Hence, further study on thermoresponsive emulsions will be carried out in order to generate engineered emulsions of enhanced performance using surfactants made from di(ethylene glycol) methyl ether methacrylate (DEGMA) branched copolymers as this belongs to the versatile and biocompatible oligo(ethylene glycol) methacrylate family offering a promising foundation for developing these materials. This innovative approach holds potential for creating novel materials suitable for healthcare applications, as well as design principles for these advanced functional materials.

2.9 Stimuli responsive emulsions: applications and future perspectives

Stimuli-responsive emulsions have gained significant attention due to their wide range of applications in various fields. These emulsions which are stabilised with stimuli-responsive polymers consisting of droplets dispersed in a continuous phase, can undergo controlled changes in their properties in response to external stimuli such as pH[56,86–88], temperature[89–92], magnetic field[93–95], CO_2[96,97], light [98–101] and redox-reaction[102,103].

One prominent area for application is drug delivery, where the ability to controlled release of encapsulated drugs in response to specific stimuli is highly desirable.[104] For instance, temperature-responsive emulsions can be employed to deliver drugs in a controlled manner via *in situ* gelation, taking advantage of localised temperature changes for example, forming depos. Additionally, stimuli-responsive emulsions find applications in cosmetics, personal care products, and food science.[42] pH or temperature-responsive emulsions can enhance the stability and functionality of skincare formulations or improve the sensory properties of food products. Furthermore, stimuli-responsive emulsions have shown promise in advanced materials synthesis, microencapsulation, and microreactors.[42,99,104] Here are some applications of stimuli-responsive emulsions:

Drug delivery: Stimuli-responsive emulsions have been explored for controlled and targeted drug delivery systems.[105] These emulsions can respond to specific triggers such as pH, temperature, light, or magnetic fields, releasing drugs at the desired site and time. This allows for enhanced therapeutic efficacy, reduced side effects, and improved patient compliance. By incorporating responsive polymers or nanoparticles into the emulsion droplets, drug release can be triggered by specific physiological conditions or external stimuli. For example, pH-responsive emulsions can release drugs selectively in acidic environments such as tumours or inflamed tissues, enhancing therapeutic efficacy.[106] The ability of responsive emulsions to tailor their properties to individual patient needs holds great promise for personalised medicine. By adjusting the composition and responsiveness of emulsions, it becomes possible to optimise drug delivery for specific patient profiles or disease states.[104,106,107] This personalised approach can lead to improved treatment outcomes and reduced side effects.

Microencapsulation: Stimuli-responsive emulsions can be utilised for the microencapsulation of various functional materials, including active ingredients, flavours, fragrances, and bioactive compounds.[108] By incorporating stimuli-responsive polymers or materials into the emulsion system, the release of encapsulated substances can be triggered by specific stimuli, offering sustained or controlled release properties.

Sensing and detection: Stimuli-responsive emulsions can be designed as sensing platforms for detecting specific analytes or environmental changes.[88] By incorporating responsive components into the emulsion droplets, changes in properties such as colour,

fluorescence, or conductivity can be observed in response to target analytes or stimuli. This makes them useful for applications such as chemical sensing, environmental monitoring, and biomedical diagnostics.[109] Responsive emulsions can be engineered to encapsulate imaging agents or diagnostic probes, enabling targeted imaging and detection. For instance, magnetic-responsive emulsions can be guided to specific sites in the body using an external magnetic field, facilitating precise imaging and diagnosis of diseases.[95,110]

Tissue engineering: Responsive emulsions have the potential to contribute to advances in tissue engineering and regenerative medicine.[111,112] By encapsulating cells or bioactive molecules within emulsion droplets, their controlled release and spatial distribution can be achieved, facilitating the growth and regeneration of tissues. Additionally, the responsiveness of emulsions can be harnessed to create dynamic scaffolds that adapt to changing physiological conditions.

Theranostics: Responsive emulsions can integrate therapeutic and diagnostic functions into a single system, known as theranostic platform. These platforms can simultaneously deliver therapeutic agents while providing real-time imaging or monitoring of treatment response. Such systems have the potential to revolutionise disease management by enabling personalised, targeted therapies and rapid assessment of treatment efficacy.[113]

Controlled release of fragrances and cosmetics: Stimuli-responsive emulsions have been explored in the field of cosmetics for the controlled release of fragrances, active ingredients, and cosmetic agents. By formulating emulsions that respond to specific triggers such as sweat, pH changes, or temperature, the release of fragrances or active ingredients can be modulated, providing long-lasting and personalised cosmetic experiences.[114]

Reversible emulsion systems: Stimuli-responsive emulsions can exhibit reversible phase transitions in response to external stimuli. These reversible emulsion systems find applications in areas such as oil recovery, enhanced oil separation, and microreactors, where the ability to switch between different phases or states can be beneficial for efficient process control and optimisation.[104]

These are just a few examples of the diverse applications of stimuli-responsive emulsions. Ongoing research in this field continues to explore new possibilities and expand their utility in various industries. While significant progress has been made in the field of stimuli-responsive emulsions, several challenges remain. Achieving precise control over the stimuli-triggered responses and understanding the underlying mechanisms are key areas of ongoing research. Additionally, scalability and cost-effectiveness of large-scale production methods need to be addressed for practical applications. Moreover, the design of stimuli-responsive emulsions with multi-responsive behaviours and hierarchical structures presents an exciting avenue for future exploration.

2.10 Conclusion

In conclusion, stimuli-responsive emulsions have emerged as a promising drug delivery platform with significant implications for pharmaceutical applications. Looking ahead, continued research and development in the field of stimuli-responsive emulsions hold the promise of expanding their applications, enabling controlled drug release strategies, and revolutionising drug delivery paradigms. By exploiting external stimuli such as temperature, pH, magnetic, and CO_2, these emulsions offer a new dimension of control over drug release kinetics or site-specific delivery through sol-gel mechanisms. Moreover, their capacity to encapsulate a diverse range of hydrophobic and hydrophilic compounds underscores their adaptability, making them an attractive choice for delivering a wide range of therapeutic agents.

The thermoresponsive BCSs architecture seems to be effective in forming thermoreversible gels. However, there have been limitations from the existing study on NIPAM which include the mechanical strength of the gel being very low and existing concerns about toxicity of NIPAM. So far only one study reports thermoresponsive engineered emulsions, they have not been investigated in the drug delivery applications and the structure-function relationships in these systems is unknown.

This thesis aims to explore a new class of thermoresponsive BCS and polymer architecture for formulation of engineered emulsions and study for applications in drug delivery. To achieve this, the following objectives are required: alteration of polymer chemistry of the BCS framework to include OEGMA, optimisation of the BCS for thermogelation of engineered emulsions at physiologically relevant temperature, and explore the effect of additives in the formulation, probe the ability of themoresponsive BCS stabilised emulsions to encapsulate drugs and release kinetics will also be assessed, in addition to their compatibility with devices for administration.

2.11 References

1. Shinohara, H. Reports on Progress in Physics Related content. *Rep. Prog. Phys.* **64**, 297–381 (2001).

2. Chen, Q. *et al.* PH-responsive high internal phase emulsions stabilized by core cross-linked star (CCS) polymers. *Polym. Chem.* **4**, 4092–4102 (2013).

3. Walstra, P. 8 Emulsions. *Fundam. Interface Colloid Sci.* **5**, 1–94 (2005).

4. Aulton, M. E. *Aulton's Pharmaceutics: The Design and Manufacture of Medicines*. (Elsevier Limited, 2007).

5. Mahato, R. I. *Pharmaceutica Dosage Forms and Drug Delivery*. (CRC Press LLC, 2007).

6. Hu, M. & Russell, T. P. Polymers with advanced architectures as emulsifiers for multi-functional emulsions. *Mater. Chem. Front.* **5**, 1205–1220 (2021).

7. Zhang, H. & Cooper, A. I. Synthesis and applications of emulsion-templated porous materials. *Soft Matter* **1**, 107–113 (2005).

8. Feng, H., Verstappen, N. A. L., Kuehne, A. J. C. & Sprakel, J. Well-defined temperature-sensitive surfactants for controlled emulsion coalescence. *Polym. Chem.* **4**, 1842–1847 (2013).

9. Richtering, W. Responsive emulsions stabilized by stimuli-sensitive microgels: Emulsions with special non-pickering properties. *Langmuir* **28**, 17218–17229 (2012).

10. Cabane, E., Zhang, X., Langowska, K., Palivan, C. G. & Meier, W. Stimuli-responsive polymers and their applications in nanomedicine. *Biointerphases* **7**, 1–27 (2012).

11. Wang, D., Green, M. D., Chen, K., Daengngam, C. & Kotsuchibashi, Y. Stimuli-Responsive Polymers: Design, Synthesis, Characterization, and Applications. *Int. J. Polym. Sci.* **2016**, 2–4 (2016).

12. Wang, D., Jin, Y., Zhu, X. & Yan, D. Synthesis and applications of stimuli-responsive hyperbranched polymers. *Prog. Polym. Sci.* **64**, 114–153 (2017).

13. Kragt, A. J. J., Zuurbier, N. C. M., Broer, D. J. & Schenning, A. P. H. J. Temperature-

Responsive, Multicolor-Changing Photonic Polymers. *ACS Appl. Mater. Interfaces* **11**, 28172–28179 (2019).

14. Isapour, G. & Lattuada, M. Bioinspired Stimuli-Responsive Color-Changing Systems. *Adv. Mater.* **30**, 1–36 (2018).

15. Brugger, B. & Richtering, W. Emulsions stabilized by stimuli-sensitive poly(N-isopropylacrylamide)-co-methacrylic acid polymers: microgels versus low molecular weight polymers. *Langmuir* **24**, 7769–7777 (2008).

16. Dai, S., Ravi, P. & Tam, K. C. pH-Responsive polymers: synthesis, properties and applications. *Soft Matter* **4**, 435 (2008).

17. Wang, L. *et al.* Preparation and aqueous solution behavior of a ph-responsive branched copolymer based on 2-(diethylamino)ethyl methacrylate. *J. Appl. Polym. Sci.* **132**, n/a-n/a (2015).

18. Zhao, C. *et al.* Ca2+ ion responsive pickering emulsions stabilized by PSSMA nanoaggregates. *Langmuir* **29**, 14421–8 (2013).

19. Brugger, B., Rosen, B. A. & Richtering, W. Microgels as stimuli-responsive stabilizers for emulsions. *Langmuir* **24**, 12202–12208 (2008).

20. Sanyal, S., Huang, H.-C., Rege, K. & Dai, L. L. Thermo-Responsive Core-Shell Composite Nanoparticles Synthesized via One-Step Pickering Emulsion Polymerization for Controlled Drug Delivery. *J. Nanomed. Nanotechnol.* **02**, (2011).

21. Thananukul, K. *et al.* Smart gating porous particles as new carriers for drug delivery. *Adv. Drug Deliv. Rev.* (2021) doi:10.1016/j.addr.2021.04.023.

22. Bratek-Skicki, A. Towards a new class of stimuli-responsive polymer-based materials – Recent advances and challenges. *Appl. Surf. Sci. Adv.* **4**, 100068 (2021).

23. Panayiotou, M. SYNTHESIS AND CHARACTERIZATION OF THERMORESPONSIVE POLYMERS, HYDROGELS AND MICROGELS, BASED ON POLY (N-SUBSTITUTED ACRYLAMIDES). (2004).

24. Chen, J. Immobilization of a -Ch y motr y psin to a Temperature-Responsive Reversibl y Soluble – Insoluble Oligomer Based on N -Isoprop y lacr y lamide. (1998).

25. Okano, T., Bae, Y. H., Jacobs, H. & Kim, S. W. Thermally on-off switching polymers for drug permeation and release. *J. Control. Release* **11**, 255–265 (1990).

26. N.Nujoma, Y. & Kim, C.-J. A Designer's Polymer as an Oral Drug Carrier (Tablet) with Pseudo-Zero-Order Release Kinetics. *J. Pharm. Sci.* **85**, 1091–1095 (1996).

27. Freitag, R., Costioli, M. & Garret-flaudy, F. Stimulus-Responsive Polymers for Bioseparation. 196–200 (2001).

28. Hoffman, A. S. Hydrogels for biomedical applications. *Adv. Drug Deliv. Rev.* **54**, 3–12 (2002).

29. Ohya, S., Nakayama, Y. & Matsuda, T. Thermoresponsive artificial extracellular matrix for tissue engineering: Hyaluronic acid bioconjugated with poly(N-isopropylacrylamide) grafts. *Biomacromolecules* **2**, 856–863 (2001).

30. Wei, M., Gao, Y., Li, X. & Serpe, M. J. Stimuli-responsive polymers and their applications. *Polym. Chem.* **8**, 127–143 (2017).

31. Priya James, H., John, R., Alex, A. & Anoop, K. R. Smart polymers for the controlled delivery of drugs – a concise overview. *Acta Pharm. Sin. B* **4**, 120–127 (2014).

32. Ofridam, F. *et al.* pH-sensitive polymers: Classification and some fine potential applications. *Polym. Adv. Technol.* **32**, 1455–1484 (2021).

33. Zhang, J. & Peppas, N. A. Synthesis and characterization of pH- and temperature-sensitive poly(methacrylic acid)/poly(N-isopropylacrylamide) interpenetrating polymeric networks. *Macromolecules* **33**, 102–107 (2000).

34. Zhang, X., Wu, D. & Chu, C. C. Synthesis and characterization of partially biodegradable, temperature and pH sensitive Dex-MA/PNIPAAm hydrogels. *Biomaterials* **25**, 4719–4730 (2004).

35. Aguilar, M. R. & San Román, J. Smart Polymers and their Applications. *Smart Polym. their Appl.* 1–568 (2014) doi:10.1533/9780857097026.

36. Teotia, A. K., Sami, H. & Kumar, A. Thermo-responsive polymers: structure and design of smart materials. in *Switchable and Responsive Surfaces and Materials for Biomedical Applications* (ed. Zhang, Z.) 3–43 (Woodhead Publishing, 2015). doi:https://doi.org/10.1016/B978-0-85709-713-2.00001-8.

37. Kim, Y. J. & Matsunaga, Y. T. Thermo-responsive polymers and their application as smart biomaterials. *J. Mater. Chem. B* **5**, 4307–4321 (2017).

38. Zuppardi, F., Malinconico, M., D'agosto, F., D'ayala, G. G. & Cerruti, P. Well-defined thermo-responsive copolymers based on oligo(Ethylene glycol) methacrylate and pentafluorostyrene for the removal of organic dyes from water. *Nanomaterials* **10**, 1–16 (2020).

39. Bordat, A., Boissenot, T., Nicolas, J. & Tsapis, N. Thermoresponsive polymer nanocarriers for biomedical applications. *Adv. Drug Deliv. Rev.* **138**, 167–192 (2019).

40. Schmaljohann, D. Thermo- and pH-responsive polymers in drug delivery. *Adv. Drug Deliv. Rev.* **58**, 1655–70 (2006).

41. Liang, C., Liu, Q. & Xu, Z. Synthesis of Surface-Responsive Composite Particles by Dehydration of Water-in-Oil Emulsions. *ACS Appl. Mater. Interfaces* **7**, 20631–20639 (2015).

42. Cook, M. T., Haddow, P., Kirton, S. B. & McAuley, W. J. Polymers Exhibiting Lower Critical Solution Temperatures as a Route to Thermoreversible Gelators for Healthcare. *Adv. Funct. Mater.* **31**, (2021).

43. Arai, T. *et al.* Novel drug delivery system using thermoreversible gelation polymer for malignant glioma. *J. Neuro-Oncology Vol.* **77**, 9–15 (2006).

44. Weaver, J. V. M., Rannard, S. P. & Cooper, A. I. Polymer-Mediated Hierarchical and Reversible Emulsion Droplet Assembly. *Angew. Chemie* **121**, 2165–2168 (2009).

45. Woodward, R. T. & Weaver, J. V. M. The role of responsive branched copolymer composition in controlling pH-triggered aggregation of 'engineered' emulsion droplets: Towards selective droplet assembly. *Polym. Chem.* **2**, 403–410 (2011).

46. Woodward, R. T. *et al.* Controlling responsive emulsion properties via polymer design. *Chem. Commun.* 3554–3556 (2009) doi:10.1039/b904320a.

47. Weaver, J. V. M. *et al.* PH-Responsive branched polymer nanoparticles. *Soft Matter* **4**, 985–992 (2008).

48. Weaver, J. V. M., Rannard, S. P. & Cooper, A. I. Polymer-mediated hierarchical and

reversible emulsion droplet assembly. *Angew. Chemie - Int. Ed.* **48**, 2131–2134 (2009).

49.   Woodward, R. T., Chen, L., Adams, D. J. & Weaver, J. V. M. Fabrication of large volume, macroscopically defined and responsive engineered emulsions using a homogeneous pH-trigger. *J. Mater. Chem.* **20**, 5228–5234 (2010).

50.   Woodward, R. T. *et al.* Reversible aggregation of responsive polymer-stabilized colloids and the pH-dependent formation of porous scaffolds. *Soft Matter* **7**, 7560–7566 (2011).

51.   Patel, A. R., Drost, E., Seijen Ten Hoorn, J. & Velikov, K. P. Fabrication and characterization of emulsions with pH responsive switchable behavior. *Soft Matter* **9**, 6747–6751 (2013).

52.   Cameron, N. R. & Sherrington, D. C. High internal phase emulsions (HIPEs) — Structure, properties and use in polymer preparation. in *Biopolymers Liquid Crystalline Polymers Phase Emulsion* 163–214 (Springer, Berlin, Heidelberg, 2004). doi:https://doi.org/10.1007/3-540-60484-7.

53.   Pickering, S. U. 72, 156),. *J. Chem. Soc.* **91**, 2001–2021 (1907).

54.   Bongiovanni Abel, S., Molina, M., Rivarola, C. R. & Barbero, C. A. Pickering emulsions stabilized with PANI-NP. Study of the thermoresponsive behavior under heating and radiofrequency irradiation. *J. Appl. Polym. Sci.* 1–9 (2021) doi:10.1002/app.50625.

55.   Zhu, Y. *et al.* Thermoresponsive Pickering Emulsions Stabilized by Silica Nanoparticles in Combination with Alkyl Polyoxyethylene Ether Nonionic Surfactant. *Langmuir* **33**, 5724–5733 (2017).

56.   Sun, G., Li, Z. & Ngai, T. Inversion of particle-stabilized emulsions to form high-internalphase emulsions. *Angew. Chemie - Int. Ed.* **49**, 2163–2166 (2010).

57.   Gao, H. Development of star polymers as unimolecular containers for nanomaterials. *Macromol. Rapid Commun.* **33**, 722–734 (2012).

58.   Blencowe, A., Tan, J. F., Goh, T. K. & Qiao, G. G. Core cross-linked star polymers via controlled radical polymerisation. *Polymer (Guildf).* **50**, 5–32 (2009).

59. Chen, Q., Deng, X. & An, Z. PH-induced inversion of water-in-oil emulsions to oil-in-water high internal phase emulsions (HIPEs) using core cross-linked star (CCS) polymer as interfacial stabilizer. *Macromol. Rapid Commun.* **35**, 1148–1152 (2014).

60. Garcia-Tunon, E. *et al.* Designing smart particles for the assembly of complex macroscopic structures. *Angew. Chemie - Int. Ed.* **52**, 7805–7808 (2013).

61. Maçon, A. L. B., Rehman, S. U., Bell, R. V. & Weaver, J. V. M. Reversible assembly of pH responsive branched copolymer-stabilised emulsion via electrostatic forces. *Chem. Commun.* **52**, 136–139 (2016).

62. Chen, Y. *et al.* Hierarchical and reversible assembly of graphene oxide/polyvinyl alcohol hybrid stabilized Pickering emulsions and their templating for macroporous composite hydrogels. *Carbon N. Y.* **111**, 38–47 (2017).

63. Santa Chalarca, C. F., Letteri, R. A., Perazzo, A., Stone, H. A. & Emrick, T. Building Supracolloidal Fibers from Zwitterion-Stabilized Adhesive Emulsions. *Adv. Funct. Mater.* **28**, 1–10 (2018).

64. Verbrugghe, S., Bernaerts, K. & Du Prez, F. E. Thermo-Responsive and Emulsifying Properties of Poly(N-vinylcaprolactam) Based Graft Copolymers. *Macromol. Chem. Phys.* **204**, 1217–1225 (2003).

65. Koh, A. Y. C. & Saunders, B. R. Thermally induced gelation of an oil-in-water emulsion stabilised by a graft copolymer. *Chem. Commun.* **6**, 2461–2462 (2000).

66. Koh, Prestidge, C. & Saunders, B. R. Temperature-induced gelation of emulsions stabilised by responsive copolymers : A rheological study. **c**, (2001).

67. Saigal, T. *et al.* Stable emulsions with thermally responsive microstructure and rheology using poly(ethylene oxide) star polymers as emulsifiers. *J. Colloid Interface Sci.* **394**, 284–292 (2013).

68. Hiranphinyophat, S., Asaumi, Y., Fujii, S. & Iwasaki, Y. Surface Grafting Polyphosphoesters on Cellulose Nanocrystals to Improve the Emulsification Efficacy. *Langmuir* **35**, 11443–11451 (2019).

69. Chen, Y., Ballard, N. & Bon, S. A. F. Moldable high internal phase emulsion hydrogel objects from non-covalently crosslinked poly(N-isopropylacrylamide) nanogel

dispersions. *Chem. Commun.* **49**, 1542–1544 (2013).

70. Yamagami, T., Kitayama, Y. & Okubo, M. Preparation of stimuli-responsive 'mushroom-like' janus polymer particles as particulate surfactant by site-selective surface-initiated AGET ATRP in aqueous dispersed systems. *Langmuir* **30**, 7823–7832 (2014).

71. Zhao, Z. *et al.* Dually Responsive Janus Composite Nanosheets. *Macromolecules* **48**, 3598–3603 (2015).

72. Li, Z., Ming, T., Wang, J. & Ngai, T. High internal phase emulsions stabilized solely by microgel particles. *Angew. Chemie - Int. Ed.* **48**, 8490–8493 (2009).

73. Li, Z. & Ngai, T. Stimuli-responsive gel emulsions stabilized by microgel particles. *Colloid Polym. Sci.* **289**, 489–496 (2011).

74. Li, H., Yang, D., Gao, Y., Li, H. & Xu, J. Dual responsive macroemulsion stabilized by Y-shaped amphiphilic AB2 miktoarm star copolymers. *RSC Adv.* **5**, 96377–96386 (2015).

75. Chen, Q., Xu, Y., Cao, X., Qin, L. & An, Z. Core cross-linked star (CCS) polymers with temperature and salt dual responsiveness: Synthesis, formation of high internal phase emulsions (HIPEs) and triggered demulsification. *Polym. Chem.* **5**, 175–185 (2014).

76. Jia, F., Liang, F. & Yang, Z. Janus Composite Nanorod from a Molecular Bottlebrush Containing a Block Copolymer. *Langmuir* **34**, 1718–1724 (2018).

77. Li, H., Li, Q., Hao, J., Xu, Z. & Sun, D. Preparation of CO_2-responsive emulsions with switchable hydrophobic tertiary amine. *Colloids Surfaces A Physicochem. Eng. Asp.* **502**, 107–113 (2016).

78. Dai, S. *et al.* Controllable CO_2-responsiveness of O/W emulsions by varying the alkane carbon number of a tertiary amine. *Phys. Chem. Chem. Phys.* **20**, 11285–11295 (2018).

79. Liang, C., Liu, Q. & Xu, Z. Surfactant-free switchable emulsions using CO_2-responsive particles. *ACS Appl. Mater. Interfaces* **6**, 6898–6904 (2014).

80. da Silva, M. A. *et al.* Engineering Thermoresponsive Emulsions with Branched

Copolymer Surfactants. *Macromol. Mater. Eng.* **307**, 1–14 (2022).

81. Hoffman, A. S. Stimuli-responsive polymers: Biomedical applications and challenges for clinical translation. *Adv. Drug Deliv. Rev.* **65**, 10–16 (2013).

82. Jennings, J. *et al.* Synthesis of High χ–Low N Diblock Copolymers by Polymerization-Induced Self-Assembly. *Angew. Chemie - Int. Ed.* **59**, 10848–10853 (2020).

83. Cortez-Lemus, N. A. & Licea-Claverie, A. Synthesis and characterization of 'living' star-shaped poly(N-vinylcaprolactam) with four arms and carboxylic acid end groups. *J. Polym. Sci. Part A Polym. Chem.* **54**, 2156–2165 (2016).

84. Hoogenboom, R. *et al.* Tuning the LCST of poly(2-oxazoline)s by varying composition and molecular weight: Alternatives to poly(N-isopropylacrylamide)? *Chem. Commun.* 5758–5760 (2008) doi:10.1039/b813140f.

85. Lutz, J. F., Akdemir, Ö. & Hoth, A. Point by point comparison of two thermosensitive polymers exhibiting a similar LCST: Is the age of poly(NIPAM) over? *J. Am. Chem. Soc.* **128**, 13046–13047 (2006).

86. Wang, Y., Zhu, L., Zhang, H., Huang, H. & Jiang, L. Formulation of pH and temperature dual-responsive Pickering emulsion stabilized by chitosan-based microgel for recyclable biocatalysis. *Carbohydr. Polym.* **241**, 116373 (2020).

87. Binks, B. P. & Rodrigues, J. A. Inversion of emulsions stabilized solely by ionizable nanoparticles. *Angew. Chemie - Int. Ed.* **44**, 441–444 (2005).

88. Besnard, L. *et al.* Multiple emulsions controlled by stimuli-responsive polymers. *Adv. Mater.* **25**, 2844–2848 (2013).

89. Chen, F. *et al.* Nitrogen-aeration tuned ultrasonic synthesis of SiO2@PNIPAm nanoparticles and preparation of temperature responsive Pickering emulsion. *Ultrason. Sonochem.* **58**, 1–6 (2019).

90. Jiang, Y. *et al.* A Novel Temperature-Dependent Hydrogel Emulsion with Sol/Gel Reversible Phase Transition Behavior Based on Polystyrene-co-poly(N-isopropylacrylamide)/Poly(N-isopropylacrylamide) Core–Shell Nanoparticle. *Macromol. Rapid Commun.* **42**, 1–7 (2021).

91. Gao, Y., Xiang, Z., Zhao, X., Wang, G. & Qi, C. Pickering Emulsions Stabilized by

Diblock Copolymer Worms Prepared via Reversible Addition-Fragmentation Chain Transfer Aqueous Dispersion Polymerization: How Does the Stimulus Sensitivity Affect the Rate of Demulsification? *Langmuir* **37**, 11695–11706 (2021).

92. Ranka, M., Katepalli, H., Blankschtein, D. & Hatton, T. A. Schizophrenic Diblock-Copolymer-Functionalized Nanoparticles as Temperature-Responsive Pickering Emulsifiers. *Langmuir* **33**, 13326–13331 (2017).

93. Peng, J., Liu, Q., Xu, Z. & Masliyah, J. Novel magnetic demulsifier for water removal from diluted bitumen emulsion. *Energy and Fuels* **26**, 2705–2710 (2012).

94. Flores, J. A., Jahnke, A. A., Pavia-Sanders, A., Cheng, Z. & Wooley, K. L. Magnetically-active Pickering emulsions stabilized by hybrid inorganic/organic networks. *Soft Matter* **12**, 9342–9354 (2016).

95. Lin, K. Y. A., Yang, H., Petit, C. & Lee, W. der. Magnetically controllable Pickering emulsion prepared by a reduced graphene oxide-iron oxide composite. *J. Colloid Interface Sci.* **438**, 296–305 (2015).

96. Sun, Z., Zhao, Q., Haag, R. & Wu, C. Responsive Emulsions for Sequential Multienzyme Cascades. *Angew. Chemie - Int. Ed.* **60**, 8410–8414 (2021).

97. Jiang, J., Ma, Y., Cui, Z. & Binks, B. P. Pickering Emulsions Responsive to CO_2/N_2 and Light Dual Stimuli at Ambient Temperature. *Langmuir* **32**, 8668–8675 (2016).

98. Zhao, X. *et al.* Light-tuning amphiphility of host-guest Alginate-based supramolecular assemblies for photo-responsive Pickering emulsions. *Carbohydr. Polym.* **251**, 117072 (2021).

99. Li, Z. *et al.* Light-Responsive, Reversible Emulsification and Demulsification of Oil-in-Water Pickering Emulsions for Catalysis. *Angew. Chemie - Int. Ed.* **60**, 3928–3933 (2021).

100. Chen, Z. *et al.* Light controlled reversible inversion of nanophosphor-stabilized pickering emulsions for biphasic enantioselective biocatalysis. *J. Am. Chem. Soc.* **136**, 7498–7504 (2014).

101. Bai, R. X. *et al.* Light-Triggered Release from Pickering Emulsions Stabilized by TiO2 Nanoparticles with Tailored Wettability. *Langmuir* **32**, 9254–9264 (2016).

102. Zhang, H., Wu, J., Jiang, J., Cui, Z. & Xia, W. Redox-Responsive Oil-In-Dispersion Emulsions Stabilized by Similarly Charged Ferrocene Surfactants and Alumina Nanoparticles. *Langmuir* **36**, 14589–14596 (2020).

103. Yu, S. *et al.* Pickering emulsions of alumina nanoparticles and bola-type selenium surfactant yield a fully recyclable aqueous phase. *Green Chem.* **22**, 5470–5475 (2020).

104. Wu, Y., Zeng, M., Cheng, Q. & Huang, C. Recent Progress toward Physical Stimuli-Responsive Emulsions. *Macromol. Rapid Commun.* **43**, 1–15 (2022).

105. Verma, G. & Hassan, P. A. Self assembled materials: Design strategies and drug delivery perspectives. *Phys. Chem. Chem. Phys.* **15**, 17016–17028 (2013).

106. Hu, Q., Katti, P. S. & Gu, Z. Enzyme-responsive nanomaterials for controlled drug delivery. *Nanoscale* **6**, 12273–12286 (2014).

107. Vijayakameswara Rao, N., Ko, H., Lee, J. & Park, J. H. Recent progress and advances in stimuli-responsive polymers for cancer therapy. *Front. Bioeng. Biotechnol.* **6**, (2018).

108. Panthi, K., Singh, R. & Mohanty, K. K. Microencapsulation and Stimuli-Responsive Controlled Release of Particles Using Water-in-Air Powders. *Langmuir* **33**, 3998–4010 (2017).

109. Cao, Y., Wang, Z., Zhang, S. & Wang, Y. Synergetic regulation of CO_2 and light for controllable inversion of Pickering emulsions. *Mater. Chem. Front.* **1**, 2136–2142 (2017).

110. Lakkadwala, S., Nguyen, S., Nesamony, J., Boddy, S. H. & Narang, A. S. Smart Polymers in Drug Delivery. *Excip. Appl. Formul. Des. Drug Deliv.* 169–199 (2015).

111. Khattak, S. F., Bhatia, S. R. & Roberts, S. C. Pluronic F127 as a cell encapsulation material: Utilization of membrane-stabilizing agents. *Tissue Eng.* **11**, 974–983 (2005).

112. Kretlow, J. D., Klouda, L. & Mikos, A. G. Injectable matrices and scaffolds for drug delivery in tissue engineering. *Adv. Drug Deliv. Rev.* **59**, 263–273 (2007).

113. Chen, F., Ehlerding, E. B. & Cai, W. Theranostic nanoparticles. *J. Nucl. Med.* **55**,

1919–1922 (2014).

114. Saura-Sanmartin, A. & Andreu-Ardil, L. Recent Advances in the Preparation of Delivery Systems for the Controlled Release of Scents. *Int. J. Mol. Sci.* **24**, (2023).

Chapter 3: Polymer architecture dictates thermoreversible gelation in engineered emulsions stabilised with branched copolymer surfactants

3.1 Introduction

Emulsions are made up of at least two immiscible phases in which one phase is dispersed into another and forms droplets.[1,2] The immiscible fluids in emulsion systems may be kinetically stabilised by lowering interfacial tension,[3] traditionally achieved using small-molecule or polymeric surfactants which adsorb at the liquid-liquid interface.[1] The use of macromolecules at the interface offers manipulation of chemistry such that in addition to stabilising the emulsion system, they impart stimuli-responsive – so-called "smart" – functionality.[4,5] These stimuli-responsive polymeric materials undergo a modification in their physical and chemical properties in response to changes in their environment, such as mechanical stress, pH, light, temperature, and biological stimuli.[6–9]

Thermoresponsive polymers modify their physical properties in response to temperature. Typically this manifests as an alteration of the solubility of the constituent units with temperature, which can be coupled to the intrinsic ability to control polymer properties through modification of architecture and inclusion of co-monomers to lead to complex materials.[10] Thermoresponsive materials are being widely employed in healthcare research, enabling novel and improved therapies and diagnostics, amongst a plethora of applications such as drug delivery platforms, additive manufacturing and tissue engineering.[11] Polymer solutions that are capable of transforming to a gel state with elevation of temperature to a critical point are referred to as "Thermoreversible gels" or "Thermogelling materials".[11] A sol-gel transition occurs when heating a thermoreversible gel above a critical temperature, affected by an overall increase in hydrophobicity above the lower critical solution temperatures (LCST), triggering self-assembly processes and physical interaction, which increases the viscosity of the system.[12] These materials could transition from liquid to gel at body temperature, enabling *in situ* gelation and thus enhanced retention and therapeutic effect.[11] However, the vast majority of these materials are aqueous polymer solutions which often limits the application of the materials to hydrophilic encapsulants.

In 2008, Weaver introduced the term "emulsion engineering"[13] to describe a droplet trapping concept in which the droplet surface functionality is designed to kinetically trap the droplets giving a percolating network structure in the material, resulting in solidification. Droplet assembly and dispersion were dependent on inter-droplet hydrogen bonding, controlled by acidic or basic pH conditions.[13] Weaver and colleagues achieved these phenomena by stabilising emulsions with branched copolymer surfactants (BCSs) composed of a pH-responsive monomer, a hydrophilic macromonomer for steric stabilisation, a crosslinker for branching, and a chain transfer agent to introduce hydrophobic alkyl chain ends.[14,15] The hydrophobic chain ends of the branched copolymers offer excellent attachment to the surface of the oil droplets and the capacity to alter the stabilisation and surface functionality of the droplets in the continuous aqueous phase.[16] These features are the essentials of "engineered emulsions". This concept was demonstrated with weakly acidic polymeric surfactants that were able to cooperatively form hydrogen-bonds between emulsion droplets in the unionised state, imparting a pH-dependent sol-gel behaviour. As is typical of emulsions, these systems are complex and polymers imparting stimuli-responsive behaviour are required to stabilise emulsions with oils of widely varied polarity, droplet size and oil/water ratio, as well as varied emulsification techniques.[3] Thus, the field is both promising, and highly challenging. Our group has recently demonstrated for the first time that thermoresponsive engineered emulsions may be generated from poly(N-isopropylacrylamide) BCSs, in which poly(N-isopropyl acrylamide) exhibits an LCST. These emulsions successfully exhibited thermoreversible gelation, however the gel state was weak (G' of ca 30 Pa) and existed over a narrow temperature range.[17] The study found that polymer exists at the O/W interface and as nanoscale aggregates in the bulk, with rising temperature inducing changes to nanostructure which induces gelation. There is a need to generate thermoresponsive engineered emulsions of higher performance, which requires an understanding of how polymer architecture links to rheology.

This study reports the first thermoresponsive engineered emulsions from di(ethylene glycol) methyl ether methacrylate (DEGMA) branched copolymer surfactants. DEGMA, as a member of the highly versatile and biocompatible oligoethylene glycol methacrylate class,[18] offers a promising blueprint for the generation of these materials. Polymer

architecture will be varied to establish correlations with the temperature-dependent rheological behaviour of these systems, in particular how it is affected by branching degree, hydrophobic chain ends and molecular weight. The nanoscale processes underpinning thermoresponse will be determined by small-angle neutron scattering. This approach is promising to generate novel materials for healthcare applications, along with design principles for these advanced functional materials.

3.2 Materials and methods

3.2.1 Materials

Di(ethylene glycol) methyl ether methacrylate (DEGMA, 95%), Poly(ethylene glycol) methyl ether methacrylate (PEGMA, M_n 950 gmol^{-1}), Ethylene glycol dimethacrylate (EGDMA, 98%), and 1-Dodecanethiol (DDT, 99%), dodecane anhydrous (99%) were purchased from Sigma-Aldrich (UK). α,α-azoisobutyronitrile (AIBN, >99%) was obtained from Molekula (UK). 1-Hexadedecanethiol (HDT, 97%) and 1-tetradecanethol (TDT, 94%) were purchased from Alfa Aesar (UK). Ethanol and dimethylformamide (DMF) were supplied by VWR (UK). Lithium bromide (99%) and 2-mercaptoethanol (ME, 99%) were purchased from Acros Organics (UK). Dialysis tubing with molecular weight cut off (MWCO) of 14 kg/mol was purchased from Sigma Aldrich (UK). GPC EasiVial poly(methyl methacrylate) mixed standards and a poly(methyl methacrylate) single standard (72 kg/mol) were procured from Agilent (UK). Deionised H_2O was employed in all experiments. All chemicals were used as received.

3.2.2 Synthesis of PDEGMA-co-PEGMA branched copolymer surfactant by free radical polymerisation

A series of thermoresponsive branched copolymer surfactants (BCSs) were synthesised by free radical polymerisation based on the method reported by Weaver et al.[13-15] In a general synthesis, DEGMA, PEGMA, cross-linker (EGDMA) and chain transfer agent (DDT/HDT/TDT/ME) were dissolved in 190 mL ethanol and bubbled with nitrogen gas. After 1 h of nitrogen purging, an ethanolic solution of AIBN (10 mL) was added to the

solution. The apparatus was set at 70 °C for 48 h for polymerisation to proceed. After 48 h, the synthesised polymer was distilled at 80 °C to remove excess ethanol. The resultant crude polymer was then dissolved in water and transferred to a pre-soaked dialysis bag. The dialysis bag was immersed in a beaker containing de-ionised water for 7 to 10 days and the water was replaced at regular intervals to facilitate the purification process. The resultant polymer solution was subjected to lyophilisation for 48 h to obtain a freeze-dried product. The yields for all the lyophilised polymers were 85 ± 1% (Table 3.1) based on the mass of the initial monomers.

A library of 9 polymers were produced, labelled P1-P9. P1-P3 explored the effect of branching degree by variation of cross-linker in the feed (Table 3.1) and P4-P6 explored the effect of molecular weight by control of initiator/chain transfer agent:monomer ratio (Table 3.1). P7-P9 explored the effect of hydrophobic end group using the feed for P1 (Table 3.1) but switching DDT for TDT (P7), HDT (P8) and ME (P9).

Table 3.1: Reagent quantities for the synthesis of BCS P1-P9.

Sample ID:	DEGMA (mmol)	PEGMA (mmol)	EGDMA (mmol)	DDT (mmol)	AIBN (mmol)	TDT (mmol)	HDT (mmol)	ME (mmol)
P1	174	6	12	12	1.2			
P2	174	6	6	12	1.2			
P3	174	6	0	12	1.2			
P4	174	6	12	8	0.8			
P5	174	6	12	6	0.6			
P6	174	6	12	3	0.3			
P7	174	6	12		1.2	12		
P8	174	6	12		1.2		12	
P9	174	6	12		1.2			12

3.2.3 Characterisation of thermoresponsive BCSs

^{1}H NMR was used to characterise the BCS on Bruker Advance AM 600 NMR instrument using CDCl$_3$ as a solvent at ambient temperature. As an internal standard, the residual solvent peak was used. Delta 5.3.1 NMR software was used to process the data.

The number average molecular weight (M_n) and polydispersity of synthesised BCSs were characterised using an Agilent 1260 Infinity II GPC equipped with a refractive index (RI) detector. The system was equipped with an Agilent Varian PLGel 5 μm mixed D column offering a linear range of molecular weight of 200 – 400 kDa. 0.1% w/v lithium bromide in dimethylformamide was used as the eluent, at a flow rate of 0.8 mL/min with the column temperature set at 30 °C. All samples were prepared in dimethylformamide at a concentration of 2 mg/mL prior to analysis. 20 μL sample was injected to the GPC system and the molecular weight of the BCSs were determined relative to the poly(methyl methacrylate) calibration standards. The samples were analysed in a single replicate.

Dynamic light scattering was conducted on 1 mg/mL BCS samples in deionised water without filtration using a Malvern Nano-ZS instrument from 20-60 °C at 1 °C intervals. The particle hydrodynamic diameter (D$_H$), polydispersity index and scattering intensity were measured at a scattering angle of 173° with a He-Ne laser of wavelength 633 nm. The refractive index was approximated to polystyrene latex (1.6) and the medium used was water. The samples were analysed in a single replicate and were equilibrated before each run with a total of 3 runs per reading.

3.2.4 Emulsion preparation

A series of 1:1 w/w oil in water emulsions were prepared to study the thermoresponsive behaviour by rheology. 2.5 g polymer solutions of 2.5, 5 and 10 wt% were prepared in ice cold water with stirring in a 30 mL glass vial. 2.5 g of dodecane oil phase was added to the polymer solution which was then homogenised for 2 min at 2,400 rpm to obtain a 1:1 w/w oil in water emulsion using a Silverson L4R Heavy Duty Mixer Emulsifier (US). The resulting emulsions were kept undisturbed for 36 h under ambient conditions. Approximately 1.1 g of the water phase separated as the lower phase of the creamed emulsion was withdrawn, and the rheological behaviour of the emulsion cream was studied as a

function of temperature. The approximate oil phase volume in the emulsions studied was 0.57. The oil phase volume (ϕ_{oil}) was calculated by:

$$\varphi_{oil} = \frac{\left(\frac{2.5}{\rho_{oil}}\right)}{\left(\frac{2.5}{\rho_{oil}}\right) + (2.5 - Mass\ Water)}$$

Where "Mass Water" is the mass of the lower phase extracted after creaming. Where ρ_{oil} is the density of the oil (in this case 0.75 g/mL) and 2.5 is individual mass of the oil and water added.

3.2.5 Light microscopy of emulsions

Light microscopy of emulsions was performed with Nikon Eclipse 80i (Nikon, Japan) microscope. A small volume (5 µL) of the emulsion was dropped onto a thin microscopic cover glass, covered with another cover glass and positioned on the mechanical stage. Subsequently, the images were captured.

3.2.6 Rheology of thermoresponsive emulsions

Rheological measurements were performed on an AR 1500ex rheometer (TA instruments, USA) equipped with a Peltier temperature control unit and a 40 mm parallel plate geometry with a specified gap distance of 500-750 µm at an oscillating stress of 1 Pa and frequency of 6.28 rad/s. The change in storage modulus (G') and loss modulus (G") as a function of temperature was recorded and the loss tangent (tan δ) calculated as G"/ G'. Temperature ramps were performed in the range 20 to 60 °C at 1 °C per minute heating/cooling rate. The samples were left for equilibration on rheometer before test. Frequency sweeps were conducted on emulsions stabilised with 10 wt% P1 at 30 and 50 °C between 0.628 and 100 rad/s at a fixed shear strain of 0.1%.

3.2.7 SANS studies on BCS solutions with variation of temperature

SANS experiments were performed on the D22 instrument at the Institut Laue-Langevin (Grenoble, France). The neutron wavelength was 6 Å, the sample-detector distances were

2, 5.6, and 17.6 m, and the collimation distances were 2.8, 8, and 17.6 m, respectively. The detector offset was 300 mm. These settings gave a wave vector range $2.7 \times 10^{-3} \leq q \leq 0.45$ Å^{-1}. Rectangular quartz cuvettes with a thickness of 1 mm were used for all samples. Measurements were performed at 25, 40, and 50 °C with a minimum equilibration time of 15 min prior to sample run. All polymer solutions (P1-6) were prepared at 20 wt% in D_2O prior to measurement. Rheological analysis of these samples was also conducted, using the protocols described above. Data stitching was performed on Igor Pro (Wavemetrics, USA)[19] and data fitting was conducted using SasView 4.2.2. The following factors were fixed to reduce the number of fitting parameters: scale/volume fraction (0.2) and solvent scattering length density, SLD (6.37×10^{-6}Å^{-2}). The remaining parameters were fitted using form factors and structure factors described elsewhere.[20,21] The SLDs of the BCS were calculated from the monomeric unit using the NIST Neutron activation and scattering calculator,[22] and left to float, to account for hydration of the polymers.

The scattering intensity $I(q)$ can be written as follows:

$$I(q) = A(P(q)_A S(q)_A) + BKG$$

where, A is a proportionality constant or "scale", BKG is the background, P(q) is the form factor of the scattering object, and S(q)$_A$ is the corresponding structure factor (when required).

A was set to 0.2, as described above. If more than one scattering object is present, or the objects studied have a hierarchical structure that generates scattering over distinct length scales, the expression can be extended to include further terms:

$$I(q) = A(P(q)_A S(q)_A) + B(P(q)_B) + BKG$$

where, A and B are proportionality constants, BKG is the background, P(q)$_A$ is the form factor for model A, S(q)$_A$ is the corresponding structure factor (when required), and P(q)$_B$ is the form factor for model B.

For the BCS solution data, the majority of data were fitted using the an ellipsoid form factor[20] with either a hard sphere or sticky hard sphere structure factor.[21] When a power law form factor was included, it took the form $I(q) = q^{-4}$ which is characteristic of Porod scattering arising from a sharp interface.[23]

3.3 Results and discussion

3.3.1 Synthesis of thermoresponsive BCS by free radical polymerisation

A modified one-pot synthesis was employed to generate an initial thermoresponsive branched copolymer surfactant (P1), informed by Weaver and co-worker's studies on pH-responsive Engineered Emulsions.[13,14,24] P1 was synthesised using DEGMA as the thermoresponsive unit, PEGMA-950 as the hydrophilic macromonomer, EGDMA as the cross-linker, AIBN as the initiator and DDT as the chain-transfer agent (Figure 3.1i), in ratios guided by previous publications.[25] DEGMA, a monomer which imparts temperature sensitivity with an LCST of 26 °C,[26] is expected to transition from a hydrophilic to a relatively hydrophobic state upon warming that was intended to trigger self-assembly processes leading to gelation. PEGMA, a hydrophilic macromonomer for stabilisation, is expected to preferably be solubilised in the water phase at the liquid-liquid interface and offer steric stabilisation over the measured temperature range. EGDMA is a widely used cross-linker in free radical polymerisation that provides branching in the system. DDT was chosen as a chain transfer agent to interact favourably with the dodecane oil phase due to the hydrophobicity of the C12 alkyl chain and aimed to improve the thermodynamic stability to the emulsion.
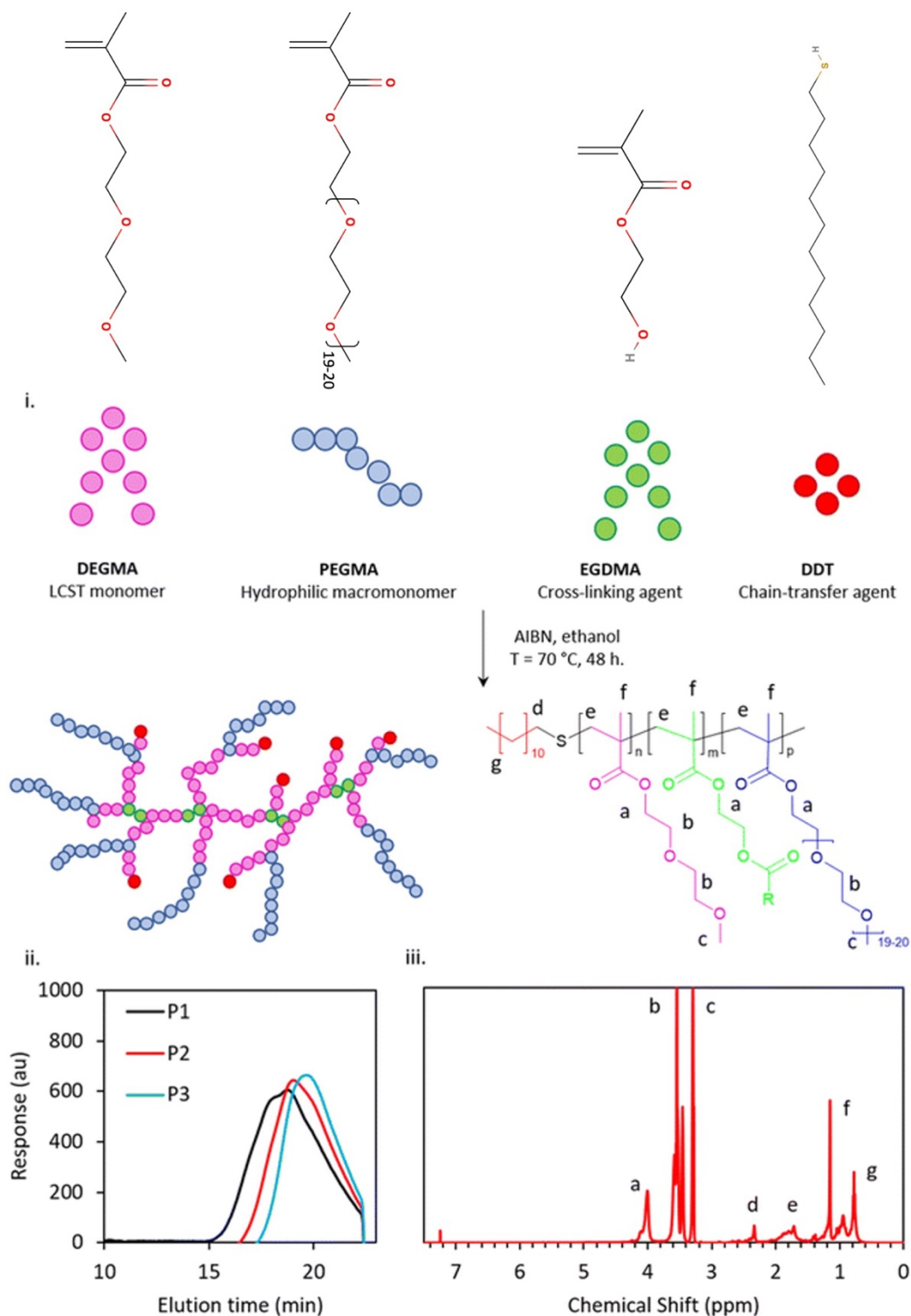
Figure 3.1: Free radical polymerisation of PDEGMA-PEGMA-EGDMA-DDT and theoretical structure of the branched copolymer surfactant (BCS) (i), exemplar GPC chromatogram of P1-3 (ii) and exemplar ¹H NMR spectrum (iii).

Following the synthesis of P1, a library of thermoresponsive BCSs were synthesised by varying composition of cross-linker, molecular weight and chain-transfer agents of longer and shorter carbon chain lengths, relative to P1, with the overall aim of linking polymer architecture to emulsion behaviour (Table 3.2). The successful synthesis of these copolymers was confirmed by GPC (Figure 3.1ii) and ^{1}H NMR (Figure 3.1iii, Figure A1 – A9 in appendix). P2 and P3 were based on the initial synthesis (i.e., P1) with half the quantity of crosslinker (EGDMA) and with no cross-linker, i.e., 6 and 0 mmol respectively, with the intention of exploring the effect, and necessity, of branching. P4, P5 and P6 were variations of P1 with reduced levels of initiator (AIBN) and chain-transfer agent (DDT) at 0.8/8 mmol AIBN/DDT, 0.6/6 mmol AIBN/DDT and 0.4/4 mmol AIBN/DDT, respectively. As chains may be propagated from either AIBN-derived radicals or those transferred to DDT, a reduction in the quantity of these elements whilst retaining their ratio offers control of molecular weight by increasing the average degree of polymerisation per chain. P7, P8 and P9 were synthesised with varying carbon chain length of the chain transfer-agents whilst keeping the composition of DEGMA, PEGMA and EGDMA constant as per P1. P7, P8 and P9 were synthesised with TDT, HDT and mercaptoethanol respectively, giving chain ends of C-14, C-16, and a "zero-length" ethyl alcohol group. This series evaluates the impact of the polymer chain-end hydrophobicity on the branched copolymer's aqueous solution characteristics, as well as explores behaviour without hydrophobic termini (P9).

The ^{1}H NMR spectra (Figure 3.1iii) confirmed the polymerisation of branched copolymers with no evidence of vinylic protons in the 6-7 ppm region (P1-P9 spectra given in the appendix). ^{1}H NMR of the crude product (Figure A15 – A18 in appendix) of the reactions indicated that the reactions achieved > 98% conversion of monomer in all cases and after purification > 85 % yield was obtained. The reactivity ratios of DEGMA and PEGMA are ca 0.3-0.6 and 3.1-1.7, respectively, and a gradient structure in the monomer sequence distribution throughout the BCS is likely.[27] Given the chemical similarity of PEGMA, DEGMA, and EGDMA, quantification of branching was not possible by ^{1}H NMR and the BCS are assumed to follow the composition driven by the feed mixture given the high conversions. GPC was employed to determine molecular weights and polydispersity indices (PDIs) of the BCSs, as well as confirming that distributions were monomodal. Indeed, GPC chromatograms (exemplar data in Figure 3.1ii, full data in Figure A19 in

appendix) for all the polymers P1 to P9 displayed monomodal distribution of molecular weight. The GPC data recorded for such complex and amphiphilic architectures are likely to deviate from the true values of molecular weight.[28] As such, recorded molecular weight parameters are not absolute, but expressed relative to PMMA standards, they do indicate that the polymerisations were successful, followed expected trends, and allow the determination of polydispersity indices (Đ). The polymers exhibited consistent and systematic compositional variation throughout the series.

Table 3.2: Composition of thermoresponsive BCSs and their characterisation by GPC

Study	Sample	Composition / Variable	M_n (kg/mol)	Mw (kg/mol)	Đ
Effect of architecture & crosslinker	P1	Full cross-linker (12 mmol)	8.2	18.5	2.3
	P2	Half cross-linker (6 mmol)	6.5	11.3	1.7
	P3	No cross-linker (0 mmol)	5.4	7.9	1.5
Effect of molecular weight	P4	0.8/8 mmol AIBN/DDT	10.8	33.0	3.1
	P5	0.6/6 mmol AIBN/DDT	14.1	68.3	4.8
	P6	0.4/4 mmol AIBN/DDT	21.3	180.9	8.5
Effect of chain-transfer agent (CTA)	P7	Tetradecanethiol (C14)	8.9	23.0	2.6
	P8	Hexadecanethiol (C16)	9.0	23.7	2.6
	P9	Mercaptoethanol (C0)	15.1	28.5	1.9

P1 to P3 evaluates the impact of cross-linker for the thermoresponsive behaviour of the emulsion systems. GPC analyses for the branched copolymers P1, P2 and P3 revealed number average molecular weights (M_n) of 8.2, 6.5 and 5.4 kg/mol, respectively. A decrease in M_n and Đ was observed with lowering cross-linker concentration (Table 3.2) whilst keeping the stoichiometry of the monomer to chain-transfer agent constant. Thus, it is intuitive that P1 with the highest concentration of cross-linker displays the greatest degree of branching and thus the highest molecular weight, with the M_n decreasing as cross-linker is reduced. P4 to P6 demonstrate that M_n may be tailored by AIBN/DDT in the feed. An increase in molecular weight and polydispersity is observed with reduced concentration of chain initiator and chain-transfer agent, allowing clear control over this parameter and granularity between Mn in emulsifiers. P7, P8, P9 are synthesised with varying carbon chain length chain-transfer agents. P7 is synthesised with TDT (C14), P8 with HDT (C16) and P9 with ME (C0). Comparing P9 (i.e., synthesis with ME) with P7 and P8, an apparent increase in M_n is observed, although ME has a shorter carbon chain length than DDT. This is attributed to the hydrophobic P7 and P8 interacting with column packing to increase elution time and reducing apparent M_n.[28] GPC analysis of BCS systems likely underestimates molecular weight where branched copolymers of this type are expected to have a compact structure of lower solvodynamic volume relative to their molecular weight than the linear systems.[29]

All BCS were capable of stabilising dodecane-in-water emulsions, giving rise to a creamed phase which was isolated and used in all further experiments. P1 demonstrated temperature-induced gelation, which could be macroscopically observed by heating of the sample followed by tilting the vial and allowing gravitational force to act on the material (Figure 3.2). When heated, the sample did not flow after vial inversion. Microscopy confirmed the presence of dodecane droplets within the emulsions at a high internal oil phase volume (ϕ = 0.57). Droplet size analysis by light microscopy (Figure A20 in appendix) revealed mean droplet radii between 7.5 and 11 μm, which gave rise to comparable levels of creaming between emulsions.
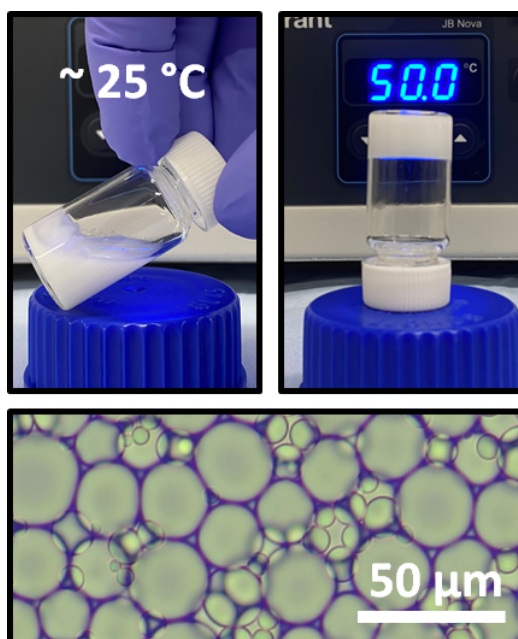
Figure 3.2: Dodecane-in-water emulsions stabilised by P1 BCS flow under the effect of gravity at room temperature but transition to a rigid gel state upon heating (top). Microscopy confirms the presence of oil droplets (bottom).

3.3.2 Effect of polymer branching on thermoresponse of BCS-stabilised emulsions

Rheology was used to measure temperature-induced changes in viscoelasticity of the creamed phase of BCS-stabilised emulsions. Viscoelasticity of the emulsions is characterised by the storage (or "elastic") modulus (G') and loss (or "viscous") modulus (G") with temperature. The emulsions behave as "solid-like" when G'>G" and "liquid-like" when G'<G". The ratio G"/ G' is defined as tan δ and allows quantification of the relative contributions of these factors to the overall resistance to deformation. In this work, the intersection of the G' and G", giving tan δ < 1, is considered as the gel point.
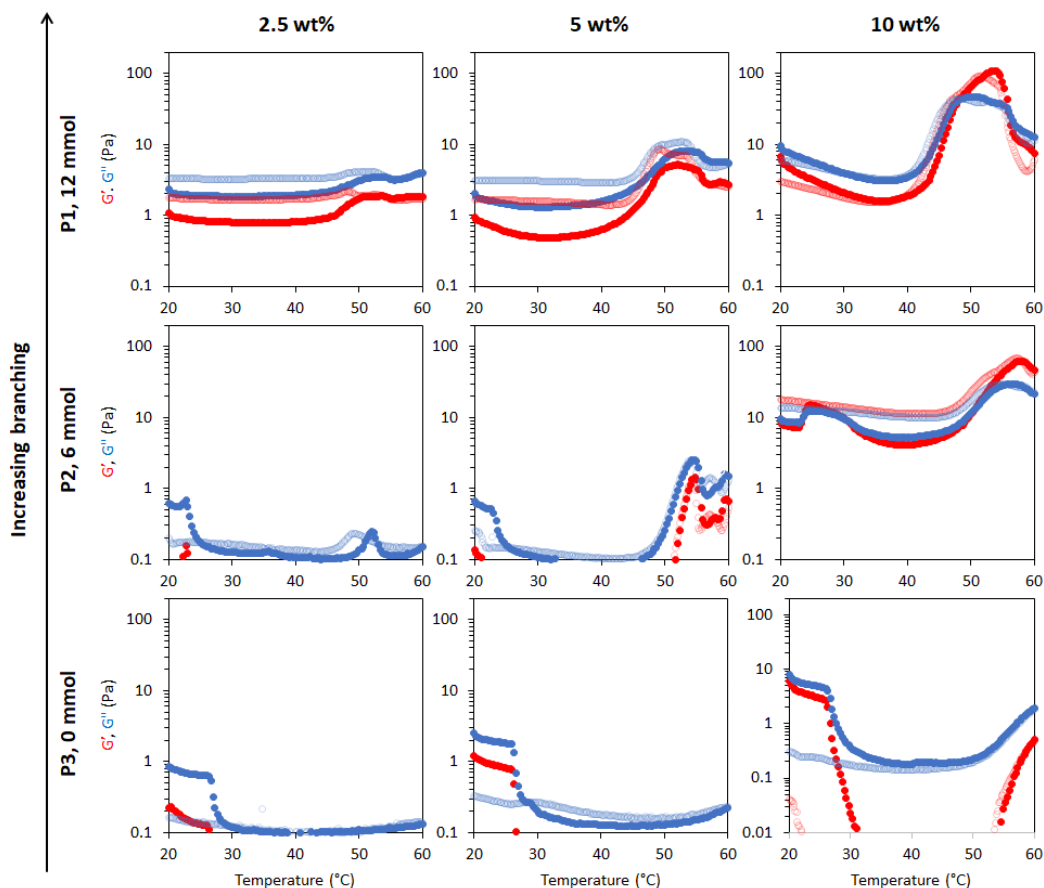
Figure 3.3: Rheological behaviour of emulsions stabilised by thermoresponsive BCSs where P1 is the sample with "full cross-linker", P2 is with "half cross-linker" and P3 has no cross-linker. Emulsions were explored at 2.5, 5 and 10 wt% polymer concentration. G' is shown in red and G" is shown in blue. Dark colours show the 'up' heating ramp whilst light colours show the subsequent 'down' cooling ramp. The Y-axis scales were chosen to enable better comparison of the different emulsion systems. Full rheograms showing the Y-axis region < 0.1 Pa are shown in Figure A21.

BCS concentration had a large effect on emulsion behaviour with temperature (Figure 3.3). For the P1 system with the highest branching degree, all emulsions showed evidence of thermoresponse. At 2.5 wt% polymer concentration, a slight rise in G' and G" was observed at 45 °C, which represents an overall increase in viscosity, and was termed "thermo-thickening" behaviour. However, gelation, defined as a point where G' exceeds G", did not occur. A similar behaviour was observed with a polymer concentration of 5 wt% where the temperature-induced thickening behaviour started at approximately 40 °C, which increased with temperature up to 55 °C, however the emulsion again remained

predominantly liquid-like at all temperatures (G''>G'). The magnitude of G' and G'' increase with temperature was greater in the 5 wt% emulsion than in the 2.5 wt% system. For emulsion systems with 10 wt% polymer concentration, a significant rise in G' and G'' was observed at 40 °C followed by a cross-over point (i.e., when solid-like behaviour was first observed, as G' > G'') at ca 48 °C, defined as the gelation temperature (T_{gel}). This T_{gel} is believed to correspond to the establishment of an inter-droplet percolating gel-network, as hypothesised in prior studies on responsive emulsions.[13,14,17] As aggregation progresses, both G' and G'' increased up to 55 °C, which coincided with a minima for tan δ, indicating a point of maximum relative elasticity (Figure A22 in appendix). Beyond this temperature, the network giving rise to the gel state appeared to break down, due to a reduction in both G' and G'' and elevation of tan δ. Thus, the region 40-55 °C is associated with the formation of an elastic structure due to an LCST-induced alteration in BCS hydrophilicity, whereas the region >55 °C is associated with the loss of elastically-active interactions.

This study showed that the polymer concentration is an important factor that could be manipulated in an emulsion system to increase the thermal response and/or trigger thermo-gelation. Indeed, the high concentrations required for gelation suggest that the polymer is likely to be spatially distributed both at the droplet interface and in the bulk in order to enable the formation of a percolating network. All systems demonstrated reversibility of the rheological transitions, which is desirable to retain functionality after heating/cooling, barring the small increase in viscosity (G'') noticeable in the "down" curve of the P1 emulsions at 2.5 and 5 %w/w. Overall, the results obtained with P1-emulsions demonstrate that the polymerisation of DEGMA, which present a LCST, and the hydrophilic macromonomer PEGMA in the BCS architecture produce the desired thermoreversible gelation behaviour.

The viscoelastic nature of the emulsions stabilised with 10 wt% P1 was further probed by rheology frequency sweeps both sides of the transition, at 30 and 50 °C (Figure 3.4). At 30 °C, the system behaved as a viscoelastic liquid exhibiting Maxwell-type behaviour with a cross-over at 16 rad/s, giving a relaxation time of ca. 0.06 s. When heated above T_{gel} to 50 °C the materials exhibited classic gel-like behaviour with G' > G'' over the range of frequencies measured.[30]
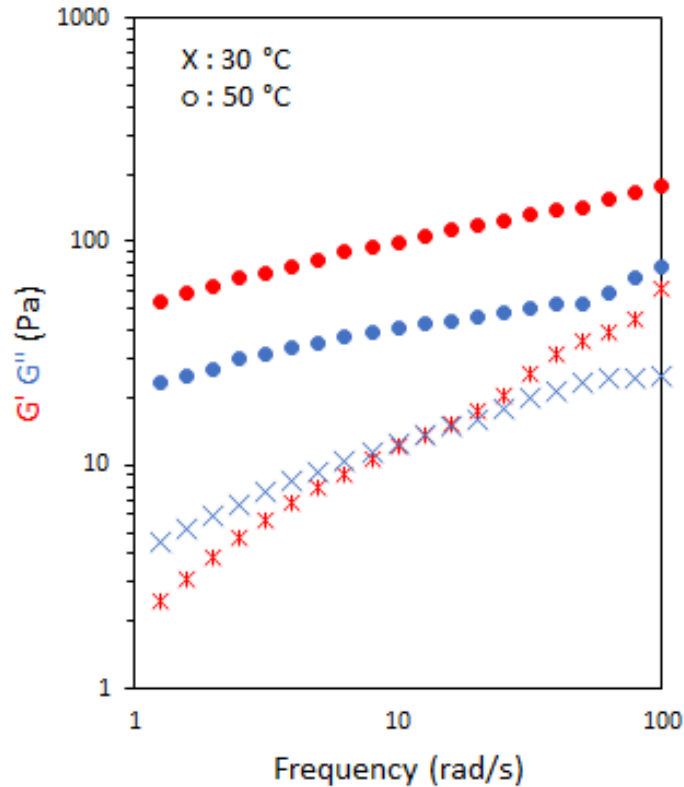
Figure 3.4: Frequency sweeps of emulsions stabilised with 10 wt% P1. G' is shown in red and G'' is shown in blue.

Variation of EGDMA in the monomer feed allowed control of branching and its exploration as a factor in emulsion thermoresponse. P1 is the most highly branched, followed by P2, while P3 has no branching (Table 3.1). In different systems, the cross-linker to monomer ratio allowed tuning of the LCST, polymer size and colloidal stability[31,32], and thus was hypothesised to affect BCS performance. As discussed above, thermoresponsive emulsions stabilised by P1 ("full cross-linker") showed thermo-thickening behaviour at 2.5 and 5 wt% and thermoreversible gelation at a concentration of 10 wt%. The rheology of the emulsions stabilised by the BCS synthesised with half the quantity of cross-linker (P2) was assessed at the same polymer concentrations (Figure 3.3). With 2.5 wt% BCS, emulsion thinning was observed at 23 °C which was stable up to 47 °C and a small rise in G'' was then observed at 50 °C. A similar behaviour was observed with 5 wt% polymer, however, the increase seen in G' and G'' observed at 47 °C was greater in magnitude. Beyond this point, both moduli collapsed. Emulsions stabilised at 10 wt% polymer

concentration showed two thermal events, which occurred at 25 and 50 °C. A second event of thermo-thickening was observed with a rise in temperature to 40 °C, with T_{gel} occurring at 50 °C. The gel state was then stable up to 60 °C, the highest temperature assessed.

The P3 construct contains no cross-linker and is expected to have a linear structure of PDEGMA-co-PEGMA with dodecyl chain ends. Temperature-induced thinning was observed at 25 °C and no sign of thickening behaviour was observed up to 60 °C. A gradual increase in polymer concentration from 2.5 to 5 and 10 wt% did not lead to any significant change to the thermal response. Considering the evolution of tan δ with temperature shows that whilst P1 and P2 achieved a transition to a predominantly elastic state, P3 reduced its elasticity during a heating cycle (Figure A13 in appendix). This indicates that the presence of cross-linker to form the BCSs, and therefore a branched structure, is essential to produce a thermal response of the emulsions. This finding is consistent with Weaver and co-workers' study of engineered emulsions, who attributed the pH-triggered gelation to the presence of multiple hydrophobic DDT domains per polymer chain in the branched systems, allowing stronger tethering to the oil phase, and ultimately the ability to form elastically active bridges between emulsion droplets.[14,33]

Small-angle neutron scattering measurements were performed on BCS solutions to explore the thermal behaviour of the polymers, with the aim to shed light on the mechanisms underlying the thermoresponsive behaviour of the engineered emulsion systems. Three temperatures were investigated to capture the behavior across the gelation process, namely: 25, 40 and 50 °C, where 25 °C lies below the LCST, 40°C around the expected onset of transition and 50°C above the transition. 20 %w/v solutions were explored for each temperature, which is equivalent to the aqueous phase used in the generation of 10 wt% emulsion systems. The data were fitted with the combination of form factors, P(q), and a structure factor, S(q). The form factor describes the morphology of the scattering objects and the structure factor accounts for interactions between the particles. Form factors used to fit the data were ellipsoids (El), associated with a power law (PL) where needed, whilst a hard sphere (HS) or a sticky hard sphere (SHS) structure factor were required to account for interactions.
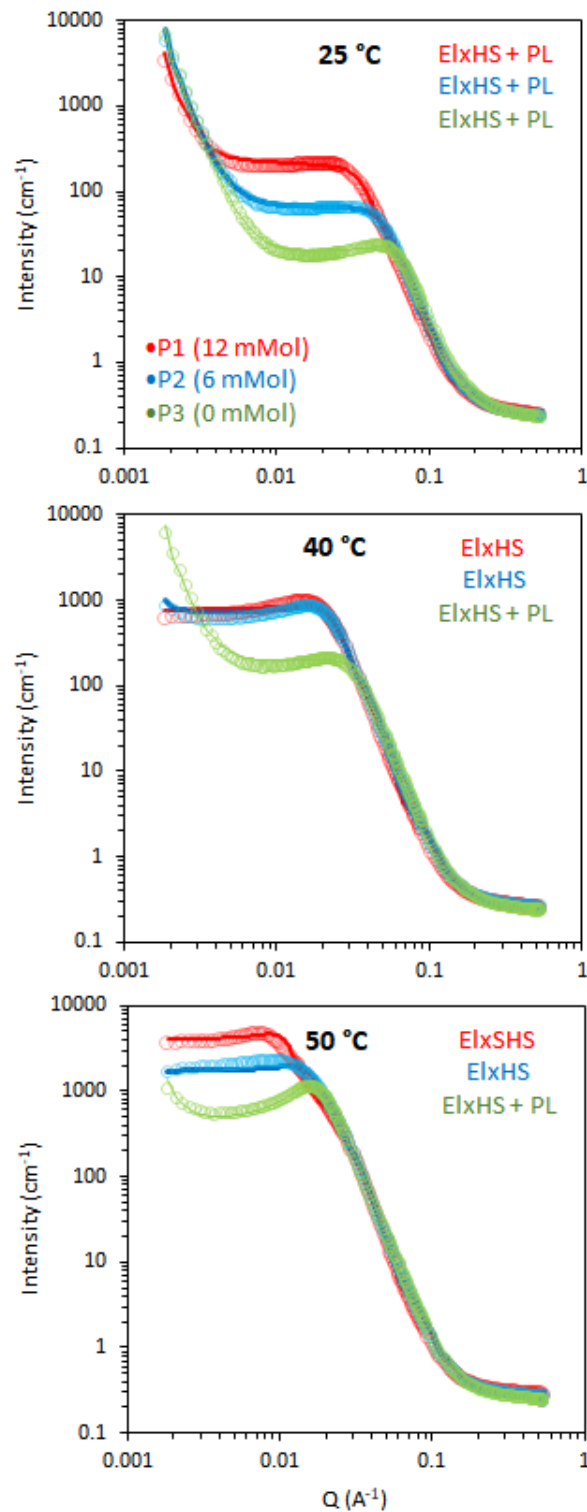
Figure 3.5: SANS data (circles) with fits (lines) of 20 wt% BCS solutions in D$_2$O with variation of cross-linking measured at 25, 40 and 50 °C temperature. Legend inset shows sample ID and cross-linker feed. Models used to fit data are inserted at the top right. El is an ellipsoid

form factor, HS and SHS are hard sphere and sticky hard sphere structure factors, respectively, whilst x and + are mathematical operators. PL is a power law with a q^{-4} decay.

Initially, the BCS series exploring branching density (P1, P2, P3) was examined by SANS. This series had cross-linker feed at 12, 6, and 0 mmol, for P1, P2, and P3, respectively (Figure 3.5). At 25 °C (below the LCST), the 20% w/v solutions were best described by an ellipsoid form factor with a polar radius greater than equatorial radius, indicating an oblate spheroid (Figure 3.6). Fitting was attempted with spherical and prolate spheroid models, but adequate fits could not be achieved. Cylinder form factors resulted in disk-like objects of large radii and short length, giving poorer fits than the oblate spheroids. The fitting required a contribution from a hard-sphere structure factor in most instances. A power-law form factor was also required to fit the low q region, and attributed to large aggregates or clusters of polymer, as observed in many polymer systems, for example PEO homopolymers.[34] The precise nature of these objects cannot be determined reasonably within this q range but fit to a q^{-4} decay, indicative of a sharp interface. Upon warming to 40 and 50 °C, the oblate ellipsoid model gave strong fits to the data but the power law contribution was greatly reduced and was no longer required to fit the data in the branched systems (P1, P2), which can be interpreted as a reduced fraction of polymer chains in solution giving rise to this clustering.

In the absence of steric constraints, surfactant molecules tend to form spherical micelles, however, it is known that depending on surfactant structure other micellar shapes with lower curvature can be attained.[35] In particular, when the tail-group of the surfactant is large compared the head-group, the surfactant will tend to form anisotropic structures such as cylinders, ellipsoids, or lamellae, based on the "critical packing parameter".[36] This theory has also been applied with great success to block copolymers.[37] In the BCS reported here, it may be hypothesised that, particularly above the LCST, the volume of the "hydrophobic" moieties (DEGMA above the LCST and DDT chain-ends) will be large relative to the PEG headgroups, given the excess DEGMA in the feed, which may prevent the formation of spherical micelles. Furthermore, given the presence of multiple DDT chain ends per BCS and steric constraints from the branched structure, it is plausible that the macromolecules cannot take a spherical conformation and instead tend towards objects of lower curvature, such as these oblate ellipsoids.

The dimensions of the oblate ellipsoidal (equatorial radius > polar radius) aggregates formed by P1-P3 solutions are given in Figure 3.6. Strikingly, all ellipsoids increase in dimensions with heating and P1 becomes increasingly oblate. For example, P1 has an elliptical form which upon heating increases approximately 11.5-fold in volume and becomes more disk-like in shape, with the ratio of equatorial to polar radius increasing from 3.5 to 6.3 (Figure 3.6b). Whilst P1-P3 have similar polar radii, the equatorial radii are greatly increased with branching, indicating an increased oblate character in the order P1>P2>P3. This is likely the result of the greater restrictions on acquiring high curvature as branching is introduced. For example, P3 at 25 °C has the lowest degree of ellipsoidal character and could be fitted as a polydisperse sphere but was kept as an ellipsoid for consistency.
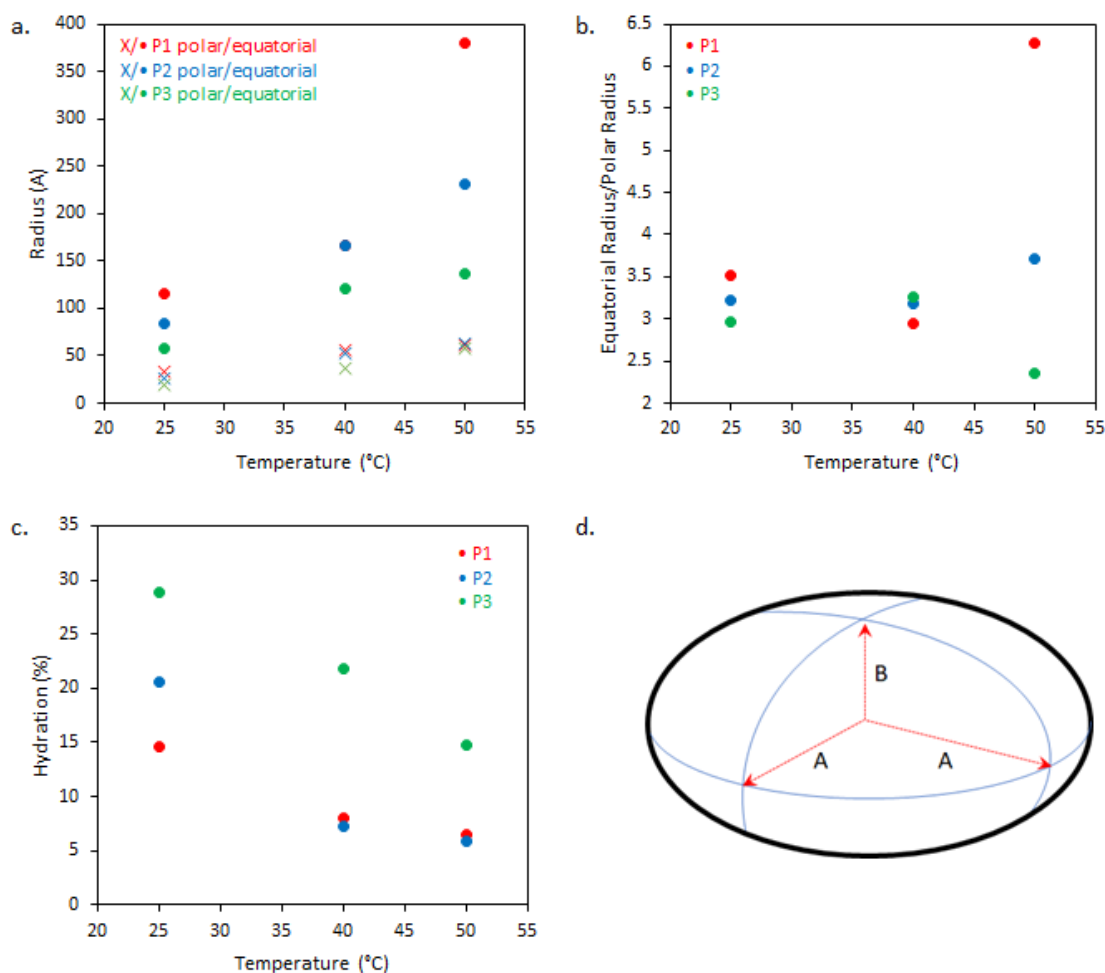
Figure 3.6: a) Dimensions of BCS ellipsoidal aggregates with variation of cross-linking and temperature, derived from SANS fitting, b) the ratio of equatorial to polar radii, and c) degree of hydration of BCS particles estimated from SLD values obtained from the fits. d)

shows the geometric structure of an ellipsoid where A and B are the equatorial and polar radii, respectively. When A>B the ellipsoid is oblate.

Furthermore, the systems appear to become increasingly dehydrated as they are heated. Hydration of the BCS aggregates was estimated using SLD values from the fits against SLD values calculated for pure DEGMA ($0.620\times10^{-6}Å^{-2}$)[22] and D_2O ($6.37\times10^{-6}Å^{-2}$). Figure 3.6 shows that all BCS aggregates become increasingly dehydrated with heating. This is consistent with the thermoresponsive DEGMA component undergoing a desolvation when heated above the LCST and expelling D_2O. Given the potentially counterintuitive combination of particle growth and desolvation, the hypothesised process occurring during heating is the association of ellipsoidal species as DEGMA desolvates, resulting in growth. P1 and P2 show a lower extent of hydration than P3, which is attributed to the dense branching structure hindering solvation of the inner moieties of the BCS.

Overall, the BCS formed ellipsoids which became less solvated with temperature. The nature of thermothickening (P1, P2) vs thermothinning (P3) (Figure 3.3) from this data may be prescribed to the differing nature of aggregates, with P1 and P2 forming larger, more oblate, aggregates facilitating jamming and connectivity in the system. Indeed, P1 at 50 °C, which gave the strongest gel-like response, was fitted to a sticky hard-sphere structure factor, indicative of inter-ellipsoid attractions. Obviously, an additional key factor in gel formation observed when emulsions are formulated with the BCSs which cannot be observed from SANS of the polymer solutions is the interfacial behaviour of the BCS at the oil/water interface. It has previously been postulated that pH-responsive BCS exhibited multiple tethering points to oil droplets when a branched structure with multiple dodecyl- chain ends was present.[25] This strength of tethering to the oil phase could be essential to enabling droplet-droplet connectivity to achieve gel formation, providing a rationale for the thermothickening behavior of the branched (P1,P2) vs non-branched (P3) polymers, given that the branched (P1,P2) systems have multiple hydrophobic chain ends per macromolecule.

3.3.3 Effect of polymer molecular weight on the rheology of BCS-stabilised emulsions

The effect of molecular weight on the rheological behaviour of thermoresponsive emulsions was then studied. Figure 3.7 shows the rheology of thermoresponsive emulsions stabilised with P1, P4, P5 and P6 (increasing M_n, Table 3.2) at concentrations 2.5, 5 and 10 %w/w. The rheological behaviour of P1 was discussed above, and this data is included as a reference point. At 2.5 wt%, the rheological behaviour of emulsions stabilised with P4, P5 and P6 did not show clear differences with P1, with weak thermal response. The thermo-thickening was enhanced relative to P1 at 5 wt% for emulsions stabilised with P4, however, gelation did not occur (G' < G''). Emulsions stabilised with 5 wt% P5 demonstrated a T_{gel} at ca. 45 °C. However, this gel was not stable over a broad range of temperatures, breaking down at 50 °C. Similarly, the emulsion stabilised with the highest molecular weight polymer, P6, at 5 wt% exhibited a T_{gel} at 45 °C, with the gel phase extending up to 55 °C. Thus, larger molecular weights appear to favour gel formation, shifting the concentrations required for gelation to lower values, as well as displaying higher moduli. This effect may be attributed in part to longer polymer chains being more likely to form physical connections with other polymer chains. With an increase in polymer concentration to 10 wt%, the emulsions stabilised with P4, P5, and P6 exhibited a T_{gel} at 46, 45, and 40 °C and showed a similar thermo-reversible behaviour while cooling. Moreover, the gel region extended up to the highest temperature assayed, 60 °C. This effect is clearly seen in the value of tan δ with temperature (Figure A13 in appendix). The storage moduli (G') of P5 and P6 is ca ten-fold greater in the gel state (up to ca 300 Pa) than the previously reported PNIPAM BCS systems (ca 30 Pa).[17] Furthermore, the onset of thickening for these two constructs was ca 35 °C, such that hardening could be triggered upon exposure to the body's heat, which is advantageous for drug delivery.[38] Thus, this new blueprint for BCS is able to generate materials with much more appropriate thermoresponsive properties for applications requiring resistance to shear, such as drug delivery to topical sites or depot injections.
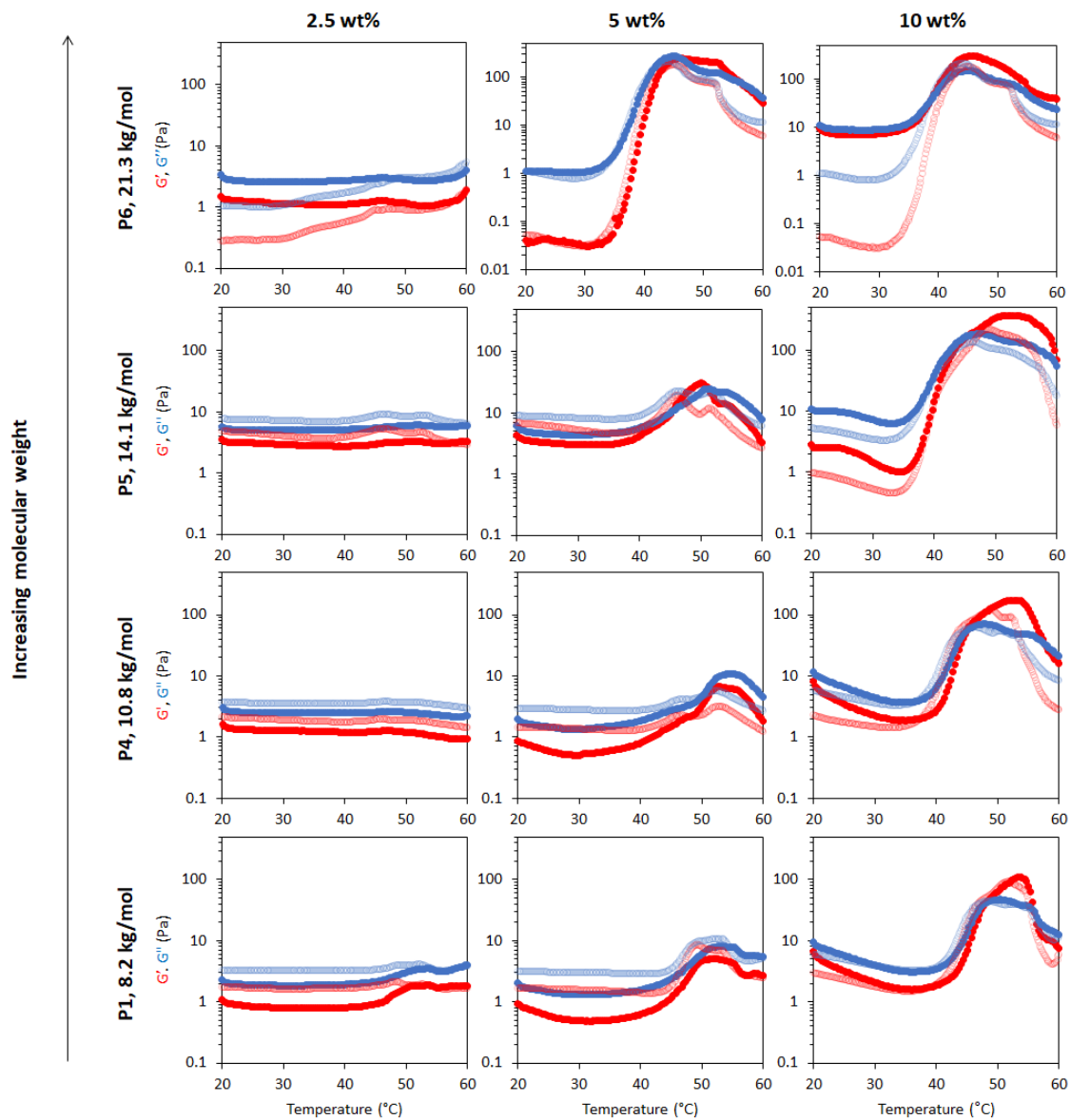
Figure 3.7: Effect of molecular weight and polymer concentration on thermoresponse of emulsions stabilised with BCSs. The molecular weight of BCSs follows: P1<P4<P5<P6. G′ is shown in red and G″ is shown in blue. Dark colours show the 'up' heating ramp whilst light colours show the subsequent 'down' cooling ramp. Full rheograms showing the Y-axis region < 0.1 Pa for P6 at 5 and 10 wt% are shown in Figure A23.
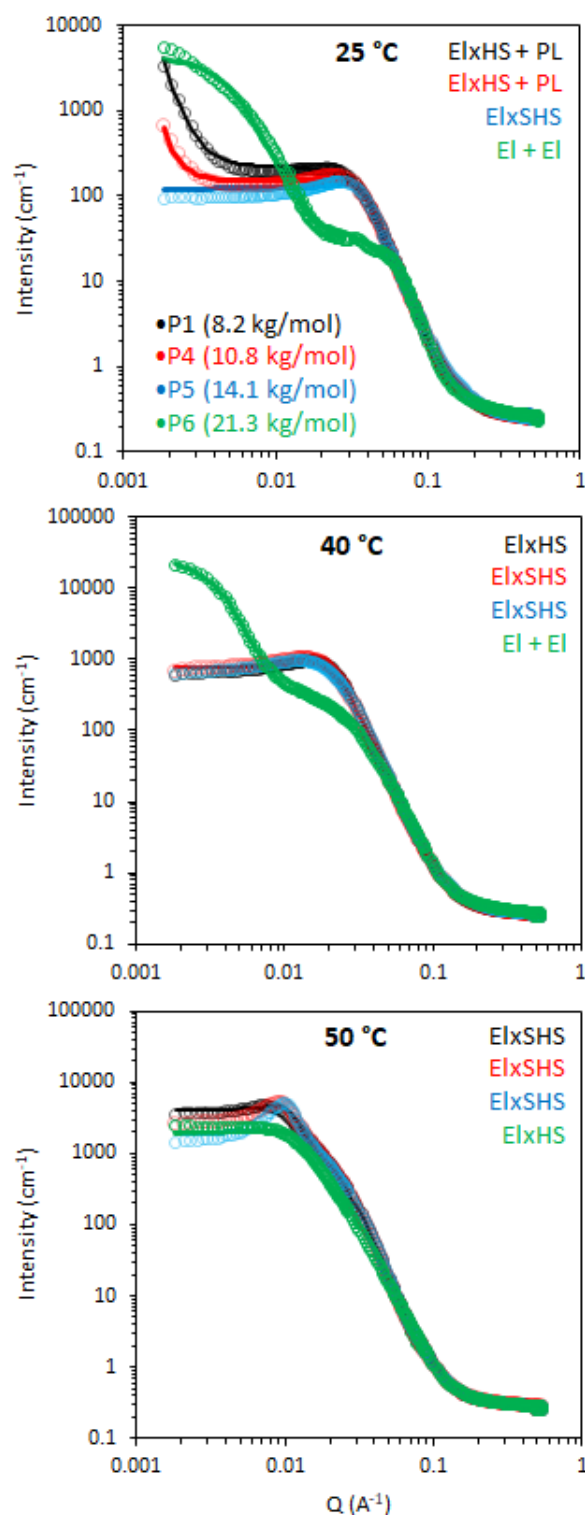
Figure 3.8: SANS data (circles) with fits (lines) of 20 wt% BCS solutions in D_2O with constructs of varying molecular weight and temperature. Legend inset with sample id and M_n determined by GPC. Models used to fit data are inserted top right. El is an ellipsoid form factor, HS and SHS are hard sphere and sticky hard sphere structure factors, respectively, whilst x and + are mathematical operators. PL is a power law with a q^{-4} decay.

The effect of molecular weight of BCSs on the nanostructures they form in solution was then evaluated by SANS (Figure 3.8). This series explored M_n at 7.7, 10.5, 13.6, and 20.6 for P1, P4, P5, and P6, respectively. It is worth noting that polydispersity also increased with M_n (Table 3.2). At 25 °C, the P4 data could again be fitted to ellipsoids with a power law contribution, however the power law was not needed with P5. Once samples were heated to 40 and 50 °C, SANS data for P1, P4 and P5 showed only subtle variations in structure, in-line with their comparable rheology at these temperatures. Parameters extracted from the fits reflect this, with only small deviations in hydration and aggregate dimensions (Figure 3.9). SANS analysis of P6 solutions instead showed vastly different scattering profiles, which were tentatively assigned to multiple ellipsoids at 25 and 40 °C, before forming an ellipsoid of equivalent dimensions to the other M_n samples at 50 °C, without the need however for a structure factor. The presence of multiple objects in P6 solutions is likely a result of its high polydispersity (Đ = 8.8). Overall, these SANS experiments with varying M_n BCS reproducibly demonstrate the presence of oblate ellipsoids at high temperatures, amenable to a gel state.
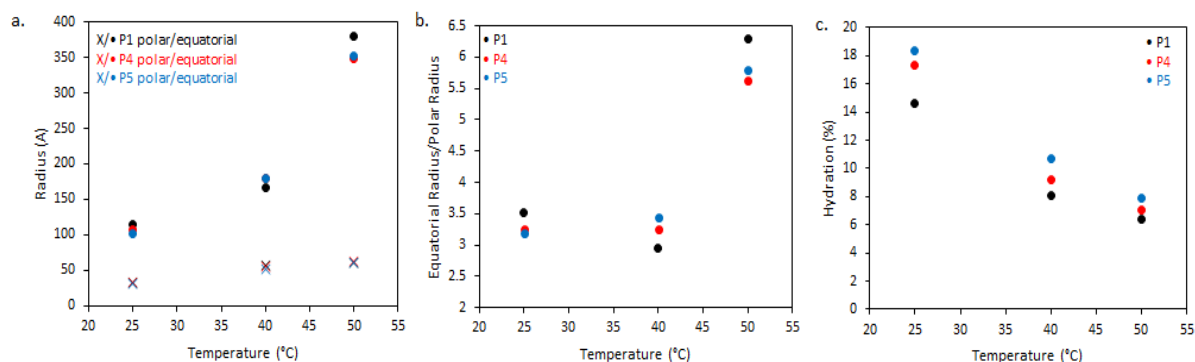

Figure 3.9: a) Dimensions of BCS ellipsoidal aggregates with variation of M_n and temperature, derived from SANS fitting, b) ratio of equatorial to polar radii, and c) degree of hydration of BCS particles estimated from the values of the SLDs returned by the fits. The parameters for P6 are omitted due to the different approach to fitting used and the presence of multiple species in solution.

### 3.3.4 Effect of chain-transfer agent (CTA)

The effect of the polymer chain end hydrophobicity on the thermoresponsive behaviour of the emulsions was studied. P1, P7 and P8 were synthesised with mercaptoalkanes comprising of C12, C14 and C16 carbon chain lengths, leading to hydrophobic tails on the BCS. BCS P9 was synthesised with mercaptoethanol as a CTA to generate a "zero-length" chain end with 2-hydroxyethyl- functionality, which is expected to be hydrophilic. Emulsions prepared with hydrophilic and hydrophobic thiols as CTAs at different polymer concentrations provided an insight on the thermoresponsive activity as shown in Figure 3.10.

The thermoresponsive activity of emulsions at 2.5 wt% polymer concentration P1, P7, P8 and P9 showed a very weak response and were comparable. At 5 wt% polymeric concentration, thermo-thickening was enhanced with P7 and P8 compared to P1. T_{gel} occurred at 50 °C, however this gel state was only stable over a narrow temperature range. Similarly, emulsions stabilised with 10 wt% P7 showed thermo-thickening but no gelation. The thermoresponsive behaviour of emulsions stabilised with P8 resembled P1 with gelation occurring at ca. 47 °C, however, the gel phase was unstable beyond 55 °C. The rheology of the emulsions stabilised with P9 (Figure 3.10) demonstrated that hydrophobic CTA is necessary for thermoresponsive activity. It was observed that P9 stabilised the emulsions despite a lack of hydrophobic tails, forming emulsions at various polymer concentrations of 2.5, 5 and 10 wt%, but demonstrating a weak thermoresponse. Analysis of tan δ indicated that the material had some degree of elasticity at low temperatures (tan δ ≈ 1) but became increasingly liquid-like when heated up. The rheology data suggested that the CTAs exert control over the thermo-thickening behaviour of the emulsions because these hydrophobic alkyl groups with strong interaction with the oil phase are required for gelation to occur.
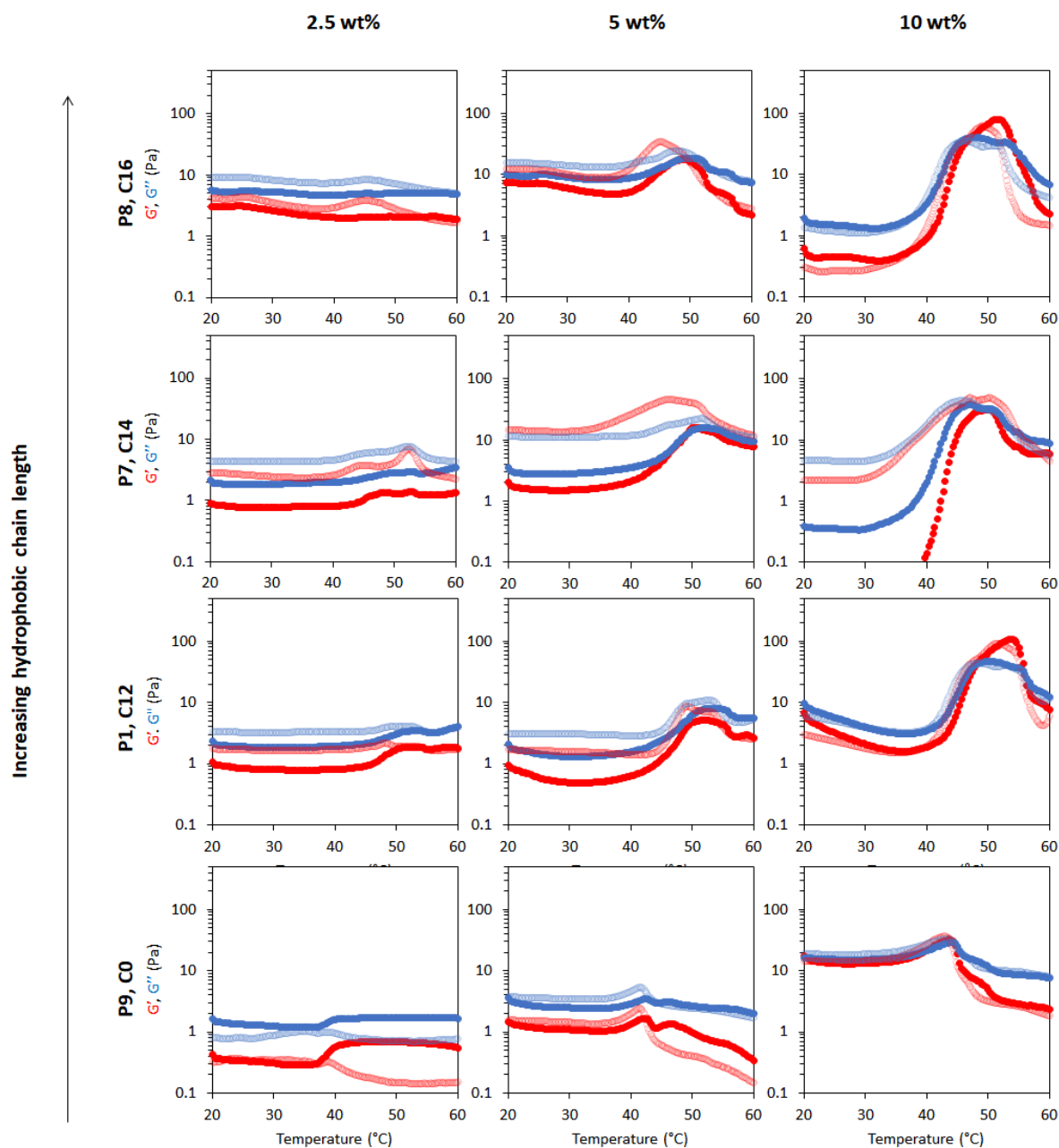
Figure 3.10: Effect of hydrophobic alkyl tail length on thermo-gelation activity of emulsions as determined by a rheology temperature ramp. P9 is synthesised with mercaptoethnol, P1 with dodecanethiol, P7 with tetradecanethiol and P8 with hexadecanethiol, leading to alkyl chain lengths of 0, 12, 14, and 16 C atoms, respectively. G' is shown in red and G'' is shown in blue. Full rheograms showing the Y-axis region < 0.1 Pa for P7 at 10 wt% are shown in Figure A24.

Dynamic light scattering (Figure 3.11) revealed further differences in self-assembly between the BCS with hydrophobic alkyl groups (P7) and those terminated with -CH_2CH_2-OH (P9). P9 (C0) showed a single, sharp transition at 29 °C, with a sharp increase in scattering, and a large D_H and PDI (270 nm, 0.27 PDI). P7 (C14) scattered light below 25 °C, associated with clusters of polymer (169 nm diameter, 0.09 PDI), before transitioning to smaller aggregates (ca 34 nm, 0.12 PDI, at 30 °C) in the region 27-35 °C. A second transition then occurred above 35 °C, with aggregates of higher D_H (51 nm, 0.07 PDI). In line with SANS, the DLS of P7 evidenced larger aggregates at low temperatures, followed by the formation of well-defined aggregates above the LCST of PDEGMA, which grew with temperature. Without the presence of hydrophobic alkyl groups, P9 (C0) simply underwent a transition from polymer in solution to heterogeneous aggregates.
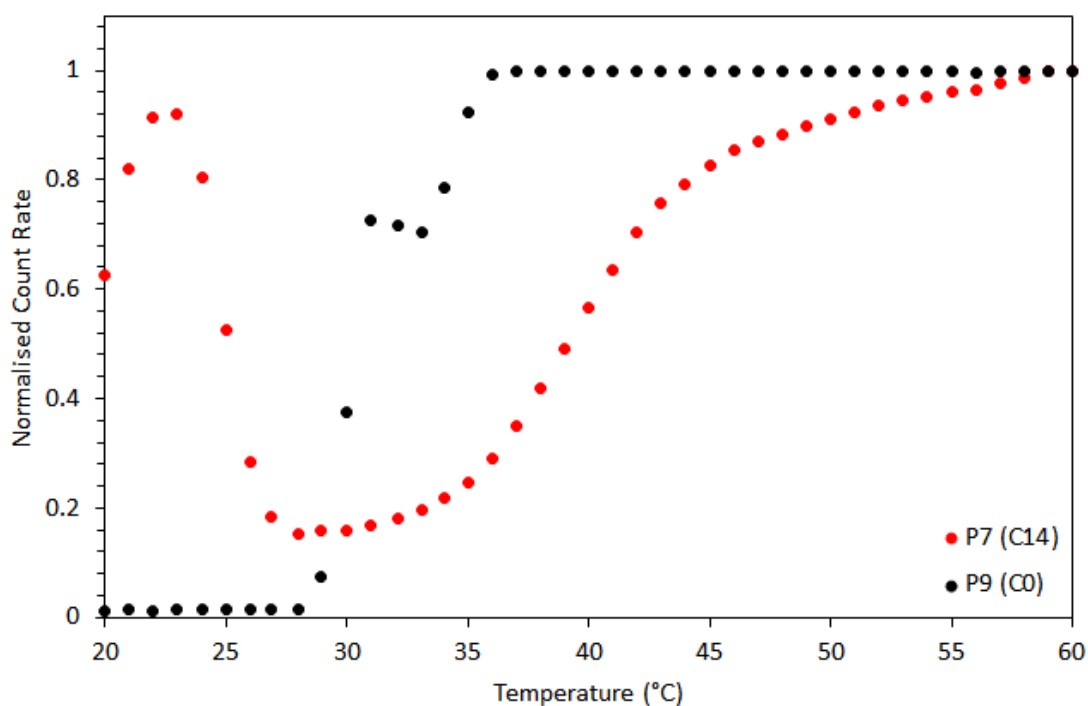
Figure 3.11: Dynamic light scattering (DLS) of P7 (C14) and P9 (C0) solutions showing normalised scattered count rates with temperature.

The rheology of BCS solutions (20 wt%) in D_2O was also studied to probe whether structuration in SANS is associated with rheological changes and if the presence of emulsion droplets is required for network formation (Figure 3.12). This concentration is equivalent to the concentration of polymer expected in the aqueous phase of 10 wt% BCS-stabilised emulsions, assuming all the polymer is in the continuous phase (which is, therefore, an over-estimation since a large amount is likely to be at the interface). All BCS solutions retained thermal transitions which were in accordance with the emulsion's rheology, showing sharp thickening with temperature, except for P9 which has no hydrophobic chain ends and showed a weaker response. However, a notable difference is in the overall liquid-like behaviour of the systems, in which G' never exceeds G'', showing overall a predominantly liquid-like response. Thus, the presence of emulsion droplets is crucial for the formation of a gel network. This connectivity could arise from the interactions of BCS at the oil-water interface with the polymer aggregates in the bulk, acting as junctions to connect droplets, or from interface-interface interactions between droplets, as hypothesised by Weaver et al in their pH-responsive engineered emulsions.[15] The rheology of emulsions does not, however, show thermal gelation at low BCS concentrations (2.5 wt%) which are however sufficient to stabilise the emulsions. In this 2.5 wt% system it is expected that concentration of polymer in the bulk water is low and that presence of the BCS at the O/W interface alone is not sufficient to enable gel formation.
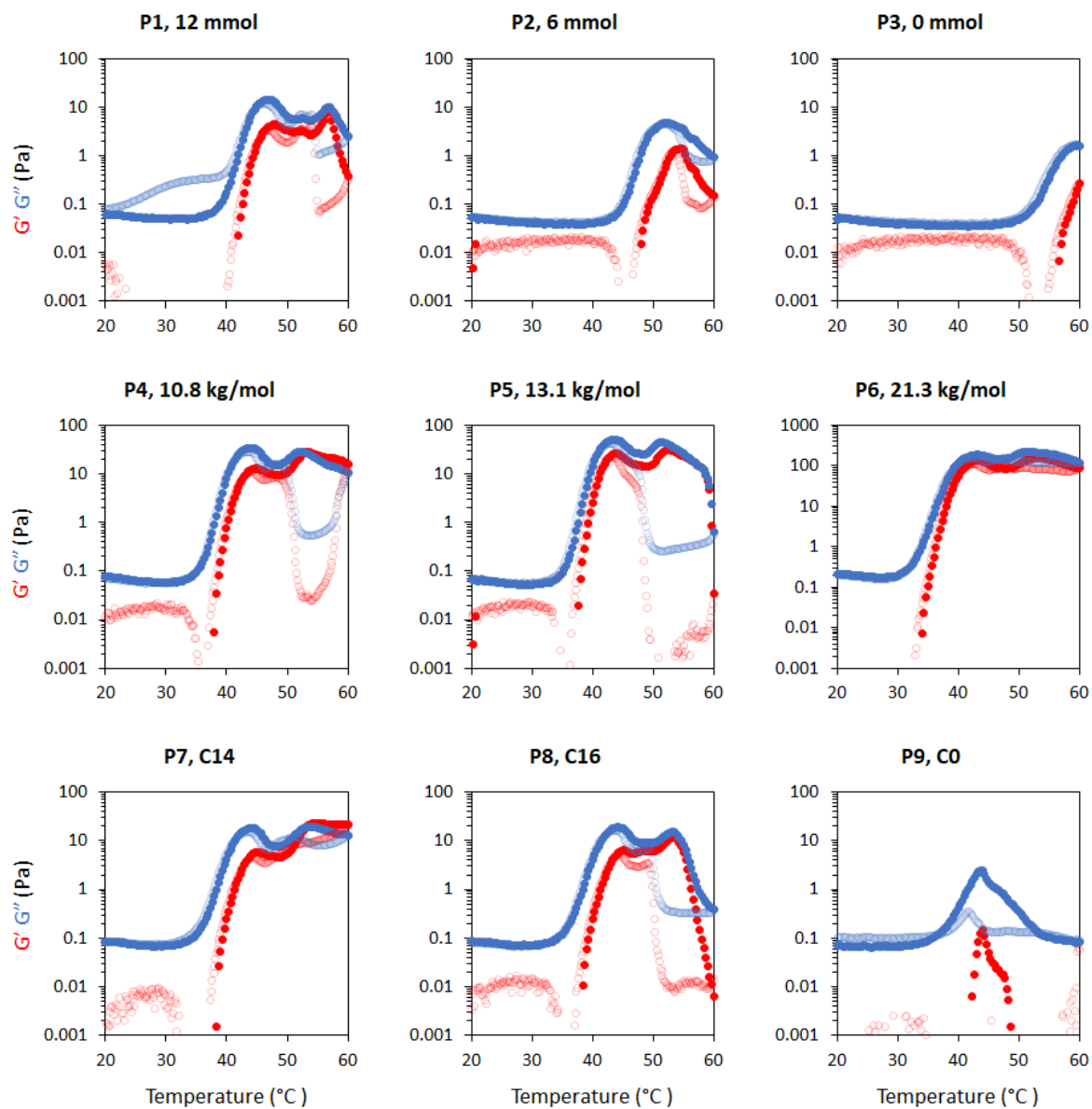
Figure 3.12: Temperature ramp rheology of 20 wt% BCS solutions in D_2O. Filled and open circles show the heating and cooling cycles, respectively.

3.4 Conclusions

This research demonstrated that thermoresponsive engineered emulsions may be generated from branched copolymers of polyDEGMA and PEGMA that act as emulsifiers and trigger gelation. The materials exhibit a sol-gel transition upon warming across a range of concentrations and architectures, generating materials up to ten-times stronger (storage modulus ca. 300 Pa) than the previously reported thermoresponsive engineered emulsions by Da Silva et al.[17] Variation of cross-linker density proves for the first time that a branched structure is required for an effective thermal transition to the gel state, as the phenomenon is "turned off" when non-branched polymers are used to stabilise the emulsions. Increasing the molecular weight of the BCS improves the gel strength (as assessed by the elastic modulus G') and shifts the onset of thickening into a physiologically relevant temperature range (ca 35 °C). Variation of alkyl length on the BCS chain ends shows that the architecture reliably exhibits a thermoreversible gelation across C12-C16, but that the phenomenon is lost when this hydrophobic character is removed. This demonstrates that effective tethering to the emulsion droplets with this hydrophobic anchor is required to form a gel phase, which is likely to require both BCS-BCS interaction in the bulk and at the droplets interface. Bulk behavior of the BCS was explored by SANS and revealed that the materials form oblate ellipsoids in solution which grow anisotropically with temperature, accompanying the thermothickening/ thermoreversible gelation events. This builds-up a hierarchical picture of self-assembly. At low temperatures, the polymer is present at the oil/water interface, tethered by hydrophobic end groups into the oil phase, and in the bulk as a mixture of ellipsoidal aggregates and larger clusters. Upon heating, the aggregates increase in size, with growth along the equatorial radius exceeding growth of the polar radius. It is expected that connectivity of these aggregates in solution and polymer adsorbed at the interface leads to the formation of a percolating network. This new class of BCS allows the effective generation of thermoresponsive engineered emulsions and establishes some principles for the design of advanced materials for exploitation in a wide range of fields, particularly in pharmaceuticals.

3.5 References

1. Shinohara, H. Reports on Progress in Physics Related content. *Rep. Prog. Phys.* **64**, 297–381 (2001).

2. Chen, Q. *et al.* PH-responsive high internal phase emulsions stabilized by core cross-linked star (CCS) polymers. *Polym. Chem.* **4**, 4092–4102 (2013).

3. Richtering, W. Responsive emulsions stabilized by stimuli-sensitive microgels: Emulsions with special non-pickering properties. *Langmuir* **28**, 17218–17229 (2012).

4. Aulton, M. E. *Aulton's Pharmaceutics: The Design and Manufacture of Medicines*. (Elsevier Limited, 2007).

5. Mahato, R. I. *Pharmaceutica Dosage Forms and Drug Delivery*. (CRC Press LLC, 2007).

6. Brugger, B. & Richtering, W. Emulsions stabilized by stimuli-sensitive poly(N-isopropylacrylamide)-co-methacrylic acid polymers: microgels versus low molecular weight polymers. *Langmuir* **24**, 7769–7777 (2008).

7. Dai, S., Ravi, P. & Tam, K. C. pH-Responsive polymers: synthesis, properties and applications. *Soft Matter* **4**, 435 (2008).

8. Wang, L. *et al.* Preparation and aqueous solution behavior of a ph-responsive branched copolymer based on 2-(diethylamino)ethyl methacrylate. *J. Appl. Polym. Sci.* **132**, n/a-n/a (2015).

9. Zhao, C. *et al.* Ca2+ ion responsive pickering emulsions stabilized by PSSMA nanoaggregates. *Langmuir* **29**, 14421–8 (2013).

10. Cabane, E., Zhang, X., Langowska, K., Palivan, C. G. & Meier, W. Stimuli-responsive polymers and their applications in nanomedicine. *Biointerphases* **7**, 1–27 (2012).

11. Cook, M. T., Haddow, P., Kirton, S. B. & McAuley, W. J. Polymers Exhibiting Lower Critical Solution Temperatures as a Route to Thermoreversible Gelators for Healthcare. *Adv. Funct. Mater.* **31**, (2021).

12. Arai, T. *et al.* Novel drug delivery system using thermoreversible gelation polymer

for malignant glioma. *J. Neuro-Oncology Vol.* **77**, 9–15 (2006).

13. Weaver, J. V. M., Rannard, S. P. & Cooper, A. I. Polymer-Mediated Hierarchical and Reversible Emulsion Droplet Assembly. *Angew. Chemie* **121**, 2165–2168 (2009).

14. Weaver, J. V. M. *et al.* PH-Responsive branched polymer nanoparticles. *Soft Matter* **4**, 985–992 (2008).

15. Weaver, J. V. M., Rannard, S. P. & Cooper, A. I. Polymer-mediated hierarchical and reversible emulsion droplet assembly. *Angew. Chemie - Int. Ed.* **48**, 2131–2134 (2009).

16. Woodward, R. T., Chen, L., Adams, D. J. & Weaver, J. V. M. Fabrication of large volume, macroscopically defined and responsive engineered emulsions using a homogeneous pH-trigger. *J. Mater. Chem.* **20**, 5228–5234 (2010).

17. Silva, M. A., Rajbanshi, A., Achampong, D. & Cook, M. T. Engineering thermoresponsive emulsions with branched copolymer surfactants. *Undergoing Revis. Follow. Rev.* (2022).

18. Lutz, J. F., Akdemir, Ö. & Hoth, A. Point by point comparison of two thermosensitive polymers exhibiting a similar LCST: Is the age of poly(NIPAM) over? *J. Am. Chem. Soc.* **128**, 13046–13047 (2006).

19. Kline, S. R. Reduction and analysis of SANS and USANS data using IGOR Pro. *J. Appl. Crystallogr.* **39**, 895–900 (2006).

20. Feigin, L. A. & Svergun, D. I. *Structure Analysis by Small-Angle X-Ray and Neutron Scattering.* (Springer New York LLC, 1987).

21. Kotlarchyk, M. & Chen, S. H. Analysis of small angle neutron scattering spectra from polydisperse interacting colloids. *J. Chem. Phys.* **79**, 2461–2469 (1983).

22. NIST SLD Calculator.

23. King, S. M. Small-Angle Neutron Scattering. in *Modern Techniques for Polymer Characterisation* (eds. Pethrick, R. A. & Dawkins, J.) 171–232 (John Wiley & Sons, Ltd, 1999).

24. O'Brien, N., McKee, A., Sherrington, D. C., Slark, A. T. & Titterton, A. Facile, versatile

and cost effective route to branched vinyl polymers. *Polymer (Guildf).* **41**, 6027–6031 (2000).

25. Weaver, J. V. M., Rannard, S. P. & Cooper, A. I. Polymer-Mediated Hierarchical and Reversible Emulsion Droplet Assembly. *Angew. Chemie Int. Ed.* **48**, 2131–2134 (2009).

26. Lutz, J. F. Polymerization of oligo(ethylene glycol) (meth)acrylates: Toward new generations of smart biocompatible materials. *J. Polym. Sci. Part A Polym. Chem.* **46**, 3459–3470 (2008).

27. Pietsch, C., Fijten, M. W. M., Lambermont-thijs, H. M. L., Hoogenboom, R. & Schubert, U. S. Unexpected Reactivity for the RAFT Copolymerization of Oligo(ethylene glycol) Methacrylates. *J. Polym. Sci. Part A Polym. Chem.* **47**, 2811–2820 (2009).

28. Philipps, K., Junkers, T. & Michels, J. J. The block copolymer shuffle in size exclusion chromatography: the intrinsic problem with using elugrams to determine chain extension success. *Polym. Chem.* 2522–2531 (2021) doi:10.1039/d1py00210d.

29. Koichi, I., Tomi, Y. & Kawaguchi, S. Poly(ethylene oxide) Macromonomers. 10. Characterization and Solution Properties of the Regular Comb Polymers with Polystyrene Main Chains and Polyethylene oxide) Side Chains. *Macromolecules1* **25**, 1534–1538 (1992).

30. Biais, P. *et al.* Thermoresponsive dynamic BAB block copolymer networks synthesized by aqueous PISA in one-pot. *Polym. Chem.* **12**, 1040–1049 (2021).

31. Welsch, N. & Lyon, L. A. Oligo(ethylene glycol)-sidechain microgels prepared in absence of cross-linking agent: Polymerization, characterization and variation of particle deformability. *PLoS One* (2017) doi:| https://doi.org/10.1371/journal.pone.0181369 J.

32. Nun, N. *et al.* Tuning the Size of Thermoresponsive Poly(N-Isopropyl Acrylamide) Grafted Silica Microgels. *Gels* **3**, 34 (2017).

33. Woodward, R. T. & Weaver, J. V. M. The role of responsive branched copolymer composition in controlling pH-triggered aggregation of 'engineered' emulsion

droplets: Towards selective droplet assembly. *Polym. Chem.* **2**, 403–410 (2011).

34. Hammouda, B., Ho, D. L. & Kline, S. Insight into clustering in poly(ethylene oxide) solutions. *Macromolecules* (2004) doi:10.1021/ma049623d.

35. Nagarajan, R. The Neglected Role of the Surfactant Tail Self-Assembly. *Langmuir* **18**, 31–38 (2002).

36. Israelachvili, J. *Intermolecular and Surface Forces*. (Academic Press, London, 1992).

37. Blanazs, A., Armes, S. P. & Ryan, A. J. Self-assembled block copolymer aggregates: From micelles to vesicles and their biological applications. *Macromol. Rapid Commun.* **30**, 267–277 (2009).

38. Haddow, P., McAuley, W. J., Kirton, S. B. & Cook, M. T. Poly(N-isopropyl acrylamide) ñ poly(ethylene glycol) ñ poly(N-isopropyl acrylamide) as a thermoreversible gelator for topical administration. *Mater. Adv.* **1**, 371–386 (2020).

Chapter 4: Branched copolymer surfactants as versatile templates for responsive emulsifiers with bespoke temperature-triggered emulsion-breaking or gelation

4.1 Introduction

Chapter 3 introduced a new class of thermoresponsive BCS based on DEGMA, offering "smart" functionality of emulsions in response to temperature. These systems exhibited complex gelation mechanisms, relying on polymer self-assembly in the bulk and concomitant network formation with BCS at the oil-water interface.[1,2] The polymer architecture effects are highly complex, affecting both the solution and interfacial behaviours that underpin the macroscopic phase changes. However, the thermoresponsive engineered emulsions exhibited gelation temperatures too high for the desired topical/mucosal applications. The need for higher performing thermoresponsive engineered emulsions with controlled gelation at body temperature led to the exploration of novel materials in this chapter.

The liquid-gel transition enabled by stimuli-responsive BCS has particular application in areas such as drug delivery and cosmetics, where manipulation in a low viscosity state permits application to the body, after which the transition to a gel state allows retention and temporal stability,[3,4] for example in prolonged drug delivery to the eye.[5] There are, however, alternative stimuli-responsive behaviours that are desirable in emulsion systems, such as the induction of emulsion breaking. Stimulus-triggered emulsion coalescence and breaking has application in fields such as chemically-enhanced oil recovery, where reservoir rock is flooded with surfactant to extract oil that subsequently requires extraction through destabilisation of the emulsion.[6,7] Typically, these processes require additional chemical treatment or high temperatures adding to cost, both monetary and environmental.[7]

Herein, the control of BCS architecture by a single factor, the pendant poly(ethylene glycol) chain length, has been shown to dictate whether emulsions stabilised by the polymer exhibit thermoresponsive gelation or breaking. Furthermore, a second factor, the monomer ratio, offers control over the liquid-gel transition temperature, allowing the

bespoke generation of emulsions that respond to body temperature for *in situ* gelation to occur. The mechanisms dictating these behaviours have been explored using small-angle neutron scattering (SANS) and pendant drop tensiometry to elucidate nanoscale and interfacial behaviours in the system, where hierarchical assembly processes from the polymer to droplet level underpin thermoresponse.

4.2 Materials and methods

4.2.1 Materials

Di(ethylene glycol) methyl ether methacrylate (DEGMA, 95%), poly(ethylene glycol) methyl ether methacrylate (PEGMA-950, Mn 950 g/mol), poly(ethylene glycol) methyl ether methacrylate (PEGMA-500, Mn 500 g/mol), poly(ethylene glycol) methyl ether methacrylate (PEGMA-300, Mn 300 g/mol), ethylene glycol dimethacrylate (EGDMA, 98%, Mn 198 g/mol), 1-dodecanethiol (DDT, 99%), and anhydrous dodecane (99%) were purchased from Sigma-Aldrich (UK). Dodecane-d26 was purchased from QMX (UK). α, α-Azoisobutyronitrile (AIBN, >99%) was obtained from Molekula (UK). Absolute ethanol was supplied by VWR (UK). Dialysis tubing with molecular weight cut off (MWCO) of 12-14 kDa was purchased from Sigma Aldrich (UK). Deionised H_2O was employed in all experiments. All chemicals were used as received. Unless otherwise stated all methods here on were replicated once.

4.2.2 Synthesis of branched copolymer surfactant (BCS) by free radical polymerisation

Thermoresponsive BCS comprising of DEGMA, PEGMA-950/PEGMA-500/PEGMA-300, EGDMA and DDT (Table 4.1) were prepared following the synthesis procedure described previously under Section 3.2.2 in Chapter 3.[2] Six polymers were synthesised, labelled as P10-15, using DEGMA as LCST-imparting thermoresponsive monomer (Table 4.1). P10-12 were synthesised with varying chain length of PEGMA functioning as non-LCST hydrophilic macromonomer for BCS stabilisation. P10 was synthesised with PEGMA-950, P11 was stabilised by replacing PEGMA-950 with PEGMA-500 and P12 with PEGMA-300. P13-15 reduced the quantity of PEGMA-950 in the feed from 6 (P10) to 1.5 (P15).

In a general synthesis, DEGMA, PEGMA, EGDMA and DDT (quantities in Table 4.1) were dissolved in ethanol (190 mL) and sparged with nitrogen gas for 1 h. A solution of AIBN (190 mg) in ethanol (10 mL), also sparged with nitrogen gas for 1 h, was then added to the solution. The reaction was heated to 70 °C for polymerisation to proceed and stirred continuously. After 48 h, the reaction mixture was subjected to distillation to remove excess ethanol. The resultant crude polymer was dissolved in water and transferred to a pre-soaked dialysis bag. The dialysis bag was immersed in deionised water for 7 to 10 days and the water was replaced at regular intervals to facilitate the purification process. The resultant polymer solution was subjected to lyophilisation for 48 h to obtain a freeze-dried product. The lyophilised polymer was weighed, and the yield for all the polymers (P10 – P15) was determined to be 85 ± 1 %. This calculation was based on the initial amount of individual monomers used in the feed during synthesis.

Table 4.1: Feed composition for the synthesis of P10 - P15

Sample ID:	P10	P11	P12	P13	P14	P15
PEGMA-950 (mmol)	6	-	-	4.5	3	1.5
PEGMA-500 (mmol)	-	6	-	-	-	-
PEGMA-300 (mmol)	-	-	6	-	-	-
DEGMA (mmol)	174	174	174	174	174	174
EGDMA (mmol)	12	12	12	12	12	12
DDT (mmol)	12	12	12	12	12	12
AIBN (mmol)	1.2	1.2	1.2	1.2	1.2	1.2

4.2.3 Characterisation of thermoresponsive BCSs

^{1}H NMR spectroscopy was used to characterise the BCS using a Bruker Advance AM 600 NMR instrument. All samples were prepared in CDCl$_3$, using the residual solvent peak as internal standard.

Gel-permeation chromatography was conducted using an Agilent Infinity II MDS instrument equipped with differential refractive index, viscometry, dual angle light scatter and variable wavelength UV detectors. The system was equipped with 2 x PLgel Mixed D columns (300 x 7.5 mm) and a PLgel 5 µm guard column. The eluent was DMF with 5 mmol NH$_4$BF$_4$ additive. Samples were run at 1 mL/min at 50 °C. Poly(methyl methacrylate) standards (Agilent EasiVials) were used for conventional and universal calibration between 955,000 - 550 g/mol. Analyte samples were filtered through a nylon membrane with 0.22 µm pore size before injection. Number-average molar mass (Mn) and dispersity (Đ) values were determined by universal calibration using Agilent GPC/SEC software.

4.2.4 Preparation of water-in-oil emulsion stabilised by BCS

A series of 1:1 w/w oil-in-water emulsions were prepared to study the thermoresponsive behaviour by rheology. Aqueous polymer solution (2.5 g) at concentration levels of 2.5, 5 and 10 wt% were prepared in ice cold water in a 30 mL glass vial and left overnight in the refrigerator (~4 °C) to solubilise. This was followed by the addition of dodecane oil phase (2.5 g) and the solution emulsified at 2400 rpm for 2 min using a Silverson L4R Heavy Duty Mixer Emulsifier (USA). The emulsions were left on the bench top to rest for 36 h at room temperature. Approximately 1.1 g of the water phase separated as the lower phase of the creamed emulsion and was withdrawn; the emulsion cream was studied in further experiments. Where quoted, the oil phase volume (φ$_{oil}$) was calculated by:

$$\varphi_{oil} = \frac{\left(\frac{2.5}{\rho_{oil}}\right)}{\left(\frac{2.5}{\rho_{oil}}\right) + (2.5 - Mass\ Water)}$$

Where "Mass Water" is the mass of the lower phase extracted after creaming. Where ρ$_{oil}$ is the density of the oil (in this case 0.75 g/mL) and 2.5 is individual mass of the oil and water added.

4.2.5 Rheology of thermoresponsive emulsions

Rheology experiments were performed on an AR 1500ex rheometer by TA instruments (USA) equipped with a Peltier temperature control unit and a 40 mm parallel plate geometry with a specified gap distance of 500–750 μm. Each emulsion's creamed layer was placed on the rheometer lower plate prior to the measurement, after which temperature ramps were performed. Three minutes of equilibration at the desired temperature was conducted prior to measurement. Temperature ramps were performed in the range 20 to 60 °C, at 1 °C per minute heating rate, an oscillating stress of 1 Pa and a frequency of 6.28 rad/s. The change in storage modulus (G') and loss modulus (G") as a function of temperature was recorded.

4.2.6 Pendant drop analysis

Pendant drop analysis was undertaken using a Krüss DSA 100 Drop Shape Analyzer system and Advance software was used to analyse the droplets. Measurements were taken at 20, 25 and 37 °C, with the sample open to the atmosphere. The heat was applied to the drop in a jacketed cell. The polymer system under study was loaded into a syringe and then liquid was extruded in 2 μL increments until the trigger line was exceeded (~ 15 μL). At this point, the droplet was held for 300 seconds and the surface tension continually monitored. An average surface tension was then calculated.

4.2.7 Small-angle neutron scattering (SANS) of BCS solutions and emulsions

SANS experiments were conducted on the time-of-flight diffractometer instrument SANS2d at the STFC ISIS Neutron and Muon Source (UK). Incident wavelengths from 1.75 to 12.5 Å were used at a sample-to-detector distance of 12 m, which gave a scattering vector (q) range from 1.6×10^{-3} to 0.25 Å^{-1}. Temperature of the samples was controlled by an external circulating water bath (Julabo, DE). Samples were loaded in 1 cm wide rectangular quartz cells with 1 mm pathlength. Solutions of BCS were prepared as described in prior sections. Emulsions were then prepared with the addition of deuterated dodecane. The raw SANS data were processed with wavelength-dependent correction to the incident spectrum, detector efficiency, and sample transmission.[8] The data were

absolutely scaled, giving scattering intensity I(Q) as a function of Q, using the scattering from a standard sample (a solid blend of protiated and perdeuterated polystyrene) based on established methods.[9] All samples were confirmed to be free of multiple scattering. SANS data were fitted using SASView 4.2.2.[10] Scattering length densities (SLDs) were calculated from the monomer using the Neutron activation and scattering calculator website from the NIST centre for neutron research.[11]

4.2.8 Transmission electron microscopy (TEM) of BCS solutions

TEM of BCS solutions was conducted using a 120kV Tecnai G2 Spirit Twin microscope (FEI, Czech Republic). To prepare the specimens for TEM, a 4 µL sample solution was dropped onto a 300-mesh copper TEM grid coated with a thin, electron-transparent carbon film. The excess solution was then removed after 15 min of sedimentation using the "fast drying method" (removal of excess solution by touching the bottom of the grid with filter paper) to minimise oversaturation during the drying process. The particles were negatively stained with a 2 wt% solution of uranyl acetate, which was dropped onto the dried nanoparticles and left for 15 seconds before being removed in the same manner as the previous solution. The sample was then left to dry completely and observed using the TEM microscope.

To observe the sample morphology at elevated temperature, specimens were prepared using a similar method but with an electric oven heated to 40°C. The solutions and all tools for sample preparation, including grids, tweezers, and uranyl acetate solutions, were incubated in the oven before being deposited onto the TEM grid and left to sediment for 15 minutes at 40°C. The excess solution was then removed, and the particles were negatively stained with pre-heated solution of uranyl acetate and left to dry completely at 40°C. This approach allowed for the stabilisation of the sample morphology at elevated temperature, was then be observed using the TEM microscope at laboratory temperature with 150,000 magnification.[12,13]

4.2.9 Hot stage light microscopy of emulsions

The emulsions were subjected to hot stage light microscopy, with use of a Nikon Eclipse 80i microscope with a Linkam THMS600 temperature control stage (UK). To begin, a small quantity of the emulsion (which was kept in the refrigerator at 4°C before the experiment) was placed on a microscope cover glass, followed by another cover glass, and then inserted into the temperature control stage. The initial temperature of the stage was set to 5°C. The sample was left to equilibrate for 5 min and micrograph was recorded. Then the temperature was gradually raised (heating rate 1°C/min) until it reached 10°C, where it was kept for another 5 minutes, and an LM micrograph was captured. This process was repeated for temperatures of 10, 15, 20, 25, and 30°C.

4.3 Results and discussion

Thermoresponsive BCSs can be synthesised by AIBN-mediated free radical polymerisation of a feed mixture containing di(ethylene glycol)l methyl ether methacrylate (DEGMA), poly(ethylene glycol) methyl ether methacrylate (PEGMA), ethylene glycol dimethacrylate (EGDMA) and 1-dodecanethiol (DDT). In the resultant materials, DEGMA is thermoresponsive, exhibiting a lower critical solution temperature (LCST), PEGMA is hydrophilic, EGDMA induces branching, and DDT imparts dodecyl (C-12) chain ends to the BCS. A library of BCSs were synthesised to probe structure-function relationships imparted by the length and amount of the PEGMA component (Table 4.1, Figure 4.1i). In principle, this component serves several functions: crucially, PEGMA can allow steric stabilisation of the oil-water interface in emulsion systems;[14] furthermore, its relative abundance potentially mediates transition temperatures, as observed in linear polymer systems.[15,16] Two series of BCS were successfully synthesised and characterised by ^{1}H NMR spectroscopy (Figure 4.1ii) and GPC (Figure 4.1iii, Table A1 in appendix). The purity of all polymers was > 99% by ^{1}H NMR with no evidence of vinylic protons in the 6-7 ppm region (Figure A10-A14 in appendix). Additionally, it was compared with the 1H NMR of the crude monomers (Figure A15-A18 in appendix). The GPC traces showed that the polymer molecular weight distribution was monomodal. M_n was impacted in the samples by the 12–14 kDa membrane used for purification by dialysis. However, this purification method was previously found to be necessary for the BCS to exhibit thermogelation.[1] The first series evaluated the effect of PEG M_n within the PEGMA component, with P10 to 12 progressively reducing the length of these pendant PEG chains from 950 to 500 to 300 g/mol M_n PEGMA, having 19–20, 9–10, and 4–5 ethylene oxide units, respectively (Figure 4.1iv, with full composition in methods, Table 4.1). The hydrophilicity and LCST in aqueous solution of PEGMA analogues increase with an increase in molecular weight.[17] However, these PEGMA components exhibit LCST in aqueous solution between 60 °C to 90 °C as homopolymers, beyond the temperature range studied.[15,18,19] The second series evaluated the effect of the PEGMA abundance, with P10 through P13-15 containing serial reduction in PEGMA feed concentration of 6, 4.5, 3, and 1.5 mmol, respectively (Figure 4.1iv). In both series, the feed ratio of thermoresponsive macromonomer (DEGMA), crosslinker (EGDMA), initiator (AIBN) and chain transfer agent (DDT) were kept constant.

The effect of the systematic variation in structure in the BCS series is diagrammatically shown in Figure 4.1iv.
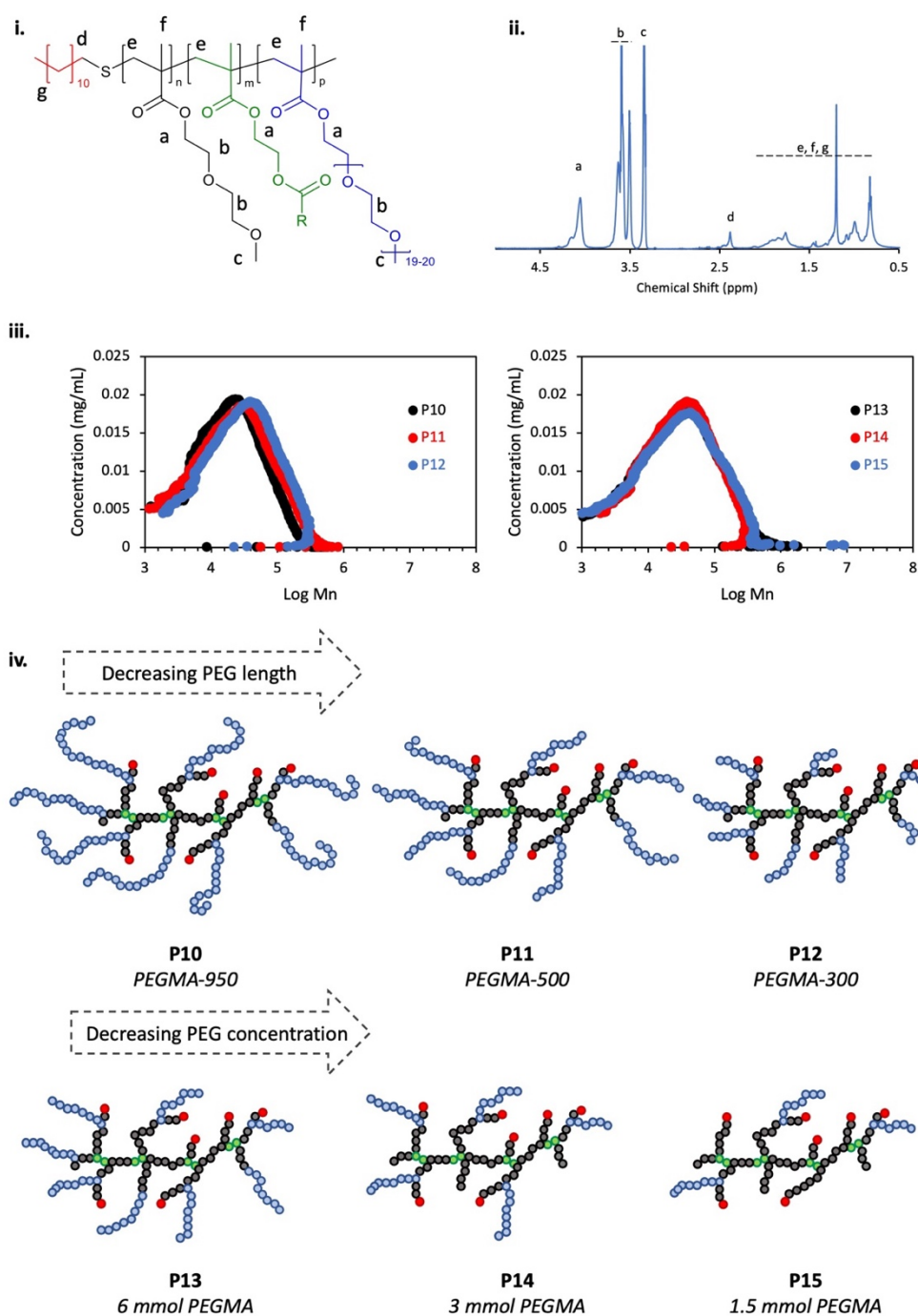
Figure 4.1: Schematic representation of the chemical structure of DEGMA BCS (i.) on which a polymer library is based and exemplar ^{1}H NMR spectrum of P10 (ii.). GPC chromatograms for the six BCS systems (iii.). The factors investigated in the library, colour coded against the chemical structure (i), are shown diagrammatically (iv.), and contained in full in Table 4.1.

Emulsions were prepared by homogenisation of equal mass of dodecane and BCS solution in water. The resulting oil-in-water emulsion exhibited creaming over 36 h and the lower water phase was removed to yield concentrated emulsions (the final volume fraction of oil was ϕ_{oil} = 0.72). When heating the samples and observing their appearance by eye, two distinct thermoresponsive behaviours were observed depending on BCS architecture. Reducing the PEGMA chain length to 500 (P11) and 300 g/mol (P12) gave emulsions with temperature-induced breaking (e.g. P12, Figure 4.2i), whilst the 950 molecular weight gave thermoreversible gelation (e.g. P14, Figure 4.2i). Both phenomena have exciting potential in the design of advanced functional materials, and control over which behaviour is exhibited was enabled by a single factor; the length of PEG chains dangling from the BCS structure. The thermoresponsive breaking of emulsions was explored by hot stage microscopy. P12 emulsions were subjected to a temperature ramp from 5 to 30 °C at 1 °C/min and micrographs recorded (Figure 4.2ii). Droplets were unaffected by temperature between 5 and 20 °C, with droplet diameters between 4 and 53 µm. However, upon heating the P12 emulsion to between 25 and 30 °C, rapid droplet coalescence was observed. This supports our macroscopic observation that the emulsions began to separate upon heating over 25 °C. Similarly, P14 emulsions were heated from 25 to 35, then 40 °C to evaluate the system below and above the gelation temperature (Figure 4.2iii). No distinct changes were observed in droplet size or morphology, and no additional objects were observed in the heated system. Further evaluation of all BCS emulsion systems was conducted using rheology to explore the materials in more detail.
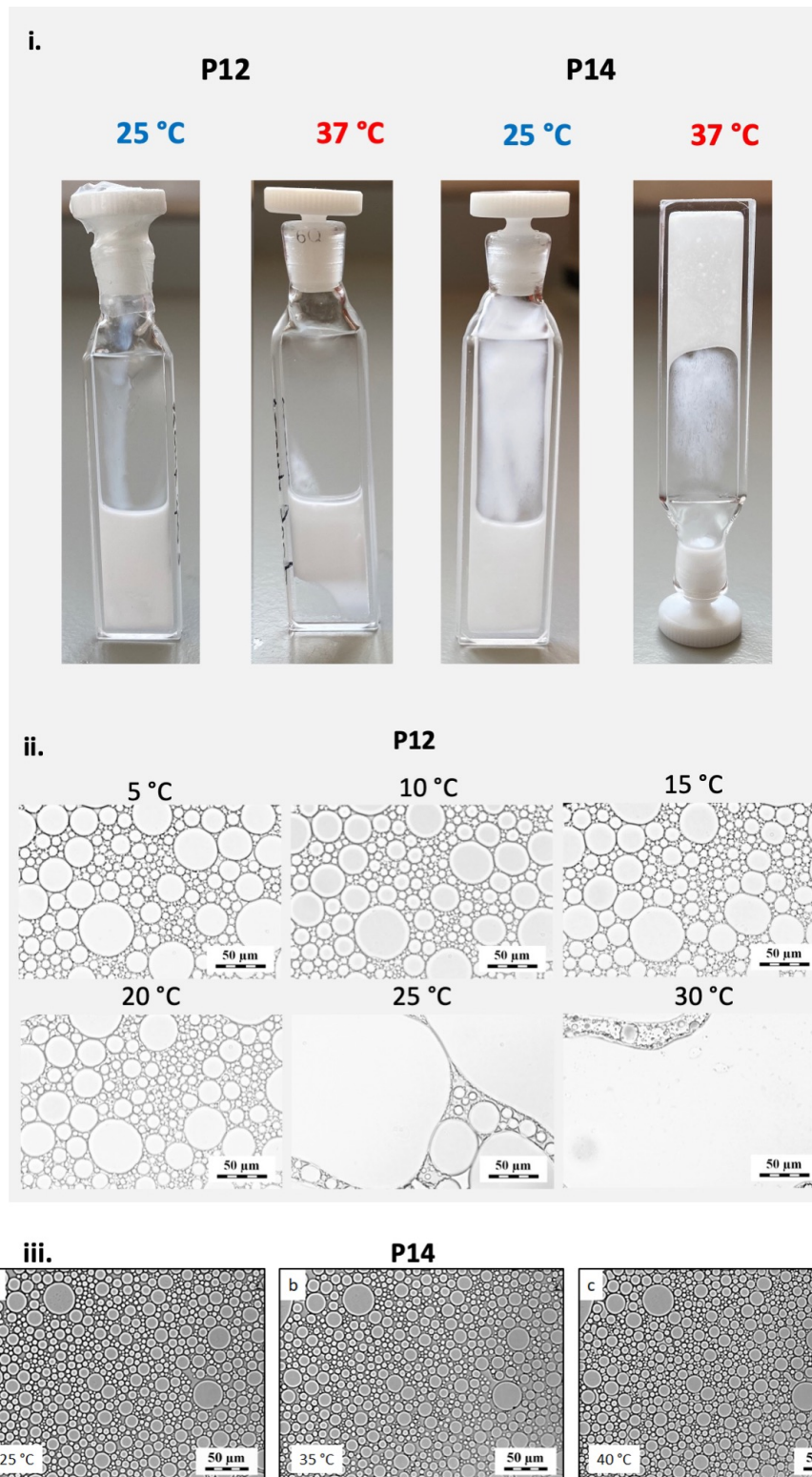
Figure 4.2: BCS-stabilised emulsions can exhibit either temperature-induced breaking or gelation at physiologically relevant temperatures. Emulsions shown are stabilised by 10 wt% BCS and displayed macroscopic phase changes (i). Microscopic evaluation at 20 x magnification demonstrates fast coalescence in the P12 system at T > 20 °C (ii), images of dodecane-in-water emulsions stabilised by P14 at 25, 35 and 40 °C (iii).

The rheological evaluation of the 1:1 oil-in-water emulsion system stabilised by varying concentrations of BCS was performed by small-amplitude oscillatory shear temperature ramps (Figure 4.3). The rheology data demonstrate the dependence of the storage, (G′) and loss, (G″) moduli with temperature at a fixed, small stress amplitude (1 Pa) and angular frequency (6.28 rad/s). BCS concentration showed a strong influence on the thermoresponsive activity, which could be manipulated to trigger thermo-gelation. P10 is the reference system, representing the emulsions stabilised by the BCS synthesised with PEGMA-950. At 2.5 wt% and 5 wt% polymer concentrations, emulsion G′ and G″ increased with the influence of temperature at 45 °C but a gel did not form. However, at 10 wt% polymer concentration, a significant rise in G′ and G″ is observed, leading to gelation at 48 °C (defined here by the G′ cross over G″ point).[20] The process was then reversed on the cooling cycle. Emulsions stabilised with P11 (i.e., BCS copolymerised with PEGMA-500 instead of PEGMA-950) demonstrated a contrasting response to temperature. At 2.5 wt%, a slight rise in G′ and G″ was observed initially, which was not stable, leading to emulsion thinning at approximately 23 °C and eventually the breaking of the emulsion at 40 °C, appearing as a sharp reduction in G′ and G″. A similar behaviour was observed for the emulsion stabilised at 5 wt% BCS, with slight thickening at the start of the temperature ramp, leading to thinning at 23 °C and emulsion break-up at 40 °C. At 10 wt% polymer concentration, emulsion breaking was observed visually with a rise in temperature at approximately 25 °C. The emulsion stabilised with P12 (i.e., BCS copolymerised with PEGMA300) also demonstrated emulsion thinning, with response to temperature eventually leading to emulsion breaking. Emulsion breaking was observed at 25 °C at all P12 concentrations of 2.5, 5 and 10 wt%. The breaking of the emulsions was observed visually for the emulsions stabilised by P11 and P12 at 10 wt% concentration.
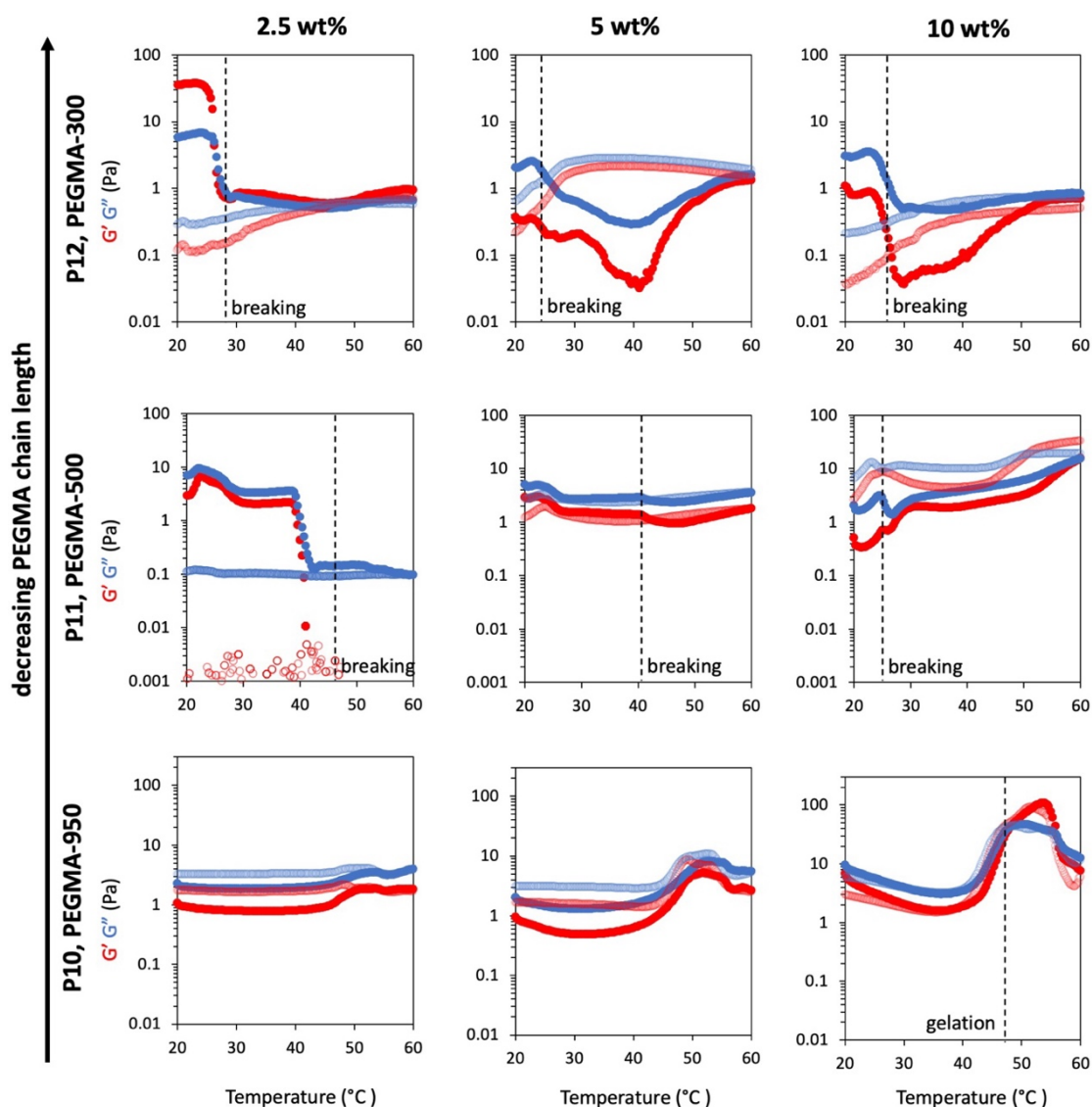
Figure 4.3: Rheological behaviour of emulsions stabilised by thermoresponsive P10-12, probing the effect of PEGMA chain length. Emulsions were explored at 2.5, 5 and 10 wt% polymer concentrations. G' is shown in red and G" is shown in blue. Dark colours show the 'up' ramp whilst light colours show the subsequent 'down' ramp.

This study of the rheological behaviour of emulsions stabilised by P10-12 suggested that emulsion thickening or thermo-gelation, and emulsion thinning or even emulsion breaking, could be controlled by varying the chain length of PEGMA. This may be due to the PEGMA moiety, which is believed to offer steric stabilisation to the emulsion after the BCS tethers to the oil-water interface.[14] Thus, when DEGMA switches to a relatively hydrophobic state above the LCST, the PEGMA is hypothesised to offer sufficient steric

stabilisation to halt coalescence events. Thus, it is likely that the reduced chain length of the PEG chains adorning the BCS reduce the ability to stabilise the emulsion when DEGMA is hydrophobic above the LCST. An additional factor is that the hydrophilicity of PEGMA increases with an increase in molecular weight and the thermoresponsive behaviour is related to the amphiphilic character of these macromolecules.[21] This factor most likely impacts transition temperatures by reducing the LCST with lower PEGMA chain lengths, particularly evident in the 2.5 wt% emulsions. Overall, these thermoresponsive BCSs can be widely employed due to this ability to switch thermoresponsive behaviour. This approach of synthesising thermoreversible gels can be used, for example, in the healthcare sector to develop drug delivery platforms with *in situ* gelation combined to the capacity to solubilise hydrophobic molecules. However, with the current systems, the gelation temperatures are not physiologically relevant.

The LCST of oligoethylene glycol methacrylates is dependent upon the degree of polymerisation of the macromonomer.[15] It is known that in copolymers of oligoethylene glycol methacrylates with different chain lengths, the LCST may be tuned with a tendency towards the LCST expected from the constituent monomer of greatest abundance.[22] Thus, it was anticipated that increasing the relative abundance of DEGMA would show a trend towards the LCST of poly(DEGMA), ca 26 °C.[22,23] Adapting this concept, analogues of P10 were synthesised with varying molar feed ratio of PEGMA-950. P10 was synthesised with 6 mmol of PEGMA-950 whereas P13, P14 and P15 were synthesised with 4.5, 3 and 1.5 mmol of PEGMA-950 keeping the feed ratio of DEGMA, EGDMA, 1-DDT constant.

Figure 4.4 shows the rheology of thermoresponsive emulsions stabilised with P10, P13-15 (decreasing the molar feed ratio of PEGMA-950, Figure 4.1iv, Table 4.1) at BCS concentrations of 2.5, 5 and 10 wt%. The emulsion systems stabilised at 2.5 wt% concentration of P10, P13-15 demonstrated a slight rise in G' and G'' indicating thermothickening behaviour. It is observed that the temperature at which the emulsion showed thickening decreased from approximately 45 °C to 30 °C with a decrease in the molar ratio of PEGMA-950. Similar rheological behaviour was observed for emulsions stabilised at 5 wt%, with the thickening temperature declining with a decrease in PEGMA-950 molar concentration. The emulsion remained predominantly liquid-like, and gelation did not occur (G' < G''). For the emulsion system stabilised with P10 at 10 wt%

concentration, thermogelation (G' > G") was observed at 48 °C, which was reversed on the cooling cycle. Similarly, reversible thermogelation occurred at 40 °C, 35 °C and 25 °C for emulsions stabilised by P13, P14 and P15 at 10 wt% concentration. In the P15 system this is gelation is particularly subtle but does meet the criterion G' > G". Overall, this study demonstrates that the gelation temperature of thermoresponsive engineered emulsion stabilised by BCSs can be controlled through varying the mole ratio of PEGMA-950 during synthesis. This design principle can generate advanced functional materials allowing the tuning of thermoresponsive engineered emulsions to gel at physiological temperature for applications including drug delivery to topical sites or depot injections.[24]
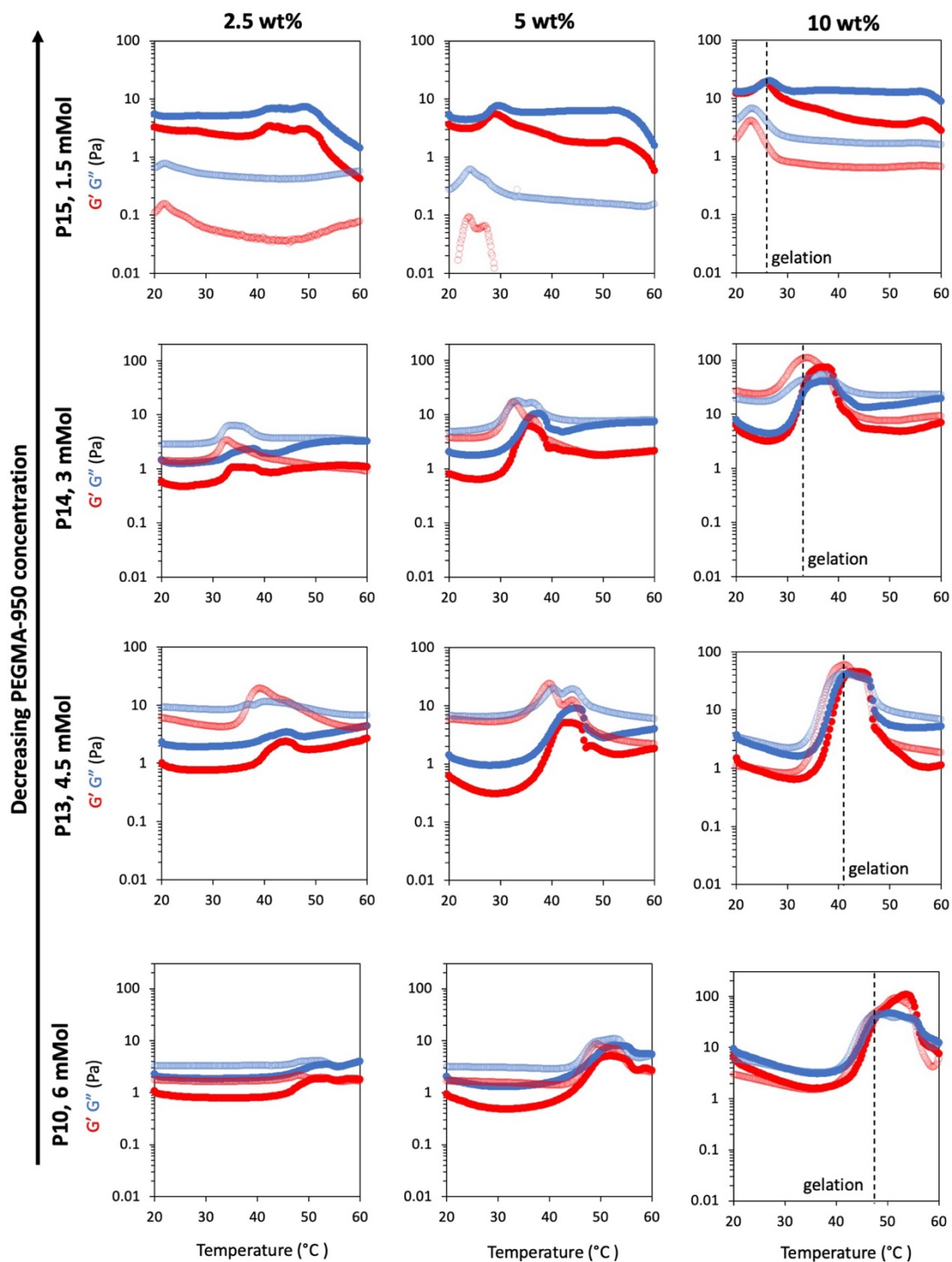
Figure 4.4: Effect of PEGMA-950 concentration on the gelation temperature of thermoresponsive engineered emulsions. Emulsions were stabilised by BCSs with P10 synthesised with 6 mmol, P13 with 4.5 mmol, P14 with 3 mmol and P15 with 1.5 mmol of PEGMA-950.

Next, pendant drop tensiometry was used to probe the effects of BCS characteristics and of temperature on surface tension, as little information is known about DEGMA BCS behaviour at interfaces (Figure 4.5). P12 and P14 were selected as two representative systems where P12 leads to emulsions which break with temperature, and P14 leads to emulsions with thermoreversible gelation. Both BCS reduced the surface tension of water substantially (from 72 mN/m to 43-45 mN/m at 25 °C), evidencing their ability to adsorb to this interface, similar to observations for *N*-isopropylacrylamide BCS.[1] Heating the system from 20 to 37 °C led to a small increase in surface tension in solutions ($p < 0.05$ by 2 way ANOVA with Bonferroni post hoc test) for both BCSs measured, which was still lower than the surface tension of water. A time study indicated that the surface tension was stable over a period of five minutes in both systems and at both temperatures, but with some evidence of drift to higher surface tension in the P14 system at 37 °C with time. However, this was at a longer timescales than that required for emulsion breaking (1 min) (Figure 4.5iii).

It can be suggested that the difference between emulsion breaking (P12) and emulsion stability (P14) when heated is due to steric effects from the PEGMA component. This is included in the BCS structure to sterically stabilise the emulsion droplets, as it is expected that over the temperature range studied PEG is highly hydrophilic and will extend into the water phase, providing a steric barrier to coalescence.[25,26] P12 and P14 contain PEGMA with molecular weight 300 and 950 g·mol^{-1}, respectively. The reduced degree of polymerisation of the PEGMA component in P12 may mean that once DEGMA is above its LCST, there is insufficient steric stabilisation of the droplets. In P14, the degree of polymerisation of PEGMA is greater, leading to stability even above the LCST.
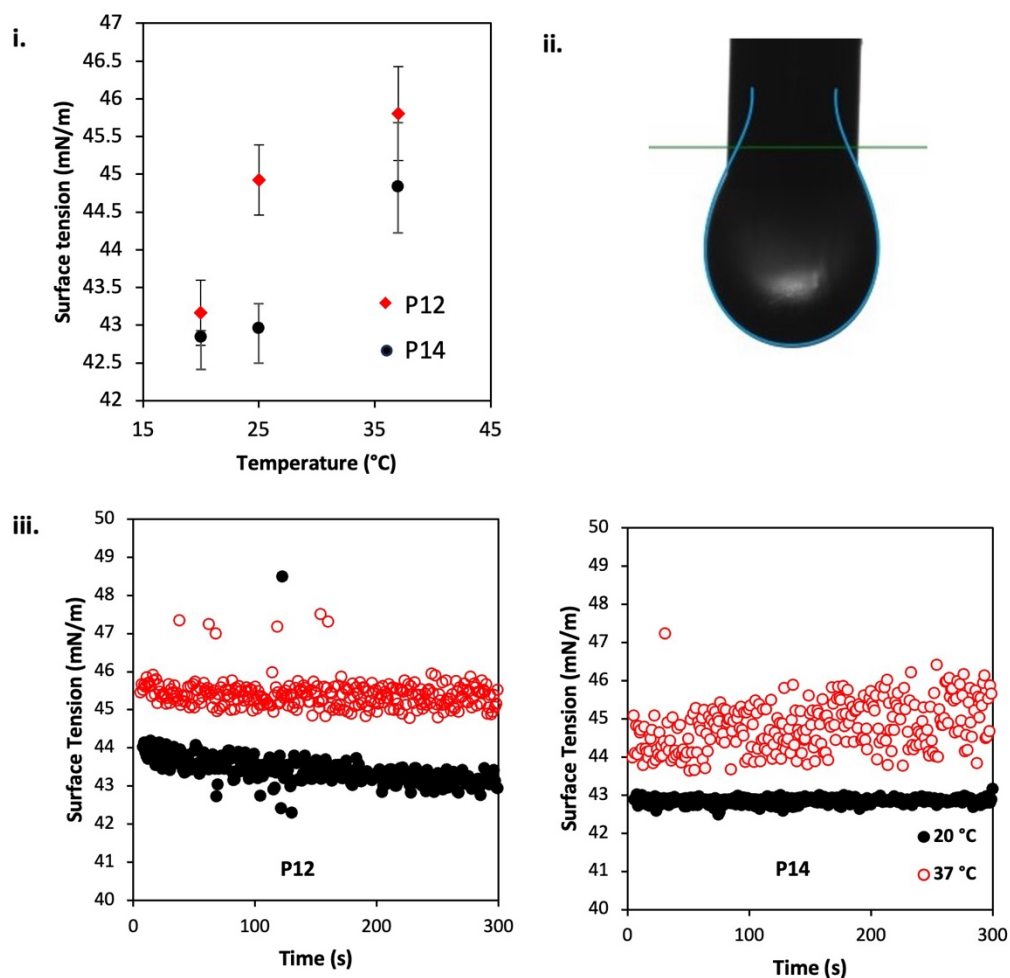
Figure 4.5: Pendant drop tensiometry of P12 and P14 aqueous solutions (20 wt%) with variation of temperature. Surface tension measurements were conducted (i) 20 wt% aqueous solution of P14 with fitting using the Owens, Wendt, Rabel and Kaelble method (ii). Time-dependence of surface tension is also shown (iii).

Small-angle Neutron Scattering (SANS) was employed to probe the nanostructure of the BCS solutions in D$_2$O (Figure 4.6). The BCS architecture has previously been reported to give oblate ellipsoidal particles, particularly above the LCST of DEGMA. Data fitting was conducted using an ellipsoidal form factor to account for scattering in BCS solutions. The volume fraction of the scattering objects was initially assumed to be equivalent to the weight fraction due to the similar density of the BCS constituents (PEG density: 1.125 g/mL) and D$_2$O (density: 1.11 g/mL), and only altered when a satisfactory fit could

otherwise not be obtained. The scattering length density of D_2O is known (6.37×10^{-6} Å^{-2}), and the SLD of the BCS components may be calculated (e.g. DDT: -0.368×10^{-6} Å^{-2}, DEGMA: 0.471×10^{-6} Å^{-2}),[11] however it is expected that the aggregates remain solvated to some degree by D_2O even above the LCST[27] so the scattering length density was fitted (and not fixed). The ellipsoidal form factor gave satisfactory fits to the intermediate and high q region (ca $0.01 < q < 0.3$ Å), but in some instances a power law was required to fit the low q region (ca 0.01 Å $> q$). In all cases this power law took the form $I(q) = q^{-4}$, consistent with Porod-type scattering from larger aggregates with a sharp interface. The exact nature of these aggregates cannot be determined, and discussion around their nature is limited.
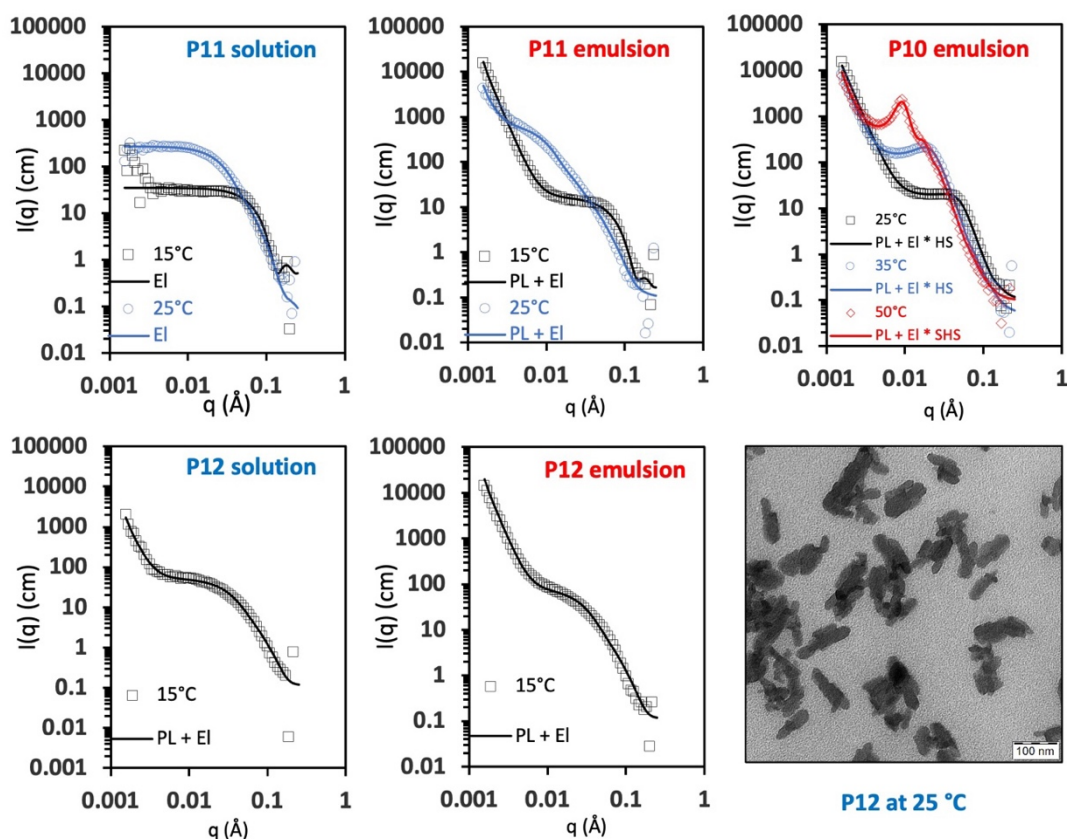
Figure 4.6: SANS of P11/12 solutions (20 wt%) in D_2O and P10-3 (10wt%) d-dodecane/D_2O emulsions. Data presented at 25, 35, and 45 °C in black, blue, and red symbols, respectively. Fits to data are shown as continuous lines, with the models used displayed in the legend. El is an ellipsoid, PL is a power-law, SHS is the sticky-hard-sphere structure factor. A TEM image of P12 is included at 25 °C.

Reducing PEGMA chain length demonstrated a switch from thermogelation (P10) to a temperature-responsive demulsification (P11 - P12). SANS was used to probe solution and emulsion behaviour of the PEGMA-500 and PEGMA-300 systems, designated P11 and P12, respectively, at temperatures below their macroscopic phase separation (Figure 4.6, Tables A4.2, A4.3). The emulsion of P10 with PEGMA-950 was also measured by SANS as a reference, where solution behaviour is already known.[2] Fitting P11 solutions to an ellipsoid form factor gave spheres (i.e. equatorial = polar radius) of radius 32 Å at 15 °C, but transitioned into an ellipsoid at 25 °C (equatorial radius/polar radius = 4.34). This ellipsoid was oblate with equatorial radius of 98 Å and a polar radius of 22 Å, in-line with prior studies of BCS systems.[2] The spherical form at 15 °C is the expected thermodynamically favourable colloidal structure to assume, however deviation from this, as observed at 25 °C, is possible due to steric constraints in the polymer. It is known that these BCSs exhibit a CAC (critical aggregation concentration),[1] thus it is believed that the nano-objects at low temperature are formed by the assembly of multiple BCSs *via* hydrophobic interaction of the polymer terminus. Upon heating to 25 °C, some degree of conformation change may occur in the BCS due to desolvation of the LCST-exhibiting DEGMA component. This, in turn, reduces the effective hydrophilic head group volume of the polymeric surfactant, leading to a transition to oblate ellipsoids, as described by the critical packing parameter theory, which holds for block copolymers.[28] In a similar manner, P12 forms oblate ellipsoidal aggregates at 15 °C, which may also be understood as a reduction in hydrophilic head group volume when the PEGMA-500 component of P11 is reduced to PEGMA-300 in P12. This ellipsoidal geometry is observable by TEM (Figure 4.6) when P12 is heated above the point of emulsion breaking, 25 °C. Sizing these particles in ImageJ gave dimensions of 69 ± 13 x 26 ± 6 nm (n = 5, particles), giving an equatorial/polar ratio of 2.6. Despite differences in sample preparation method, TEM provides further proof of the existence of these ellipsoidal nano-objects.

In emulsion systems of P11 and P12, the spherical/ellipsoidal structures remain observable in the SANS profiles, however with a marked q^{-4} decay at low q. This is believed to arise from the interface of the larger d-dodecane droplets. Above 25 and 15 °C for P11 and P12, respectively, the BCS solutions/emulsions underwent macroscopic phase separation and SANS measurements were not conducted. The P10 emulsion, which

displays thermogelation, exhibited features not seen in the P11/P12 systems. Again, oblate ellipsoidal nano-objects are present with Porod behaviour at low q. The ellipsoidal objects grew anisotropically, from 28 x 61 Å at 25 °C to 67 x 350 Å at 50 °C (polar x equatorial radii). This effect is attributed to further desolvation of the DEGMA component reducing headgroup size as heating increases. The P10 emulsion also requires a structure factor to fit the data adequately, indicating the presence of strong interactions between the colloidal assemblies. At low temperature, a fit to a hard-sphere structure factor indicates that the objects interact via hard-sphere interactions without interpenetration. Instead, at 50 °C, where the emulsions are in the gel state, a sticky hard sphere structure factor was required to fit the very marked peak at $q = 9.16 \times 10^{-3}$ Å^{-1}. This indicates the presence of an attractive well and interactions between the BCS aggregates, giving information that the gel state occurring under this condition is underpinned by supracolloidal aggregates of oblate ellipsoids formed by multiple BCSs.
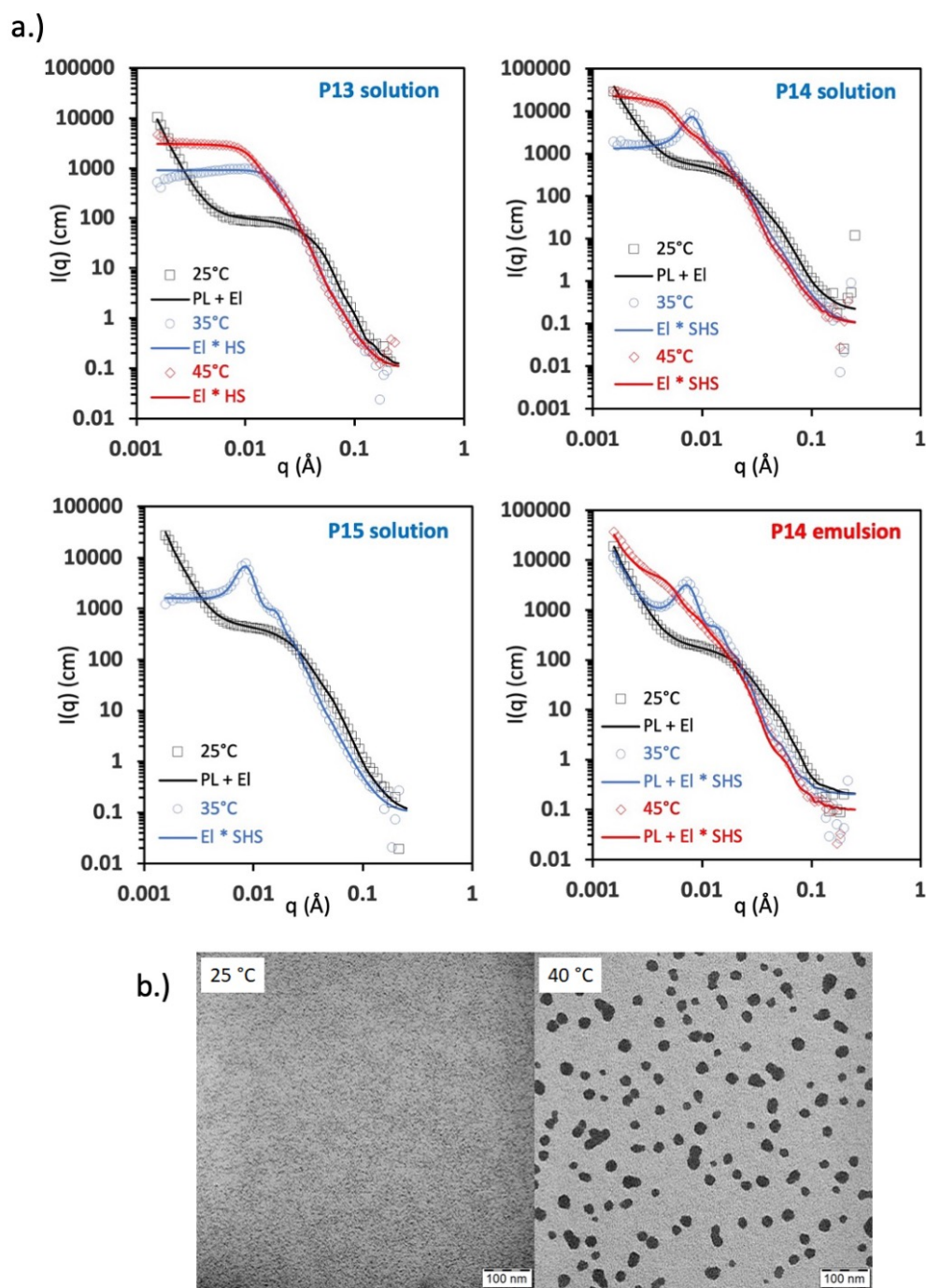
Figure 4.7: a.) SANS of P13-15 solutions (20 wt%) in D$_2$O and P14 (10 wt%) d-dodecane/D$_2$O emulsion. Data presented at 25, 35, and 45 °C in black, blue, and red symbols, respectively. Fits to data are shown in the continuous lines, with the models used shown in the legend. El is an ellipsoid, PL is a power-law, SHS is the sticky-hard-sphere structure factor. b.) TEM micrographs of P14 dried at 25 °C and 40 °C, indicating transition from small clusters to larger nano-objects.

The P13-15 series was then examined by SANS (Figure 4.7, Tables S4.4, S4.5), which explores a reduction in PEGMA concentration in the feed mixture, from 6 mmol in P10 to 4.5, 3, and 1.5 mmol, in P13, P14 and P15, respectively. All these emulsions exhibited thermothickening behaviour, as measured by rheology, with the temperature at which an increase in G' and G" was observed decreasing with the PEGMA content of the BCS. SANS was conducted on BCS solutions at 25, 35, and 45 °C to compare the systems that allowed emulsions to switch between liquid and gel states. At 25 °C, P13-15 solutions contained oblate ellipsoidal nano-objects with a Porod character at low q, assigned to clustering of the polymer.[29] Upon heating, the ellipsoids increased in size and had an increasing oblate character, with the ratio of equatorial to polar radius increasing (Figure 4.8). P13 required a hard sphere structure factor for fitting, whereas P14 required a sticky-hard-sphere structure factor to fit the data, as did P15. P15 phase separated at high temperatures, hence the data at 45 °C are omitted. The lack of attractive interactions in P13, which did not require a sticky-hard-sphere structure factor, is attributed to the temperature at which the SANS was conducted. The corresponding emulsion is in a liquid state at 25 and 35 °C and transitions into a gel between 42 and 45 °C. The measurement is therefore taken at a transition temperature where the elastic character starts to reduce. P14, which exhibited gelation at the most appropriate temperature for healthcare applications (32 °C), was also studied by SANS in an emulsion system (Figure 4.7). The existence of oblate ellipsoidal particles complemented by TEM experiment (Figure 4.7) were retained and exhibited comparable transitions to the solution system, giving evidence that solution behaviour reported thus far is retained in the emulsion system. A pronounced upturn at low q was also present, associated to the interface of the emulsion droplets.
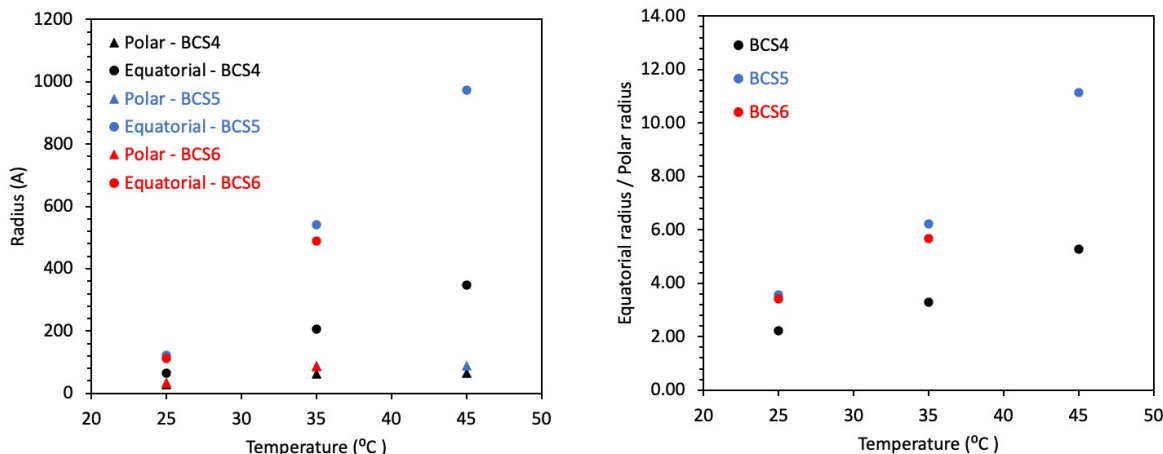
Figure 4.8: Fitting parameters extracted from the ellipsoidal form factor used in analysis of P13-15 solutions. In the figure BCS4, BCS5 and BCS6 are P13, P14 and P15 respectively.

4.4 Conclusions

The BCS architecture is highly versatile in generating thermoresponsive emulsions with either reversible gelation or emulsion breaking, even with mild temperature changes. The PEG component of BCS is crucial to control the thermoresponsive behaviour of the emulsions. With longer PEG lengths (950 g/mol), the emulsions exhibit thermogelation, whereas shorter PEG chains (500 or 300 g/mol) lead to emulsion breaking upon mild warming. This is attributed to reduced steric stabilisation of the droplets above the LCST of DEGMA by the hydrophilic PEG chains with reduced length. The relative abundance of PEGMA in the BCS tightly controls the gelation temperature of BCS-stabilised emulsions. Decreasing the concentration of PEGMA leads to a reduction in the temperature at which gelation occurred. SANS reveals that the BCSs formed oblate ellipsoids in both solution and emulsion systems, which grew anisotropically with temperature. In samples that formed a gel, there was evidence that these nano-objects formed supracolloidal structures, which would be responsible for gelation. An optimal BCS architecture, P14, can form emulsions that transition from a liquid to a gel state when warmed above 32 °C, making this system ideal for *in situ* gelation upon contact with the body.

4.5 References

1. da Silva, M. A. *et al.* Engineering Thermoresponsive Emulsions with Branched Copolymer Surfactants. *Macromol. Mater. Eng.* **307**, 1–14 (2022).

2. Rajbanshi, A. *et al.* Polymer architecture dictates thermoreversible gelation in engineered emulsions stabilised with branched copolymer surfactants. *Polym. Chem.* **13**, 5730–5744 (2022).

3. Caramella, C. M., Rossi, S., Ferrari, F., Bonferoni, M. C. & Sandri, G. Mucoadhesive and thermogelling systems for vaginal drug delivery. *Adv. Drug Deliv. Rev.* **92**, 39–52 (2015).

4. Kan, P., Lin, X. Z., Hsieh, M. F. & Chang, K. Y. Thermogelling emulsions for vascular embolization and sustained release of drugs. *J. Biomed. Mater. Res. - Part B Appl. Biomater.* **75**, 185–192 (2005).

5. Kim, Y. C. *et al.* Gelling hypotonic polymer solution for extended topical drug delivery to the eye. *Nat. Biomed. Eng.* **4**, 1053–1062 (2020).

6. Ni, C. *et al.* Phase transformation of thermoresponsive surfactant triggered by its concentration and temperature. *J. Pet. Sci. Eng.* **193**, 107410 (2020).

7. Raffa, P., Broekhuis, A. A. & Picchioni, F. Polymeric surfactants for enhanced oil recovery: A review. *Journal of Petroleum Science and Engineering* at https://doi.org/10.1016/j.petrol.2016.07.007 (2016).

8. Heenan, R. K., Penfold, J. & King, S. M. SANS at Pulsed Neutron Sources: Present and Future Prospects. *J. Appl. Crystallogr.* **30**, 1140–1147 (1997).

9. Wignall, G. D. & Bates, F. S. Absolute calibration of small-angle neutron scattering data. *J. Appl. Crystallogr.* **20**, 28–40 (1987).

10. SasView version 4.2.2.

11. NIST SLD Calculator.

12. Kolouchova, K. *et al.* Thermoresponsive Triblock Copolymers as Widely Applicable Magnetic Resonance Imaging Tracers. *Chem. Mater.* **34**, 10902–10916 (2022).

13. Skvarla, J., Zednik, J., Slouf, M., Pispas, S. & Stepanek, M. Poly(N-isopropyl

acrylamide)-block-poly(n-butyl acrylate) thermoresponsive amphiphilic copolymers: Synthesis, characterization and self-assembly behavior in aqueous solutions. *Eur. Polym. J.* **61**, 124–132 (2014).

14. Weaver, J. V. M., Rannard, S. P. & Cooper, A. I. Polymer-mediated hierarchical and reversible emulsion droplet assembly. *Angew. Chemie - Int. Ed.* **48**, 2131–2134 (2009).

15. Lutz, J. F. Thermo-switchable materials prepared using the OEGMA-platform. *Adv. Mater.* **23**, 2237–2243 (2011).

16. Lutz, J. F., Akdemir, Ö. & Hoth, A. Point by point comparison of two thermosensitive polymers exhibiting a similar LCST: Is the age of poly(NIPAM) over? *J. Am. Chem. Soc.* **128**, 13046–13047 (2006).

17. Lutz, J. F. Polymerization of oligo(ethylene glycol) (meth)acrylates: Toward new generations of smart biocompatible materials. *J. Polym. Sci. Part A Polym. Chem.* **46**, 3459–3470 (2008).

18. Lutz, J. F., Hoth, A. & Schade, K. Design of oligo(ethylene glycol)-based thermoresponsive polymers: An optimization study. *Des. Monomers Polym.* **12**, 343–353 (2009).

19. Cook, M. T., Haddow, P., Kirton, S. B. & McAuley, W. J. Polymers Exhibiting Lower Critical Solution Temperatures as a Route to Thermoreversible Gelators for Healthcare. *Adv. Funct. Mater.* **31**, (2021).

20. Da Silva, M. A., Farhat, I. A., Arêas, E. P. G. & Mitchell, J. R. Solvent-induced lysozyme gels: Effects of system composition and temperature on structural and dynamic characteristics. *Biopolymers* **83**, 443–454 (2006).

21. Badi, N. Progress in Polymer Science Non-linear PEG-based thermoresponsive polymer systems. *Prog. Polym. Sci.* **66**, 54–79 (2017).

22. Yamamoto, S.-I., Pietrasik, J. & Matyjaszewski, K. The Effect of Structure on the Thermoresponsive Nature of Well-Defined Poly(oligo(ethylene oxide) methacrylates) Synthesized by ATRP. *J. Polym. Sci. Part A Polym. Chem.* **46**, 194–202 (2008).

23. Badi, N. Non-linear PEG-based thermoresponsive polymer systems. *Prog. Polym. Sci.* **66**, 54–79 (2017).

24. Yu, L. & Ding, J. Injectable hydrogels as unique biomedical materials. *Chem. Soc. Rev.* **37**, 1473–81 (2008).

25. Woodward, R. T. & Weaver, J. V. M. The role of responsive branched copolymer composition in controlling pH-triggered aggregation of 'engineered' emulsion droplets: Towards selective droplet assembly. *Polym. Chem.* **2**, 403–410 (2011).

26. Woodward, R. T. *et al.* Controlling responsive emulsion properties via polymer design. *Chem. Commun.* 3554–3556 (2009) doi:10.1039/b904320a.

27. Pelton, R. Poly(N-isopropylacrylamide) (PNIPAM) is never hydrophobic. *J. Colloid Interface Sci.* **348**, 673–674 (2010).

28. Blanazs, A., Armes, S. P. & Ryan, A. J. Self-assembled block copolymer aggregates: From micelles to vesicles and their biological applications. *Macromol. Rapid Commun.* **30**, 267–277 (2009).

29. Hammouda, B., Ho, D. L. & Kline, S. Insight into clustering in poly(ethylene oxide) solutions. *Macromolecules* (2004) doi:10.1021/ma049623d.

Chapter 5: Combining branched copolymers with additives generates stable thermoresponsive emulsions with *in situ* gelation upon exposure to body temperature

5.1 Introduction

Previous chapters described the challenges in generating thermoresponsive engineered emulsions with high performance and describes the effect of BCS architecture, molecular weight and concentration to demonstrate thermogelation over a temperature range. DEGMA-based BCS allowed dispersion of dodecane in water which formed an emulsion that creamed over ca 36 h, but was otherwise macroscopically stable.[1] The isolated creamed phase exhibited the desired temperature-induced gelation, however for the efficient production of pharmaceutical emulsions elimination of this creaming event is desirable. Furthermore, the compatibility of these novel emulsifiers with pharmaceutically relevant oils is unknown. Chapter 4 revealed that the length of poly(ethylene glycol) (PEG) chains in BCSs plays a crucial role in controlling thermoresponsive behaviour. Additionally, the monomer ratio allowed control over the liquid-gel transition temperature, enabling the generation of emulsions that respond to body temperature for *in situ* gelation. This chapter explores the use of additives to take this optimal BCS and formulate into stable, pharmaceutically-relevant emulsions.

Emulsion stability, amongst other physical properties, can be enhanced by the use of a secondary co-surfactant alongside the primary surfactant.[2] Mixing surfactants enables the combination of stabilising factors found in the individual components. For example, combining small non-ionic surfactants with ionic surfactants can lead to a mixed emulsifier film which has the condensed nature typically seen in non-ionic surfactants, with charge repulsion granted by the ionic component.[3] Indeed, many commercial emulsifiers are mixtures of surfactants.[4] This process of mixing surfactants has the potential to grant this surfactant synergism but also the possibility for antagonism, thus the approach is powerful but complex.[2] Structural diversity in surfactants includes head group nature (e.g. ionic/non-ionic), tail-group nature (e.g. saturated/unsaturated), size (e.g. polymeric/small), which overall impact factors such as solubility, ability to pack at an interface, and, in mixed systems, compatibility with any primary surfactant. Additionally,

polymeric/oligomeric additives may enhance the stability of emulsion systems by interface stabilisation and by increasing the viscosity of the continuous phase, thus reducing velocities of sedimentation. Thermoresponsive BCS behaviour in mixed surfactant/additive systems is unknown but has the potential to improve emulsion stability, pushing the materials further toward commercial utility.

This study reports the combination of DEGMA BCSs with secondary surfactants and polymeric/oligomeric additives with the aim of generating stable emulsions with the potential for *in situ* pharmaceutical applications. A range of secondary surfactants and additives are explored to determine effects on thermoresponse, compatibility with BCS, and stability. The effect of oil type is also studied to evaluate compatibility of the BCS with pharmaceutically relevant oils and expand the potential vehicles for drug solubilisation in future. The ability of the BCS-stabilised emulsions to undergo thermoresponsive gelation is assessed by rheology, which allows the determination of the potential for *in situ* gel formation and T_{gel}. Small-angle neutron scattering is employed to probe the nanostructure of the systems, which is fundamental to understanding the bulk properties of the thermoresponsive emulsions.

5.2 Materials and methods

5.2.1 Materials

Di(ethylene glycol) methyl ether methacrylate (DEGMA, 95%), poly(ethylene glycol) methyl ether methacrylate (PEGMA, M_n 950 gmol^{-1}), ethylene glycol dimethacrylate (EGDMA, 98%), 1-dodecanethiol (DDT, 99%), deuterium oxide (99.9 atom % D), anhydrous dodecane (99%), tetradecane, mineral oil (batch no. MKCQ7240, CAS no. 8042-47-5), sunflower oil (batch no. BCCH0522, CAS no. 8001-21-6), sodium lauryl sulfate, lauryl alcohol, laureth-9, and methyl cellulose (2000 cP, 2% aqueous solution at 20 °C) were purchased from Sigma-Aldrich (UK). α, α -azoisobutyronitrile (AIBN, >99%) was obtained from Molekula (UK). Ethanol was supplied by VWR (UK). n-Dodecane-d26 (neat) was purchased from QMX (UK). Dialysis tubing with molecular weight cut off (MWCO) of 14 kDa was purchased from Sigma Aldrich (UK). Corn oil was purchased from Acros Organics

(UK). Brij 30 and PEG 400 were purchased from Fisher Scientific (UK). Deionised water was employed in all experiments. All chemicals were used as received.

5.2.2 Synthesis of branched copolymer surfactant (BCS) by free radical polymerisation

The thermoresponsive BCS (P14) was prepared with a procedure described previously in Section 4.2.2 in Chapter 4.[1] DEGMA (174 mmol), PEGMA (3 mmol), EGDMA (12 mmol) and DDT (12 mmol) were dissolved in ethanol (190 mL) then bubbled with nitrogen gas for 1 h. Subsequently, a solution of AIBN (1.2 mmol) in ethanol (10 mL) was added. The reaction was then heated to 70 °C and stirred continuously. After 48 h, the reaction mixture was gently distilled at 80 °C to remove ethanol. The resultant crude polymer was dissolved in water and transferred to a pre-soaked dialysis bag. The dialysis bag was immersed in deionised water for 7 days and the water was replaced at regular intervals to facilitate the purification process. The resultant polymer solution was subjected to lyophilisation for 48 h to obtain a freeze-dried product (yield 85 %).

^{1}H NMR was used to confirm product formation for the BCS using a Bruker Advance AM 600 NMR instrument with $CDCl_3$ at ambient temperature. Delta 5.3.1 NMR software was used to process the data.

Gel-permeation chromatography was conducted using an Agilent Infinity II MDS instrument equipped with differential refractive index, viscometry, dual angle light scattering and variable wavelength UV detectors. The system was equipped with 2 x PLgel Mixed D columns (300 x 7.5 mm) and a PLgel 5 μm guard column. The eluent was DMF with 5 mmol NH_4BF_4 additive. Samples were run at 1ml/min at 50 °C. Poly(methyl methacrylate) standards (Agilent EasiVials) were used for conventional and universal calibration between 955,000 - 550 $gmol^{-1}$. Analyte samples were filtered through a nylon membrane with 0.22 μm pore size before injection. Number-average molar mass (M_n) and dispersity (Đ) values were determined by universal calibration using Agilent GPC/SEC software.

5.2.3 Emulsion formation

Aqueous BCS solutions with concentration of 5, 10, or 20 wt% were prepared in cold water. If required, additives (surfactants/polymer/oligomer) were then added at the

concentration stated in the associated results. The mixture was refrigerated with intermittent vortexing every 15 min until a clear solution was obtained. The preparation of oil-in-water emulsions stabilised was then carried out by mixing 2.5 g of aqueous BCS solution with 2.5 g of dodecane oil. The mixture was emulsified for 2 min using a Silverson L4R mixer using a 5/8" micro tubular frame with integral general purpose disintegrating head at 2400 rpm and left to rest for 36 h at room temperature. The creamed phase of the emulsions was then isolated for further analysis. The emulsion mass yield was then defined in equation 1:

$$mass\ yield\ (\%) = 100 \times \frac{5 - Mass\ Water}{5}$$

Where "Mass Water" is the mass of the lower phase extracted after creaming for a total sample mass of 5g. The oil phase volume of creamed region (ϕ_{oil}) may also be determined by equation 2:

$$\varphi_{oil} = \frac{\left(\frac{2.5}{\rho_{oil}}\right)}{\left(\frac{2.5}{\rho_{oil}}\right) + (2.5 - Mass\ Water)}$$

Where ρ_{oil} is the density of the oil and 2.5 is the mass of the oil added in g.

Emulsion droplet size was determined by Laser Diffraction using a Sympatec HELOS/BR QUIXEL. 10 µl of emulsion was added to the dispenser R3 cuvette containing 50ml of water with constant stirring at 1800 rpm. Water was used as reference before sample measurement. All the samples were measured at optical concentration of approximately 30%. Trigger conditions were as follows: reference measurement duration – 10 s, signal integration time – 100 ms, trigger timeout – 90 s.

5.2.4 Rheological evaluation of emulsion systems

The rheological properties of the resulting emulsions were studied using an AR 1500ex rheometer with a Julabo cooling system. Analysis was conducted with a gap size of 500 µm using a 40 mm parallel plate geometry. Samples were placed onto the lower plate and trimmed after lowering of the upper plate to the geometry gap stated. The sample was then enclosed using a solvent trap. Temperature ramps were performed from 20 to 60 °C

at 1 °C/min intervals (controlled by a Peltier), with a strain of 0.1 % and a frequency of 6.28 rad/s, following a 2 min equilibration period at 20 °C. The cooling cycle was determined by reducing the temperature from 60 to 20 °C at 1 °C/min intervals, at a strain of 0.1 % and a frequency of 6.28 rad/s. Frequency sweeps were conducted at a shear strain of 0.1 % between 0.628 and 100 rad/s with a 2 min equilibration period at the stated temperature.

5.2.5 Transmission electron microscopy (TEM) of BCS solutions

Transmission electron microscopy of BCS solutions was conducted with a 120 kV TEM microscope Tecnai G2 Spirit Twin (FEI, Czech Republic) with 150,000x magnification. 10 wt% BCS and 10 wt% BCS with 0.25 wt% methylcellulose were prepared in water as described previously. The specimens for TEM were prepared by dropping 4 µL of sample solution onto a microscopic copper TEM grid (300 mesh) coated with thin, electron-transparent carbon film. After 15 min of sedimentation the excess solution was removed by touching the bottom of the grid with a filter paper (designated the "fast drying method"). This fast removal of solution was performed in order to minimise oversaturation during the drying process.[5,6] Subsequently, the particles were negatively stained with uranyl acetate (2 wt.% solution dropped onto the dried nanoparticles and removed after 15 s in the same manner as the previous solution). The sample was finally left to dry completely and observed with the TEM microscope.

In the next step, the specimens were prepared at elevated temperature using an analogous procedure. The solutions and all tools for sample preparation (grids, tweezers, uranyl acetate solutions etc.) were incubated in an electric oven heated to 40 °C. Then the pre-heated solutions were deposited to the TEM grid and left to sediment for 15 min (the sedimentation took place in the oven at 40 °C). Then the excess solution was removed, and the particles were negatively stained with pre-heated solution of uranyl acetate (as described in the previous paragraph) and left to dry completely (again in the oven at 40 °C). With this approach, the sample morphology could be stabilised at elevated temperature and then observed with TEM microscope at laboratory temperature, as documented in previous studies.[6,7]

5.2.6 Small angle neutron scattering (SANS)

SANS experiments were conducted on the time-of-flight diffractometer instrument SANS2d at the STFC ISIS Neutron and Muon Source (UK). Incident wavelengths from 1.75 to 12.5 Å were used at a sample-to-detector distance of 12 m, which gave a scattering vector (q) range from 1.6×10^{-3} to 0.25 $Å^{-1}$. Temperature of the samples was controlled by an external circulating water bath (Julabo, DE). Samples were loaded in 1 cm wide rectangular quartz cells with 1 mm pathlength. Solutions of BCS and BCS with methylcellulose were prepared as described in Section 2.3 in D_2O. Emulsions were then prepared with the addition of deuterated dodecane. The raw SANS data were then processed using wavelength-dependent corrections to the incident spectrum, detector efficiencies, and measured sample transmissions.[8] The data were then absolutely scaled to give profiles of scattering intensity I(q) as a function of q, using the scattering from a standard sample (comprising a solid blend of protiated and perdeuterated polystyrene) based on established methods.[9] All samples were confirmed to be free of multiple scattering. SANS data were fitted using SASView 4.2.2.[10] Where required, scattering length densities (SLDs) were calculated from the monomeric unit using the Neutron activation and scattering calculator website from NIST centre for neutron research.[11]

5.2.7 Hot stage light microscopy of emulsions

Light microscopy (LM) of the emulsions at selected temperatures was performed with a LM microscope Nikon Eclipse 80i (Nikon, Japan) equipped with a Linkam THMS600 (Linkam, UK) temperature control stage. A small volume of the emulsion was dropped onto a thin microscopic cover glass, covered with another cover glass and inserted in the temperature control stage. The temperature was increased slowly (1 °C/min) to 25 °C, held for 5 min and LM micrograph was recorded. The same procedure was applied for 30, 35, 40, 45 and 50 °C.

5.3 Results and discussion

The BCS was successfully synthesised using DEGMA, PEGMA, EGDMA, and DDT (Figure 5.1), then used to produce thermoresponsive emulsions. NMR analysis confirmed that the purity of the polymer was > 99.8 % using the residual monomer protons visible at 5.8 and 5.3 ppm against the signal from the polymer backbone (0.5-1.5 ppm), and proton signals were consistent with previous publications.[1] GPC confirmed that the BCS had M_n 12.5 kDa with Đ of 4.16, with a monomodal size distribution. From the universal calibration, the average radius of gyration of the BCS was 2.25 nm. A 20 wt% solution of the polymer was then homogenised in the presence of an equal mass of dodecane to disperse the oil phase. This emulsion was then designated to be 10 wt% BCS. The process gave a cloudy phase which exhibited creaming. The creamed phase was then isolated after 36 h to give BCS-stabilised emulsions of dodecane-in-water. No further creaming was observed over the duration of the experiments reported. The mass of this creamy phase compared to the initial mass of all components (5 g) was designated to be the yield, in this case 76 %. The final oil phase volume, ϕ_{oil}, was determined to be 0.72. It should be noted that due to the sample preparation method, these two parameters are inversely proportional to each other.
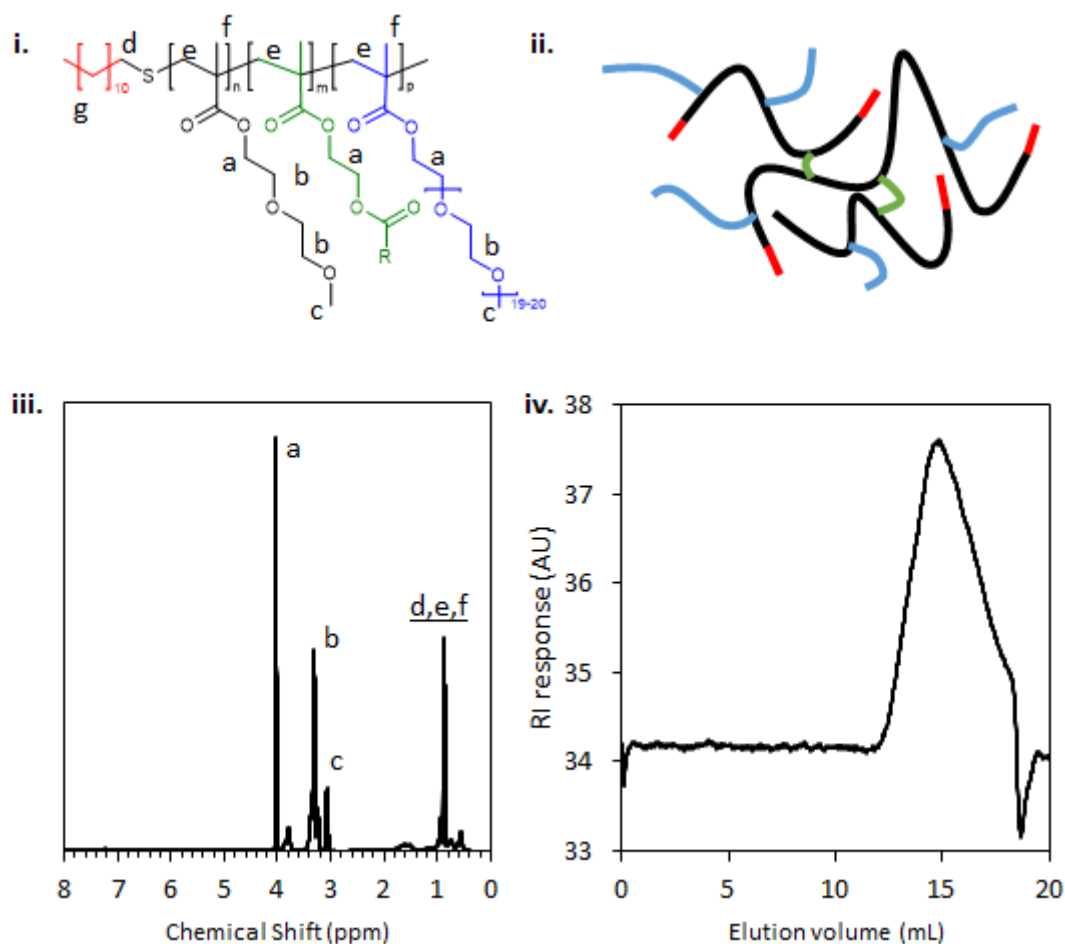
Figure 5.1: Chemical structure (R represents another polymer chain to indicate branching) (i) and schematic diagram (ii) of BCS (P14 system) containing DDT (red), DEGMA (black), EGDMA (green), and PEGMA (blue). NMR spectra with overlaid signal allocation (iii) and GPC trace are also shown (iv).

Rheological analysis of the BCS-stabilised emulsion was conducted. Initially, small-amplitude oscillatory rheology at a fixed frequency was used to study the effect of temperature on the emulsions. This experiment allows the determination of the storage (G') and loss (G") moduli at shear strains sufficiently small to lie within the linear viscoelastic region of the system (0.1% strain), thus retaining the sample structure. The fixed frequency allows for initial investigation of temperature effects alone. The temperature ramp (Figure 5.2) shows clear thermoresponsive behaviour in the BCS-stabilised emulsion. At low temperatures, G' (red) and G" (blue) are low (ca. 3-8 Pa) with the material in a predominantly liquid-like state (G" > G'). Upon heating above ca. 30 °C,

both moduli increase and the system transition to a predominantly elastic state (G'> G") at 32 °C, which is a commonly used criterion to indicate gel formation.[12,13] As such, 32 °C was designated as T_{gel}. Further heating (above ca. 40°) reduced G' and G", which is attributed to reducing interaction between droplets as further kinetic energy is added to the system or structural evolution of the BCS system at higher tempeatures. The sol-gel transition was clearly observed upon heating by vial inversion, without any observable syneresis (Figure 5.2). This transition is presumed to arise from the LCST of DEGMA, which is known to be ca 31-35 °C when copolymerised with PEGMA.[14] Above T_{gel}, the system reached a plateau at ca 35 °C with a G' of ca 80 Pa. This temperature makes the emulsion a potential *in situ* gel-former for pharmaceutical applications, where the surface temperature of the body is estimated to be 32-35 °C and internal temperature is 37 °C. The cooling of the system shows a reversibility of this transition with a hysteresis of ca 2 °C. Thus, there is potential for removal of the dosage form by local cooling and extraction.
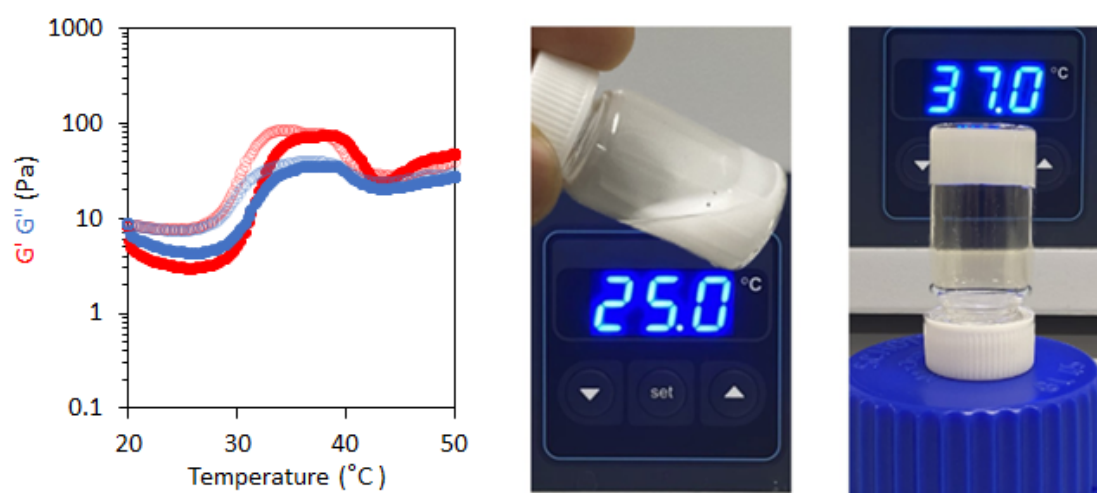
Figure 5.2: Small-amplitude oscillatory rheology (left) of dodecane-in-water emulsions stabilised with P14 thermoresponsive BCS with heating (filled circles) and cooling (open circles) and a fixed angular frequency (6.28 rad/s) and strain (0.1%) showing G' (red) and G" (blue). The emulsions exhibited macroscopic switch (right) from a liquid state (25°C) to a gel state (37°C) by vial inversion without any observed syneresis.

Small-amplitude frequency sweeps were conducted to evaluate the rheological properties of the BCS-stabilised emulsion above and below T_{gel} (Figure 5.3). At 30 °C, below T_{gel}, the emulsion displayed predominantly liquid-like behaviour, with $G'' > G'$ at all frequencies measured. Upon heating above T_{gel} (35 and 37 °C), two major effects may be noted at both temperatures. Firstly, the emulsions become predominantly elastic at all frequencies, with $G' > G''$, which provides further evidence for the formation of a gel state.[15] Secondly, the magnitude of both moduli increases ca. ten-fold compared to those at T_{gel}, and as such, the overall resistance to deformation of the material increases substantially. At 35 °C, the low frequency region of the rheogram appears to trend toward intersection of the moduli, however no relaxation time was reached within the frequencies measured. At 37 °C the emulsion did not exhibit this reduction in relative elasticity with frequency (i.e., a reduction in loss tangent), and as such, the emulsions stabilised by BCS alone are better suited to internal body sites at 37 °C (such as intravaginal, rectal, and nasal delivery) to reduce any viscous flow over long timescales.
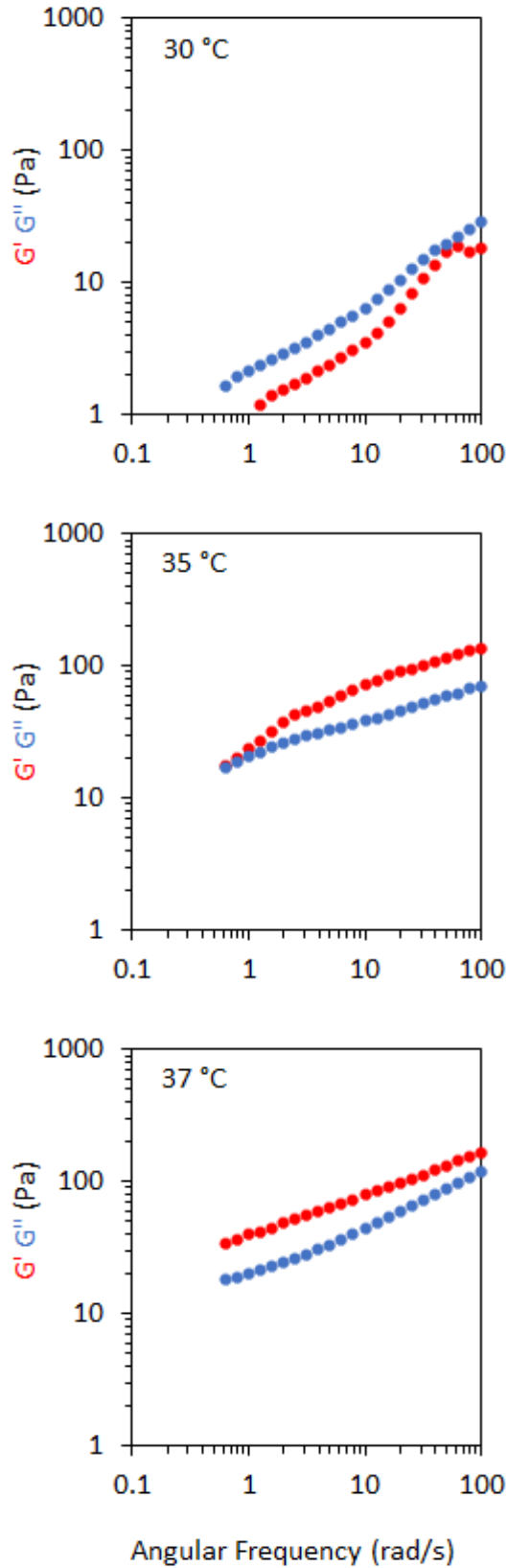
Figure 5.3: Rheological behaviour of emulsions stabilised by thermoresponsive BCSs (P14) at 10 wt% concentration evaluated by frequency sweeps below (30 °C) and above T_{gel} (35 and 37 °C). G′ is shown in red and G″ is shown in blue.

The BCS was then evaluated as an emulsifier for a broader range of oils, to investigate compatibility with oils outside of the model dodecane system (Table 5.1). Tetradecane was initially explored to probe an oil chain length which was not matched to the C12-terminated BCS. Mineral oil, composed of a mixture of hydrocarbons from crude oil, was also studied to further test the system. Sunflower oil and corn oil were also emulsified with BCS, where these oils are typically composed of triglycerides with greater polarity than simple hydrocarbons.[16] Mineral oil, sunflower oil, and corn oil are all used as pharmaceutical excipients and help probe the potential exploitation of BCS in the pharmaceutical industry.[17] All oils were successfully emulsified by the BCS at 10 wt% concentration in the emulsion, and the emulsion yield and ϕ_{oil} were recorded after isolation of the creamed phase (Table 5.1). Laser diffraction allowed measurement of droplet size distributions, giving X_{10}, X_{50}, and X_{90} values, which correspond to diameter values below which 10, 50 and 90 % of the population are found, respectively. Typically, X_{50}, representing the median is used as an average with the other two values giving a numerical description of dispersity. Full distributions can be found in Figure A25. Overall, the median droplet size appeared to increase from ca 4 to 6 μm as oil density increased. The mass yield of the creamed phase also increased with the density of the oil, likely due to the velocity of creaming being directly related to the difference in density between the two phases of the emulsion.[18] Creaming becomes reduced as the density of the oils approach the density of water. This is despite an increase in droplet size, which would typically accelerate the velocity of creaming, highlighting density changes as the dominant factor. Likewise, the final ϕ_{oil} decreased as the yield increased due to the larger fraction of water in these samples. Overall, the emulsions were effectively stabilised at internal phase volumes greater than 0.5, albeit with the occurrence of creaming.

Table 5.1: Yield and oil phase volume (ϕ_{oil}) of BCS-stabilised emulsions following isolation of the creamed phase (n=1).

Oil phase	Density of oil (kg/L)	Yield (wt%)	ϕ_{oil}	Droplet size (µm)		
				X_{10}	X_{50}	X_{90}
Dodecane	750	76	0.72	1.28	4.00	8.61
Tetradecane	762	78	0.70	1.11	4.17	9.23
Mineral oil	820	80	0.67	1.34	4.13	8.29
Sunflower oil	920	84	0.62	0.85	5.86	17.31
Corn oil	920	84	0.62	0.93	6.12	14.31

The oscillatory rheology of BCS-stabilised emulsions was then probed by temperature ramps, as described previously (Figure 5.4). The BCS was successful in imparting a sol-gel transition to all emulsified oils studied, without substantial changes to T_{gel}. The plateau region where the gel state (G' > G") was maintained at its maximal value of G' occurred over a smaller temperature range in tetradecane (33-40 °C) and mineral oil (35-40 °C) relative to dodecane (30-42 °C), however all emulsions were gels at body temperature (37 °C). Sunflower and corn oils appeared to be amenable to sol-gel behaviour, with relatively minor variation in G' and G" above T_{gel} (33 °C). These oils are mixtures of triglycerides and minor components such as phospholipids [16]. The BCS system is thus both effective at forming emulsions with this range of oils as well as imparting the desired thermoresponsive gelation which can lead to *in situ* gel-forming materials.
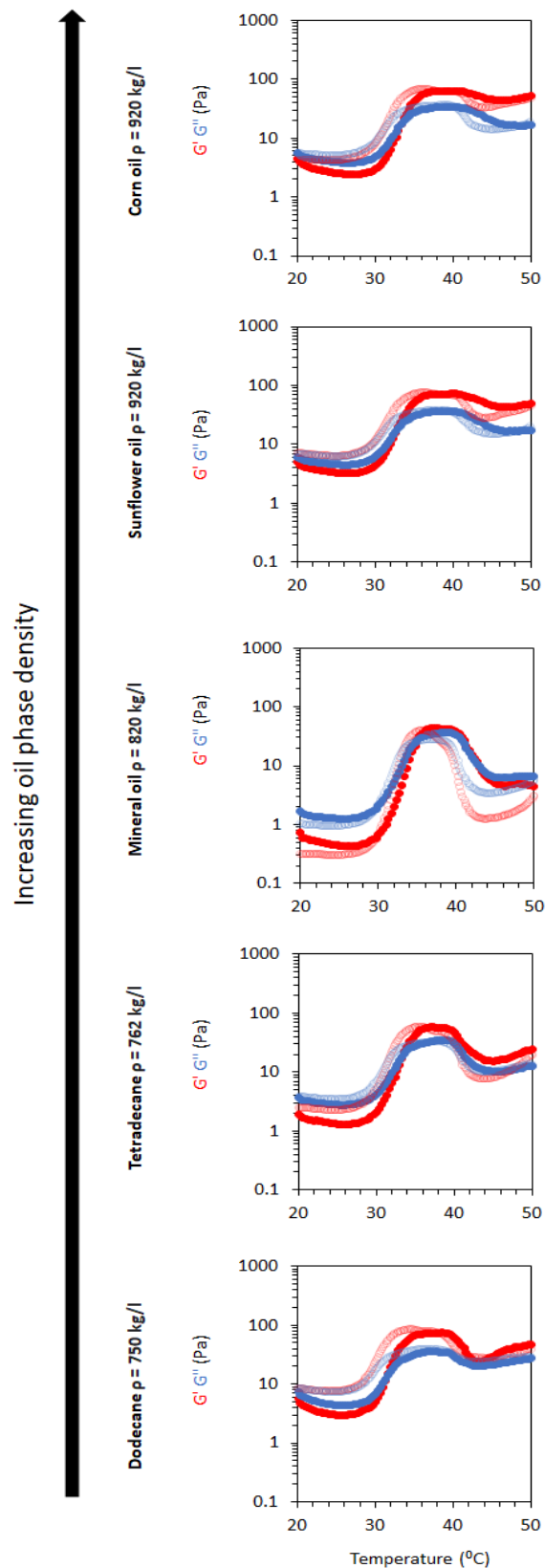
Figure 5.4: Small-amplitude oscillatory rheology of emulsions of various oil types with heating (filled circles) and cooling (open circles) and a fixed angular frequency (6.28 rad/s) and strain (0.1%). G' (red) and G" (blue) are shown.

Despite successes in generating thermoresponsive emulsions with a diverse range of oils, all the emulsions exhibited significant creaming. Secondary co-surfactants were explored to further stabilise the emulsion systems (Figure 5.5). In this study, head group chemistry was explored, using C12 alkyl tail surfactants to match the alkyl chain length on the DDT end groups of the BCS. This increases the likelihood of compatibility of the two tail groups, where mixed small-molecule surfactants are better able to form condensed films at interfaces when tail length is matched.[19] The first series of additives explored are lauryl (dodecyl) alcohol, lauryl (dodecyl) sulfate, Brij-30 and laureth-9. Lauryl alcohol has an -OH head group and is selected as a model small non-ionic surfactant with limited steric hinderance in the aqueous phase. Lauryl sulfate is an ionic surfactant used to explore the effect of ionic/non-ionic head group on emulsion behaviour. Brij-30 and laureth-9 are non-ionic surfactants, like lauryl alcohol, but have increasingly long oxyethylene chains as their head group, with degrees of polymerisations of 4 and 9, respectively. This allows the effect of head group size to be explored. A second pair of polymeric/oligomeric additives were also explored, namely, polyethylene glycol (PEG) 400 and methylcellulose, which have a degree of surface activity and can also increase the viscosity of the continuous water phase and reduce the velocity of creaming.
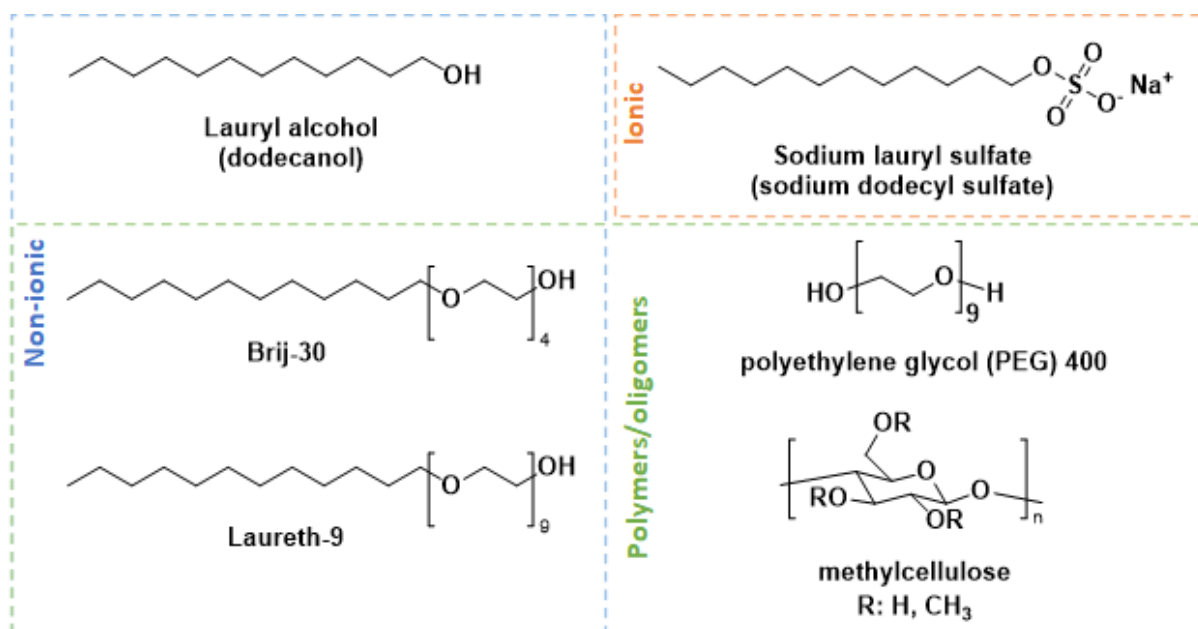
Figure 5.5: Chemical structures of additives to BCS-stabilised emulsions

Initially, the first surfactant series (lauryl alcohol, sodium lauryl sulfate, Brij-30 and Laureth-9) were mixed with 10 wt% BCS at increasing surfactant concentration (0.5, 1.0, 1.5 and 2.0 wt%) and homogenised to disperse the oil phase. All mixtures successfully formed emulsions (Table 5.2), however degrees of creaming varied and hence emulsion yields. The final value of ϕ_{oil} is inversely proportional to the yield, due to the removal of the lower aqueous phase. Overall, the non-ionic surfactants gave a greater yield than the ionic surfactant (sodium lauryl sulfate), however all surfactants reduced creaming relative to the BCS alone (yield = 76%, ϕ_{oil} = 0.72). Laser diffraction was used to determine droplet sizes of the emulsions (Table 5.3). Median particle size (X_{50}) of all systems was close to that of BCS emulsions without additive, ca 4 μm. Due to the similarity in droplet size, it is suggested that the homogenisation technique is the major factor that determines the diameter. Particle size distributions (Figure A26 in appendix) indicated a stronger bimodal distribution in the sodium lauryl sulfate system than the other surfactants, with peaks centred on ca 3 and 9 μm. Other systems were largely monomodal with a minor shoulder at lower diameter.

Table 5.2: Yield and oil phase volume (ϕ_{oil}) of BCS/additive emulsions after isolation of the creamed phase at 36 h.

	Yield (wt%)				ϕ_{oil}			
Concentration:	0.5 wt%	1.0 wt%	1.5 wt%	2 wt%	0.5 wt%	1.0 wt%	1.5 wt%	2 wt%
Lauryl alcohol	86	90	92	94	0.74	0.74	0.72	0.68
Sodium lauryl sulfate	74	74	76	82	0.69	0.66	0.60	0.59
Laureth-9	80	84	94	96	0.65	0.63	0.61	0.60
Brij 30	76	80	90	96	0.72	0.69	0.63	0.59
PEG 400	76	80	84	88	0.72	0.69	0.66	0.64

Table 5.3: Droplet size of BCS/additive (2 wt%) emulsions after isolation of the creamed phase at 36 h (n=1).

Additive (2 wt %)	Droplet Size (μm)		
	X_{10}	X_{50}	X_{90}
Lauryl alcohol	1.38	5.28	9.90
Sodium lauryl sulfate	1.47	4.75	10.74
Laureth-9	1.26	4.23	8.69
Brij 30	1.32	4.40	8.98
PEG 400	1.32	4.08	7.53
Methylcellulose	1.87	3.13	5.35

Shear rheology of the BCS/surfactant-stabilised emulsions was then explored with temperature (Figure 5.6). Overall, the addition of surfactant appeared to hinder thermogelation events, particularly at concentrations > 0.5 wt%. Lauryl alcohol was the best-performing surfactant, with thermogelation occurring in all samples measured, with T_{gel} ca 33 °C. Comparison with sodium lauryl sulfate showed that the ionic sulfate head group was detrimental to the emulsion relative to the hydroxy group of the lauryl alcohol. Furthermore, increasing the volume of the head group also limited the ability of the emulsion to undergo gelation, completely eliminating the phenomenon at concentrations > 0.5 wt%. All rheograms showed some level of thermoresponsive character, however in the Brij 30, laureth-9, and sodium lauryl sulfate emulsions this was a reduction in viscosity upon heating, which was not of interest in this study. Overall, lauryl alcohol was the most effective cosurfactant, increasing the yield by ca 20 % and allowing the emulsion to undergo thermogelation at a physiologically relevant temperature.
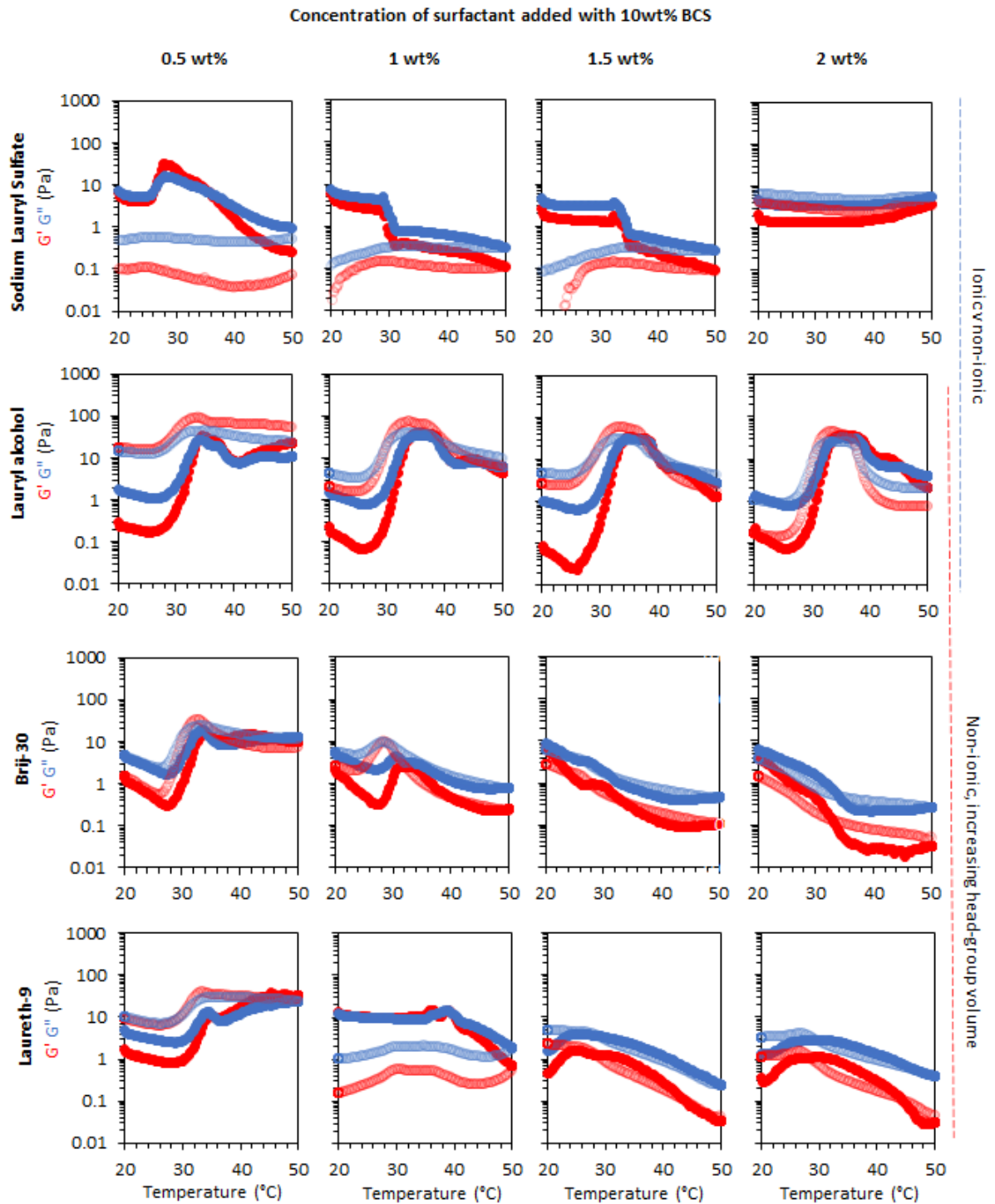
Figure 5.6: Temperature-ramp shear rheology of dodecane-in-water emulsions stabilised with 10 wt% BCS with added surfactant. G' (red) and G" (blue) are shown. Closed symbols indicate heating, whilst open symbols indicate cooling.

Mechanisms of gelation have been reported in thermoresponsive BCS-stabilised emulsions.[1,20] At low temperatures, BCS is present at both the oil interface and in the bulk as nano-sized oblate ellipsoids. Upon heating, the nano-ellipsoids grow in size due to the LCST of the DEGMA component, driving polymer-polymer associations. In aqueous solutions of BCS, this leads to an increase in viscoelasticity but not gelation.[1] At the oil-water interface, a thickening of the stabilising polymer layer occurs due to the LCST effect, drawing polymer from the bulk to the interface.[20] Connectivity between BCS at the interface and BCS in the bulk is critical for gelation to occur. Elimination of thermogelation events in the rheology of the BCS/cosurfactant emulsions (Figure 5.6) may be the result of: polymer-surfactant interaction in the bulk affecting the connective polymer aggregates; displacement of BCS from the emulsion surface; or hindering the emulsion droplets from coming into suitable proximity to allow connectivity to occur. As lauryl alcohol did not eliminate thermogelation, it is not believed that polymer-surfactant interaction in the bulk is a dominant effect limiting the ability of the emulsions to undergo gelation. Typically, the interaction of surfactant with thermoresponsive polymer leads to increases in the LCST, which was not observed in this case.[21] Thus, the negative effects of sodium lauryl sulfate, Brij-30 and laureth-9 are ascribed to charge and steric effects, respectively, hindering the BCS to connect from one O/W interface, through the bulk, to another. Hypothesised mechanisms for this are displacement of BCS from the interface and hindrance of the droplets from reaching close proximity.

Table 5.4: Yield and oil phase volume (ϕ_{oil}) of BCS/methylcellulose emulsions after isolation of the creamed phase at 36 h.

	Methylcellulose concentration			
	0.1 wt%	0.2 wt%	0.25 wt%	0.5 wt%
Yield	90	98	100	100
ϕ_{oil}	0.63	0.58	0.57	0.57
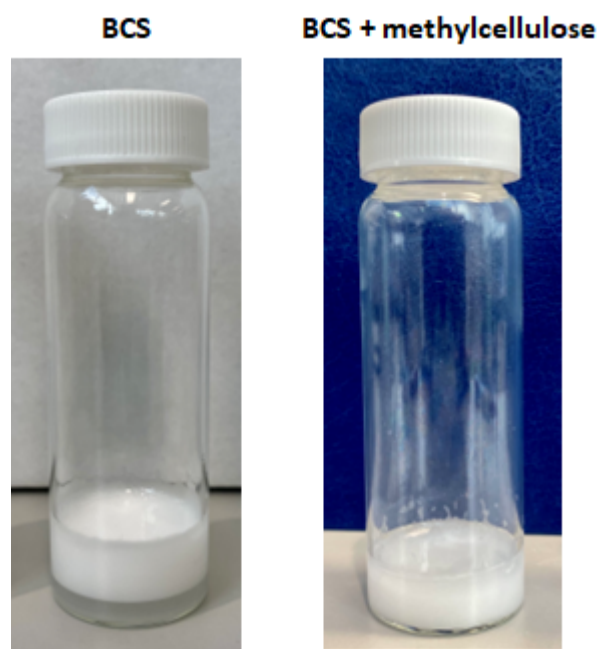
Figure 5.7: Dodecane-in-water emulsions stabilised by BCS alone (10 wt%, left) or BCS/methylcellulose (10/0.25 wt%, right) after 36 h storage at room temperature.

Polymeric/oligomeric additives were then explored for their compatibility with BCS-stabilised emulsions. Both PEG 400 (Table 5.2) and methylcellulose (Table 5.4) greatly reduced emulsion creaming. Methylcellulose was particularly effective, eliminating any evidence of creaming by 0.25 wt%, giving a final emulsion with ϕ_{oil} of 0.57 (Figure 5.7). Methylcellulose generated emulsions with the smallest median droplet diameter of any additive (Table 5.3) with a narrower size distribution (Figure A17 in appendix), which is a contributor to the stability of the system. Emulsions stabilised with mixtures of BCS and both additives exhibited the desired themogelation profile (Figure 5.8), with T_{gel} of 33 and 30 °C for PEG 400 and methylcellulose, respectively. It is believed that one reason for this effectiveness is that these additives typically form multilayer structures at interfaces rather than monolayers, and thus may be less likely to displace BCS from the interface. There may also be specific synergic effects seen in the BCS/methylcellulose mixtures. Interestingly, methylcellulose extended the G' plateau region over which the gel state was present, up to the highest temperature measured (50 °C) with 0.5 wt% additive concentration. Combining this effect with the stability of the system, methylcellulose was identified as the optimal additive in this study. Once the emulsions were formed, they

were visually stable for at least 3 months on the benchtop where the use of BCS alone lead to additional creaming over this time period (Figure A27 in appendix). In addition, the thermoreversible gel formation in the emulsions stored for 3 months was confirmed by rheology (Figure A28 in appendix). The remainder of the study focussed on exploring the properties and structure of this optimised formulation.
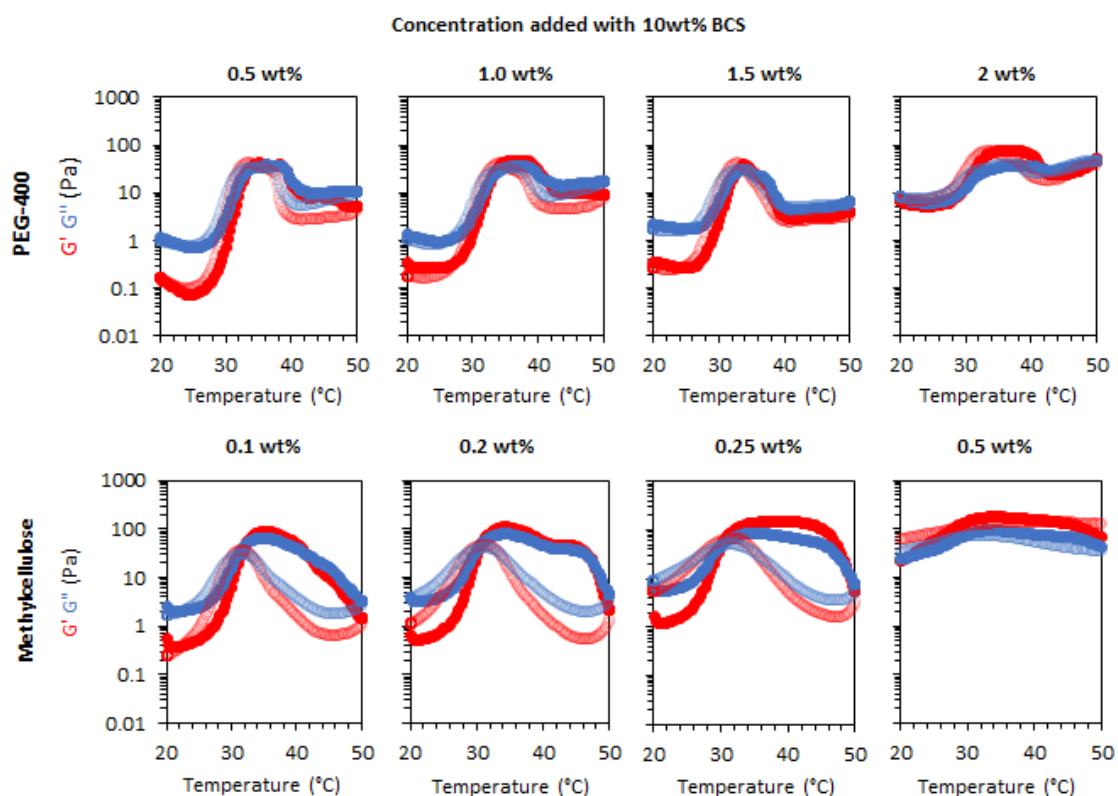
Figure 5.8: Temperature-ramp shear rheology of emulsions stabilised with 10wt% BCS with added PEG 400 or methylcellulose. G' (red) and G" (blue) are shown. Closed symbols indicate heating, whilst open symbols indicate cooling.

The shear rheology of the BCS/methylcellulose (10/0.25 wt%) emulsions was then explored with small-amplitude oscillatory frequency sweeps at temperatures below (25 °C), around (30 °C) and above (35, 37 and 40 °C) gelation (Figure 5.9). At 25 °C, the system showed a liquid-like behaviour, with G" > G'. At 30 °C, the emulsion showed a ten-fold increase in viscosity and transitioned to a viscoelastic material with a maximum relaxation time of 0.1 s, taken as the inverse of the cross-over frequency between G' and G". At 35-

40 °C, the emulsion was predominantly solid-like G' > G" at all frequencies measured. At the highest frequency measured (100 rad/s), G' increased from 42 Pa at 25 °C to 341 Pa at 37 °C, an approximately 8-fold increase in elasticity of the materials. This highlights the potential of the materials as *in situ* gel forming agents in drug delivery.
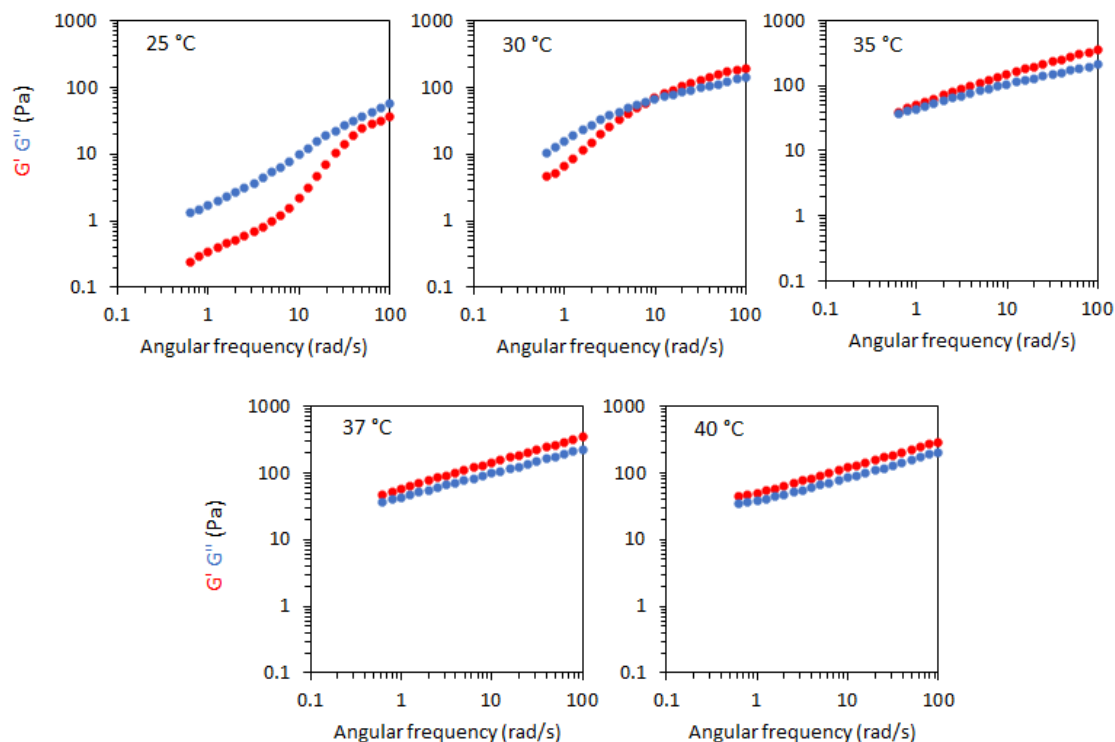
Figure 5.9: Rheological behaviour of emulsions stabilised by thermoresponsive BCSs at 10 wt% concentration with 0.25 wt% methylcellulose evaluated by frequency sweeps below (25 and 30 °C) and above T_{gel} (35, 37, and 40 °C). G' is shown in red and G'' is shown in blue.

Transmission electron microscopy (TEM) was initially conducted to probe nanostructures present in solutions of BCS (Figure 5.10). At 25 °C the TEM images show exceedingly small objects without clearly defined structure. At 40 °C the appearance of nanoscale objects can clearly be visualised. These nano-objects of ca 10-50 nm dimensions appeared to be a mixture of circular and elongated elliptical objects. As TEM gives a projected two-dimensional shape, it is plausible that these structures are oblate elliptical objects viewed from above, appearing as a circle, and side-on, appearing as an ellipse. A key limitation of

the TEM technique is the drying procedure required for imagining to be conducted, thus solution behaviour was probed by SANS.
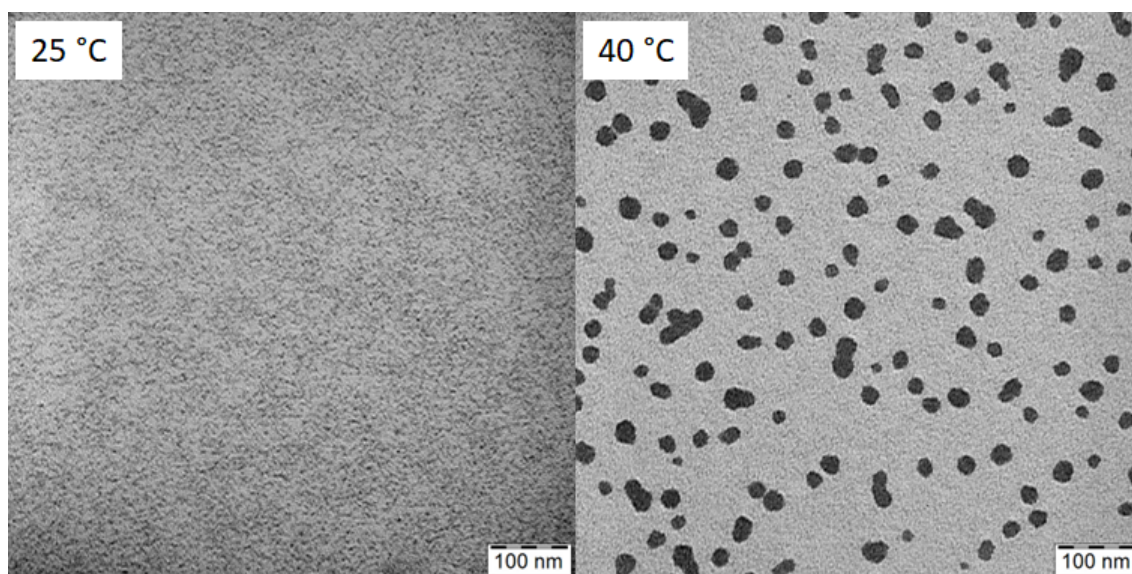
Figure 5.10: TEM micrographs of BCS dried at 25 °C and 40 °C, indicating transition from small clusters to larger nano-objects.

Small-angle neutron scattering (SANS) was employed to understand the nanostructures present in the emulsions. It is known that thermoresponsive gelation is linked to hierarchical processes occurring at the polymer level, self-assembled nano-aggregate level, and in the supracolloidal assemblies of these aggregates.[22,23] Thus, SANS is a powerful technique to probe nanostructure of aggregates and their interactions underpinning the gel state. In the SANS study, BCS was measured at 20 wt% in D_2O, equivalent to the water phase used in 10 wt% emulsion, at 25, 35, and 45 °C to measure nanostructure below and above the LCST in water alone. Additionally, 0.5 wt% methylcellulose and 20 wt% BCS with 0.5 wt% methylcellulose in D_2O was measured at these temperatures to understand any effect of adding methylcellulose to the structure of BCS. Emulsions of both BCS and BCS/methylcellulose were prepared with deuterated dodecane and D_2O, masking both the water and oil phases in the emulsion system and showing only polymer in the scattering profile. Scattering profiles required both form factors, which describes the morphology of the scattering objects, and structure factors which account for interactions between the objects.

SANS of solutions of BCS alone show structural transitions with temperature (Figure 5.11). At 25 °C the scattering pattern was fitted to an ellipsoidal form factor, consistent with TEM, with uniform scattering length density combined with a power law.[24] The polar and equatorial radii of this ellipsoid are 34 by 122 Å, indicating that the ellipsoid is oblate. This is in-line with a previous study of the BCS class.[1] In brief, it is hypothesised that steric constraints from the BCS branched structure does not allow the more typical spherical morphology to occur in aggregates of BCS, leading to this oblate morphology. The nano-objects at this temperature, below the LCST transition, are assumed to be formed in water due to the hydrophobic terminal groups driving a self-assembly process into an aggregate. The object has a scattering length density (SLD) of $4.8 \times 10^{-6} \text{Å}^{-2}$, indicating hydration of the aggregate (SLD PEG: ca $0.88 \times 10^{-6} \text{Å}^{-2}$, SLD D_2O: $6.37 \times 10^{-6} \text{Å}^{-2}$).[11] Given the uncertainty around the degree of hydration and the volume fraction of the aggregates formed, fitting was typically attempted using the approximate volume fraction of BCS and conclusions drawn from the value of the SLD are limited. A power law was required to fit the low q region. The exponent of this form factor is - 4, indicative of Porod-type scattering arising from objects larger than the q range studied. This can be attributed to larger aggregates or clusters of polymers.[25] When the sample was heated to 35 °C, the upturn at low q disappeared, which is attributed to a larger fraction of the polymer chains forming the well-defined ellipsoidal aggregates. These aggregates have polar and equatorial radii of 88 and 522 Å, respectively, showing growth of the objects, particularly along the equatorial radii. The ellipsoidal form factor required a "sticky-hard-sphere" structure factor, describing hard-sphere interactions with a narrow attractive well.[26] At 45 °C the scattering was again fitted with an ellipsoid form factor with a sticky hard-sphere structure factor, albeit with alterations to both the perturbation and stickiness term in the fits. Additionally, at 45 °C the ellipsoids have grown along their equatorial radii (972 Å) with a polar radius nearly unchanged (87 Å). This anisotropic growth has been observed previously for similar BCS systems.[1]

Considering the temperature effects on SANS of BCS solutions the following conclusions are drawn:

- At 25 °C, below the LCST, the BCS exist as nano-objects with an oblate ellipsoidal geometry, driven by hydrophobic interactions from DDT (polymer termini). Larger aggregates with sharp interfaces exhibiting Porod scattering are also present.

- At 35 °C, above the LCST, the larger aggregates disappear and the nano-objects present grow larger and more oblate. These aggregates then interact attractively. These effects are attributed to increased hydrophobicity of the constituent BCS above DEGMA LCST.

- At 45 °C, further anisotropic growth of the BCS aggregates occurs with the attractive interactions retained.
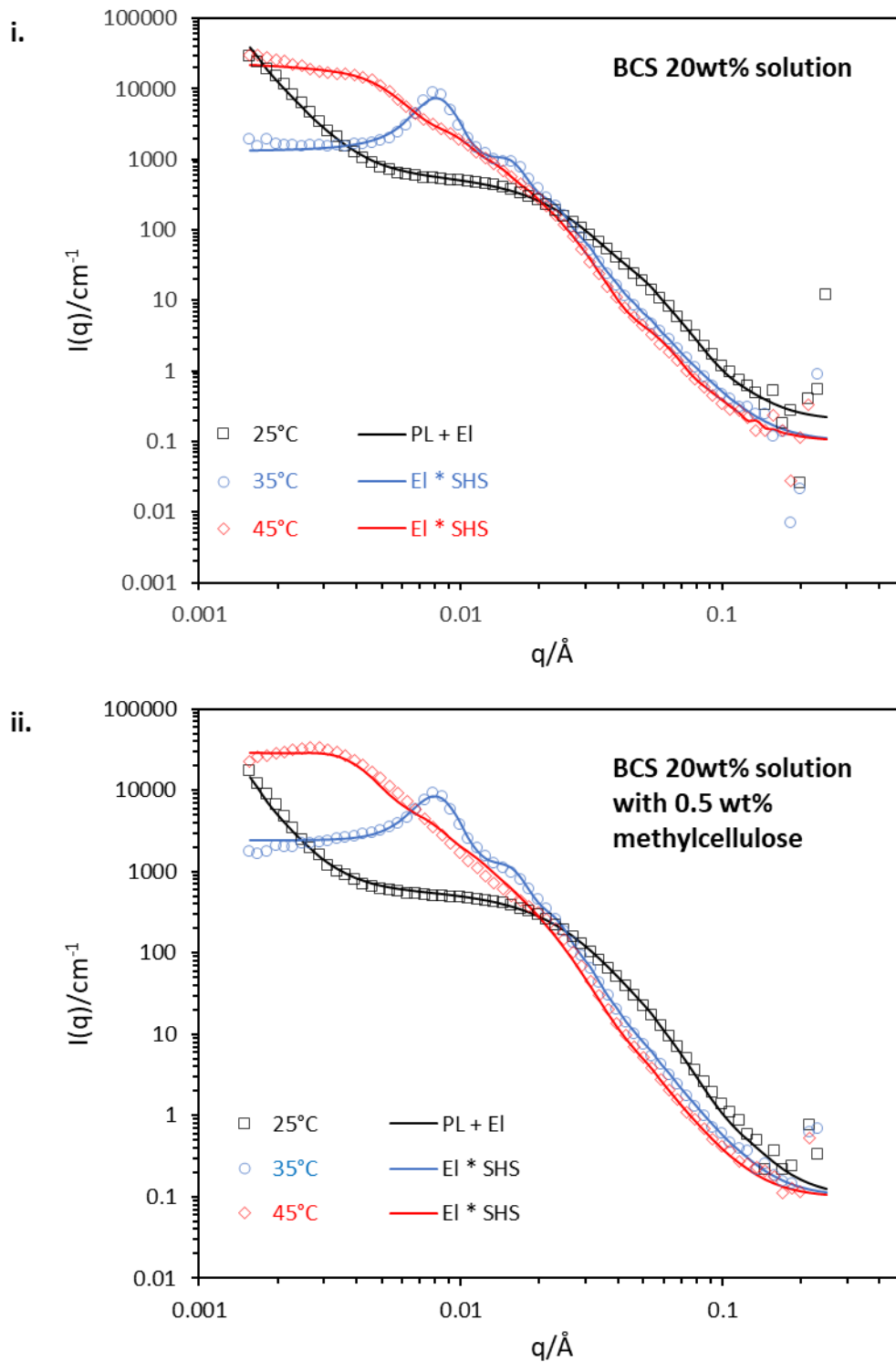
Figure 5.11: SANS of BCS solutions (20 wt%) in D_2O (i) and in D_2O with methycellulose added (0.25 wt%) (ii). Data presented at 25, 35, and 45 °C in black, blue and red symbols, respectively. Fits to data are shown as continuous lines, with the models used shown in the legend. EL is an ellipsoid, PL is a power-law, SHS is the sticky-hard-sphere structure factor.

SANS of BCS (20 wt%) and methylcellulose (0.25 wt%) were also measured in D_2O to probe the effect of methylcellulose on BCS nanostructure. SANS of methylcellulose (0.25 wt% in D_2O) was also determined to aid comprehension of the system, however no signal was observed in the q range studied (Figure A29). Thus, it is assumed that any changes to the neutron scattering patterns observed, relative to the BCS system, are due to interactions between the BCS and methylcellulose, rather than to the scattering of methylcellulose aggregates. Initial observation of the SANS for the BCS/methylcellulose solutions shows only minor changes from BCS alone (Figure 5.11ii). At all temperatures, the BCS and BCS/methylcellulose SANS data are nearly superimposable, except for a small broadening of the correlation peak at 0.01 Å for the 35 °C sample and changes to the low q region at 45 °C. Only minor alterations to the fitting parameters were required (Figure A30-A32). Thus, there is no evidence of major structural alterations to BCS in aqueous solution upon addition of methylcellulose in the temperature range studied.

SANS of BCS-stabilised emulsions was also conducted at 25, 35, and 45 °C (Figure 5.12). In this experiment, both the oil and water phases were deuterated, and scattering is dominated by BCS at the interface and in the bulk where the difference in SLD between the deuterated dodecane and D_2O phases is small (6.71 vs. 6.37 x 10^{-6} Å^{-2}, respectively). All emulsions exhibited features consistent with the BCS solutions alone but with lower scattering intensity. This is indicative of a reduced concentration of BCS in the bulk which is attributed to a fraction of the BCS moving to the O/W interface and losing structure, as well as a reduction in the volume fraction of water due to the emulsion system. Other thermoresponsive polymers, such as poly(N-isopropyl acrylamide), are known to move to interfaces and lose structuration as they spread across the interface.[27,28] Furthermore, study of structurally related poly(N-isopropylacrylamide) BCS by neutron reflectivity at the perfluorooctane/water interface demonstrated the ability of the BCS architecture to move to this interface.[20] At 25 °C, the emulsion's scattering could be fitted using the same parameters (SLD, equatorial/polar radii) as the BCS in solution, but with a reduced volume fraction of 0.056. It is known that the volume fraction of water in the system is 0.34 – if the volume fraction of BCS in this water phase was unchanged by the emulsification process it would give an overall BCS volume fraction in the emulsion of 0.068. Thus, there

is a ca. 18 % reduction in BCS volume in the bulk water after emulsion formation. At 35 °C, the data could again be fitted with the parameters from the BCS solution with a reduced scale, associated with a reduced volume fraction, relating to the ellipsoid form factor. However, the appearance of an upturn at low q was observed, which fits to a power law with a - 4 exponent. This is assumed to arise from the emulsion droplets themselves. At 45 °C, a similar effect was observed. Fitting was adequately conducted using the parameters from the BCS solution at 45 °C but with a reduced scale (0.052). An upturn at low q was again fitted to a - 4 exponent power law. Parameters from all fits are shown in supplementary information (Figure A21-A23, Table A6).
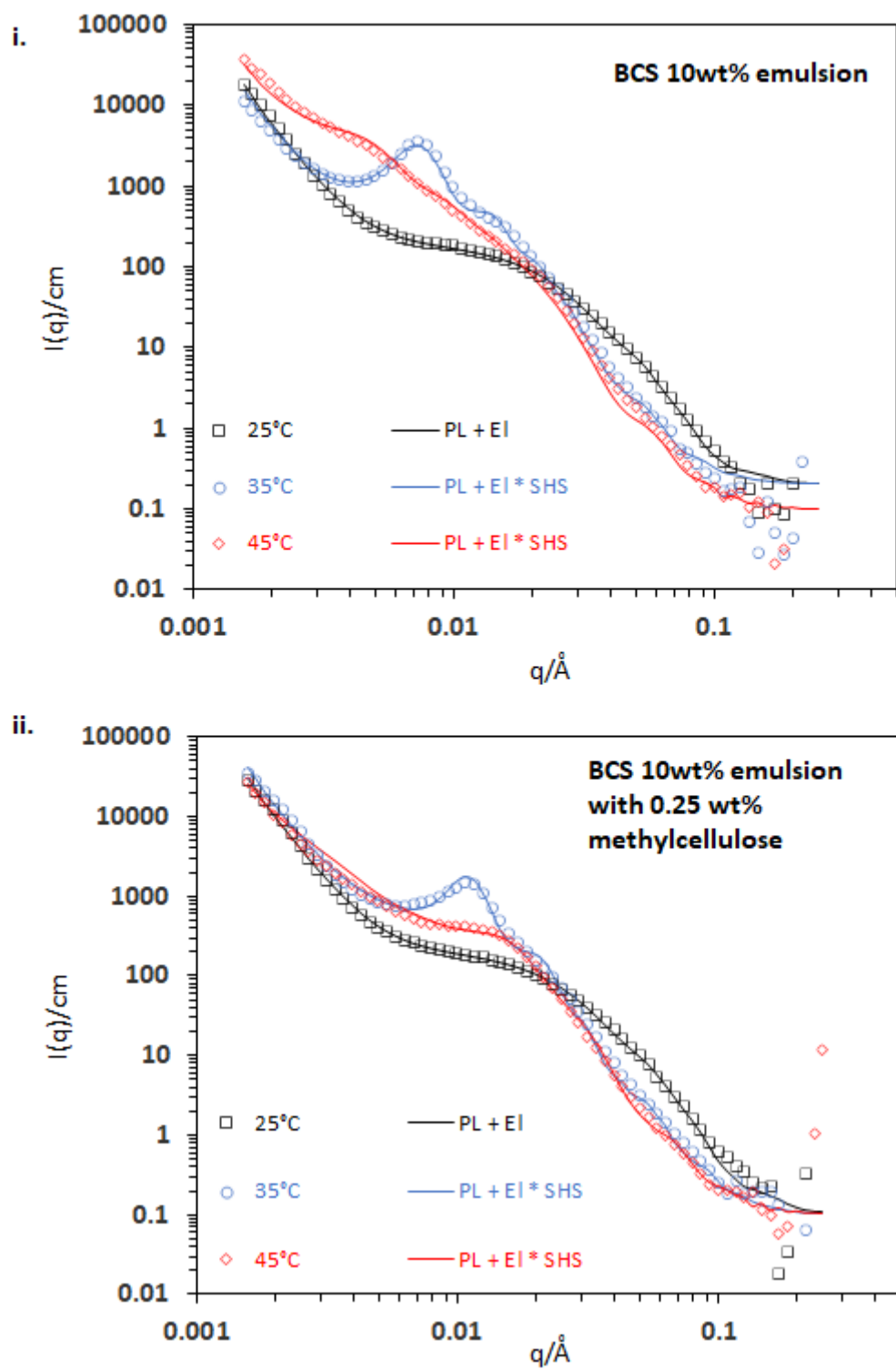
Figure 5.12: SANS of BCS emulsions (10 wt%) in D_2O (i) and in D_2O with methylcellulose added (0.25 wt%) (ii). Deuterated dodecane used as oil phase. Data presented at 25, 35, and 45 °C are in black, blue and red symbols, respectively. Fits to the data are shown as continuous lines, with the models used shown in the legend. EL is an ellipsoid, PL is a power-law, SHS is the sticky-hard-sphere structure factor.

Finally, the BCS plus methylcellulose emulsions were studied by SANS with increasing temperature. At 25 °C, a similar trend was seen as for the BCS emulsion alone. The emulsion's scattering could successfully be fitted with the same parameters as the solution with a reduced scale. At 35 °C, the mixed system could again be fitted with this approach, however the correlation peak moved from q = 0.00727 in the BCS emulsion alone to q = 0.01068 upon addition of methylcellulose to the emulsion system. This corresponds to distances (d) of 864 and 588 Å before and after methylcellulose addition, respectively, using the relationship d = 2π/q. At 45 °C the SANS could again be fitted to an ellipsoidal form factor with a sticky hard-sphere structure factor combined to a power law (-4) appearing at low q. The dimensions of this aggregate were fitted using the parameters for the solution alone. Relative to the BCS emulsion alone; this fitting required a reduction in effective radius from 800 to 176 Å.

Considering the SANS data from the emulsions as a whole, the following conclusions are drawn:

- Nanoscale aggregates formed in aqueous solutions of BCS and BCS with methylcellulose are preserved in the emulsion system. However, there is evidence that larger structures are also present due to the upturn at low q, which may arise from aggregates or more likely the interface of the oil droplets, outside the q-range measured.
- A reduction in effective concentration of the nanoscale aggregates occurs, which provides evidence for movement of BCS to the oil/water interface and reduction of the structured scattering objects in the bulk.
- The addition of methylcellulose to the emulsions appears to reduce the effective distance between BCS aggregates whilst preserving their nanostructure.

Finally, dodecane-in-water emulsions stabilised by 10 wt% BCS alone and with 0.25 wt% methylcellulose were imaged by light microscopy (LM) with a hot stage to observe possible morphological changes on the microscale as a function of temperature (Figure 5.13). The droplet size of BCS-stabilised emulsions was polydisperse with a range ca 6-38 μm, whilst the droplet size of the BCS/methylcellulose emulsions was significantly reduced

with the majority at 4-5 µm. This reduction in droplet size explains prior observations that creaming was greatly reduced in the BCS plus methylcellulose emulsion. The emulsions were heated from 25 to 35, then 40 °C to evaluate the system below and above the gelation temperature. No distinct changes were observed in droplet size or morphology, and no additional objects were observed in the heated system. The rheological features observed are therefore not strongly attributed to any changes to the droplets themselves.
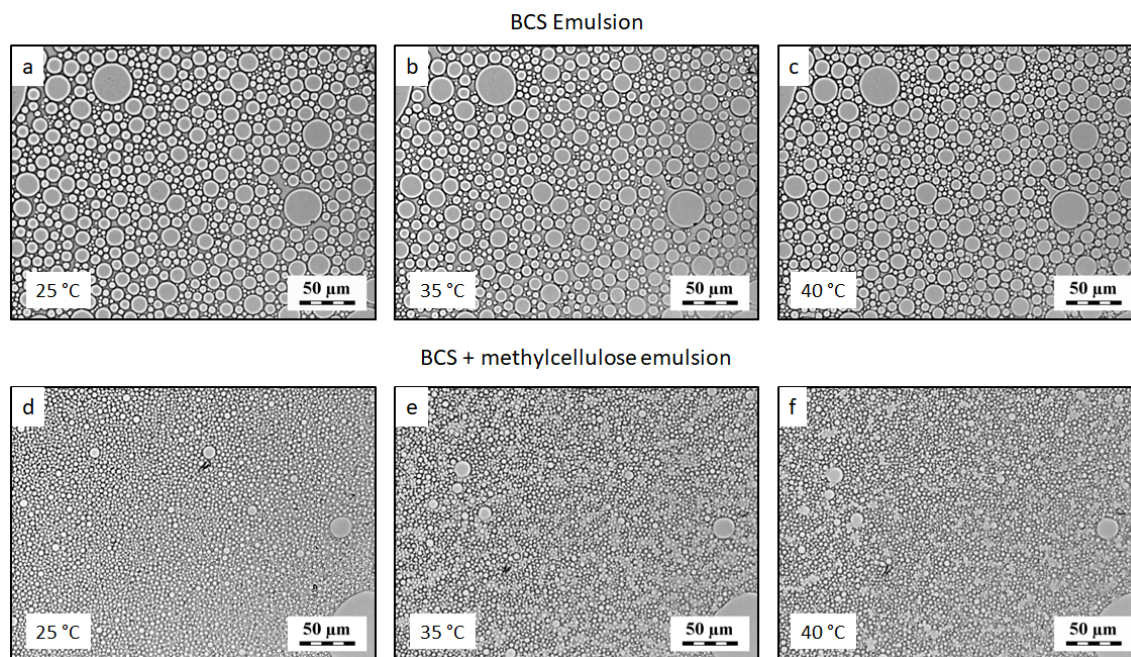
Figure 5.13: Light microscopy (LM) images of dodecane-in-water emulsions stabilised by 10 wt% BCS alone (a–c) and with 0.25 wt% methylcellulose (d–f) at different temperatures at 20x magnification.

5.4 Conclusion

BCS synthesised by free radical polymerisation of DEGMA, PEGMA, EGDMA, and DDT is effective as an emulsifier for oil-in-water emulsions whilst imparting temperature-responsive gelation to the emulsion systems. This transition occurs at ca 32 °C, making these thermoresponsive emulsions attractive for *in situ* gelation upon contact with body sites and thus exploitation in pharmaceuticals where the gel state may enhance retention at the target site. The BCS was able to both stabilise and impart thermoresponsive behaviour to a range of pharmaceutically-relevant oils. The addition of small molecule surfactants and polymer/oligomer additives to BCS emulsions was explored to reduce instability due to creaming. An optimal formulation of BCS with methylcellulose was identified which eliminated creaming over the experimental period and extended the range of temperatures over which the gel state was stable. SANS study of the system allowed the investigation of the nanostructure, which underpins the rheological response to temperature. BCS in solution formed nanoscale oblate ellipsoidal aggregates which grew and interacted with each other when heated. In aqueous solution, there was limited evidence of methylcellulose affecting the nanoscale organisation, however, in the emulsion systems, a different effect was observed. Both the BCS and the BCS/methylcellulose mixed emulsions retained the nanostructures observed in solution but with larger aggregates present. Methylcellulose appeared to reduce the distance between BCS aggregates, tentatively assigned to additional steric crowding in the aqueous phase. Overall, this study reports a novel thermoresponsive emulsion formulation for use as an in-situ gel forming dosage form, along with comprehension of nanostructural mechanisms in the system. Future studies will seek to incorporate the material into delivery devices and explore the effect of drug-incorporation on performance of the emulsion.

5.5 References

1.   Rajbanshi, A. *et al.* Polymer architecture dictates thermoreversible gelation in engineered emulsions stabilised with branched copolymer surfactants. *Polym. Chem.* **13**, 5730–5744 (2022).

2.   McClements, D. J. & Jafari, S. M. Improving emulsion formation, stability and performance using mixed emulsifiers: A review. *Adv. Colloid Interface Sci.* **251**, 55–79 (2018).

3.   Schulman, J. H. & Cockbain, E. G. Molecular Interactions at Oil / Water Interfaces. *Trans. Faraday Soc.* **35**, 651–661 (1940).

4.   USP Monographs: Emulsifying Wax. *United States Pharmacopeoia* (2008).

5.   Stepanek, M. *et al.* Association of Poly (4-hydroxystyrene) - block -Poly (Ethylene oxide) in Aqueous Solutions : Block Copolymer Nanoparticles with Intermixed Blocks. *Langmuir* **28**, 307–313 (2012).

6.   Kolouchova, K. *et al.* Thermoresponsive Triblock Copolymers as Widely Applicable Magnetic Resonance Imaging Tracers. *Chem. Mater.* **34**, 10902–10916 (2022).

7.   Skvarla, J., Zednik, J., Slouf, M., Pispas, S. & Stepanek, M. Poly(N-isopropyl acrylamide)-block-poly(n-butyl acrylate) thermoresponsive amphiphilic copolymers: Synthesis, characterization and self-assembly behavior in aqueous solutions. *Eur. Polym. J.* **61**, 124–132 (2014).

8.   Heenan, R. K., Penfold, J. & King, S. M. SANS at Pulsed Neutron Sources: Present and Future Prospects. *J. Appl. Crystallogr.* **30**, 1140–1147 (1997).

9.   Wignall, G. D. & Bates, F. S. Absolute calibration of small-angle neutron scattering data. *J. Appl. Crystallogr.* **20**, 28–40 (1987).

10.   SasView version 4.2.2.

11.   NIST SLD Calculator.

12.   Da Silva, M. A., Bode, F., Grillo, I. & Dreiss, C. A. Exploring the Kinetics of Gelation and Final Architecture of Enzymatically Cross-Linked Chitosan/Gelatin Gels. *Biomacromolecules* (2015) doi:10.1021/acs.biomac.5b00205.

13. Constantinou, A. P. & Georgiou, T. K. Tuning the gelation of thermoresponsive gels. *European Polymer Journal* vol. 78 366–375 at https://doi.org/10.1016/j.eurpolymj.2016.02.014 (2016).

14. Bassi, J., Haddow, P., Luciano, M. & Thomas, M. Thermoresponsive poly (di (ethylene glycol) methyl ether methacrylate) - ran- (polyethylene glycol methacrylate) graft copolymers exhibiting temperature-dependent rheology and self-assembly. *J. Mol. Liq.* **346**, 117906 (2022).

15. Zhao, Y., Cao, Y., Yang, Y. & Wu, C. Rheological study of the sol-gel transition of hybrid gels. *Macromolecules* **36**, 855–859 (2003).

16. Yara-Varón, E. *et al.* Vegetable oils as alternative solvents for green oleo-extraction, purification and formulation of food and natural products. *Molecules* **22**, 1–24 (2017).

17. FDA. Inactive Ingredient Database for Approved Drug Products.

18. Hu, Y., Ting, Y., Hu, J. & Hsieh, S. Techniques and methods to study functional characteristics of emulsion systems. *J. Food Drug Anal.* **25**, 16–26 (2016).

19. Shiao, S. Y. *et al.* Chain length compatibility effects in mixed surfactant systems for technological applications. *Adv. Colloid Interface Sci.* **74**, 1–29 (1998).

20. da Silva, M. A. *et al.* Engineering Thermoresponsive Emulsions with Branched Copolymer Surfactants. *Macromol. Mater. Eng.* **307**, 1–14 (2022).

21. Meewes, M., Ricka, J., de Silva, M., Nyffenegger, R. & Binkert, T. Coil-Globule Transition of Poly(N-isopropylacrylamide). A Study of Surfactant Effects by Light Scattering. *Macromolecules* **24**, 5811–5816 (1991).

22. Blanazs, A., Armes, S. P. & Ryan, A. J. Self-assembled block copolymer aggregates: From micelles to vesicles and their biological applications. *Macromol. Rapid Commun.* **30**, 267–277 (2009).

23. da Silva, M. A. *et al.* Thermoresponsive Triblock-Copolymers of Polyethylene Oxide and Polymethacrylates: Linking Chemistry, Nanoscale Morphology, and Rheological Properties. *Adv. Funct. Mater.* **32**, 2109010 (2022).

24. Feigin, L. A. & Svergun, D. I. *Structure Analysis by Small-Angle X-Ray and Neutron*

Scattering. (Springer New York LLC, 1987).

25.   Hammouda, B., Ho, D. L. & Kline, S. Insight into clustering in poly(ethylene oxide) solutions. *Macromolecules* (2004) doi:10.1021/ma049623d.

26.   Kotlarchyk, M. & Chen, S. H. Analysis of small angle neutron scattering spectra from polydisperse interacting colloids. *J. Chem. Phys.* **79**, 2461–2469 (1983).

27.   Zhang, J. & Pelton, R. Poly(N-isopropylacrylamide) at the Air/Water Interface. *Langmuir* **12**, 2611–2612 (1996).

28.   Li, Z., Geisel, K., Richtering, W. & Ngai, T. Poly(N-isopropylacrylamide) microgels at the oil–water interface: adsorption kinetics. *Soft Matter* **9**, 9939–9946 (2013).

Chapter 6: Development of engineered emulsions for nasal drug delivery

6.1 Introduction

Administering drugs via intranasal drug delivery is a popular choice due to its non-invasive nature. The nasal cavity contains a large and highly vascularised surface area, making it a highly efficient method for drug absorption while bypassing first-pass metabolism.[1–3] Intranasal drug delivery is commonly used to administer locally acting drugs for treating conditions such as nasal congestion, infections, and allergic rhinitis.[4] However, nasal delivery can also be employed for the systemic delivery of drugs to treat diseases like osteoporosis, migraine, pain, and for vaccine administration.[5] This delivery route is painless, non-invasive, and offers rapid drug onset due to the highly vascularised and permeable nasal mucosa, while avoiding first-pass metabolism, resulting in high patient convenience and compliance.[6] Nasal drug delivery also offers opportunity to bypass the blood-brain barrier via absorption through the olfactory bulb.[7] The advantages of intranasal drug delivery for neurotherapeutic agents include rapid onset of drug action, improved local bioavailability, reduced dosage requirements, and fewer side effects, making it a promising approach in drug administration.[8–10]

Various dosage forms are available for nasal drug delivery, with nasal sprays and nasal drops being the most popular examples, typically formulated as solutions or suspensions.[11] Aqueous nasal spray formulations are commonly used for intranasal drug delivery due to their simplicity, compatibility with various drugs, potential for rapid onset and ease of administration.[11,12] These formulations typically consist of water as the main solvent, along with other excipients to stabilize the drug and enhance its effectiveness. However, aqueous nasal sprays have their own limitations such as shorter residence time, limited drug retention and difficulty in achieving controlled drug release.[11,13] Short residence times arise from mucocilary clearance, and natural flow out of the nasal cavity by gravity.

Residence time on mucosal surfaces such as the nasal mucosa may be enhanced by the use of mucoadhesive and/or viscous materials. Certain "mucoadhesive" polymeric

156

materials have the ability to adhere to the mucosal surface due to their interactions with the mucin layer.[14] This interaction creates a longer residence time for the applied substance on the mucosal surface, which can be advantageous for drug delivery through the nasal route due to prolongation of local effects or increased duration at the site of absorption for systemic effects. Retention can also be enhanced by viscous materials that have resistance to flow and can reduce clearance due to shear or gravitational force. For instance, it has been shown that high-viscosity polymers, such as carbomers or xanthan gum, can adhere to the nasal mucosa for longer periods, allowing for prolonged and controlled drug release.[15] However, there is a challenge associated with spraying viscous liquids. Viscous fluids may not be able to be actuated through nozzles, have a tendency to "jet" into single streams, and may not atomise into a fine mist.[16] Viscous formulations can also clog or block the nozzle of the spray device, reducing the efficiency and consistency of the spray. This can lead to inconsistent dosing, uneven distribution, and potentially affect the overall effectiveness of the treatment. While viscous formulations can offer extended contact time, challenges related to spraying and consistent delivery need to be addressed for optimal therapeutic outcomes. Optimising the viscosity and rheological properties of the formulation is crucial to ensure efficient aerosol generation and delivery while maintaining the desired retention on mucosal surfaces, but knowledge in this area is limited.

The primary aim of the research presented in this thesis was to investigate and develop thermoresponsive engineered emulsions as an innovative drug delivery platform. The materials will be applied to intranasal drug delivery, which was identified as a field which could benefit from these new systems. Thermoresponsive emulsions can offer solutions to address some of the challenges associated with spraying viscous liquids in nasal drug delivery. Thermoresponsive emulsions undergo a sol-gel transition in response to temperature variations. When heated, these emulsions can transition from a less viscous state to a more viscous state or a gel state, which can be beneficial for nasal spray applications. The thermosensitive emulsions developed might be suitable for administration as sprays when designed to undergo a sol-gel transition at the temperature of the nasal cavity (32-35 °C).[17,18] The formulations are low viscosity liquids at room temperature and can potentially achieve efficient atomisation and produce smaller

droplet sizes, leading to improved spray consistency. Upon warming by body temperature, these emulsions transition to a gel resulting in better drug retention in the nasal cavity due to resistance to flow.[19–22] Hence, their characteristics hold great promise for efficient therapeutic delivery at target sites, enhanced adhesion to the nasal mucosa, leading to prolonged drug contact, controlled drug release kinetics and adsorption.

The emulsions prepared with the branched copolymer surfactant (P14 – as described in Chapter 4) and P14 (BCS) / methylcellulose were identified as optimal formulation systems with *in-situ* gelation for drug delivery as discussed in Chapter 5. The focus of this chapter is on evaluating the ability of the optimised emulsions to solubilise different drugs with varying solubility and lipophilicity (i.e. partition coefficients), assessing controlled drug release kinetics, and evaluating the compatibility of the thermoresponsive emulsions with nasal drug delivery devices. Three different drugs (phenylephrine hydrochloride, lidocaine hydrochloride, and budesonide) with varied solubility and partition coefficients (details in Table 6.2) were selected to assess the ability of the emulsions to solubilise different drug types and control their liberation. Rheological analysis of the drug-loaded emulsions was also conducted to determine the effect of drug on thermal transitions. The ability to spray the emulsions was conducted in collaboration with Bespak (Recipharm). Overall, the preclinical suitability of the BCS-stabilised thermoresponsive emulsions for nasal administration is reported in this chapter.

6.2 Materials and methods

6.2.1 Materials

Di(ethylene glycol) methyl ether methacrylate (DEGMA, 95%), poly(ethylene glycol) methyl ether methacrylate (PEGMA, M_n 950 gmol^{-1}), ethylene glycol dimethacrylate (EGDMA, 98%), 1-dodecanethiol (DDT, 99%), anhydrous dodecane (99%), absolute ethanol, acetonitrile (gradient grade) and methyl cellulose (2000 cP, 2% aqueous solution at 20 °C) were purchased from Sigma-Aldrich (UK). α, α -azoisobutyronitrile (AIBN, >99%) was obtained from Molekula (UK). Sodium dihydrogen phosphate dihydrate (99%), orthophosphoric acid (85%), potassium dihydrogen phosphate (99%) and 1-octanesulphonic acid sodium salt (98%) were supplied by VWR (UK). Dialysis tubing with

molecular weight cut off (MWCO) of 14 kDa was purchased from Sigma Aldrich (UK). Phenylephrine hydrochloride and lidocaine hydrochloride were purchased from Sigma Aldrich (UK). Micronised budesonide was supplied from LMG Pharma (Boca Raton, USA). Phosphate buffered saline (PBS) tablets were purchased from Oxoid, UK. Tween 20 was purchased from Fluka Analytical, UK. Potassium dihydrogen orthophosphate, octane sulphonic acid sodium salt, orthophosphoric acid, sodium dihydrogen phosphate dihydrate, absolute ethanol, and gradient grade acetonitrile were purchased from VWR (UK). Deionised water was employed in all experiments. All chemicals were used as received. Mechanical nasal spray pumps delivering 100 µl of formulation per actuation were provided by Bespak, Recipharm. The optimal system P14 (referred to as BCS in this chapter) as synthesised and described in Chapter 4 was used for this study.

6.2.2 Emulsion formation with drug loading

Aqueous BCS solution with concentration of 20 wt% was prepared in cold water. If required, 0.25 wt% methylcellulose (MC) additive was then added in the associated results. For emulsion formulations with active pharmaceutical ingredients incorporated, 0.5 wt% phenylephrine HCl, 5 wt% lidocaine HCl and 0.064 wt% budesonide (as a suspension) was then added to the aqueous solution to match the reference products. The mixture was refrigerated with intermittent vortexing every 15 min to aid solubilisation of BCS until a clear solution was obtained. The preparation of oil-in-water emulsions was then carried out by mixing 2.5 g of aqueous BCS solution with 2.5 g of dodecane oil. The mixture was emulsified for 2 min using a Silverson L4R mixer with a 5/8" micro tubular frame and integral general purpose disintegrating head at 2400 rpm then left to rest for 36 h at room temperature. The creamed phase of the emulsions was then isolated for further analysis. The emulsion mass yield was then defined in equation 1:

$$mass\ yield\ (\%) = 100\ \times \frac{5 - Mass\ Water}{5}$$

Where "Mass Water" is the mass of the lower phase extracted after creaming. The oil phase volume of creamed region (ϕ_{oil}) may also be determined by equation 2:

$$\varphi_{oil} = \frac{\left(\dfrac{2.5}{\rho_{oil}}\right)}{\left(\dfrac{2.5}{\rho_{oil}}\right) + (2.5 - Mass\ Water)}$$

where, ρ_{oil} is the density of the oil and 2.5 is the mass of the oil added in g.

6.2.3 Rheology of thermoresponsive emulsions

Rheology experiments were performed on an AR 1500ex rheometer by TA instruments (USA) equipped with a Peltier temperature control unit and a 40 mm parallel plate geometry with a specified gap distance of 500–750 µm. Each emulsion's creamed layer (after 36 h of isolation) was placed on the rheometer lower plate prior to the measurement, after which temperature ramps were performed. The sample was equilibrated for 2 minutes prior to measurement. Temperature ramps were performed in the range 20 to 50 °C, at 1 °C per minute heating rate, an oscillating stress of 1 Pa and a frequency of 6.283 rad/s. The change in storage modulus (G') and loss modulus (G") as a function of temperature was recorded.

6.2.4 Droplet size determination of emulsion by laser diffraction

Emulsion droplet (after 36 h of isolation) size was determined by Laser Diffraction using a Sympatec HELOS/BR QUIXEL. 10 µL of emulsion was added to the dispenser R3 cuvette containing 50 mL of water with constant stirring at 1800 rpm. Water was used as a reference before sample measurement. All the samples were measured at an optical concentration of approximately 30%. Trigger conditions were as follows: reference measurement duration – 10 s, signal integration time – 100 ms, trigger timeout – 90 s.

6.2.5 HPLC method for determination of phenylephrine and lidocaine

A gradient method was used to determine the concentration of phenylephrine and lidocaine released from the emulsion formulations. The aqueous mobile phase consisted of 0.02 M potassium dihydrogen phosphate and 0.01 M of octane sulphonic acid sodium salt adjusted to pH 2.8 with dilute orthophosphoric acid and gradient grade acetonitrile

as the organic phase. A Waters symmetry C18, 5 μm column of dimension 250 mm X 4.6 mm was used with a flow rate of 1 mL per minute. 30 °C was used as column temperature at 272 nm detection wavelength with 20 μL injection volume for each solution. An analytical method was developed (Table 6.1) for the determination of phenylephrine and lidocaine as per ICH method validation guidelines.[23,24] The specificity, accuracy, precision, and repeatability parameter of analytical method validation was assessed. The specificity was performed to demonstrate that the analytical method is selective for the determination of phenylephrine and lidocaine and can distinguish them from other components that may be present in the sample matrix. In the evaluation of controlled release, the validation range covered 0 – 120 % of the target concentration (0.05 mg for phenylephrine and 0.5 mg for lidocaine). Accuracy testing involved six determinations across concentration levels of 0, 0.01, 0.02, 0.03, 0.04, 0.05 and 0.06 mg/mL for phenylephrine and 0, 0.1, 0.2, 0.3, 0.4, 0.5 and 0.6 mg/mL for lidocaine. Precision and repeatability assessments were conducted with six determinations at the target concentration of phenylephrine and lidocaine, i.e., 0.05 mg/mL and 0.5 mg/mL respectively. The calibration curves were constructed using the accuracy data obtained across the concentration levels for both phenylephrine and lidocaine. Peak area vs concentration was extrapolated to assess and verify the linearity of the calibration curve.

Table 6.1: Gradient flow HPLC method for determination of phenylephrine and lidocaine

Time (min)	Aqueous phase	Organic phase
0	75	25
10	70	30
20	70	30
21	75	25
25	75	25

6.2.6 HPLC method for determination of budesonide

An isocratic elution HPLC method was used to quantify budesonide. The isocratic method used a mobile phase composed of 2 volumes of ethanol, 34 volumes of acetonitrile and 66 volumes of phosphate buffer solution prepared using 0.026 M sodium dihydrogen phosphate dihydrate adjusted to pH 3.2 with orthophosphoric acid. A stainless-steel Waters column of dimensions 150 mm X 4.6 mm packed with end-capped octadecyl silyl silica gel for chromatography (3 μm) was used. The chromatographic conditions were set up with a flow rate of 1.5 mL/min, a column temperature of 50 °C, a detection wavelength of 240 nm and a 20 μL injection volume of each solution. The method was then validated using ICH guidelines.[23,24] The specificity, accuracy, precision and repeatability parameter of analytical method validation was assessed. As previously described in Section 6.2.5, the specificity testing was performed to ensure that the method of analysis can accurately measure the budesonide and can distinguish it from the potential interfering substances that may be present in the sample solution. The accuracy testing involved six determinations across concentration levels of 0, 0.01, 0.02, 0.04, 0.06, 0.08, 0.1, 0.12 mg/mL for budesonide. In evaluation of controlled release, the validation range covered 0 – 120 % of the target concentration of budesonide, i.e., 0.1 mg/mL. Precision and repeatability assessments were performed six determinations at 0.1 mg/mL. The construction of the calibration curve involved utilising accuracy data obtained across various concentration levels, with six repetitions conducted at each concentration level. The extrapolation of this data to peak area versus concentration was performed to assess and verify the linearity of the calibration curve.

6.2.7 Drug quantification and release profile using Franz diffusion cells

Quantitative analysis of the drug loaded in the emulsion systems was determined by using the established HPLC methods as described in Section 6.2.5 and 6.2.6. A common method was used for the quantification of phenylephrine and lidocaine. 1 g of creamed emulsion (equivalent to 5 mg of phenylephrine) was weighed and dissolved in 100 mL of diluting solvent (aqueous mobile phase) with the aid of sonication. Similarly, for the determination of lidocaine, 1 g of creamed emulsion (equivalent to 25 mg of lidocaine) was weighed and

dissolved in 100 mL of diluting solvent with 10 min sonication. The sample solutions were then transferred in centrifuge tubes and centrifuged for 15 min at 5000 rpm. The clear solution was then used for further analysis using a validated HPLC method as described in section 6.2.5. The content of phenylephrine and lidocaine was calculated using the calibration curve determined.
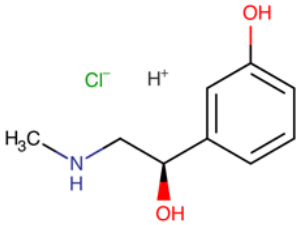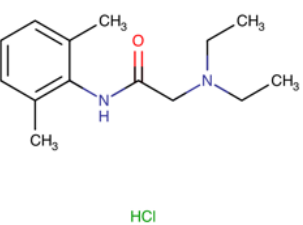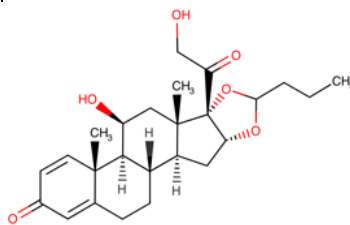
For quantification of budesonide by HPLC, 1.5 g of emulsion (equivalent to 1 mg of budesonide) was dissolved in 10 mL of mobile phase and mixed with 10 min sonication. The resulting solution was then centrifuged for 15 min at 5000 rpm. The clear solution was then used for further analysis using a validated HPLC method as described in 6.2.6. The content of budesonide in the emulsion was determined using the calibration curve. The calculation was based on the sum of the areas of the two budesonide epimer peaks.

Individually calibrated upright unjacketed Franz diffusion cells (Soham Scientific) with an average volume of 3 mL and a diameter of 1 cm were used for release studies. Dialysis membrane (MWCO 12-14 KDa) was mounted between the donor and receiver chambers of Franz cells, the receiver chamber was filled with phosphate buffer solution (PBS) for phenylephrine and lidocaine determination and 0.2 %v/v Tween-20 in PBS for Budesonide determination, to maintain sink conditions. The sink conditions were maintained as per the solubility of the drugs as shown in Table 6.2. For budesonide, the solubility was assessed in 0.2 %v/v solution of Tween 20 in PBS solution for maintaining the sink conditions (Figure 6.6). Franz cells were equilibrated in a water bath at 37 °C for 0.5 h with constant stirring in the receptor chamber during the diffusion study (to achieve a skin surface temperature of 32°C). 100 μL sample (six replicates) of the receiver fluid were withdrawn at intervals of up to 24 h and replaced with fresh preheated receiver fluid. Drug quantification was then achieved using HPLC-UV.
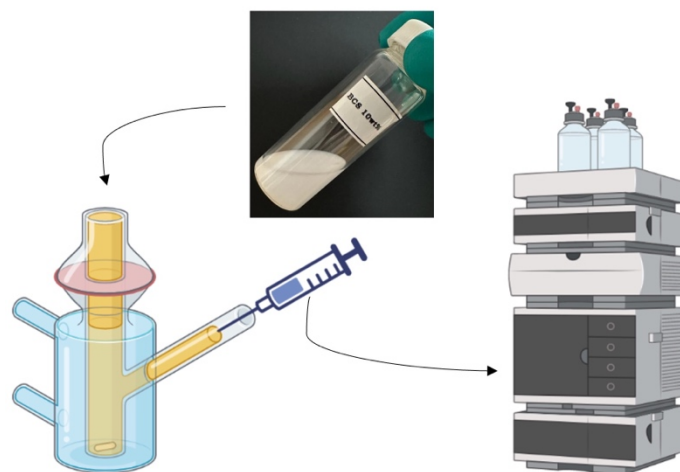
Figure 6.1: Work flow process of drug release study showing emulsion loading in the donor chamber of Franz cell, sampling at time intervals and quantitative analysis by HPLC.

Table 6.2: Illustration of properties of the drugs studied.[28]

Properties	Phenylephrine	Lidocaine	Budesonide
Structure			
Chemical Formula	$C_9H_{14}ClNO_2$	$C_{14}H_{25}ClN_2O_2$	$C_{25}H_{34}O_6$
Water solubility at 20 °C	22.0 mg/mL	0.593 mg/mL	0.0457 mg/mL
logP	-0.69	1.81	2.42

6.2.8 Mathematical modelling of drug release kinetics and statistical analysis

To study the drug release profile of all 3 drugs studies, Korsmeyer-Peppas model was considered to fit the experimental data which is given by the equation:

$$M_t/M_\infty = K_m \, t^n$$

164

where, M_t and M_∞ are the cumulative drug release at time t and infinite time, respectively; K_m is a constant which depends on the structural and geometrical characteristic of the particles, t is the release time and n is the diffusional exponent which indicates the drug release mechanism. For thin film delivery system, when n=0.50, the drug release mechanism is the Fickian diffusion. When n is between 0.50 and 1.0, drug release mechanism is anomalous (non-Fickian) transport and when the value of n is greater than 1.0, the drug release mechanism is zero order. For budesonide, the data was also fitted with linear regression indicating zero order release to predict the best possible release kinetics.

The statistical significance of the obtained values was analysed using Bonferroni post-hoc t-test for analysis of variance (ANOVA) using GraphPad Prism.

6.2.9 Model formulation for nasal device

The 1: 1 dodecane in water emulsion stabilised with 10 wt% BCS was used for the investigation of nasal spray generation using a unit dose nasal spray device (Unidose[25] nasal spray). 10 unit dose nasal sprays were assembled and the parameters such as shot weight, droplet size distribution, plume geometry and spray pattern were tested. The aforementioned parameters are requirement for *in vitro* bioequivalence study, quality control and development of nasal spray.

6.2.9.1 Determination of shot weights

In order to determine the shot weights, the nasal sprays were filled with 0.1 g of the dodecane in water emulsion stabilised with 10 wt% BCS. The device was actuated with an automated actuator (SPRAYER-module, Sympatec), and after each actuation, the device was weighed on an analytical balance (A 200 S, Sartorius, Göttingen, Germany) to determine the delivered mass.

6.2.9.2 Determination of droplet size distribution (DSD)

The droplet size distribution (DSD) was determined by laser diffraction using Spraytec, Malvern instrument. This technique is a fast and efficient way to measure the size of droplets and particles in real-time. The distance to the measuring zone was performed at 3 cm and 6 cm. The data was acquired during the fully developed spray phase and droplet sizes were represented by D_{10}, D_{50}, and D_{90}. Additionally, the span, calculated to signify distribution width using the following equation:

$$(D_{90} - D_{10})/D_{50}$$

where, D_{10}, D_{50} and D_{90} represent 10, 50 and 90 percent of the droplet population below the obtained droplet size. Moreover, the fraction of droplets smaller than 10 µm was also part of the reported information.

6.2.9.3 Determination of plume geometry and spray pattern

For the determination of plume geometry, an Imager E-lite CCD-camera (charge-coupled device camera) and sheet light (LaVision, Göttingen, Germany) were used. The images were corrected for distortion, due to the skewed camera perspective, and plume angle was determined manually using CorelDraw X6 software (Corel, Ottawa, ON, Canada).

The characterisation of spray pattern was performed by automated image analysis. The approximate center of mass (COM) was identified, and the maximum diameter (Dmax) and minimum diameter (Dmin) was drawn through this centre to determine the size of the pattern. Additionally, the ovality ratio (Dmax/Dmin) was calculated as the control of the shape pattern. The spray pattern was determined based on a single spray. Spray pattern measurement was performed at two distances from the actuator tip, 3 and 6 cm at room temperature.

6.3 Results and discussion

The optimal BCS system (P14) as described in Chapter 4 was used for further study in this chapter. 1:1 dodecane in water emulsion was formulated with 10 wt% BCS and 10 wt% BCS combined with 0.25 wt% methylcellulose (MC). The ability of BCS and BCS/MC emulsions to solubilise a range of drugs with varied solubility and partition coefficients was explored. Three drugs (phenylephrine hydrochloride, lidocaine hydrochloride and budesonide) were selected with respect to their varied solubility and partition coefficients as detailed in Table 6.2. The log P value of phenylephrine hydrochloride, lidocaine hydrochloride and budesonide are reported to be -0.69, 1.81 and 2.42 respectively.[28]

The emulsions were formulated with 0.5 wt% of phenylephrine HCl, 5 wt% lidocaine HCl and 0.064 wt% budesonide (Figure A37-A39 in appendix) to match reference licensed products.[29,30] All mixtures successfully formed emulsions (Table 6.3), however degrees of creaming varied and hence emulsion yields in the BCS-stabilised systems. The varied amounts of drugs added to the emulsion system increased the viscosity of the continuous phase thus reducing the velocities of the oil droplets to creaming. The addition of methylcellulose removed creaming in all systems, giving 100 % yields. It has been reported in Chapter 5 that BCS/MC generated emulsions with small median droplet diameter and narrower size distribution which is a contributor to the stability of the system.

Table 6.3: Yield and oil phase volume (ϕ_{oil}) of emulsion with BCS and BCS/MC; and drug-loaded emulsion with BCS and BCS/MC after isolation of the creamed phase at 36 h (n=1).

Emulsion	Yield (%)		ϕ_{oil}	
	with BCS	with BCS/MC	with BCS	with BCS/MC
without drug	76	100	0.72	0.57
0.5 wt% Phenylephrine	80	100	0.65	0.57
5 wt% Lidocaine	86	100	0.74	0.57
0.064 wt% Budesonide	80	100	0.65	0.57

Rheological analysis of the emulsion with drug molecules stabilised by BCS and emulsion with drug molecules stabilised with BCS/MC was conducted as showed in Figure 6.2. Small-amplitude oscillatory rheology at a fixed frequency was used to investigate the impact of temperature on the emulsions. This experiment determined the storage (G') and loss (G") moduli within the linear viscoelastic range of the system (at a shear strain of 0.1%), thus preserving the sample structure. By using a fixed frequency, heating and cooling temperature ramps were performed.
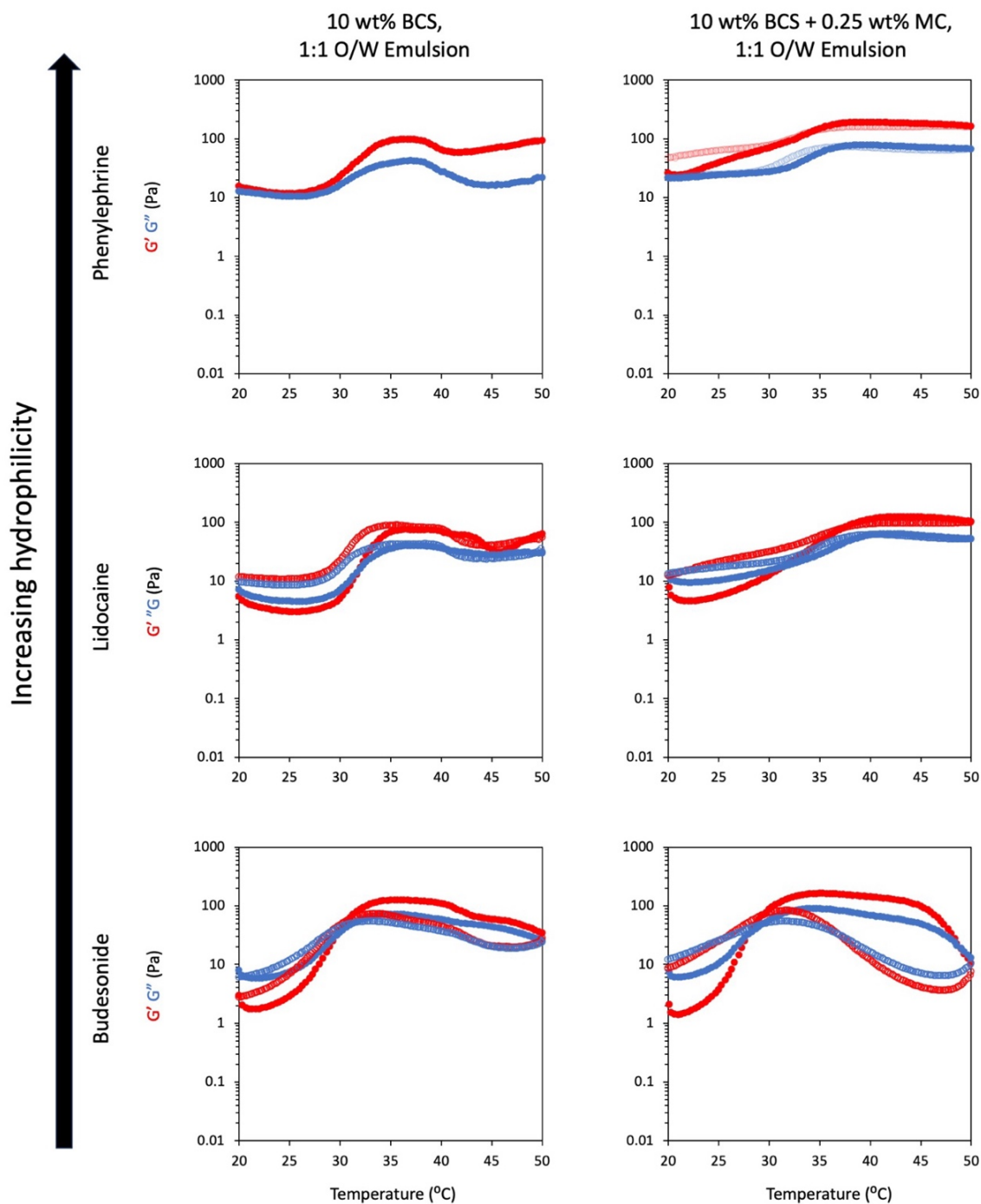
Figure 6.2: Temperature-ramp shear rheology of 1:1 o/w drug-loaded emulsions stabilised with 10wt% BCS (left column) and drug-loaded emulsions with added 0.25 wt% methylcellulose to 10wt% BCS (right column). G' (red) and G" (blue) are shown. Closed symbols indicate heating, whilst open symbols indicate cooling. The rheological analysis of the emulsions was conducted after 36 h of isolation. For the control systems (emulsion with BCS and BCS/MC) without drug, refer to Chapter 5.

For the emulsions with drug substances stabilised with BCS, the temperature ramp in Figure 6.2 revealed distinct thermoresponsive behaviour in the BCS-stabilised emulsion. At low temperatures, both G' (represented in red) and G" (in blue) remained low, ranging from approximately 3 Pa for budesonide emulsion, 8 Pa for lidocaine emulsion and 15 Pa for phenylephrine emulsion. This indicated a predominantly liquid-like state (with G" > G'). However, phenylephrine emulsion as compared to the other 2 emulsion systems behaved as a thick viscoelastic liquid with G' slightly greater than G". As the temperature increased above around 30 °C, both moduli exhibited an increase, with a shift towards a more elastic character in the system. At 32 °C the system transitioned to a predominantly elastic state (G' > G"). This temperature, designated as Tgel, demonstrated the formation of a gel-like structure. As reported in our previous finding, Tgel is believed to be triggered by the lower critical solution temperature (LCST) of DEGMA, known to be around 31-35 °C when copolymerised with PEGMA .[27] Above Tgel, the system reached a plateau at approximately 35 °C, with G' reaching around 100 Pa in all examples. With further heating, both G' and G" decreased, suggesting reduced internal friction as more kinetic energy was added to the system or due to structural changes in the BCS system at higher temperatures. Emulsions with drug substances in mixtures of BCS and methylcellulose showed T_{gel} of 30 °C (G' > G") (Figure 6.2). At low temperatures, both G' (represented in red) and G" (in blue) remained low for budesonide and lidocaine, ranging from approximately 5 to 15 Pa indicating a predominantly liquid-like state (with G" > G'). However, phenylephrine emulsion system demonstrated more viscous liquid with G' slightly greater than G". As the temperature ramped, the budesonide and lidocaine emulsion systems reached a with G' reaching around 200 Pa. This gel state plateaued at ca 120 Pa for the phenylephrine emulsion system.

All emulsions were left on the bench top without any disturbance under ambient conditions to assess any macroscopic instability events. It was observed that the emulsions formulated with phenylephrine HCl and budesonide were stable with no further creaming after 36 h. After 10 days of emulsion isolation on the bench top, it was observed that the emulsions formulated with lidocaine separated into 2 phase systems indicating the breaking of emulsions. Hence, a set of lidocaine emulsions stabilised by BCS and BCS/MC were prepared for stability studies. After 7 days of isolation, rheological

analysis was conducted as demonstrated in Figure 6.3. At low temperatures, the G' was observed to be 10 fold greater (approximately 80 Pa) as compared to the emulsions analysed after 36 h of isolation (Figure 6.2). As the temperature ramped, a reduction in viscosity was observed leading to emulsion breaking at ca 28 °C. As compared to other emulsion systems, lidocaine emulsion systems were formulated with the highest drug concentration of 5 wt%. The negative effect of lidocaine loaded emulsions is ascribed to charge and steric effects, respectively, hindering the BCS to connect from one O/W interface, through the bulk, to another. Hypothesised mechanisms for this are displacement of BCS from the interface with concurrent alteration of surface properties. Lidocaine is known to have surface activity and thus may anchor to the O/W interface.[31]
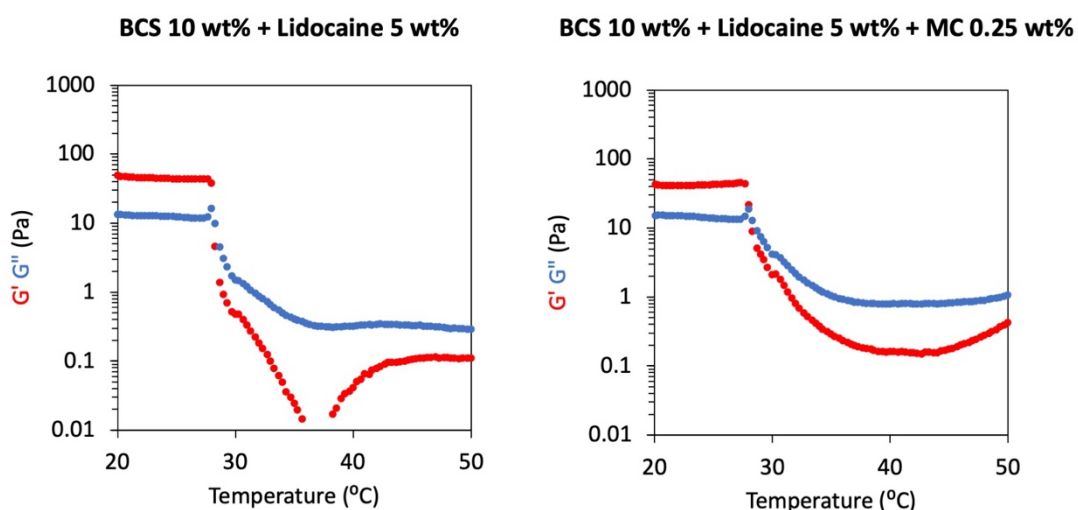
Figure 6.3: Temperature-ramp shear rheology of 1:1 o/w lidocaine loaded emulsions stabilised with 10wt% BCS (left) and drug-loaded emulsions with added 0.25 wt% methylcellulose to 10wt% BCS (right). G' (red) and G" (blue) are shown. The rheological analysis of the emulsion was conducted after 7 days of isolation.

Laser diffraction allowed measurement of droplet size distributions, giving X_{10}, X_{50}, and X_{90} values which correspond to the diameters which 10, 50 and 90 % of the population are less than, respectively. Typically, X_{50}, representing the median is used as an average with the other two values giving numerical description of dispersity. The size distributions are demonstrated in Figure 6.4. The droplet size distribution of the emulsions is illustrated

in Table 6.4. Median particle size (X_{50}) of all drug-loaded emulsion systems with 10 wt% BCS emulsions demonstrated stronger bimodal distribution in budesonide and lidocaine loaded emulsions stabilised with 10 w% BCS whereas these were largely monomodal with a minor shoulder at lower diameter in phenylephrine loaded emulsions stabilised with 10 wt% BCS. The similarity in droplet size for all 3 systems could be due to the same homogenisation technique used for the formation of droplet diameter. The drug-loaded emulsion systems with 10 wt% BCS and 0.25 wt% methylcellulose additive generated emulsions (emulsion with BCS/MC) with the smallest median droplet diameter (Table 6.4) and a narrower distribution as shown in Figure 6.4, which is a contributor to the stability of the system.
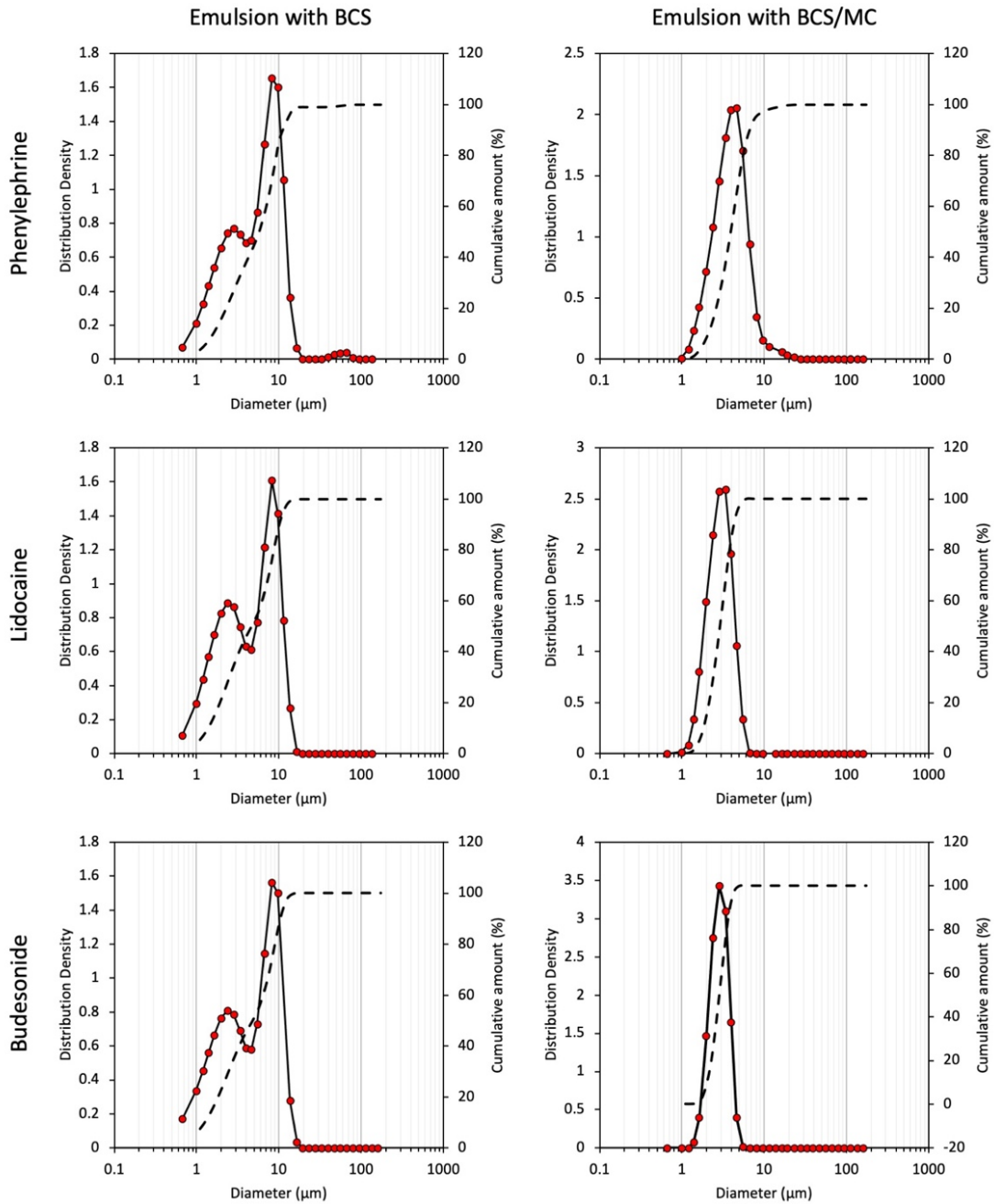
Figure 6.4: Droplet size distribution of drug-loaded o/w emulsions stabilised with 10 wt% BCS (left column) and drug-loaded o/w emulsions with added 0.25 wt% methylcellulose to 10wt% BCS (right column) as determined by laser diffraction. The red dots with solid line indicate distribution density, whilst the dotted line indicate cumulative distribution.

Table 6.4: Droplet size of drug-loaded emulsions stabilised with 10 wt% BCS (emulsion with BCS) and 0.25 wt% methylcellulose with 10 wt% BCS (emulsion with BCS/MC) after isolation of the creamed phase for 36 h.

Droplet size (μm)	Phenylephrine		Lidocaine		Budesonide	
	Emulsion with BCS	Emulsion with BCS/MC	Emulsion with BCS	Emulsion with BCS/MC	Emulsion with BCS	Emulsion with BCS/MC
X10	1.3	2.09	1.38	1.82	1.26	2
X50	4.8	3.94	4.7	2.91	4.83	2.86
X90	9.51	6.85	10.21	4.29	10.46	3.9

6.3.1 HPLC method development for determination of phenylephrine, lidocaine and budesonide

An analytical method was developed for the determination of phenylephrine as per ICH method validation guidelines.[23,24] Sample diluent (blank solution) was injected to determine the specificity. It was observed that no peaks were observed in the blank solution that interfered with the peak of interest. The precision of the method was determined by injecting 0.05 mg/mL phenylephrine solution 6 times. The retention time of phenylephrine is 5.4 min as shown in Figure A33 (in appendix). The relative standard deviation of the peak areas obtained from 6 samples injected independently was calculated to be 0.2 % and served as the measure of repeatability. The results met the acceptance criteria as per ICH method validation guidelines as tabulated in Table 6.5. According to the guidelines, specificity results myst ensure the selectivity of method for the analyte amid potential interference. Linearity, assessed through accuracy data with a concentration dependent calibration curve, requires a correlation coefficient (R^2) > 0.99. The precision, evaluated for repeatability, should be < 2%.

Table 6.5: Precision of phenylephrine, lidocaine and budesonide solutions at 0.05 mg/mL, 0.5 mg/mL and 0.1 mg/mL concentrations respectively (n=6).

No. of Samples	Phenylephrine 0.05 mg/mL solution response (mAU)	Lidocaine 0.5 mg/mL solution response (mAU)	Budesonide 0.1 mg/mL solution response (mAU)
1	540.296	527.754	2577.233
2	539.856	527.463	2576.413
3	539.833	529.546	2579.236
4	539.349	528.326	2577.376
5	541.291	526.92	2596.844
6	541.858	526.404	2596.665
Average	**540.414**	**527.736**	**2583.961**
RSD	**0.2**	**0.2**	**0.4**

The linearity and accuracy of the method were determined by preparing phenylephrine solution at different concentration levels. The target concentration of 0.05 mg/mL was considered as 100% solution and 6 different concentration levels of 20%, 40%, 60%, 80%, 100% and 120% (0.01 mg/mL, 0.02 mg/mL, 0.03 mg/mL, 0.04 mg/mL, 0.05 mg/mL, 0.06 mg/mL respectively) solutions with respect to the target concentration. The linearity curve was plotted for peak response against concentration as shown in Figure 6.5a. The correlation coefficient for the linearity plot was calculated to be 1. All analytical performance characteristics were met for the determination of phenylephrine and was validated for its intended use.
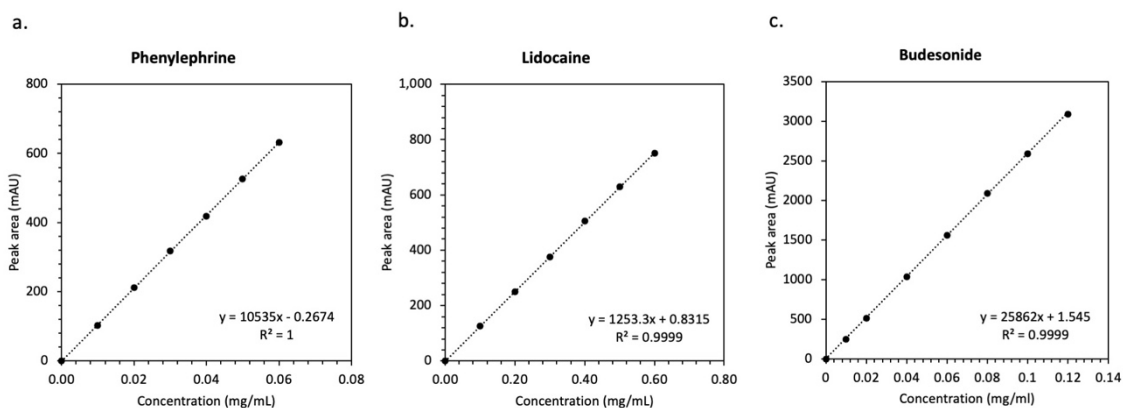
Figure 6.5: Linearity and accuracy of HPLC method for a.) phenylephrine, b.) lidocaine, and c.) budesonide.

Similarly, an analytical method was developed for the determination of lidocaine as per ICH method validation guidelines using the same chromatographic conditions as used in the phenylephrine determination. Sample diluent (blank solution) was injected to determine the specificity. It was observed that no peaks were observed in the blank solution that interfered with the peak of interest. The precision of the method was determined by injecting 0.5 mg/mL lidocaine solution 6 times. The retention time of lidocaine is 15.1 min as shown in Figure A34 (in appendix). The relative standard deviation of the peak areas obtained from 6 samples injected independently was calculated to be 0.2 % and served as the measure of repeatability. The results met the acceptance criteria as per ICH method validation guidelines as tabulated in Table 6.3.

The linearity and accuracy of the method were determined by preparing lidocaine solution at different concentration levels. The target concentration of 0.5 mg/mL was considered as 100% solution and 6 different concentration levels of 20%, 40%, 60%, 80%, 90%, 100% and 120% (0.1 mg/mL, 0.2 mg/mL, 0.3 mg/mL, 0.4 mg/mL, 0.5 mg/mL, 0.6 mg/mL respectively) solutions with respect to the target concentration (i.e., 0.5 mg/mL). The linearity curve was plotted for peak response against concentration as shown in Figure 6.5b. The correlation coefficient for the linearity plot was calculated to be 0.9999. All analytical performance characteristics were met for the determination of lidocaine and was validated for its intended use.

176

A method for budesonide quantification was developed. Again, no peaks were observed in the blank solution that interfered with the peak of interest. It was observed that the budesonide separated in two epimers, epimer A and epimer B and the retention times of the epimers are 12.5 and 13.44 min respectively as shown in Figure A35 (in appendix). The resolution between the two epimers of budesonide was observed to be 3.1. The relative standard deviation of the peak areas (calculated from the sum of two budesonide epimer peaks) obtained from 6 samples injected independently was calculated to be 0.2 % and served as the measure of repeatability. The results met the acceptance criteria as per ICH method validation guidelines as tabulated in Table 6.3.

The linearity and accuracy of the method were determined by preparing budesonide solution at 7 different concentration levels of 0.01 mg/mL, 0.02 mg/mL, 0.04 mg/mL, 0.06 mg/mL, 0.08 mg/mL, 0.1 mg/mL and 0.12 mg/mL. The correlation coefficient for the linearity plot (Figure 6.5c) was calculated to be 0.9999. All analytical performance characteristics were met for the determination of budesonide and was validated for its intended use. Thus, the techniques were accepted for use in drug release studies.

6.3.2 Solubility study of budesonide in 0.2 % v/v Tween-20 in PBS

Solubility profiling of budesonide was performed in 0.2 % v/v solution of Tween-20 in PBS to be used as a receiver fluid for a drug release experiment using a Franz cell apparatus. The inclusion of Tween-20 in the fluid was required due to the low solubility of budesonide and the need to maintain sink conditions in the experiment. Budesonide solutions in concentrations ranging from 0.01 mg/mL to 0.15 mg/mL were prepared to obtain a saturated solubility of budesonide in the receiver fluid. The higher concentrations of budesonide formed a suspension which was visually confirmed by the continued presence of drug particles in the solution. All sample solutions were stirred for 24 h at room temperature, centrifuged at 5000 rpm for 15 min and subjected to drug quantification by HPLC analysis. The maximum solubility of drug in the solvent was found to be ca 0.1 mg/mL as shown in Figure 6.6 as evidenced by the plateau of the signal at this concentration.
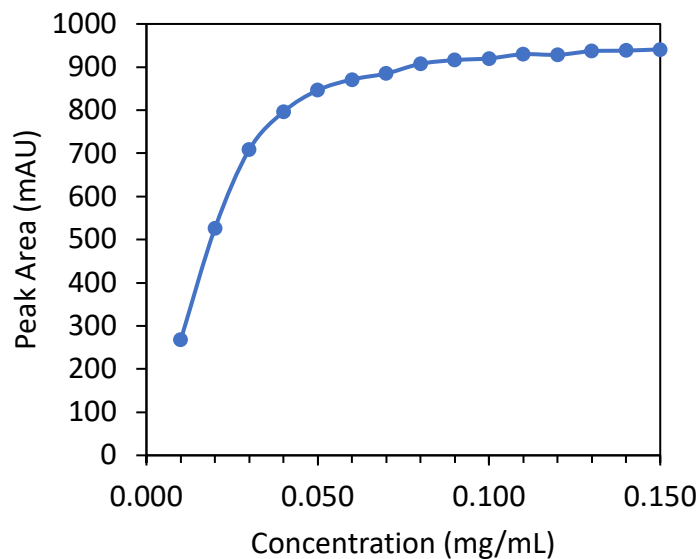
Figure 6.6: Solubility profile of budesonide plotted for peak response against concentration as determined by HPLC (n=1).

6.3.3 Drug loading and quantification

1 wt%, 10 wt% and 0.128 wt% of phenylephrine, lidocaine and budesonide were added to aqueous BCS and BCS/MC solutions and emulsified with equal weight of dodecane oil phase. The resulting emulsions were estimated to be loaded with 0.5 wt%, 5 wt% and 0.064 wt% of phenylephrine, lidocaine and budesonide theoretically. The drug loading concentrations were selected with respect to equivalent market products available. Phenylephrine 0.5 %w/v and lidocaine 5 %w/v topical solution were used as reference product for comparing lidocaine and phenylephrine emulsions formulation. For the comparison of budesonide emulsion, Benacort nasal spray (budesonide 64 mcg per actuation) was used. Upon drug quantification, drug loading for emulsion stabilised by 10 wt% BCS was 81.5% (20.375 mg), 91% (227.5 mg) and 38.1% (1.22 mg) for phenylephrine, lidocaine and budesonide formulations as tabulated in Table 6.6. The drug loading for emulsions stabilised by 10 wt% BCS and 0.25 wt% methylcellulose was found to be 98% (24. 5mg), 96% (240.0 mg) and 51.3% (1.64 mg) for phenylephrine, lidocaine and budesonide formulations (Table 6.6). Drug loading percentage was calculated with respect to the amount of drug loaded in the system before emulsification. In the

budesonide formulation, drug was added as a suspension due to its low solubility, giving rise to the lower loading efficiency reported.

Table 6.6: Drug loading and quantification in the emulsion system stabilised by BCS and BCS/MC (n=6).

| Drug | drug loaded (mg) | drug quantified (mg) | |
		Emulsion with BCS	Emulsion with BCS/MC
Phenylephrine	25	20.375	24.5
Lidocaine	250	227.5	240
Budesonide	3.2	1.22	1.64

6.3.4 Drug release profiling using Franz diffusion cells

For phenylephrine drug release, 0.5 g of emulsion was added to the donor chamber of the Franz cell giving 2.5mg of phenylephrine. The receiver fluid was comprised of phosphate buffer solution and the sampling was conducted at time intervals of 0.25, 0.5, 1, 3, 6, 9, 12 and 24 h. The quantification of drug release in the receiver fluid was performed using the validated HPLC method. Lidocaine-Phenylephrine topical solution containing 5 %w/v solution of Lidocaine and 0.5 %w/v solution of phenylephrine was used for comparative study.[29]

The cumulative release of phenylephrine formulated into either BCS-only or BCS/MC emulsions, as well as the reference product, was studied across a cellulose membrane over 24 h period (Figure 6.7). The drug release profile of the market-available topical solution (reference product) gave relatively rapid liberation. It was observed that 60% of drug was released in the first 1.5 h and above 80% of the drug was released in 3 h. Both emulsion systems retarded liberation across the membrane significantly. In the BCS-only emulsion, it was observed that 60% of the drug (calculated relative to the drug loading) was released in 10 h and 88% of the drug was released in 24 h. The emulsion formulated with BCS/MC showed a further reduction in drug release rate, liberating 60% in 20 h and a total of 65% of the drug was released in 24 h.

Statistical evaluation of the drug release data was conducted using 2-way ANOVA with Bonferroni post-hoc testing for multiple comparisons. The release of phenylephrine in time 0 between 3 formulations, reference, emulsion with BCS and emulsion with BCS/MC was 0% as expected. At the second time point, 15 min (0.25 h), drug release from emulsion with BCS and emulsion with BCS/MC were significantly different ($p > 0.05$) with release below 5% while the drug release from both the emulsion formulations were significantly different as compared to the reference product which showed release of 11.1%. Furthermore, except for these time points, in all the sampling events all 3 formulations had significantly significant differences in release ($p < 0.001$). The drug release pattern for both the BCS-stabilised emulsion formulations showed controlled release relative to the reference product with optimum release of 88% and 65% form BCS and BCS/MC emulsion in 24 h respectively. The reference product showed more than 83% in 3 h and 95.9% drug release in 24 h.

For lidocaine drug release, the study was performed similarly to phenylephrine-loaded emulsion formulations. 0.5 g of the emulsion (containing 25mg of lidocaine) was added to the donor chamber of the Franz cell and phosphate buffer solution as receiver fluid in the receiver chamber. The cumulative amount of lidocaine permeated across the membrane over 24 h period is illustrated in Figure 6.7. For the BCS-only emulsion, it was observed that 60% of the drug (calculated relative to the drug loading) was released in 15 h and 76% of the drug was released in 24 h. The emulsion formulated with BCS/MC showed drug release of 60% in 21 h and total of 64.5% of the drug was released in 24 h. Comparing the release from emulsion with BCS only and BCS with MC with the reference product, it was observed that 60% of the drug was released in 2 h.

Primarily, the first timepoint (0 h) result showed 0% drug release for all 3 products. In contrast, the samples at 15 min (0.25 h) were comparable ($p > 0.05$) between BCS and BCS/MC formulation with less than 5% drug release. Whereas, both groups were significantly different ($p < 0.001$) with the reference product which released 10.4 %w/v of lidocaine. Furthermore, at 0.5 h drug release from BCS and BCS/MC emulsion showed statistical significance ($p < 0.01$). However, both emulsion formulations showed less than 10% drug release, significantly different ($p < 0.001$) from the reference product which is

20.5%. All of the other time events resulted in significantly different from each other ($p < 0.001$).

The lidocaine release pattern was similar to phenylephrine, but with reduced rate as observed in Figure 7.6. The formulation with BCS and BCS/MC showed controlled release with 76% and 63.9% at 24 h respectively. Whereas, the reference formulation showed more than 74.7% in 3 h and 91.4% in 24 h.

The cumulative amount of budesonide permeated across the membrane over 24 h period is illustrated in Figure 6.7. In the donor chamber of the Franz cell, 0.1 g of the emulsion (32 mcg of budesonide) was added and 0.2 %v/v solution of Tween-20 in phosphate buffer solution was used as receiver fluid in the receiver chamber. In the comparison of the 2 drug-loaded emulsion systems, increased permeation of budesonide was observed with the emulsion formulated with only BCS. It was observed that 60% of the drug (calculated relative to the drug loading) was released in 9.5 h and 74% of the drug was released in 24 h. The emulsion formulated with BCS/MC showed drug release of 60% in 12 h and a total of 67.5% of the drug was released in 24 h. Interestingly, the budesonide formulations show near zero-order liberation for the first 9 h of the experiment. Similarly, drug release study was performed for a reference product (budesonide nasal spray – 64 mcg per actuation) and it was observed that 60% of the drug was released in the initial 2 h and a total of 83.9% in 24 h.
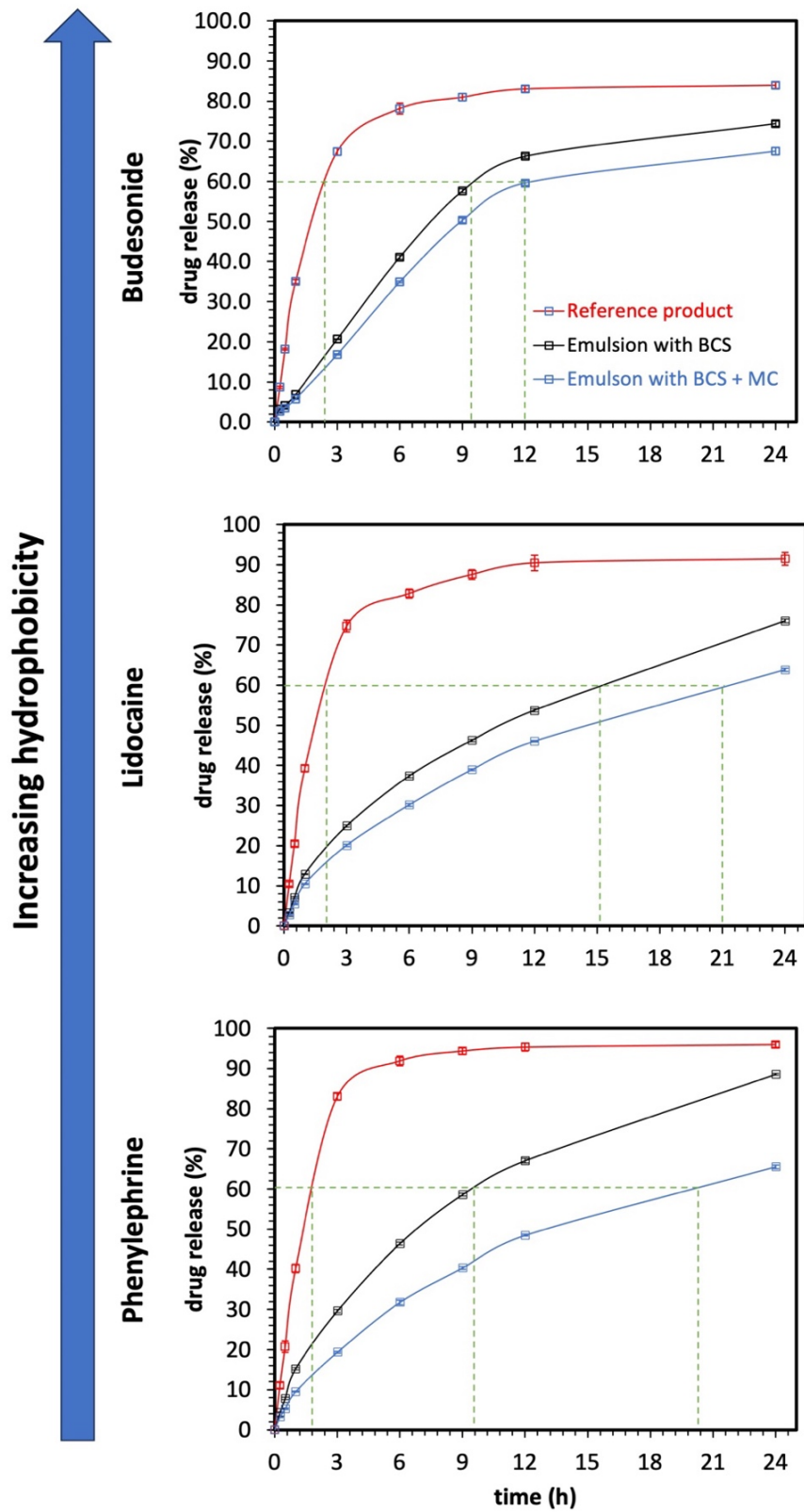
Figure 6.7: Drug release profile of phenylephrine, lidocaine and budesonide emulsion formulation using Franz diffusion cells (n=6).

The observation for the drug release in time 0 h for the reference product and the drugs formulated with BCS and BCS/MC were considered 0% The quantity of released budesonide at 0.25 and 0.5 h were comparable (p > 0.05) between two emulsion formulations with BCS and BCS/MC with less than 5% drug release. Whereas both the formulations were significantly different (p < 0.01) with the reference product which showed release of 8.7% and 18.2% of budesonide in 0.25 h and 0.5 h respectively. However, the amount of drug release at 1 h showed significance (p < 0.001) between emulsions with BCS and BCS/MC. Both emulsion formulations showed less than 10% drug release which is significantly different (p < 0.001) from the reference product which is 35%. All of the other sampling events results showed significantly different (p < 0.001) release from each other. Both emulsion formulations with BCS and BCS/MC showed drug release of 74.4% and 67.5% at 24 h respectively whereas, the reference product showed 67.5% drug release at 3 h and 83.9% release at 24 h.

The Korsmeyer-Peppas[32] equation was fitted to the drug release data to further probe the drug release kinetics from the controlled release thermoreversible gels stabilised by the BCS and BCS/MC. According to the equation, designed for fitting release data from thin films, when n=0.50 the drug release mechanism is governed by Fickian diffusion, when 0.50<n<1.0 it is anomalous (non-Fickian transport), and when n=1.0 it is zero order release. To study the drug release kinetics, the Korsmeyer-Peppas kinetic model was fitted to all drug release data. Figure 6.8 shows the nonlinear curve fitting to the experimental data of phenylephrine and lidocaine formulations using the Korsmeyer-Peppas model and a zero-order release kinetics for budesonide formulations. The release constant (*k*) is directly proportional to the diffusion constant and hence depends on the physical and structural properties of both the drug and BCS. This *k* value indicates the release rate of the drug. As shown in Table 6.7, the *k* value is higher for the emulsions with only BCS as compared to emulsions with BCS and MC. This denotes that the release rate is higher with emulsions systems prepared with only BCS. The n value is observed to be greater than 0.5 for all the systems which is attributed to anomalous (non-Fickian) transport through the dialysis membrane, indicating that the dosage form is affecting liberation from the system.[32] The kinetic parameters obtained from the *in vitro* drug release data (Table 6.7)

showed that the release of phenylephrine and lidocaine followed the diffusion model of Korsmeyer-Peppas. The correlation coefficient, "R^2", values were 0.9955, 0.9969 for phenylephrine emulsion with BCS and BCS/MC respectively and 0.9985, 0.9982 for lidocaine emulsion with BCS and BCS/MC respectively. For budesonide-loaded emulsions, the drug release obeyed zero order kinetics with R^2 values of 0.9866 and 0.9925 for BCS and BCS/MC emulsion respectively. This might be because the drug has a high affinity for the oil droplet and experiences a zero-order release profile due to partitioning out from oil to water phase. Furthermore, the better fit with zero order kinetics has been confirmed by assessing the correlation coefficient between the experimental and fitted values obtained through mathematical methodologies at various time points during the experimental duration. Mechanistically, zero order delivery can be achieved when the rate of partition of drug from oil to water is approximately equal to that rate of diffusion across the membrane from the water phase.
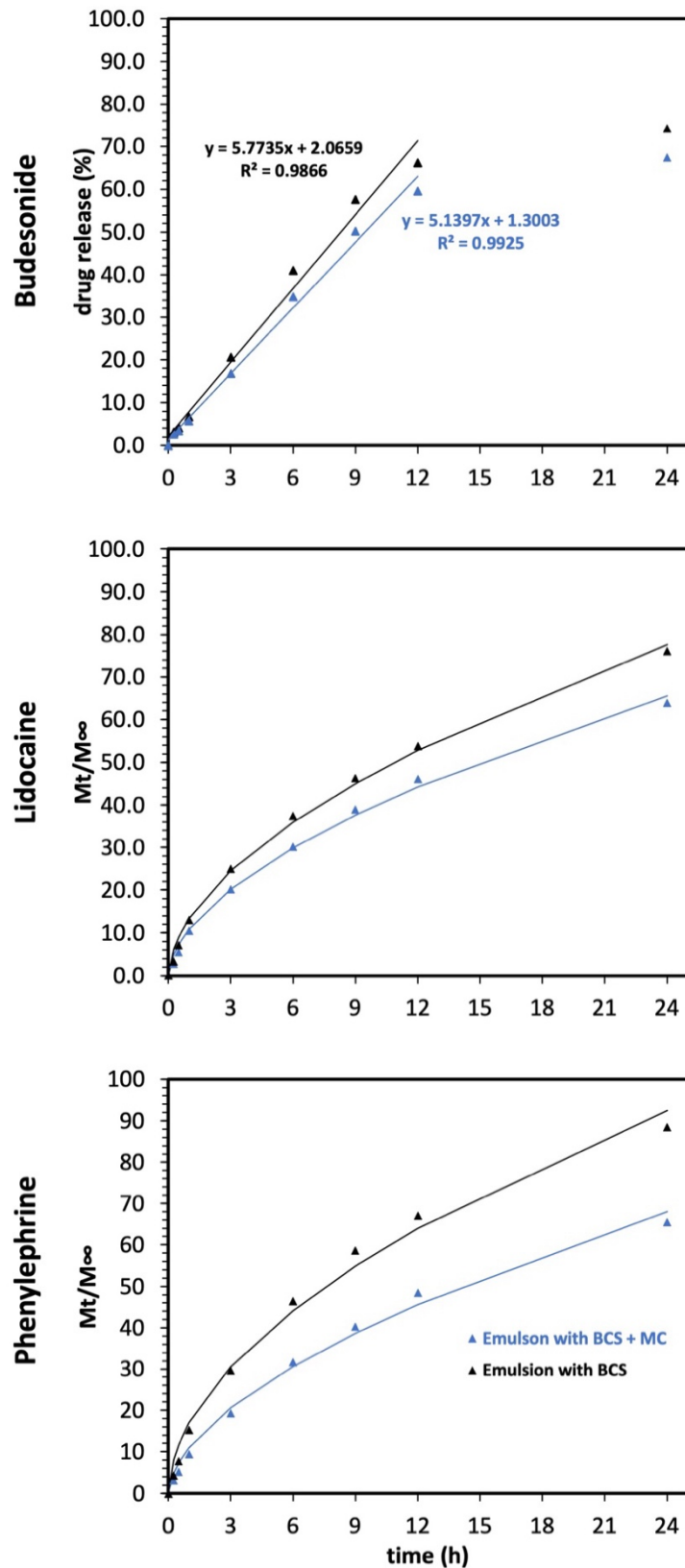
Figure 6.8: Drug release profile fitted with Korsmeyer-Peppas model fit for phenylephrine and lidocaine; and zero-order kinetic model for budesonide. Solid lines represent the predicted model.

Table 6.7: Parameters obtained from fitting experimental data to Korsmeyer-Peppas model.

Korsmeyer-Peppas fit parameters	Phenylephrine		Lidocaine		Budesonide	
	Emulsion with BCS	Emulsion with BCS/MC	Emulsion with BCS	Emulsion with BCS/MC	Emulsion with BCS	Emulsion with BCS/MC
K	17	10.94	13.35	10.81	14.24	11.91
n	0.53	0.57	0.55	0.57	0.56	0.58
R^2	0.9955	0.9969	0.9985	0.9982	0.9737	0.9749

Overall, the slowest release is observed from the BCS/MC emulsion as compared to BCS only emulsion and the reference product (Figure 6.7). The reference product for phenylephrine and lidocaine is a topical solution (lidocaine 5 %w/v and phenylephrine 0.5 %w/v topical solution)[29] and an aqueous suspension for budesonide (Benacort nasal spray)[30], hence it is obvious that the release of the drug from a membrane is immediate with more than 60 % w/v drug release in less than 3 h and more than 90 %w/v for phenylephrine and lidocaine; and more than 80 %w/v for budesonide in 24 h.

Comparing drug formulations with BCS only and BCS/MC, slower drug release is observed from the emulsion formulated with BCS/MC. In BCS-stabilised thermoresponsive gels, the drug release may be controlled by multiple factors. The release rate is hypothesised to depend on the drug's affinity for the BCS, its solubility in the oil phase, its diffusion through the BCS matrix, and the emulsion droplet size which can alter both the area of the O/W interface and the tortuosity of the aqueous inter-droplet space.[33,34] However, in the BCS/MC thermoresponsive gelation system, an additional factor is introduced. Methylcellulose is a hydrophilic polymer often used in pharmaceutical formulations to control drug release. It forms a gel-like matrix when hydrated, which can slow down the dissolution and diffusion of the drug through the matrix.[34,35] This results in delayed drug release, as the drug molecules must diffuse through polymer network before being released into the surrounding environment. The thermogelation of the emulsion and the methylcellulose's swelling properties could also be other factors that contributed to this delayed release effect. In addition, the enhanced gelation strength contributed by the addition of methylcellulose in BCS/MC stabilised thermosensitive engineered emulsions

seem to have an effect on controlling drug release. The drugs formulated with BCS only have lower gelation strength as compared to the drug formulation with BCS/MC as seen in the rheological profile (Figure 6.2). This could lead to faster drug release, as the gel matrix has fewer physical cross-links, allowing for easier diffusion of drug molecules. The addition of methylcellulose enhanced the gelation strength, and the stronger gel matrix can impede drug diffusion, leading to a slower release rate. Hence, the differences in drug release rate from BCS and BCS/MC systems can be attributed to the interplay between drug-polymer interactions and the influence of methylcellulose's hydrated layer on these interactions.

A slower release is observed with BCS/MC formulation despite the emulsion droplet size being smaller as compared to the formulation with only BCS (Table 6.3, Figure 6.4). Conventionally, smaller emulsion droplets are generally associated with a greater surface area of the oil, potentially leading to an accelerated drug release from oil to water.[33] Hence, the polymer in the bulk or at the interface or the polymer-methylcellulose is limiting the release rate.

Comparing the drug release pattern for all 3 drugs (Table A10), it was observed that the release was comparable ($p > 0.05$) between lidocaine and budesonide at 0.25 h with 3.3% and 3.2% respectively but 2 other comparison groups (phenylephrine vs lidocaine and phenylephrine vs budesonide) were significantly different ($p < 0.001$). Moreover, at 0.5 h, the drug release was 7.9% and 7.1% ($p < 0.01$) between phenylephrine and lidocaine respectively. However, for other comparison groups (phenylephrine vs budesonide and lidocaine vs budesonide) the drug releases were significantly different from each other ($p < 0.001$). Remaining other observations, the drug release amounts were significantly different ($p < 0.001$) between each comparison group at every time point. Hence, comparing the overall release profile for all 3 drugs, it is observed that phenylephrine is released faster, and it is significantly different ($p < 0.001$) at 24 h. The amount of drug released at 24 h with BCS-only formulation is 88.6, 76, 74.4%; and 65.5, 63.9 and 67.5% for BCS/MC formulation loaded with phenylephrine, lidocaine and budesonide respectively. This show that the release pattern follows the hydrophobicity rank order of the 3 drugs studied, which refers to the amount of water they repel. Phenylephrine, being

the least hydrophobic of the three, has a greater fraction of the dissolved drug present in the water phase over the oil phase. Therefore, the release is relatively quick from the formulation because it is readily dissolved in the surrounding water-based medium and hindered by polymer in the aqueous bulk and tortuosity of the system. Lidocaine has a moderate affinity for the oil phase. Consequently, lidocaine is released at an intermediate rate as it takes some time to partition from the oil phase into the surrounding medium. Finally, budesonide is the most hydrophobic of the three drugs, has a strong tendency to dissolve in the oil phase. Hence, when the drug formulation is exposed to a surrounding medium, budesonide is more likely to be released slowly from the formulation because it takes time for the drug to partition out of the oil phase. So, the release pattern, budesonide < lidocaine < phenylephrine, reflects the drugs' different tendencies to partition from the oil phase of the formulation, where they are initially embedded, into the surrounding medium. This phenomenon is tied to their hydrophobicity, with more hydrophobic drugs taking longer to partition and be released into the surrounding aqueous phase to replenish drug which is lost across the membrane.

The release pattern is also related to how these drugs diffuse through a medium. Diffusion occurs as the movement of molecules from higher to lower concentration area. The hydrophobicity of the drug affects the diffusion rate. More hydrophobic drugs tend to interact with other factors in an emulsion system (oil phase or polymer surfactants) slowing down the diffusion process.[33,34] Moreover, the diffusion of the drugs may also be limited by the polymer micelle present in the aqueous phase of the colloid system.[36] The interior of these micelle provides a hydrophobic environment. Hence, the hydrophobic drugs tend to dissolve within the micelle. This partitioning process is driven by the drug's hydrophobic nature. The drug within the micelle is now effectively encapsulated which slows down the release of the drug into the surrounding medium as the drug molecules must diffuse out of the micelle to be released. The rate at which the drugs are released from the micelles follow the hydrophobicity order. Budesonide being the most hydrophobic, takes longer to diffuse out of the micelle due to strong affinity for the hydrophobic interior whereas phenylephrine being the least hydrophobic is liberated more readily. Hence, the hydrophobicity of the drugs and their interaction with the micelles also influences the liberation kinetics of the drug.

The drug release pattern can also be explained by considering how tortuosity within the polymer matrix and the oil droplets affects the release process. The tortuous path can slow down the diffusion process. Budesonide, being highly hydrophobic, faces more tortuous paths within the polymer or emulsion droplets, resulting in a slower release rate as compared to lidocaine and phenylephrine. Moreover, the release mechanism can also be influenced by the drug's interaction with the gel structure and drug within the lipid-based get network leading to the drug diffusion through the thermogelling systems.

The behaviour of thermoreversible gelling system is complex and the drug release mechanism from these systems is influenced by a variety of factors. These factors include, the composition of emulsion, properties of BCS and other additives and their interactions, viscosity, the partition coefficient of the drug molecules, concentration effects, dug-polymer interaction, emulsion droplet size, diffusion hinderance and tortuosity path.[37] Hence, it is important to consider these factors during the formulation of thermoresponsive emulsion systems for drug delivery and their drug release mechanism.

6.3.5 Drug delivery platform/device assembly

Nasal drug delivery offers a wide range of devices including unit dose and multi dose nasal devices. The benefits of nasal drug delivery include its rapid onset of action and targeted delivery capabilities making it ideal for systemic drug delivery and CNS treatments. It is proposed that thermoresponsive engineered emulsions may be ideal drug delivery vehicle for nasal application, considering the low viscosity state at room temperature will allow the material to be sprayed. Post-spraying, switch to a gel state by warming in the nose will allow the material to better resist any shear imposed to enhance retention. As such, the emulsions developed in this project were evaluated for compatibility with a novel spray device in collaboration with Bespak.

The 0.1 g of engineered emulsion stabilised with 10 wt% BCS was filled in the metering chamber of the Unidose[25] nasal spray device (Figure 6.9a). The aim was to fill the device with viscous emulsion liquids, understand the atomisation and perform qualitative tests. The determination of droplet size distribution (DSD), plume geometry, spray pattern (Figure 6.9b) and shot weights were performed using engineered emulsion formulation

and a standard Unidose nasal spray device. The design of this device was requested to remain confidential by the company and is omitted from this thesis.
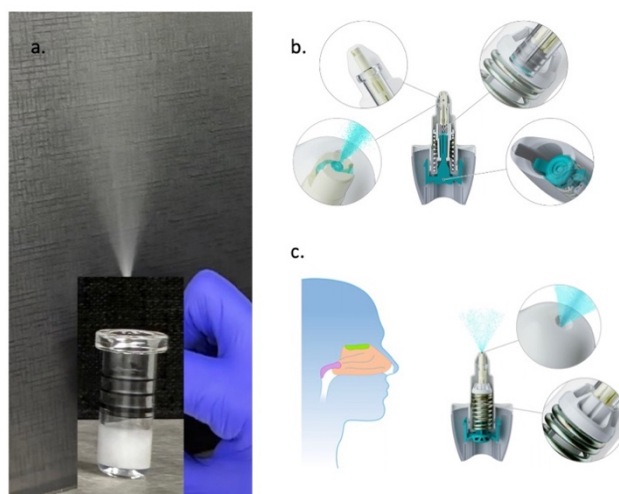
Figure 6.9: a.) Atomisation of engineered emulsions stabilised with 10 wt% BCS through unit dose nasal device b.) cross-sectional view of nasal device and its assembly consisting of actuator, spray pin, nozzle, plunger and container[25] c.) plunger controlling the droplet size and plume angle depending on the emulsion viscosity.[25]

6.3.6 Determination of shot weights/pump delivery

The determination of shot weights serves two primary purposes: first, to verify the functionality of the valve and second, to assess the consistency of pump-to-pump performance in terms of drug product effectiveness, ensuring reproducible and accurate dosing.[38,39] To determine the shot weights from the Unidose nasal spray, the devices were initially weighed both before and after each actuation using a precise analytical balance, allowing for an evaluation of the mass emitted. The metering chamber in the nasal device was loaded with 0.1 g of emulsion. Our investigation focused on the impact of actuation force on shot weight or pump delivery, and this relationship represented in Figure 6.10. A total of 45 nasal devices were tested and the results revealed that, on average, 52.5 ± 3.6 mg of the loaded emulsion were dispensed with an average force of 32.6 ± 2.6 N. The maximum and minimum deviations for the shot weights were found out to be + 9.8 to - 16.9 % and for the actuation force +29.4 to -16.4 % respectively. These findings exhibited deviations out of the acceptance criteria for nasal spray formulations. The acceptance

criteria must ensure that the weight of each individual spray remains within 15% of the designated target weight, while the average weight should be controlled within a 10% range of the target weight.[39] The latter of these two criteria has been achieved, however, indicating that the average performance was acceptable, with outliers causing the first criterion to be broken. Thus, results are promising but the device/formulation parameters will require optimisation if adopted into a medicine . Multiple factors can influence the pump delivery of a nasal spray, encompassing viscosity, surface tension, stroke length and actuation velocity employed.[40] Additionally, the dimensions of the metering chamber within the pump play a pivotal role in determining the volume and subsequent mass delivered by the device.[40]

Figure 6.10: The effect of actuation force on shot weight of the Unidose nasal device. The result represents data from 45 actuations.

6.3.7 Droplet size distribution (DSD)

Laser diffraction was used to measure the geometric size of droplets and particles in real time. The droplet sizes of a single spray were measured at 2 distances from the nozzle tip,

3 cm and 6cm as populated in Table 6.8. The data was collected during the fully developed phase of the spray and the sizes are expressed as D_{10}, D_{50}, D_{90} as well as span. An influence on D_{10}, D_{50} and D_{90} on the measurement distances (3 cm and 6 cm) was observed due to the evolution of a spray plume. The average median droplet size (D_{50}) was found to be 186.15 μm (SD $\pm$ 107.6) and 197 μm (SD $\pm$ 159.9) on the measurement distances of 3 cm and 6 cm respectively. However, there was a slight effect on span with an average of 1.515 (SD $\pm$ 0.2) and 1.584 (SD $\pm$ 0.3) for measurement distances of 3 cm and 6 cm respectively with some fluctuation. The DSD within the nasal spray is a critical parameter to access how the drug is deposited within the nasal cavity during in vivo administration. The dimensions of these droplets are primarily influenced by several factors such as the design of the nasal device, actuation force, actuation velocity, stroke length, the distance between the nozzle and the laser beam, spraying angle and the viscosity and surface tension of the formulation.[40] The acceptance criteria for the median droplet size falls within the range of 30 to 120 μm.[39] When droplets are above 120 μm, they tend to deposit in the anterior regions of the nasal passage whereas if the droplets are less than 10 μm, they could potentially be inhaled reaching the lungs and causing adverse effects. Thus, the formulations show a desirable droplet size distribution with negligible fine (< 10 μm) fine fraction to avoid inhalation of dose and target the nasal mucosa. The variability observed in the droplet size distribution may have been occurred due to the emulsion viscosity, the nozzle size and the nasal device parameters.

Table 6.8: The droplet size distribution and span measured at 3 cm and 6 cm from the nozzle.

Actuations	Droplet Size Distribution @ 3cm (μm)					Droplet Size Distribution @ 6cm (μm)				
	%<10 μm	D_{10}	D_{50}	D_{90}	Span	%<10 μm	D_{10}	D_{50}	D_{90}	Span
1	0.00	70.23	160.60	313.60	1.52	0.00	40.89	88.49	181.00	1.58
2	0.00	35.88	90.87	183.60	1.63	0.00	339.70	511.40	744.00	0.79
3	0.00	64.20	147.10	287.60	1.52	0.00	51.68	148.10	309.50	1.74
4	0.00	242.40	459.80	759.90	1.13	0.17	47.00	122.80	257.50	1.71
5	0.00	38.64	99.73	207.20	1.69	0.00	82.12	172.10	316.20	1.36
6	0.00	123.50	267.50	558.70	1.63	0.00	31.18	71.56	169.70	1.94
7	0.00	71.17	163.20	318.20	1.51	0.00	81.90	202.50	420.20	1.67
8	0.00	87.53	181.60	340.60	1.39	0.00	37.76	90.86	196.30	1.75
9	0.00	59.17	152.80	306.80	1.62	0.00	39.21	95.98	203.80	1.72
10	0.00	58.49	138.30	269.50	1.53	0.14	274.20	468.40	755.40	1.03
Mean		85.12	186.15	354.57	1.52		102.56	197.22	355.36	1.53
SD		60.59	107.59	174.52	0.16		110.22	159.87	221.52	0.36

6.3.8 Plume geometry and spray pattern

For the determination of plume geometry, a laser sheet and a high-speed digital camera were used. The images (Figure 6.11) were taken from a sideward view of the emitted spray parallel to the axis of the plume. The result showed plume angle of 51.1° to 23.1°and plume width of 28.71 to 12.25 measured at 6 cm from the tip of the nozzle (Table 6.9). Trows et al investigated the influence of viscosity and suggested that decrease in plume angle and spray area was observed with an increase in the viscosity of the formulation.[40] Moreover, the plume geometry can also be affected by the type of nozzle, measurement distance and actuation force. The average plume angle of 38° suggest efficient delivery to the turbinate region of the nasal mucosa, based on prior studies demonstrating can 80 % of dose delivered to this region for formulations of equivalent plume angle.[41] This highly vascularised and permeable region of the nasal cavity is ideal for systemic drug delivery. For optimal deposition in the nasal cavity, the plume angle needs to be carefully controlled. A plume angle that is too narrow may result in the spray being directed too high into the nostrils, potentially missing the targeted areas within the nasal passages. On the other hand, a plume angle that is too wide might cause the spray to impact the nasal septum or even exit the nasal cavity altogether.[42] To effectively deposit the spray in the desired regions of the nasal cavity, the plume angle should be adjusted to align with the anatomy and airflow patterns within the nose. This ensures that the spray particles are carried by the nasal airflow to the intended target areas, such as the nasal cavity and the mucosal surfaces, where efficient absorption can occur. Hence, the plume angle of a nasal spray is also one of the critical parameters in guiding the trajectory of the spray droplets within the nasal cavity, ensuring that they are deposited in the appropriate locations for optimal therapeutic effect.
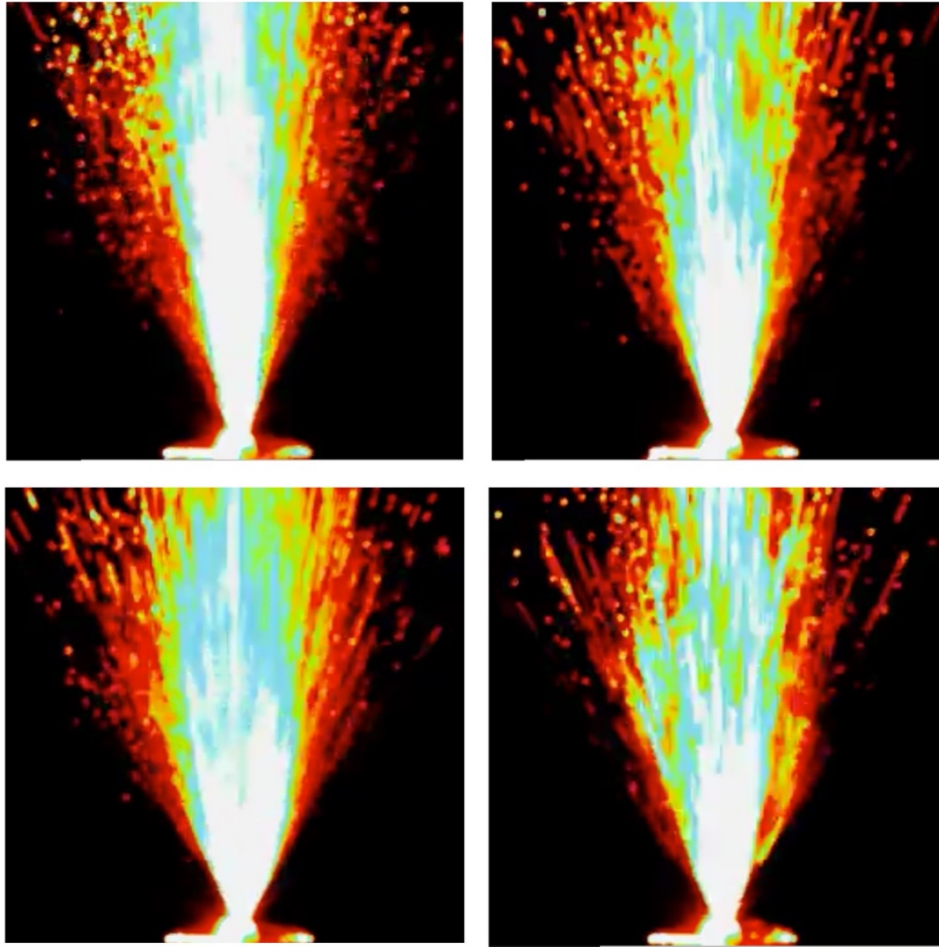
Figure 6.11: Plume geometry and spray pattern of Unidose nasal spray loaded with engineered emulsion stabilised with 10 wt% thermoresponsive BCS captured by a high-speed digital camera. 4 images captured for 4 devices actuated manually showing reproducibility with slight variations.

Table 6.9: Evaluation of plume geometry at a defined distance of 6 cm to the nozzle.

Actuations	Plume Geometry @ 6cm	
	Plume Angle 6cm	Plume Width 6cm
1	40.70	22.26
2	46.10	25.65
3	23.10	12.25
4	29.30	15.70
5	51.10	28.71
6	45.10	24.89
7	32.70	17.61
8	27.20	14.55
9	48.20	26.80
Mean	**38.17**	**20.94**
SD	**10.25**	**6.01**

To assess the spray pattern, an image capturing a cross-sectional view of the plume along the axial direction was employed at a specified distance (3 cm and 6 cm) from the actuator tip. The plume width data supplements the spray pattern data and was determined based on single actuation. The evaluation of the spray pattern measured at 3 cm and 6 cm distances is tabulated in Table 6.10. The spray pattern measured at 3 cm showed variable result for the ovality ratio ranging from 1.124 to 2.585. Whereas the spray pattern data suggested that no significant changes was observed in the ovality ratio when measured at a distance of 6 cm. It should be noted that the spray pattern increases with increasing actuation velocity and leading to slight decrease in spray pattern ovality.[43] A more circular spray pattern is desired as it ensures an even and efficient distribution of the spray within the nasal cavity. A reduction in spray pattern ovality implies a circular shape, indicating improved coverage and deposition of the spray on the nasal surfaces. Hence, this enhances the effectiveness and consistency of drug delivery and absorption, contributing to the overall performance of the nasal spray in achieving its intended therapeutic outcomes.[42]

Table 6.10: The evaluation of spray pattern measured at 2 distances, 3 cm and 6 cm.

Actuations	Spray Pattern @ 3cm			Spray Pattern @ 6cm		
	Dmax	Ovality	Area	Dmax	Ovality	Area
1	20.88	1.17	288.80	46.16	1.42	1142.50
2	22.61	1.15	347.10	34.40	1.33	662.80
3	19.09	1.27	222.50	36.17	1.35	722.80
4	16.15	2.59	74.70	29.13	1.35	474.90
5	18.91	1.25	228.10	32.10	1.29	596.40
6	21.88	1.86	191.50	36.31	1.32	813.90
7	22.28	1.12	343.50	45.99	1.24	1395.90
8	22.77	1.19	347.40	33.67	1.71	470.10
Mean	20.57	1.45	255.45	36.74	1.38	784.91
SD	2.34	0.52	95.85	6.20	0.15	327.66

The analytical parameters related to the characterisation of nasal spray device were carried out for the feasibility of the emulsions stabilised with 10 wt% thermoresponsive BCS. It was observed that the development of nasal spray is formulation dependent, and the viscosity of the formulation significantly influences DSD, shot weight, plume geometry and spray pattern. As a result, it is crucial to take the influence of viscosity of the formulation into account during the formulation development which can be contributed by the concentration of BCS and drug molecule. In this context, the molecular weight and concentration of BCS is directly affects the viscosity of the emulsions. The molecular weight and concentration serve to enhance the stability of the emulsion as well as increase the magnitude of gelation which is predicted to contribute to prolonged retention of the formulation in the nasal cavity. Despite not meeting the analytical parameter criteria in our initial attempt, these thermoresponsive engineered emulsion showed promising results for further qualitative and quantitative analysis for development of nasal sprays.

To demonstrate the broad functionality of the emulsions, passage through needles was also explored to open up future possibilities of use in parenteral delivery. Additionally, in the development of nasal sprays, the unit dose nasal spray devices feature a spray pin needle through which the emulsion must pass to be sprayed from the nozzle. The emulsion stabilised with 10 wt% BCS was able to be passed through the needles of 25 and

26G sizes as shown in Figure 6.12. These low bore sizes open up the possibility of injection into SC or IM spaces with reduced pain compared to larger size needles.
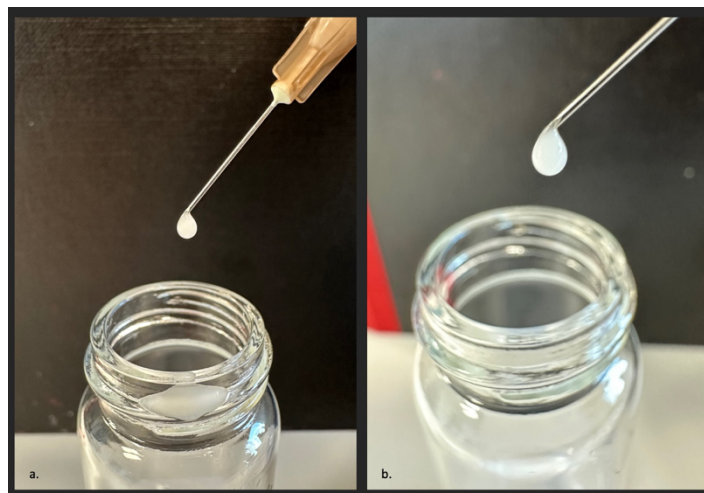
Figure 6.12: a.) emulsion stabilised 10 wt% BCS passed through a needle 25G needle b.) emulsion passed through 26G size needle.

6.4 Conclusion

The exploration of drug incorporation into thermoresponsive engineered emulsions was reported in this chapter. The emulsions were able to incorporate phenylephrine, lidocaine, and budesonide, with drug loading poorest in the poorly-soluble budesonide system. The drug release profiles of phenylephrine, lidocaine, and budesonide from the emulsions were studied using Franz diffusion cells. The drug release was significantly retarded in the emulsions compared to a reference product available on the market. Liberation from the emulsion systems occurred over several hours, opening up the possibility of sustained effects from nasal medicines. To this end, compatibility of the system with a nasal spray device was assessed. It was found that the emulsions could be sprayed and successfully atomised by these systems, with exceedingly little fine fraction. This indicates that nasal medicines developed from these systems may attenuate the fraction of inhaled dose from nasal sprays, as well as delivering emulsion to the nasal mucosa. Overall, this chapter provides valuable insights into the development and characterisation of thermoresponsive emulsions for drug delivery applications, offering potential new avenues for controlled delivery of active pharmaceutical agents through nasal routes.

6.5 References

1. Pozzoli, M. *et al.* Application of RPMI 2650 nasal cell model to a 3D printed apparatus for the testing of drug deposition and permeation of nasal products. *Eur. J. Pharm. Biopharm.* **107**, 223–233 (2016).

2. Bhise, S., Yadav, A., Avachat, A. & Malayandi, R. Bioavailability of intranasal drug delivery system. *Asian J. Pharm.* **2**, 201 (2008).

3. Ong, H. X. *et al.* Primary air-liquid interface culture of nasal epithelium for nasal drug delivery. *Mol. Pharm.* **13**, 2242–2252 (2016).

4. Illum, L. Nasal drug delivery - Possibilities, problems and solutions. *J. Control. Release* **87**, 187–198 (2003).

5. Rama Prasad, Y. V., Krishnaiah, Y. S. R. & Satyanarayana, S. Intranasal drug delivery systems: An overview. *Indian J. Pharm. Sci.* **58**, 1–8 (1996).

6. Costantino, H. R., Illum, L., Brandt, G., Johnson, P. H. & Quay, S. C. Intranasal delivery: Physicochemical and therapeutic aspects. *Int. J. Pharm.* **337**, 1–24 (2007).

7. Lee, D. & Minko, T. Nanotherapeutics for nose-to-brain drug delivery: An approach to bypass the blood brain barrier. *Pharmaceutics* **13**, (2021).

8. Kapoor, M., Cloyd, J. C. & Siegel, R. A. A review of intranasal formulations for the treatment of seizure emergencies. *J. Control. Release* **237**, 147–159 (2016).

9. Bahadur, S. & Pathak, K. Physicochemical and physiological considerations for efficient nose-to-brain targeting. *Expert Opin. Drug Deliv.* **9**, 19–31 (2012).

10. Rassu, G. *et al.* Nose-to-brain delivery of BACE1 siRNA loaded in solid lipid nanoparticles for Alzheimer's therapy. *Colloids Surfaces B Biointerfaces* **152**, 296–301 (2017).

11. Ehrick, J. D. *et al. Considerations for the Development of Nasal Dosage Forms.* (2013). doi:10.1007/978-1-4614-7978-9_5.

12. Pires, P. C., Rodrigues, M., Alves, G. & Santos, A. O. Strategies to Improve Drug Strength in Nasal Preparations for Brain Delivery of Low Aqueous Solubility Drugs. *Pharmaceutics* **14**, 1–18 (2022).

13. Saindane, N. S., Pagar, K. P. & Vavia, P. R. Nanosuspension based in situ gelling nasal spray of carvedilol: Development, in vitro and in vivo characterization. *AAPS PharmSciTech* **14**, 189–199 (2013).

14. Sau-Hung Spence Leung & Robinson, J. R. The contribution of anionic polymer structural features to mucoadhesion. *J. Control. Release* **5**, 223–231 (1987).

15. Vigani, B. *et al.* Recent advances in the development of in situ gelling drug delivery systems for non-parenteral administration routes. *Pharmaceutics* **12**, 1–29 (2020).

16. Moakes, R. J. A., Davies, S. P., Stamataki, Z. & Grover, L. M. Formulation of a Composite Nasal Spray Enabling Enhanced Surface Coverage and Prophylaxis of SARS-COV-2. *Adv. Mater.* **33**, (2021).

17. Elad, D., Wolf, M. & Keck, T. Air-conditioning in the human nasal cavity. *Respir. Physiol. Neurobiol.* **163**, 121–127 (2008).

18. Mygind, N. & Dahl, R. Anatomy, physiology and function of the nasal cavities in health and disease. *Adv. Drug Deliv. Rev.* **29**, 3–12 (1998).

19. Mayol, L., Quaglia, F., Borzacchiello, A., Ambrosio, L. & Rotonda, M. I. L. A novel poloxamers/hyaluronic acid in situ forming hydrogel for drug delivery: Rheological, mucoadhesive and in vitro release properties. *Eur. J. Pharm. Biopharm.* **70**, 199–206 (2008).

20. Wu, J., Wei, W., Wang, L. Y., Su, Z. G. & Ma, G. H. A thermosensitive hydrogel based on quaternized chitosan and poly(ethylene glycol) for nasal drug delivery system. *Biomaterials* **28**, 2220–2232 (2007).

21. Andrews, G. P., Laverty, T. P. & Jones, D. S. Mucoadhesive polymeric platforms for controlled drug delivery. *Eur. J. Pharm. Biopharm.* **71**, 505–518 (2009).

22. Madsen, F., Eberth, K. & Smart, J. D. A rheological examination of the mucoadhesive/mucus interaction: The effect of mucoadhesive type and concentration. *J. Control. Release* **50**, 167–178 (1998).

23. ICH. ICH Harmonised Guidance:Validation of Analytical Procedures Q2(R2). *ICH Harmon. Tripart. Guidel.* **2**, 1–34 (2022).

24. Harron, D. W. G. Technical Requirements for Registration of Pharmaceuticals for

Human Use: The ICH Process. *Textb. Pharm. Med.* **1994**, 447–460 (2013).

25. Recipharm. Nasal spray device manufacturer, Unidose nasal spray. https://www.recipharm.com/drug-delivery-devices/nasal-sprays.

26. Rajbanshi, A. *et al.* Polymer architecture dictates thermoreversible gelation in engineered emulsions stabilised with branched copolymer surfactants. *Polym. Chem.* **13**, 5730–5744 (2022).

27. Rajbanshi, A. *et al.* Combining branched copolymers with additives generates stable thermoresponsive emulsions with in situ gelation upon exposure to body temperature. *Int. J. Pharm.* **637**, 122892 (2023).

28. VCCLAB. Virtual Computational Chemistry Laboratory. https://vcclab.org/lab/alogps/.

29. Martindale Pharma an Ethypharm Group Company. Lidocaine Hydrochloride 5% w/v and Phenylephrine Hydrochloride 0.5% w/v Topical Solution. https://www.medicines.org.uk/emc/product/3592/smpc/print (2017).

30. Sandoz Limited. Budesonide 64 micrograms/actuation, Aqueous Nasal Spray. https://www.medicines.org.uk/emc/product/445/smpc/print (2022).

31. Sarheed, O., Dibi, M. & Ramesh, K. V. R. N. S. Studies on the effect of oil and surfactant on the formation of alginate-based O/W lidocaine nanocarriers using nanoemulsion template. *Pharmaceutics* **12**, 1–21 (2020).

32. Korsmeyer, R. W., Gurny, R., Doelker, E., Buri, P. & Peppas, N. A. Mechanisms of solute release from porous hydrophilic polymers. *Int. J. Pharm.* **15**, 25–35 (1983).

33. Calderó, G., García-Celma, M. J., Solans, C., Plaza, M. & Pons, R. Influence of composition variables on the molecular diffusion from highly concentrated water-in-oil emulsions (gel-emulsions). *Langmuir* **13**, 385–390 (1997).

34. Calderó, G., García-Celma, M. J., Solans, C. & Pons, R. Effect of pH on mandelic acid diffusion in water in oil highly concentrated emulsions (gel-emulsions). *Langmuir* **16**, 1668–1674 (2000).

35. Dewan, M. *et al.* Effect of methyl cellulose on gelation behavior and drug release from poloxamer based ophthalmic formulations. *Int. J. Biol. Macromol.* **72**, 706–

710 (2015).

36.   Babak, V. G., Stébé, M. J. & Fa, N. Physico-chemical model for molecular diffusion from highly concentrated emulsions. *Mendeleev Commun.* **13**, 254–256 (2003).

37.   Main mechanisms to control the drug release. *Strateg. to Modify Drug Release from Pharm. Syst.* 37–62 (2015) doi:10.1016/b978-0-08-100092-2.00004-7.

38.   Farina, D. J. *Regulatory Aspects of Nasal and Pulmonary Spray Drug Products*. *Handbook of Non-Invasive Drug Delivery Systems* (Vitthal S. Kulkarni, 2010). doi:10.1016/b978-0-8155-2025-2.10010-1.

39.   FDA. Nasal Spray and Inhalation Solution, Suspension, and Spray Drug Products — Chemistry, Manufacturing, and Controls. *Final* 10–15 (2002).

40.   Trows, S., Wuchner, K., Spycher, R. & Steckel, H. Analytical challenges and regulatory requirements for nasal drug products in Europe and the U.S. *Pharmaceutics* **6**, 195–219 (2014).

41.   Foo, M. Y., Cheng, Y. S., Su, W. C. & Donovan, M. D. The influence of spray properties on intranasal deposition. *J. Aerosol Med. Depos. Clear. Eff. Lung* **20**, 495–508 (2007).

42.   Gao, M., Shen, X. & Mao, S. Factors influencing drug deposition in the nasal cavity upon delivery via nasal sprays. *J. Pharm. Investig.* **50**, 251–259 (2020).

43.   Newman SP, Moren F, C. S. Deposition pattern of nasal sprays in man. *Rhinology* **26**, 111–120 (1988).

Chapter 7: Concluding remarks and future works

7.1 Conclusion

This research work explored the generation of thermoresponsive emulsions and their ability to deliver drugs via *in situ* gelling pharmaceutical formulations. Thermoresponsive branched copolymer surfactants (BCS)s had proven effectiveness in forming stable emulsions with thermoreversible gelation. Prior to this study, it had been shown that BCSs can switch low-viscosity emulsions to gels when the pH changes. This generated a concept to create thermoresponsive emulsions that change when the temperature is elevated as an alternative stimulus. The generation of materials that switch from a liquid to a gel state upon warming can enable new healthcare technologies with improved functionality, such as *in situ* gel-forming materials for drug delivery to nasal, topical or parenteral sites.[3] Da Silva et al. reported the first example of responsive emulsions stabilised with BCS that can change their properties with temperature.[4] The BCSs of Da Silva et al. were comprised of NIPAM and thermoresponsive monomer, PEGMA as hydrophilic macromonomer, EGDMA as crosslinker and DDT as a hydrophobic chain end. The research explored how these engineered emulsions respond to temperature, and how the BCS structure at both macro and nanoscale levels affects their behaviour. However, limitations from the existing study on the engineered emulsions stabilised with PNIPAM BCSs were highlighted, which included problems with the temperature and the strength of gelation. The responsive behaviour of the emulsion system can potentially be paired with a wide range of drug chemistries to enable the solubilisation of molecules. The latter study highlighted the great potential of BCSs in generating thermoresponsive emulsions for drug delivery. The aim of the current thesis was to build upon that knowledge to generate new BCS systems containing an alternative thermoresponsive component with the aim of altering gel strength and transition temperatures, as well as mitigating perceived risk of using NIPAM in BCS systems.

The research described in the previous six chapters was undertaken in order to generate smart emulsions stabilised by thermoresponsive polymers that could be applied to drug delivery. Progress has been made towards this, but further work would be required before

their full potential can be reached. Chapter 3 looked at the new class of thermoresponsive materials by the synthesis of novel BCS containing di(ethylene glycol) methyl ether methacrylate (DEGMA) as a thermoresponsive component giving a lower critical solution temperature (LCST). The BCSs were employed as emulsifiers to prepare 1:1 dodecane-in-water emulsion systems. The effect of polymer architecture proved to be intimately linked to the rheology of these systems, where branching, increase in molecular weight, and the presence of hydrophobic end groups demonstrated to be commensurate with gel formation upon heating. Mechanisms of gel formation were probed by small-angle neutron scattering, which demonstrated that the branched copolymer surfactants formed oblate ellipsoids in solution that grew anisotropically with temperature, forming larger disk-like nanoparticles. The formation of these elongated particles led to the thickening of the emulsions, whilst connectivity of the aggregates and BCS at the oil–water interface is required for gel formation to occur. However, the gelation temperature was higher than desired (ca. 48 °C). Hence, Chapter 3 provided initial design principles for a novel class of thermoresponsive material.

The aim of Chapter 4 was to expand on the systems researched in Chapter 3 by generating a second library of BCS. Chapter 4 explains the potential of PEGMA, a hydrophilic macromonomer, to control the responsive nature of the engineered emulsions. It was found that the thermoresponsive behaviour of emulsions stabilised by block copolymer surfactants (BCSs) can induce either gelation or emulsion break-up with mild temperature changes. PEGMA is crucial to control the thermoresponsive behaviour of the emulsions: longer PEG chains (950 g/mol) lead to thermogelation, whereas shorter PEG chains (500 or 300 g/mol) lead to emulsion cracking upon mild heating. Additionally, the relative abundance of PEGMA to the thermoresponsive component (DEGMA) in the BCS tightly controlled the gelation temperature of BCS-stabilised emulsions. An optimal BCS architecture (P14) with controlled PEGMA concentration and chain length (as shown in Figure 7.1), was found to form emulsions that transition from a liquid to gel state when warmed above 32 °C. This makes the system ideal for *in situ* gelation upon contact with the body, which would have significant potential in healthcare applications.
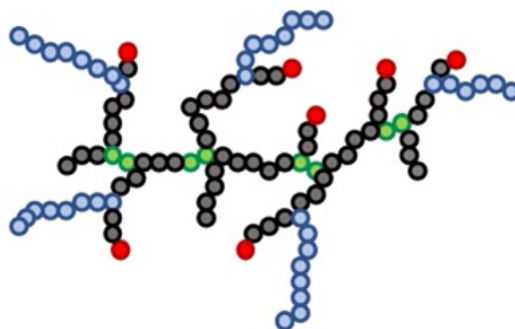
Figure 7.1: Schematic representation of the chemical structure of P14 BCS synthesised with 174 mmol DEGMA (in black), 3 mmol PEGMA-950 (in blue), 12 mmol EGDMA (in green) and 12 mmol DDT (in red).

The expansion of the previously evaluated systems to form pharmaceutically-relevant emulsions was then explored. To transition towards this application, Chapter 5 described the evaluation of a range of pharmaceutically relevant oils in the BCS system as well as evaluation of surfactants and polymeric/oligomeric additives to enhance stability. The effect of the addition of methylcellulose as an optimal additive was particularly pronounced, eliminating emulsion creaming and enhancing the temperature range (32 – 40 °C, solid-like behaviour with G'>G") over which the gel state was stable. The nanoscale processes occurring in the BCS-stabilised emulsions was probed by SANS and TEM to better comprehend the system. This system was then selected to explore in nasal drug delivery.

The principles for the design of the advanced thermoresponsive emulsion were identified in Chapter 4 and 5 and identified an optimal system for further investigation as dosage forms. Finally, in Chapter 6, BCS-stabilised emulsions were investigated as pharmaceutical formulations for their potential to incorporate drugs based on their varying solubility and partition coefficient and to understand the drug release mechanisms. Rheological analysis of drug loaded emulsions demonstrated distinctive thermoresponsive behaviour, with lidocaine eliminating the thermogelation process, highlighting the need to carefully match drug with the emulsion system to ensure performance. Emulsions stabilised by BCS showed sustained drug release profiles compared to marketed reference products for nasal administration, with BCS/MC emulsions exhibiting even slower drug release rates.

The formulations were also evaluated for compatibility with a nasal spray device. This pilot study demonstrated successful spray and atomisation of the emulsions, and various regulatory endpoints were explored to inform future emulsion design. Despite not fully meeting all analytical criteria, the thermoresponsive engineered emulsions exhibited potential for further development and optimisation toward effective nasal spray formulations. Particularly typical dose consistency was good (< 10 % RSC) and plume angles appropriate for delivery to the turbinate region of the nasal mucosa.

The work undertaken in this thesis opens new horizons in drug delivery through temperature-responsive emulsions, offering "smart" dosage forms. These innovative systems have the potential to transform treatment modalities, enhance patient outcomes, and reduce dosing frequency. The research significantly advances understanding in the field of thermoresponsive engineered emulsions, particularly outlining design principles linking polymer architecture to function. Future studies can explore diverse drug molecules to identify suitable chemistries for emulsions to function, optimise device incorporation to meet regulatory criteria, and explore *in vivo* evaluation to bridge the gap between benchtop findings and clinical applications. This project paves the way for the development of novel therapeutic strategies in personalised medicine and targeted drug delivery.

7.2 Future directions in optimising thermoresponsive emulsions for topical and nasal drug delivery

The research conducted in this thesis has provided valuable insights into the design and generation of thermoresponsive emulsions for drug delivery, with a specific focus on their potential application as topical or nasal sprays. While significant progress has been made in understanding the behaviour and properties of these emulsions, several avenues for further optimisation and exploration could lead to more effective and versatile drug delivery systems.

7.2.1 Fine-tuning thermoresponsive BCS architecture

One of the key findings of this research is the critical role of copolymer architecture in determining the behaviour of thermoresponsive emulsions. Further investigations could involve a systematic exploration of different BCS compositions and architectures to achieve precise control over gelation temperatures with enhanced mechanical strength of gelation, and drug loading capacities. The experimental design in this thesis is such that optimisation has occurred one-variable-at-a-time around a central point (P1), but more effective optimal materials may exist. The impact of varying molecular weights, hydrophilic-to-hydrophobic ratios, and other structural parameters on emulsion stability and thermoresponsive behaviour could be thoroughly studied to identify optimal copolymer configurations. Statistical designs such as design-of-experiments optimisations could be an efficient method to approach this problem.

Machine learning techniques offer a promising avenue to accelerate the BCS optimisation process, predicting optimal materials for the generation of low-viscosity emulsions with enhanced retention. With a trained and validated machine learning model, optimal polymer attributes, such as composition, molecular weight, and architecture, could be predicted that will result in the desired emulsion viscosity. By predicting the optimal BCS system, machine learning can significantly accelerate the process of formulation development with enhanced retention, reducing the number of laboratory experiments, time and cost. This integration of machine learning into pharmaceutical formulation development holds great promise for improving drug delivery systems.

7.2.2 Enhanced drug loading and release profiles

While the current research has demonstrated the potential of thermoresponsive emulsions for drug delivery, there is room for improvement in terms of drug loading capacity and release profiles where initial formulations were designed to match reference products and parameters outside this remain unexplored. Future work could focus on optimising the formulation parameters to achieve high drug loading efficiencies while maintaining controlled release kinetics. Exploring various drug molecules with different solubilities and partitioning coefficients could help uncover the full potential of these

emulsions in accommodating a wide range of drug molecules. Understanding the chemistry of drugs which leads to thermally induced breaking of the emulsion (seen for Lidocaine) is essential in this respect. The emulsions also have the potential to co-incorporate incompatible drugs through inclusion in separate phases or droplets.

7.2.3 Formulation stability and compatibility

The stability of the emulsions during storage and upon application is of paramount importance for pharmaceutical applications. Investigating methods to enhance the long-term stability of these emulsions, including preventing phase separation and maintaining consistent thermoresponsive behaviour over time, could be a significant area of research. Moreover, evaluating the compatibility of these emulsions with different drug compounds, as well as the influence of excipients and additives, will contribute to the development of robust and reliable drug delivery formulations. Considering the thermal gelation observed in the emulsion systems, it is expected that long-term stability studies at room temperature will be required and that accelerated storage conditions are unlikely to be predictive of long-term behaviour.

7.2.4 Device incorporation and administration

For topical and nasal drug delivery applications, the design and optimisation of suitable administration devices are crucial. Future studies could explore the integration of these thermoresponsive emulsions into nasal spray devices, taking into consideration factors such as emulsion viscosity, spray pattern, droplet size distribution, and ease of administration. To address the challenge of spraying viscous liquids, optimisation of the emulsion's viscosity is crucial. Formulation adjustments involving BCS architecture, concentration, and molecular weight can influence viscosity. Balancing viscosity to ensure it is sprayable yet not too thin can be achieved by fine-tuning the polymer composition and concentration. Moreover, rheological properties play a pivotal role in the success of emulsion-based sprays. While achieving a suitable viscosity is essential for spraying, it is equally important to balance viscosity with ease of administration. Thixotropic behaviour, where the emulsion becomes less viscous upon shear stress (spraying) and regains

viscosity when at rest (on the nasal mucosa), can enhance 'sprayability' and contact time. Incorporating additives that promote thixotropy, such as structuring agents, can be explored.

The compatibility of the emulsion formulations with different device materials and their impact on drug delivery efficiency could also be investigated. Optimising the spray nozzle design and mechanism to accommodate viscous emulsions is essential. Nozzle geometry, actuation pressure, and spray pattern could be adjusted to ensure efficient atomisation of the emulsion.

7.2.5 Enhancing nasal retention

Nasal retention of sprayed emulsions is influenced by multiple factors, including formulation development, administration technique, and mucociliary clearance. Incorporating mucoadhesive agents into the emulsion formulation can enhance contact with the nasal mucosa and extend retention time. Polymers with mucoadhesive properties, such as chitosan or hyaluronic acid, can be added to the emulsion to increase adhesion to nasal tissues. Emulsion droplet size also plays an important role in nasal retention. Smaller droplets can penetrate deeper into the nasal passages and adhere better to mucosal surfaces. Achieving a controlled and consistent droplet size distribution through formulation adjustments and optimised spraying techniques can improve retention. Moreover, designing emulsions with the ability to penetrate the nasal mucus layer can improve retention. There are existing *ex vivo* methods to achieve this, such as flow-through systems.

7.2.6 *In vivo* evaluation and clinical translation

While the research conducted in this thesis has laid the foundation for understanding the potential of thermoresponsive emulsions, further steps are needed to bridge the gap between laboratory findings and clinical applications. *In vivo* studies to assess the safety, efficacy, and pharmacokinetics of these emulsions in relevant animal models, once paired with an API, could provide valuable data for their potential translation to human use. Additionally, investigating the local and systemic effects of these emulsions upon

administration could help determine their suitability for different therapeutic applications. *In vivo* data is also likely to give the most accurate predictor of retention.

In conclusion, the research conducted in this thesis has opened new horizons in drug delivery through temperature-responsive emulsions. The findings highlight the potential of these innovative systems to transform treatment modalities and enhance patient outcomes. However, there are still various challenges to overcome and opportunities to fully capture the capabilities of thermoresponsive emulsions for topical and nasal drug delivery. The proposed future directions offer a roadmap for further optimising these emulsions and advancing their translation into practical pharmaceutical applications.

7.3 References

1. Weaver, J. V. M., Rannard, S. P. & Cooper, A. I. Polymer-mediated hierarchical and reversible emulsion droplet assembly. *Angew. Chemie - Int. Ed.* **48**, 2131–2134 (2009).

2. Woodward, R. T. *et al.* Reversible aggregation of responsive polymer-stabilized colloids and the pH-dependent formation of porous scaffolds. *Soft Matter* **7**, 7560–7566 (2011).

3. Cook, M. T., Haddow, P., Kirton, S. B. & McAuley, W. J. Polymers Exhibiting Lower Critical Solution Temperatures as a Route to Thermoreversible Gelators for Healthcare. *Adv. Funct. Mater.* **31**, (2021).

4. da Silva, M. A. *et al.* Engineering Thermoresponsive Emulsions with Branched Copolymer Surfactants. *Macromol. Mater. Eng.* **307**, 1–14 (2022).

Appendix

Table A1: BCS characterisation by GPC

Study	Sample	Mn (g/mol)	Mw (g/mol)	Đ
Effect of PEGMA chain length	P10	9802	23920	2.4
	P11	9125	23746	2.6
	P12	8657	24254	2.8
Effect of PEGMA molar feed	P13	9071	25026	2.8
	P14	8959	22487	2.5
	P15	9073	25727	2.8

Table A2: Parameters from fitting of P11 solutions and emulsions to the ellipsoidal form factor. Equatorial/polar ratio has been calculated.

Temperature (°C)	P11, 20 wt% solution				P11, 10 wt% emulsion			
	Polar radius (Å)	Equatorial Radius (Å)	Equatorial radius/polar radius	SLD (x 10^{-6} A^{-2})	Polar radius (Å)	Equatorial Radius (Å)	Equatorial radius/polar radius	SLD (x 10^{-6} A^{-2})
15	32.15	32.15	1.00	2.87	30.05	30.05	1.30	2.78
25	22.45	97.58	4.34	2.50	24.317	264.79	10.89	3.45

Table A3: Parameters from fitting of P12 solutions and emulsions to the ellipsoidal form factor. Equatorial/polar ratio has been calculated.

Temperature (°C)	P12, 20 wt% solution				P12, 10 wt% emulsion			
	Polar radius (Å)	Equatorial Radius (Å)	Equatorial radius/polar radius	SLD (x 10^{-6} A^{-2})	Polar radius (Å)	Equatorial Radius (Å)	Equatorial radius/polar radius	SLD (x 10^{-6} A^{-2})
15	18.33	62.54	3.41	3.91	18.02	79.2	4.40	2.67

Table A4: Parameters from fitting of P13-P15 solutions to ellipsoidal form factor. Equatorial/polar ratio has been calculated.

Temperature (°C)	P13, 20 wt% solution				P14, 20 wt% solution				P15, 20 wt% solution			
	Polar radius (Å)	Equatorial Radius (Å)	Equatorial radius/polar radius	SLD (x 10^{-6} A^{-2})	Polar radius (Å)	Equatorial Radius (Å)	Equatorial radius/polar radius	SLD (x 10^{-6} A^{-2})	Polar radius (Å)	Equatorial Radius (Å)	Equatorial radius/polar radius	SLD (x 10^{-6} A^{-2})
25	28.73	64.22	2.24	3.22	34.13	121.92	3.57	4.81	33.17	113.2	3.41	2.77
35	63.04	206.92	3.28	2.27	87.09	541.46	6.22	3.24	86.08	487.72	5.67	2.93
45	65.54	346.27	5.28	2.04	87.23	972.02	11.14	2.82		-		

Table A5: Parameters from fitting of P13-15 solutions to hard sphere (P13) or sticky hard sphere (P14-15).

Temperature (°C)	P13, 20 wt% solution			P14, 20 wt% solution			P15, 20 wt% solution		
	Vol. Fraction	Perturbation	Stickiness	Vol. Fraction	Perturbation	Stickiness	Vol. Fraction	Perturbation	Stickiness
25									
35	0.15			0.36	0.05	2.06E+09	0.30	0.1	2.33E+10
45	0.15			0.2	0.05	0.73			

Table A6: Fitting parameters for the "sticky hard sphere" structure factor.

Temperature (°C)	BCS 20 wt% Solution			BCS 10 wt% Emulsion			BCS 20 wt% + MC 0.25 wt% Solution			BCS 10 wt% + MC 0.25 wt% Emulsion		
	Vol. Fraction	Perturbation	Stickiness	Vol. Fraction	Perturbation	Stickiness	Vol. Fraction	Perturbation	Stickiness	Vol. Fraction	Perturbation	Stickiness
25	-	-	-	-	-	-	-	-	-	-	-	-
35	0.36	0.05	2.06E+09	0.33	0.1	1.38	0.33	0.05	9.49E+10	0.33	0.1	1.38
45	0.2	0.05	0.72837	0.2	0.05	3.6	0.2	0.05	3.6331	0.16854	0.05	1.79E+07

Table A7: Phenylephrine

Time (h)	Emulsion with BCS vs Emulsion with BCS/MC		Reference vs Emulsion with BCS		Reference vs Emulsion with BCS/MC	
	P value	Summary	P value	Summary	P value	Summary
0	P > 0.05	ns	P > 0.05	ns	P > 0.05	ns
0.25	P < 0.05	*	P<0.001	***	P<0.001	***
0.5	P<0.001	***	P<0.001	***	P<0.001	***
1	P<0.001	***	P<0.001	***	P<0.001	***
3	P<0.001	***	P<0.001	***	P<0.001	***
6	P<0.001	***	P<0.001	***	P<0.001	***
9	P<0.001	***	P<0.001	***	P<0.001	***
12	P<0.001	***	P<0.001	***	P<0.001	***
24	P<0.001	***	P<0.001	***	P<0.001	***

Table A8: Lidocaine

Time (h)	Emulsion with BCS vs Emulsion with BCS/MC		Reference vs Emulsion with BCS		Reference vs Emulsion with BCS/MC	
	P value	Summary	P value	Summary	P value	Summary
0	P > 0.05	ns	P > 0.05	ns	P > 0.05	ns
0.25	P > 0.05	ns	P<0.001	***	P<0.001	***
0.5	P<0.01	**	P<0.001	***	P<0.001	***
1	P<0.001	***	P<0.001	***	P<0.001	***
3	P<0.001	***	P<0.001	***	P<0.001	***
6	P<0.001	***	P<0.001	***	P<0.001	***
9	P<0.001	***	P<0.001	***	P<0.001	***
12	P<0.001	***	P<0.001	***	P<0.001	***
24	P<0.001	***	P<0.001	***	P<0.001	***

Table A9: Budesonide

Time (h)	Emulsion with BCS vs Emulsion with BCS/MC		Reference vs Emulsion with BCS		Reference vs Emulsion with BCS/MC	
	P value	Summary	P value	Summary	P value	Summary
0	P > 0.05	ns	P > 0.05	ns	P > 0.05	ns
0.25	P > 0.05	ns	P<0.001	***	P<0.001	***
0.5	P > 0.05	ns	P<0.001	***	P<0.001	***
1	P < 0.05	*	P<0.001	***	P<0.001	***
3	P<0.001	***	P<0.001	***	P<0.001	***
6	P<0.001	***	P<0.001	***	P<0.001	***
9	P<0.001	***	P<0.001	***	P<0.001	***
12	P<0.001	***	P<0.001	***	P<0.001	***
24	P<0.001	***	P<0.001	***	P<0.001	***

Table A10: Drug comparison

Time (h)	Phenylephrine vs Lidocaine		Phenylephrine vs Budesonide		Lidocaine vs Budesonide	
	P value	Summary	P value	Summary	P value	Summary
0	P > 0.05	ns	P > 0.05	ns	P > 0.05	ns
0.25	P<0.001	***	P<0.001	***	P > 0.05	ns
0.5	P<0.01	**	P<0.001	***	P<0.001	***
1	P<0.001	***	P<0.001	***	P<0.001	***
3	P<0.001	***	P<0.001	***	P<0.001	***
6	P<0.001	***	P<0.001	***	P<0.001	***
9	P<0.001	***	P<0.001	***	P<0.001	***
12	P<0.001	***	P<0.001	***	P<0.001	***
24	P<0.001	***	P<0.001	***	P<0.001	***

Figure A1: ^{1}H NMR spectrum of P1 with annotation.
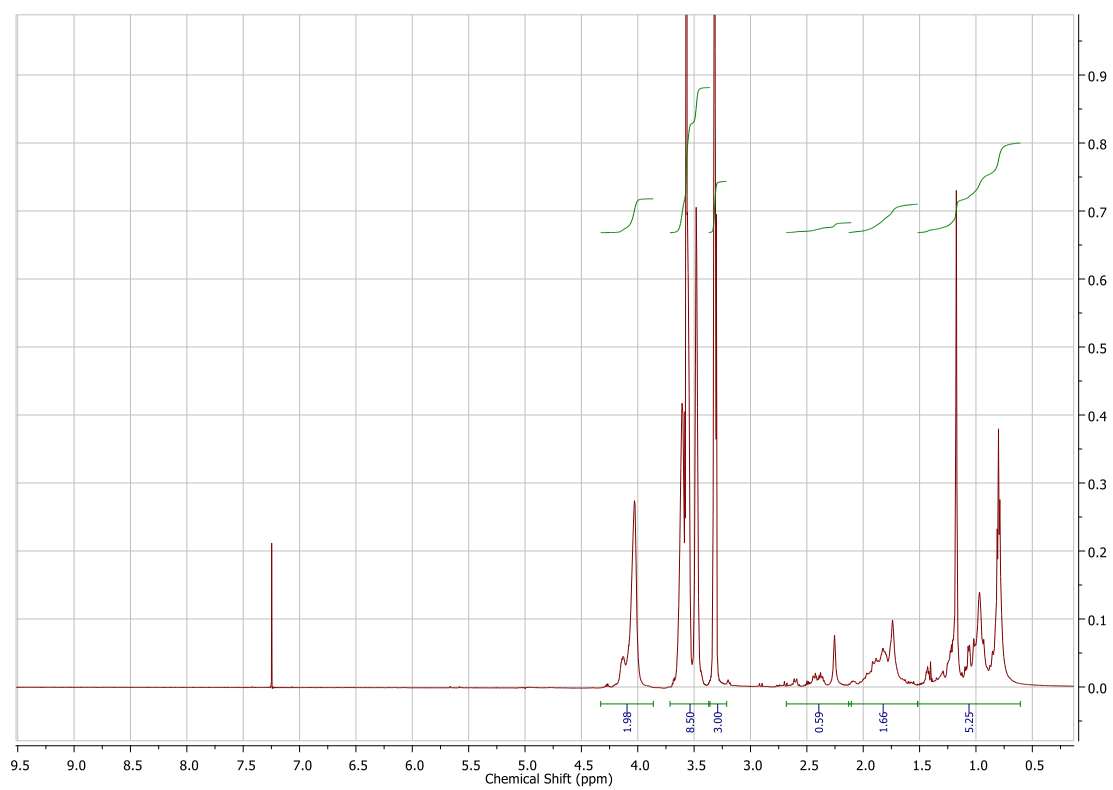
Figure A2: ^{1}H NMR spectrum of P2

216
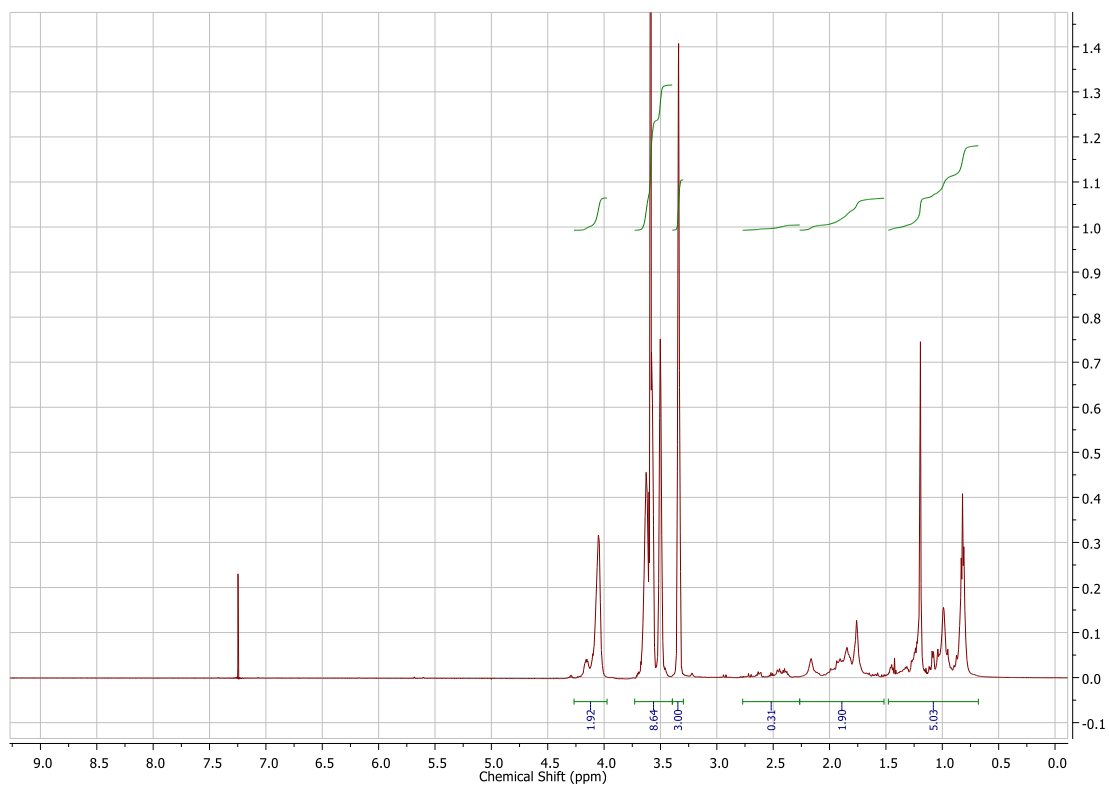
Figure A3: ^{1}H NMR spectrum of P3
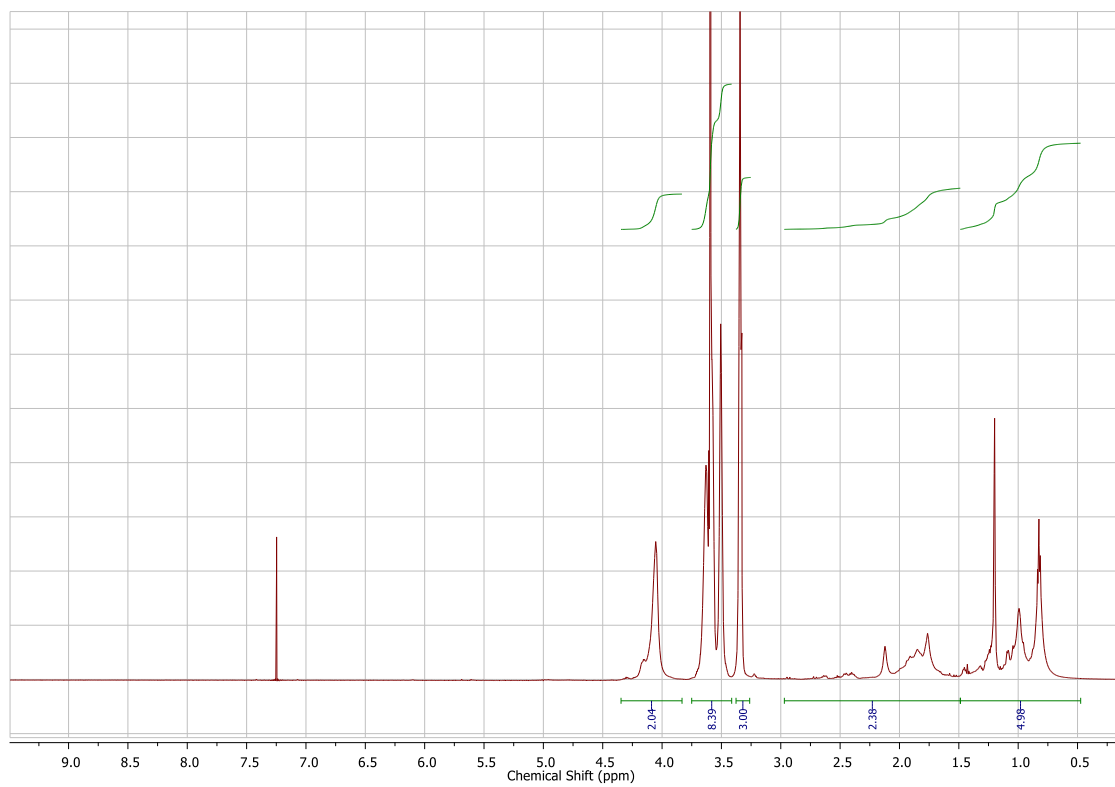
Figure A4: ^{1}H NMR spectrum of P4
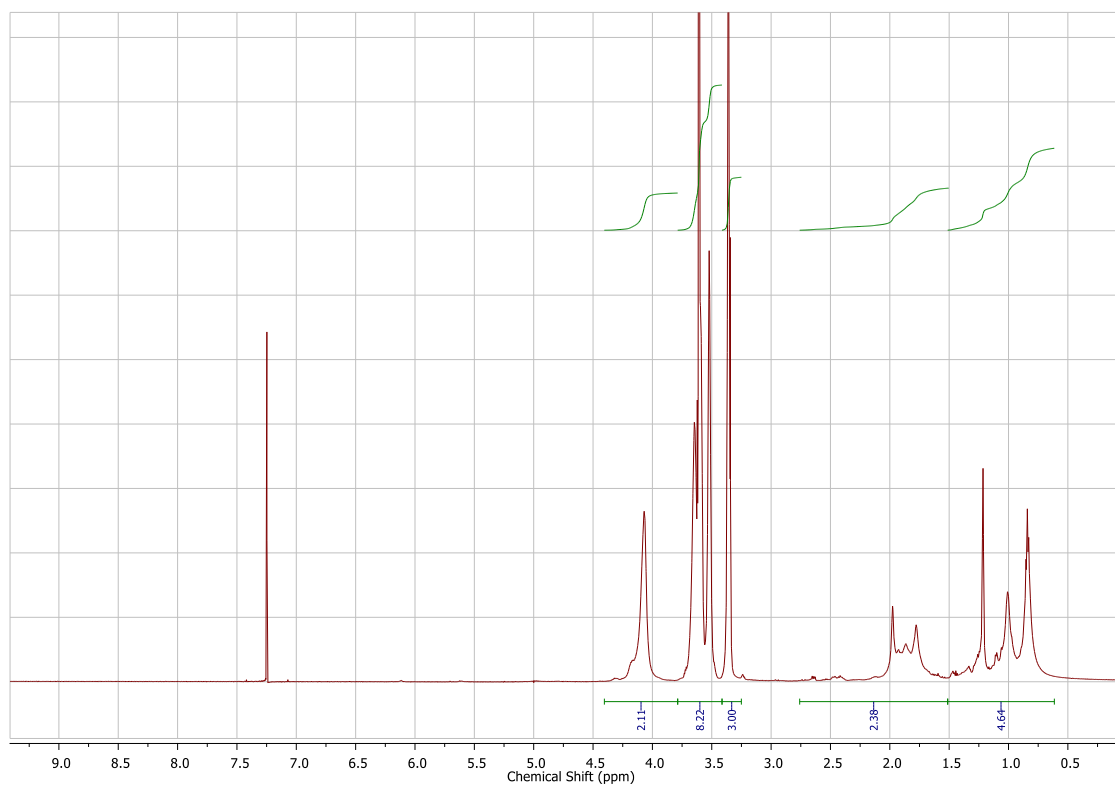
Figure A5: ^{1}H NMR spectrum of P5
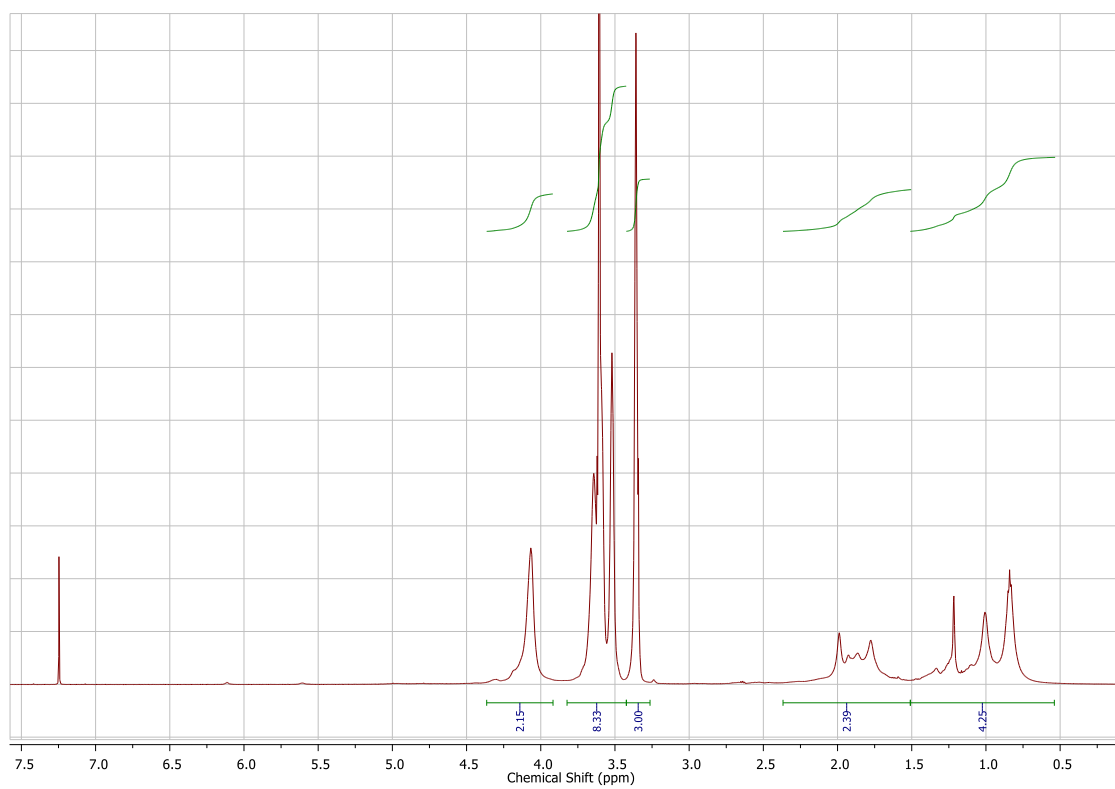
Figure A6: ^{1}H NMR spectrum of P6
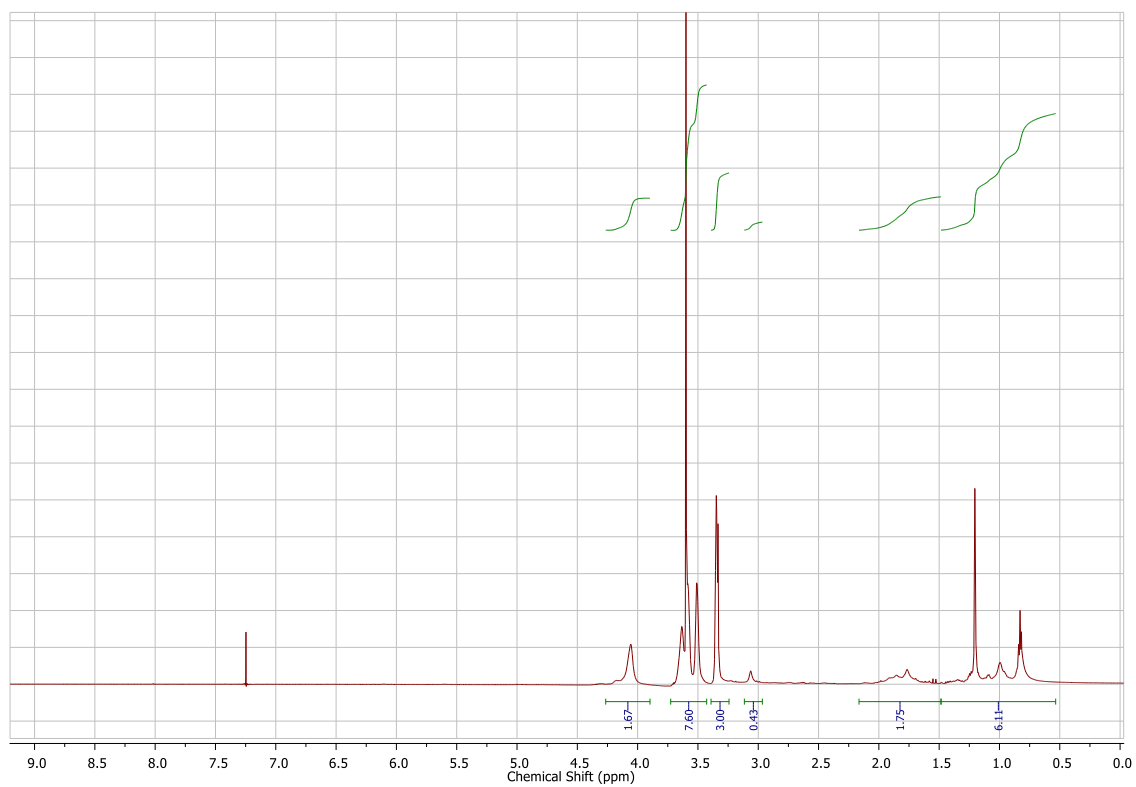
Figure A7: ^{1}H NMR spectrum of P7
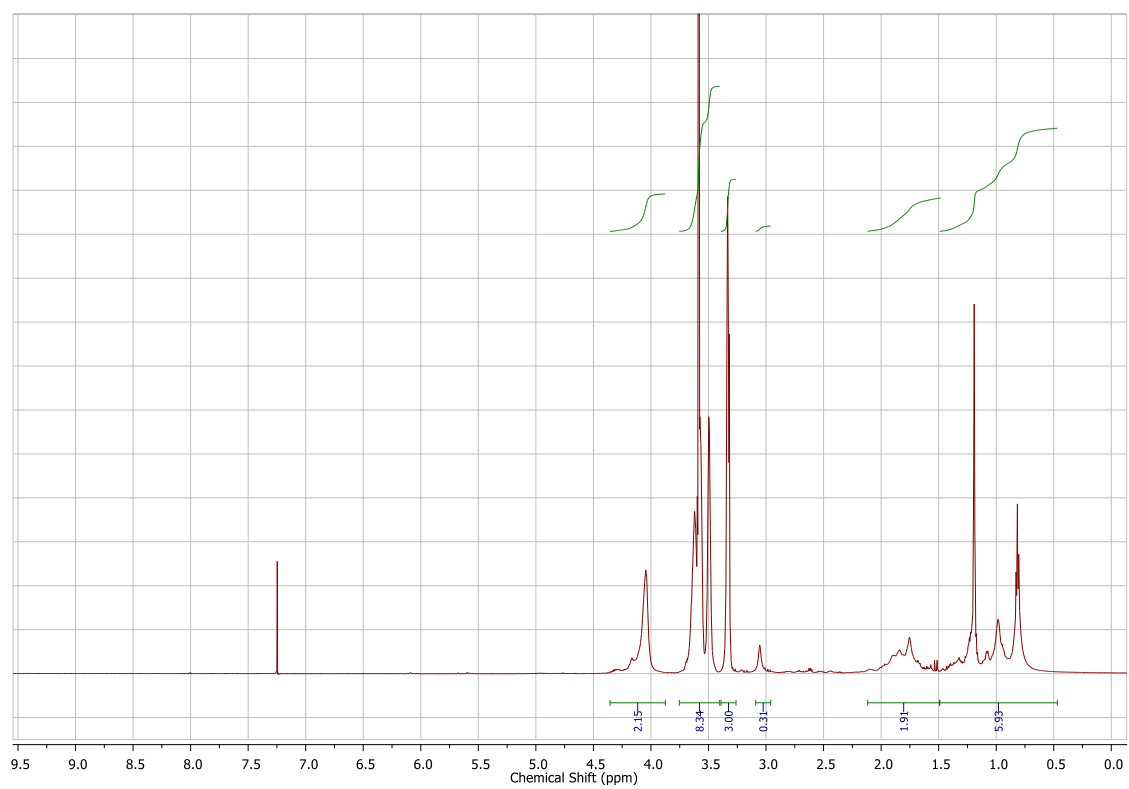
Figure A8: ^{1}H NMR spectrum of P8
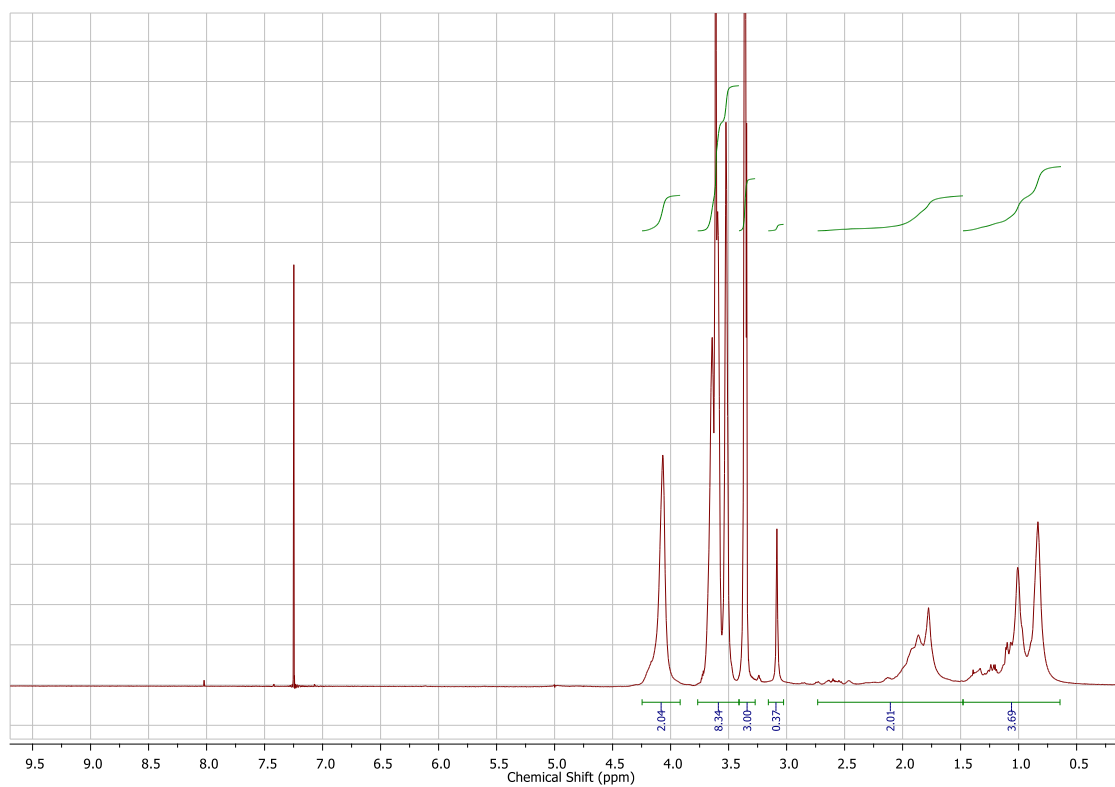
Figure A9: ^{1}H NMR spectrum of P9
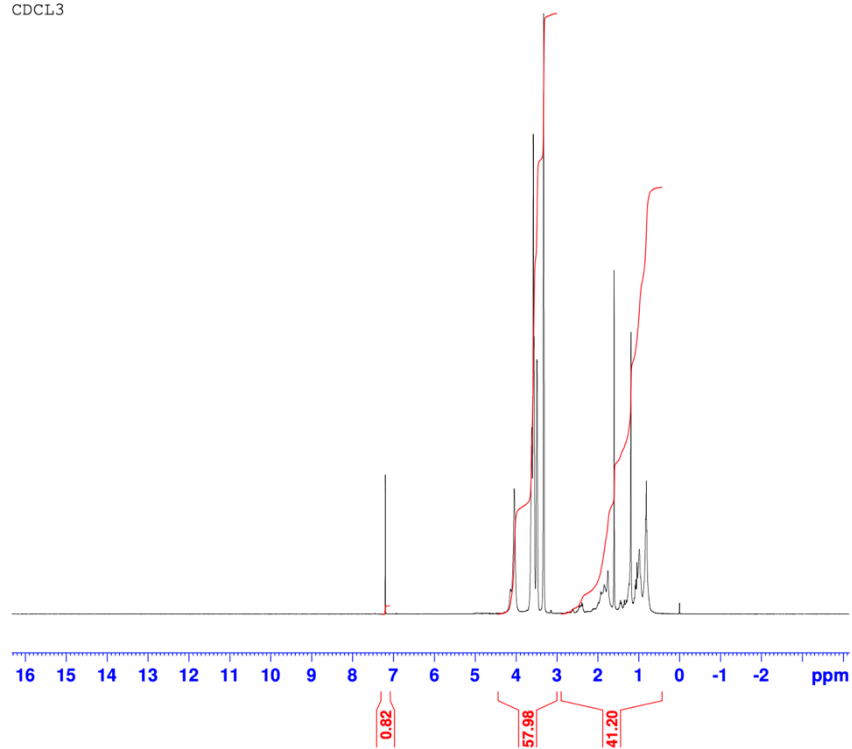
Figure A10: ^{1}H NMR spectrum of P11

16 15 14 13 12 11 10 9 8 7 6 5 4 3 2 1 0 -1 -2 ppm

0.77   58.16   41.07
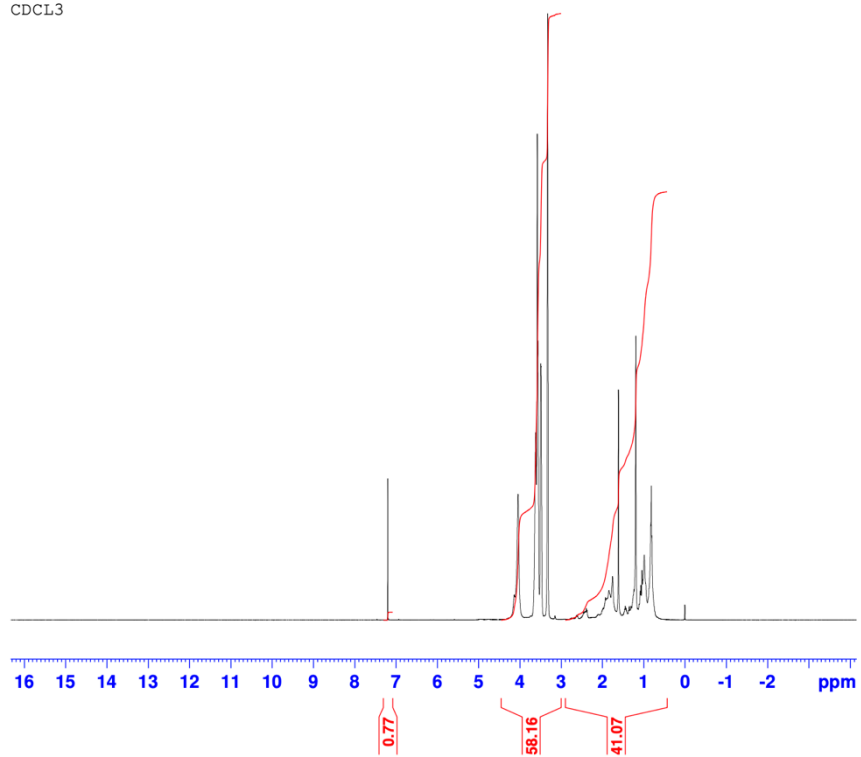
Figure A11: ^{1}H NMR spectrum of P12

16 15 14 13 12 11 10 9 8 7 6 5 4 3 2 1 0 -1 -2 ppm

1.08   57.98   40.94
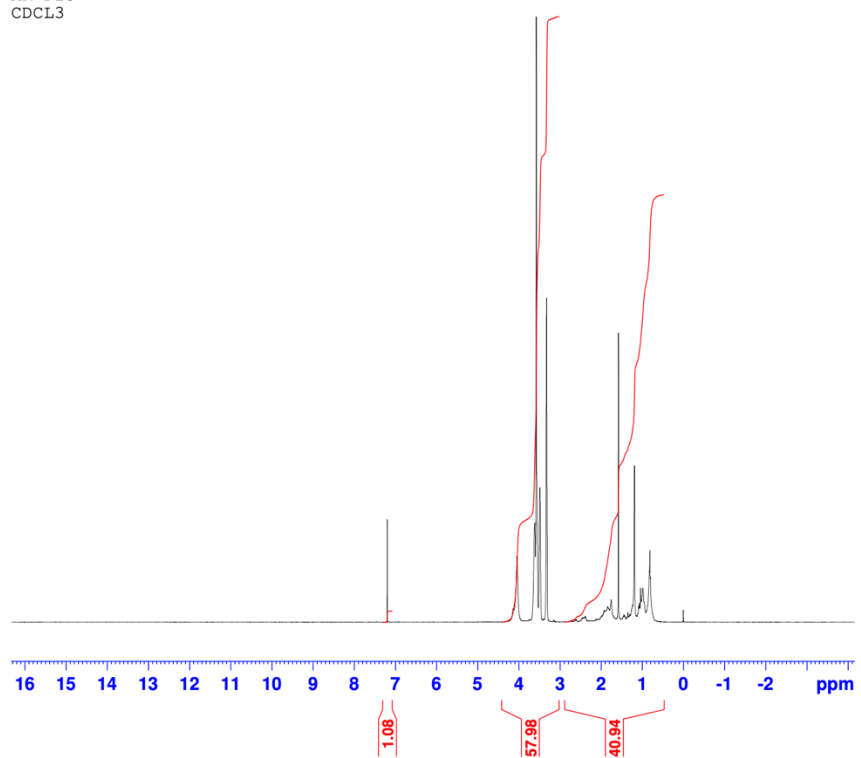
Figure A12: ^{1}H NMR spectrum of P13
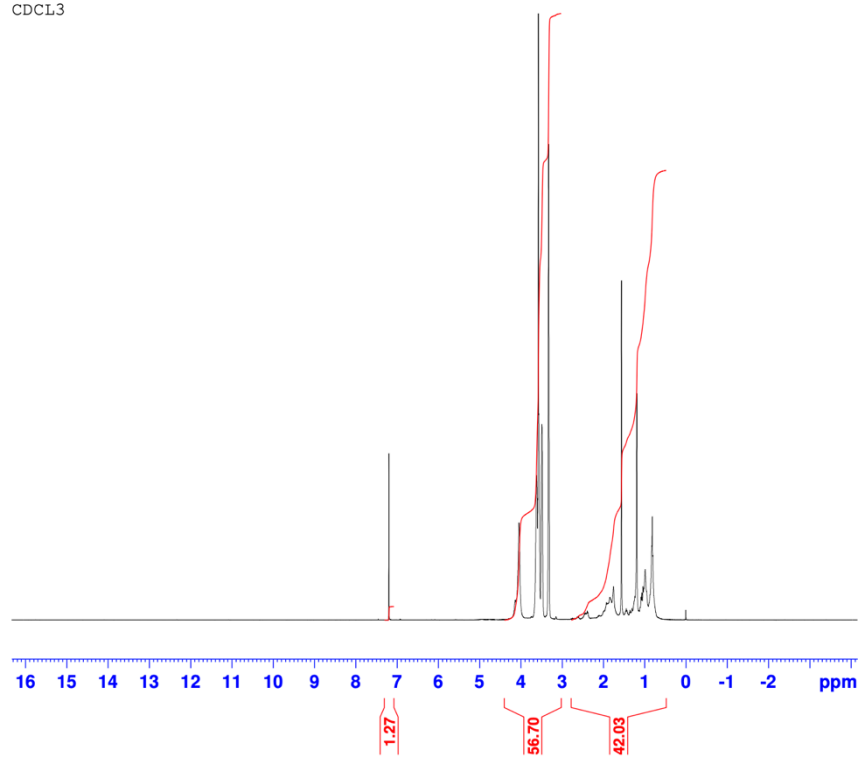
Figure A13: ^{1}H NMR spectrum of P14
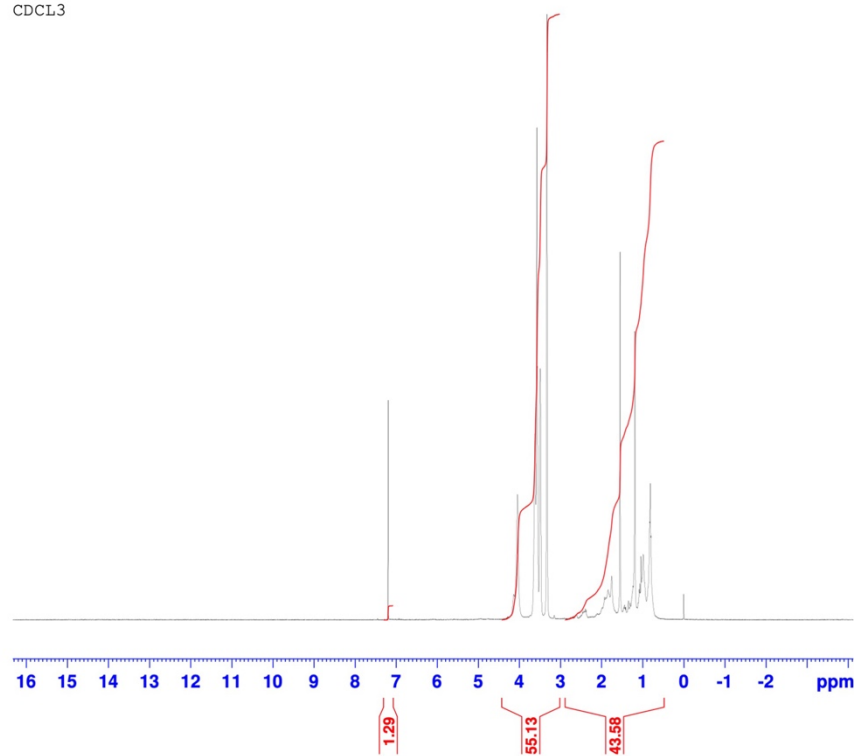
Figure A14: ^{1}H NMR spectrum of P15
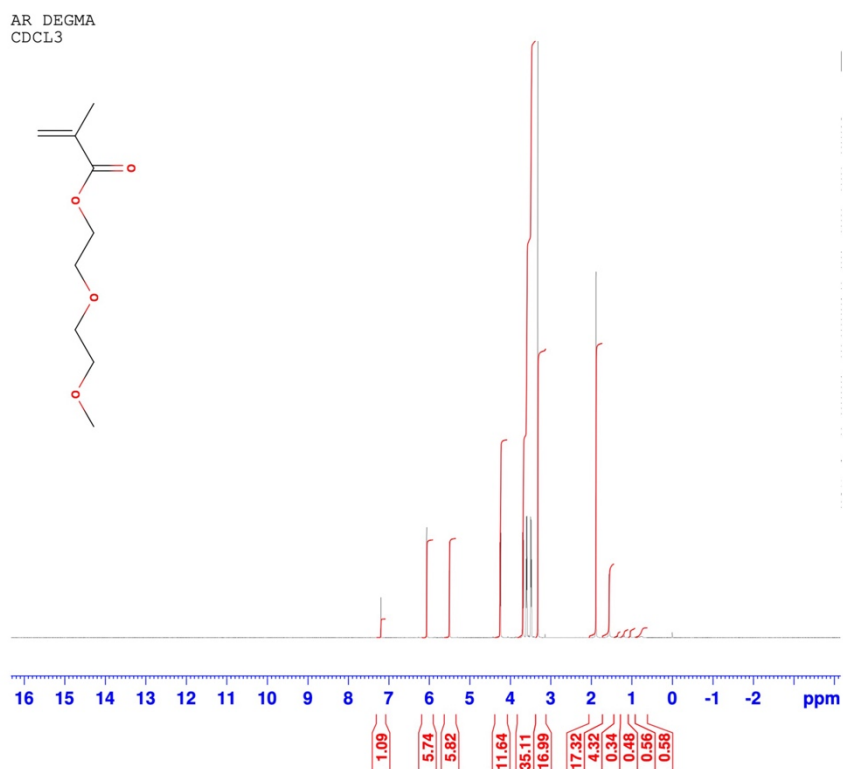
Figure A15: ^{1}H NMR spectrum of DEGMA
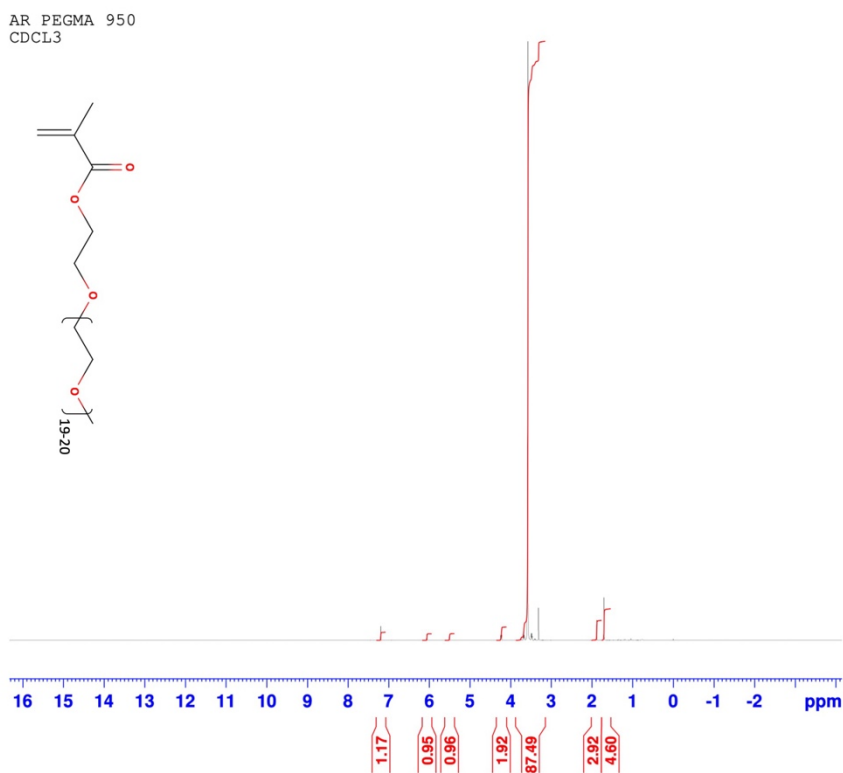
Figure A16: ^{1}H NMR spectrum of PEGMA
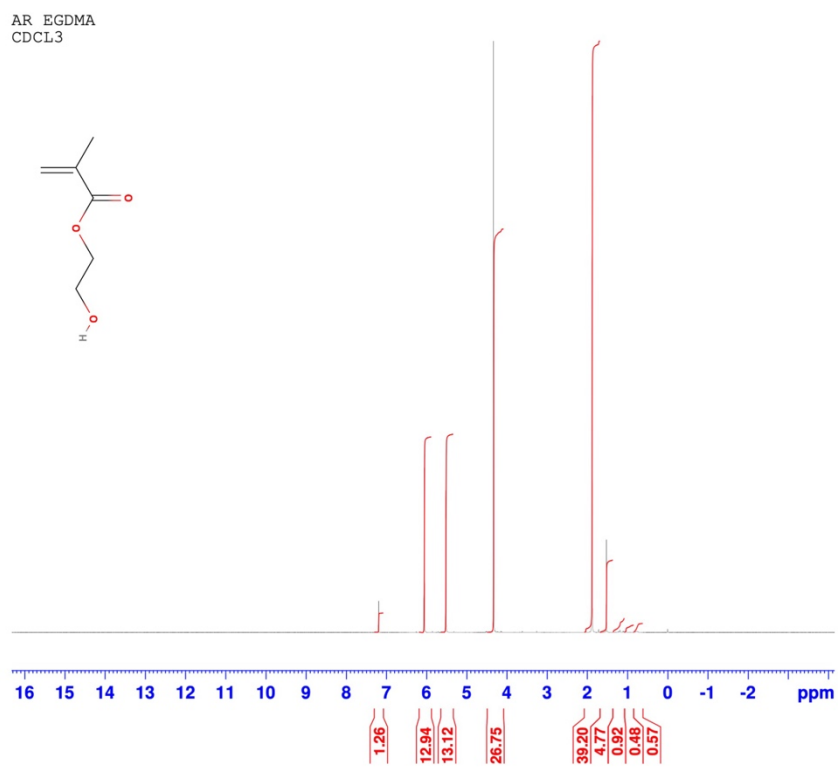
Figure A17: ¹H NMR spectrum of EGDMA
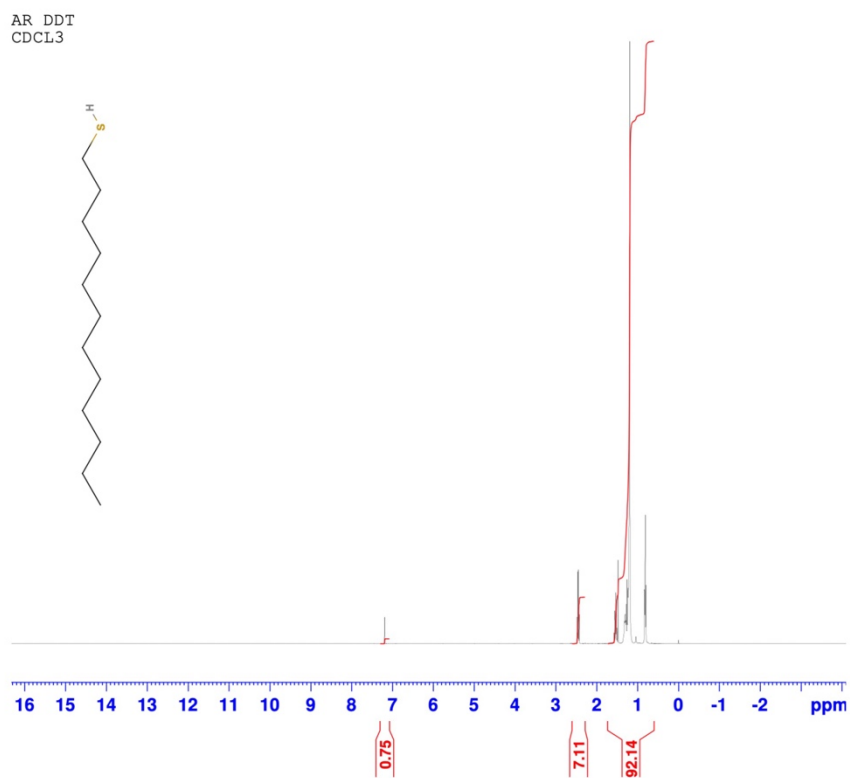
Figure A18: ¹H NMR spectrum of DDT
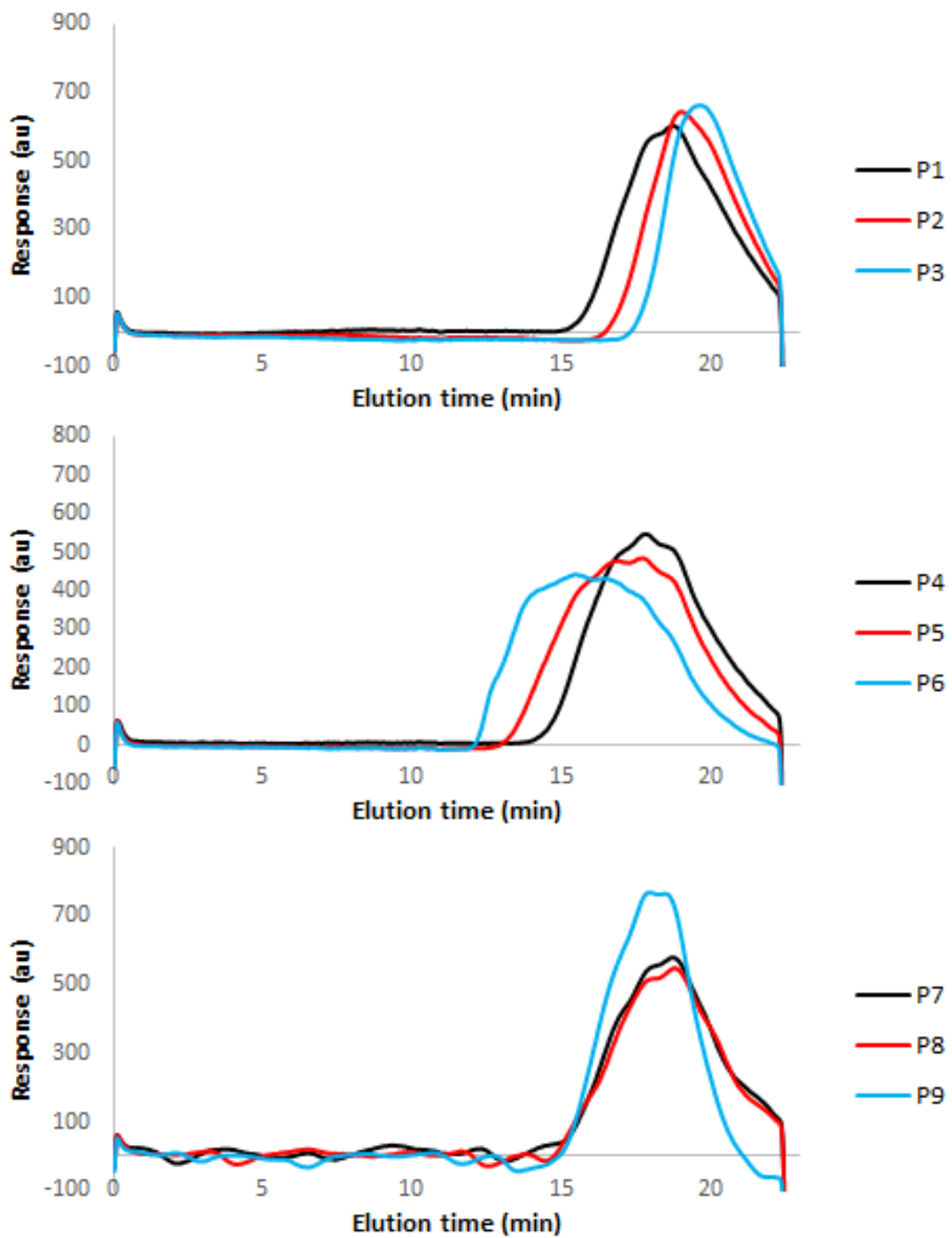
Figure A19: GPC chromatograms for P1-9.
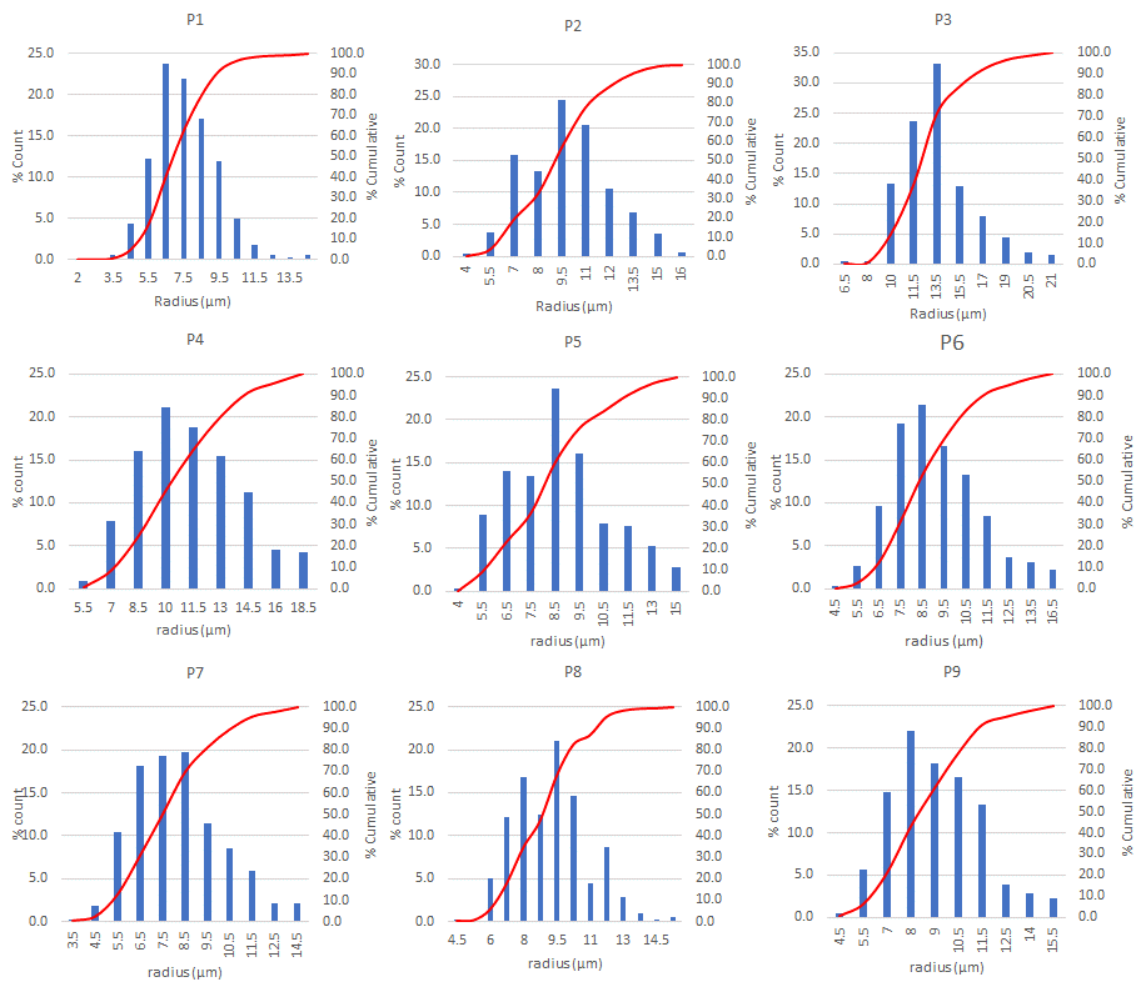
Figure A20: Emulsion droplet size distributions measured by light microscopy at 10 wt% BCS concentration. % counts are shown in blue, with cumulative data in red.
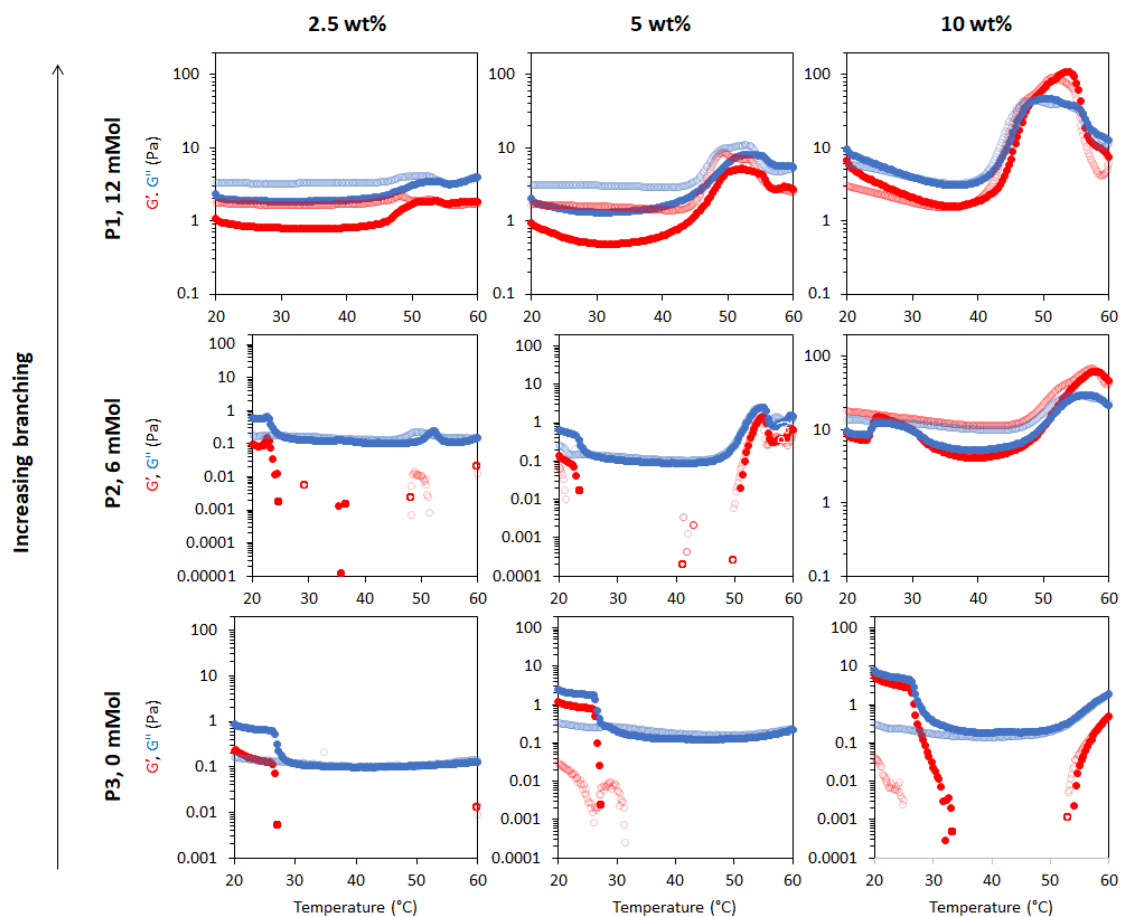
Figure A21: Rheological behaviour of emulsions stabilised by thermoresponsive BCSs, where P1 is the sample with "full cross-linker", P2 is with "half cross-linker" and P3 has no cross-linker. Emulsions were tested at 2.5, 5 and 10 wt% polymer concentration. G' is shown in red and G" is shown in blue. Dark colours show the 'up' heating ramp whilst light colours show the subsequent 'down' cooling ramp.
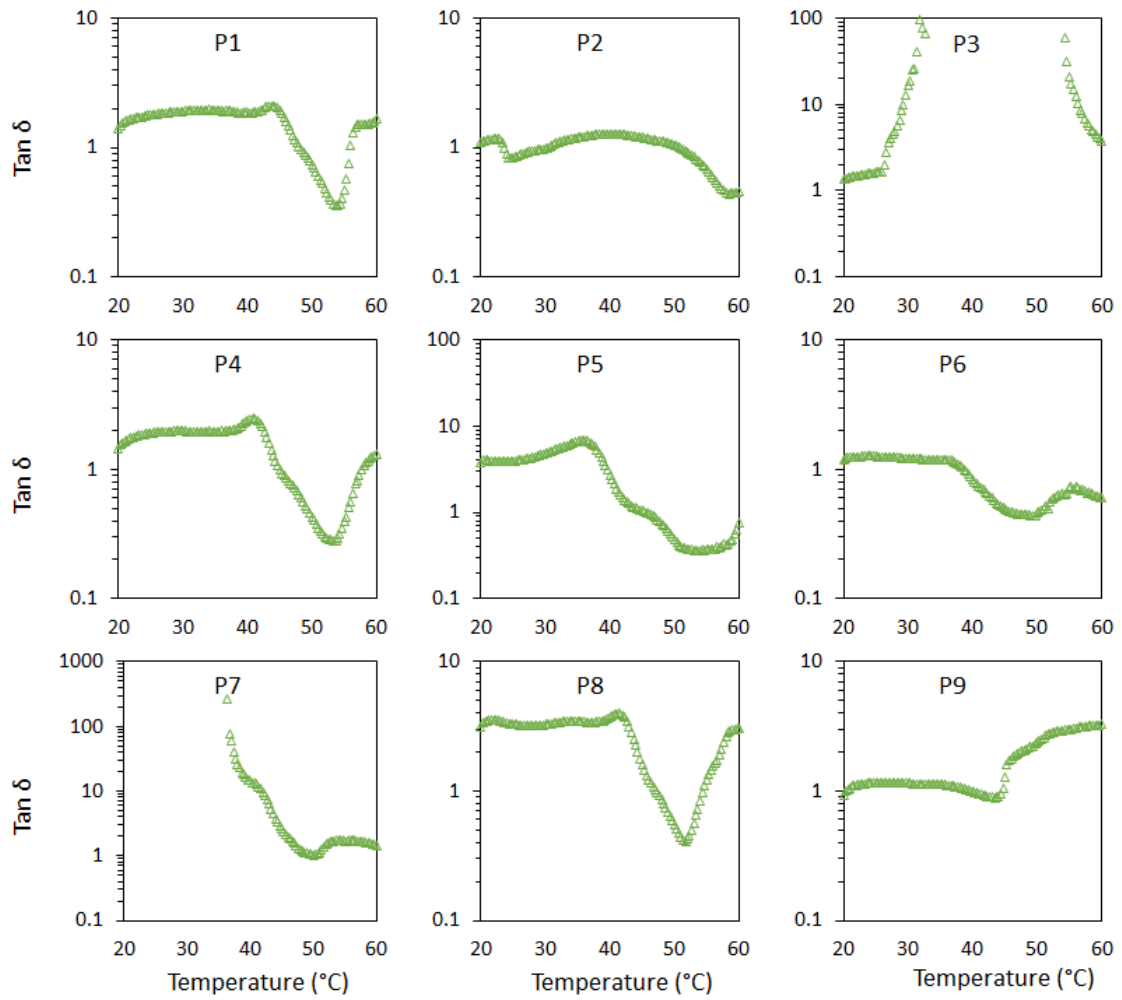
Figure A22: Evolution of tan δ with temperature for emulsions stabilised with 10 wt% BCS P1-P9.
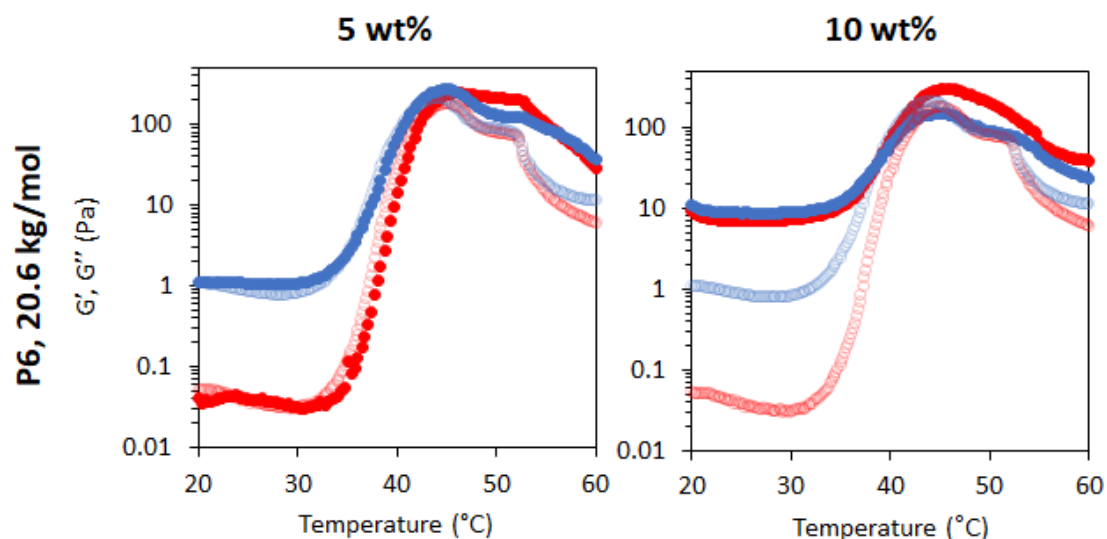
Figure A23: Rheological thermoscans for P6 emulsions at 5 and 10 wt %. G′ is shown in red and G″ is shown in blue. Dark colours show the 'up' heating ramp whilst light colours show the subsequent 'down' cooling ramp.
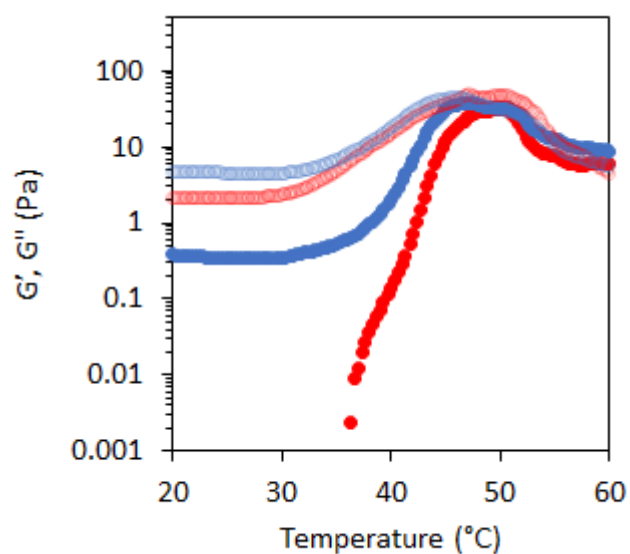
Figure A24: Rheological thermoscans for P7 emulsion at 10 wt %. G′ is shown in red and G″ is shown in blue. Dark colours show the 'up' heating ramp whilst light colours show the subsequent 'down' cooling ramp.
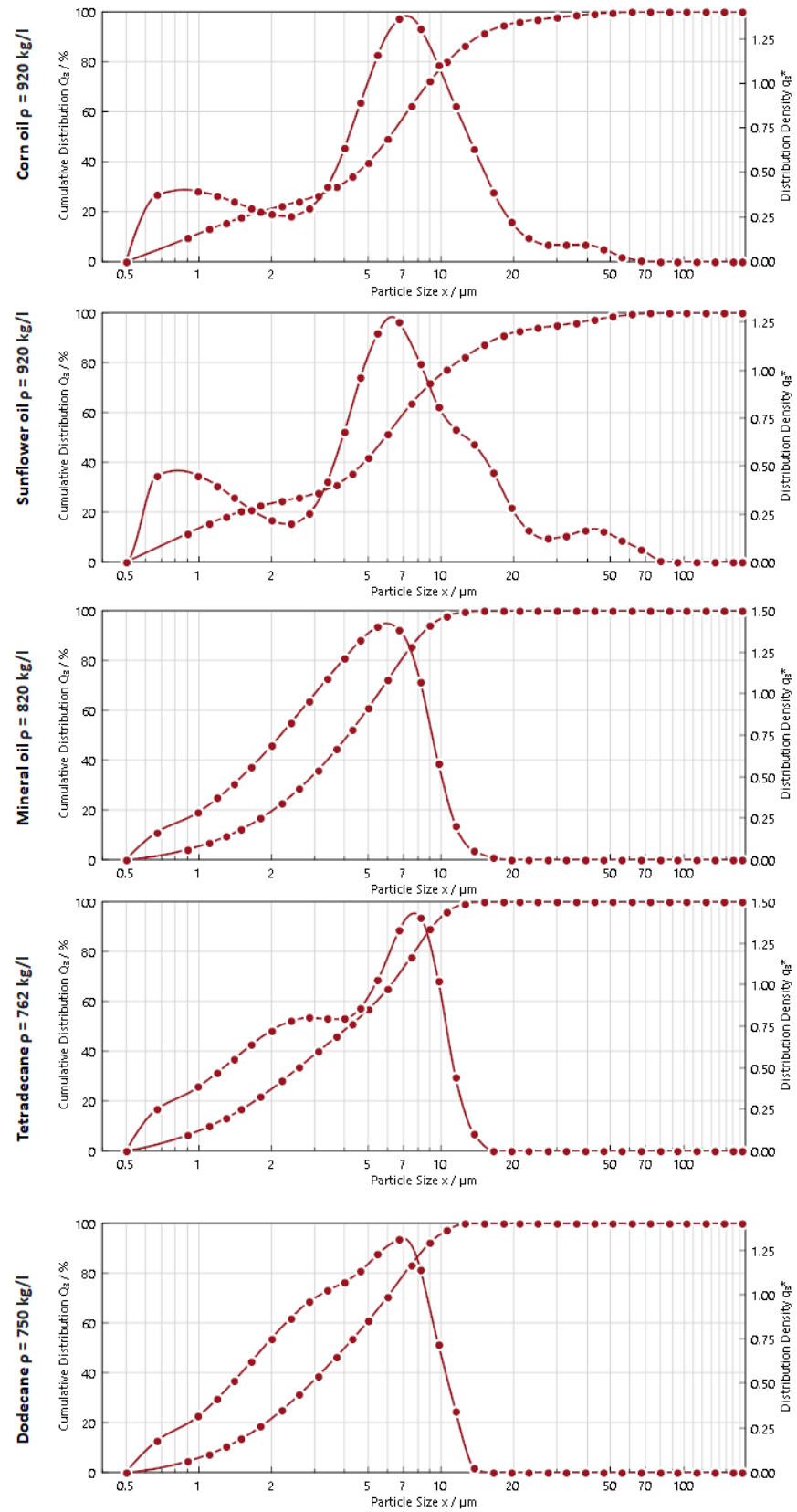
Figure A25: Droplet size distribution of O/W emulsions stabilised with 10 wt% BCS during variation of oil type, as determined by laser diffraction.
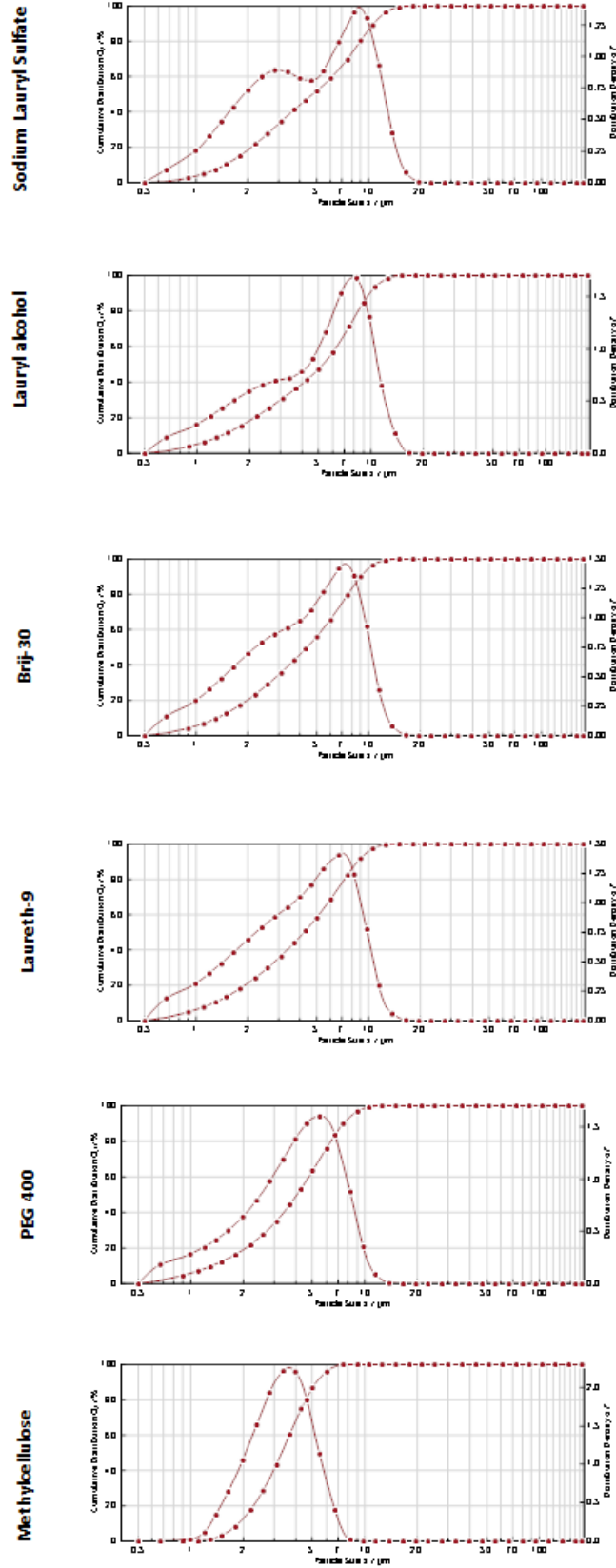
Figure A26: Droplet size distribution of O/W emulsions stabilised with 10 wt% BCS with variation of additive (2 wt%), as determined by laser diffraction.
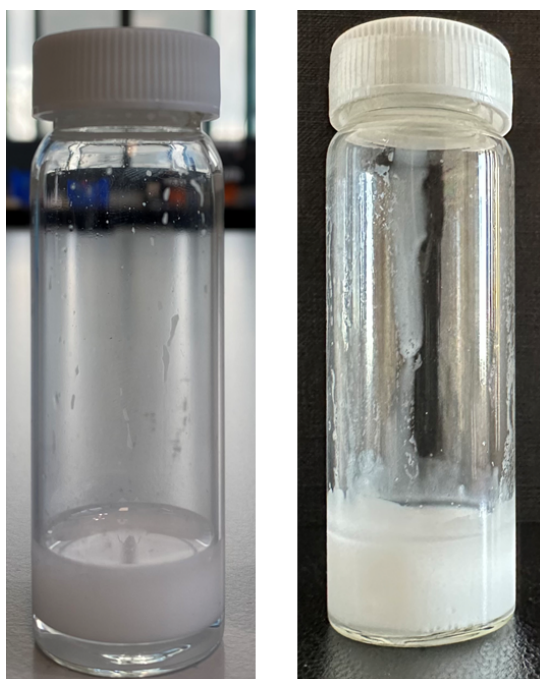
Figure A27: Appearance of BCS (10wt%)-stabilised (left) and BCS/methylcellulose (10/0.25 wt%) dodecane-in-water emulsions after 3 months storage under ambient conditions.
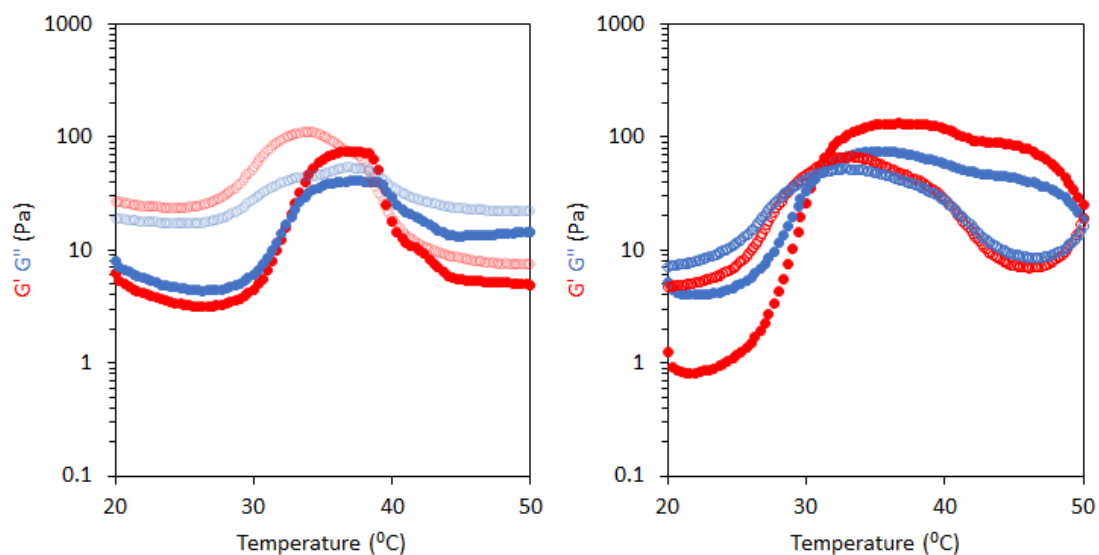

Figure A28: Rheological oscillatory temperature ramps of BCS (10 wt%)-stabilised (left) and BCS/methylcellulose (10/0.25 wt%) dodecane-in-water emulsions after 3 months storage under ambient conditions. The creamed phase was used for these experiments.
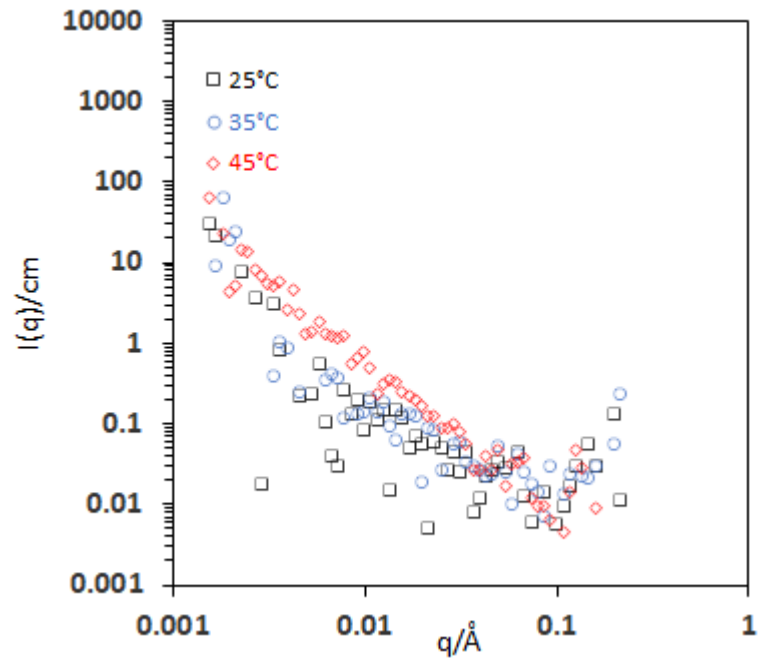
**Figure A29:** SANS of 0.5 wt% methylcellulose in D_2O.
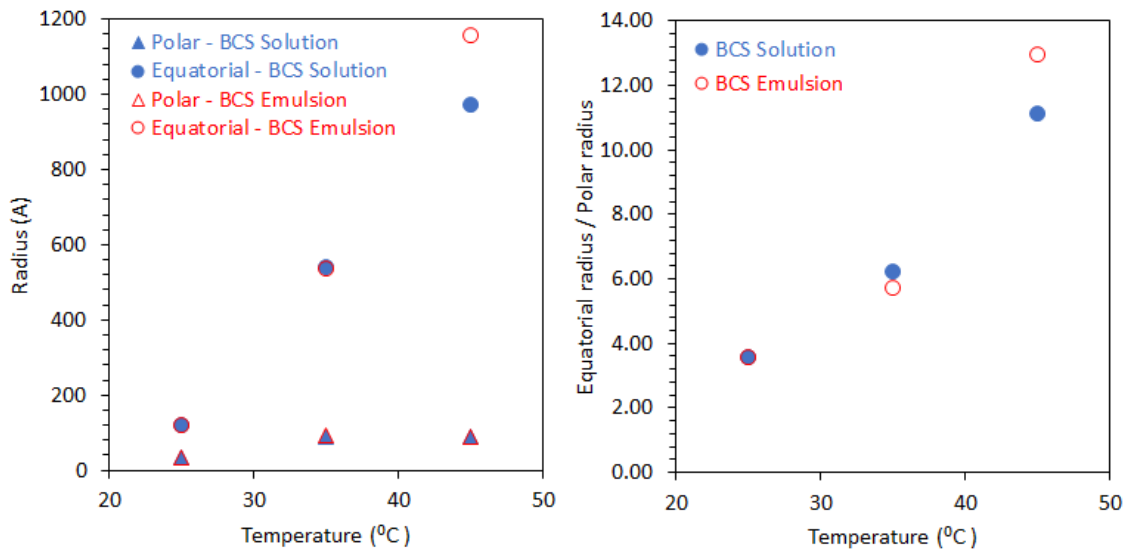
Figure A30: Dimensional parameters from fitting SANS data from BCS and BCS/methylcellulose (MC) solutions to the ellipsoid model (left). Equatorial/polar ratio, indicating the extent of flattening of the oblates (right).
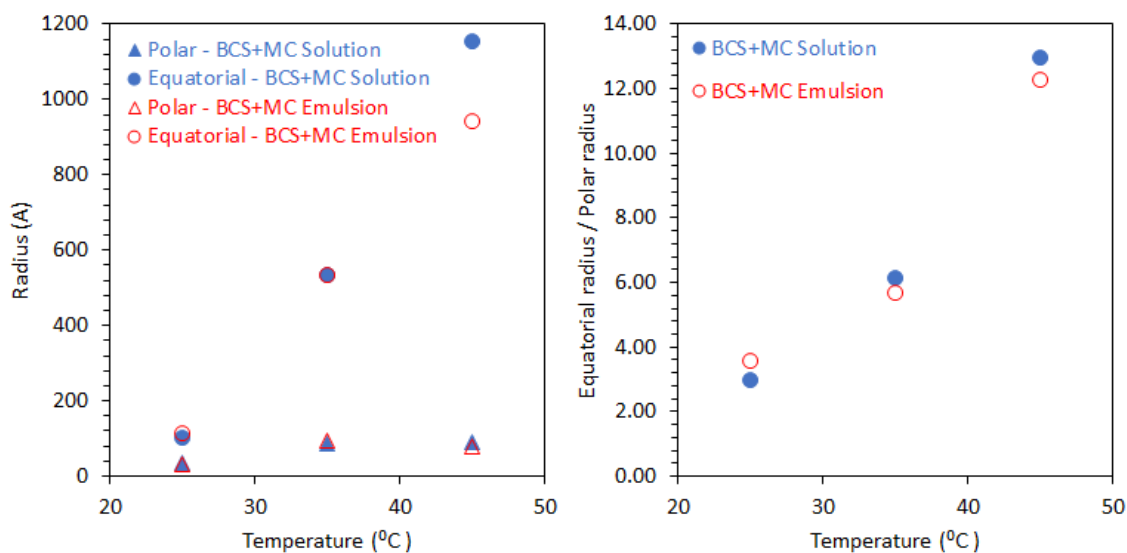
Figure A31: Dimensional parameters from fitting of data of BCS and BCS/methylcellulose (MC) emulsions to the ellipsoid model (left). Equatorial/polar ratio, indicating the degree of flattening of the oblates (right).
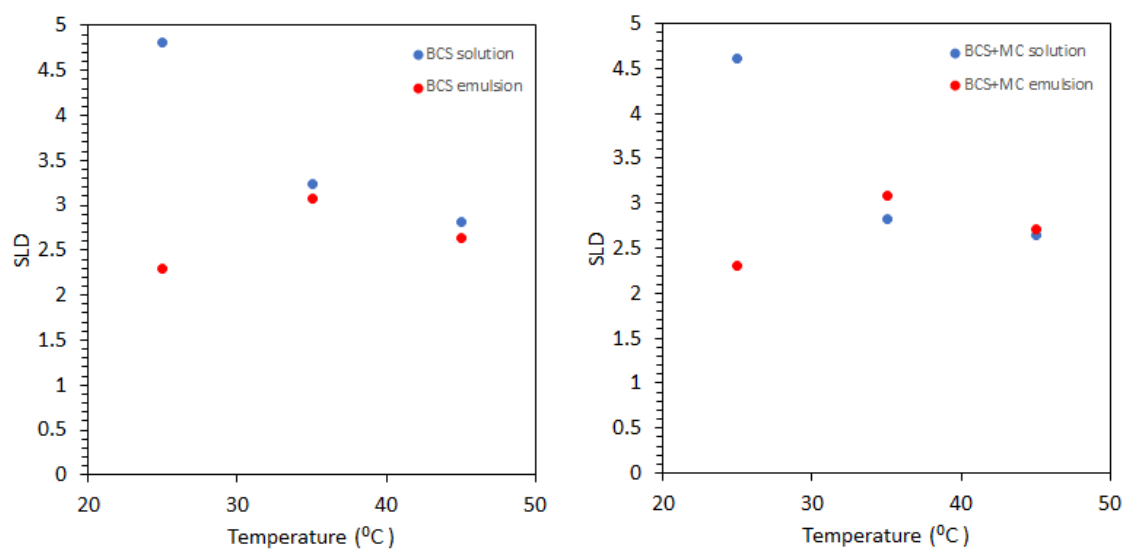

Figure A32: SLDs of nano-objects determined from fitting of data of BCS and BCS/methylcellulose (MC) solutions (left) and emulsions (right) to the ellipsoid model.
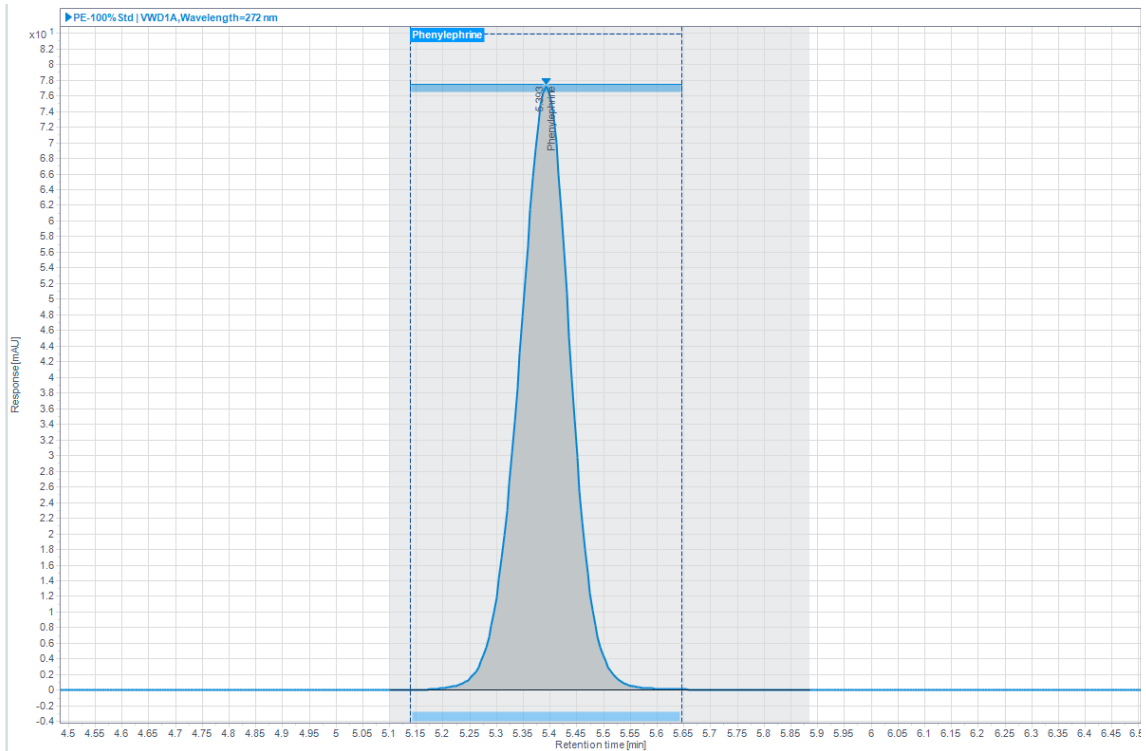
Figure A33: An example sample chromatogram representative of a 0.05 mg/mL phenylephrine standard solution in PBS analysed at 272 nm using HPLC method expanded between 4.5 – 8.5 min. The retention time of phenylephrine was observed to be 5.4 min.
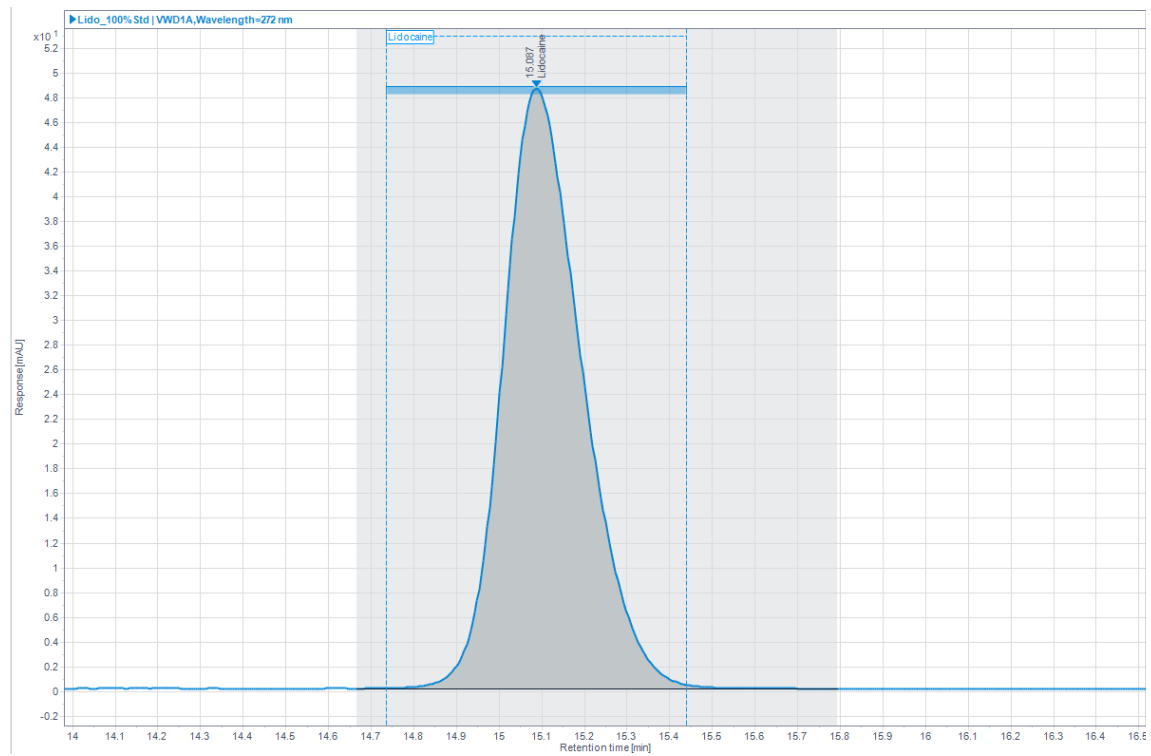
Figure A34: An example sample chromatogram representative of a 0.5 mg/mL lidocaine standard solution in PBS analysed at 272 nm using HPLC method expanded between 14 – 16.5 min. The retention time of lidocaine was observed to be 15.1 min.
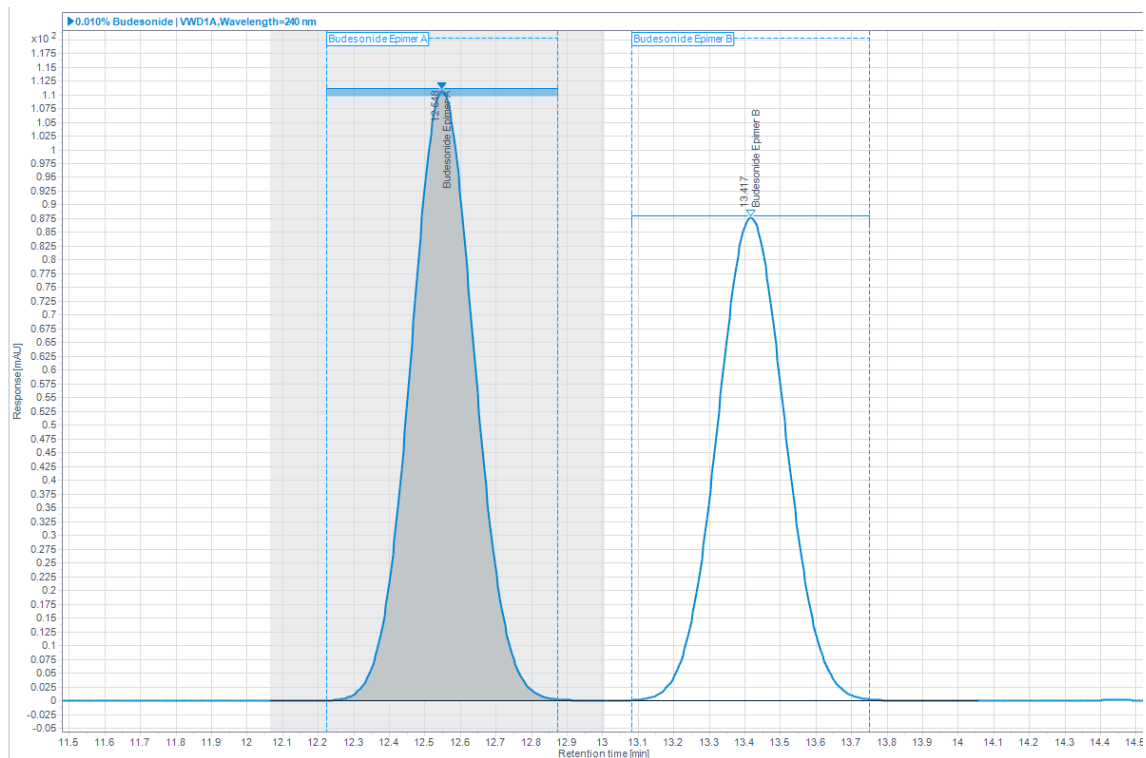
Figure A35: An example sample chromatogram representative of a 0.1 mg/mL budesonide standard solution in mobile phase analysed at 272 nm using HPLC method expanded between 11.5 – 14.5 min. The retention time of epimer A and epimer B was observed to be 12.5 and 13.4 min respectively.